AN ECONOMIC, METAMORPHIC, STRUCTURAL AND GEOCHEMICAL STUDY OF THE ISLE AUX MORTS PROSPECT, SOUTHWEST NEWFOUNDLAND

PATRICK P. O'NEILL

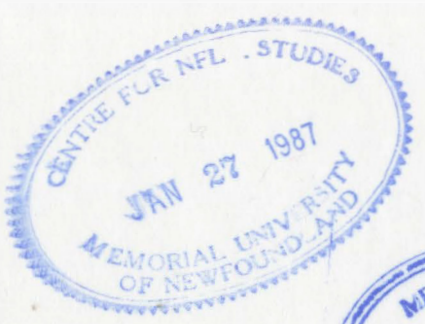
CENTRE FOR NFL . STUDIES
JAN 27 1987
MEMORIAL UNIVERSITY
OF NEWFOUNDLAND

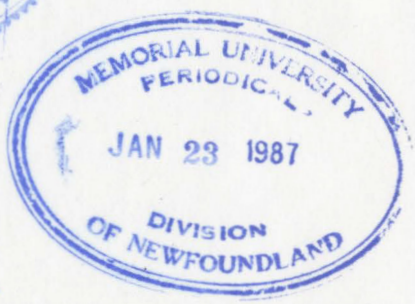
MEMORIAL UNIVERSITY
PERIODICALS
JAN 23 1987
DIVISION
OF NEWFOUNDLAND

AN ECONOMIC, METAMORPHIC, STRUCTURAL AND GEOCHEMICAL STUDY OF THE ISLE AUX MORTS PROSPECT, SOUTHWEST NEWFOUNDLAND

BY

Copyright (C) Patrick P. O' Neill, B.Sc. (Hons.)

A thesis submitted to the School of Graduate Studies in partial fulfillment of the requirements for the degree of Master of Science

Department of Earth Sciences
Memorial University of Newfoundland

May 1985

St. John's Newfoundland

FRONTISPIECE

View of the Isle aux Morts River looking NE;
location, SW corner of claim block 2327

ABSTRACT

A polymetallic sulphide occurrence, the Isle aux Morts Prospect, is located within the Port aux Basques Gneiss Complex of southwest Newfoundland. This is the first such mineralization to be found in the Complex and is the basis of the present study.

Three main lithologic units dominate the geology of the area and these comprise quartzofeldspathic, pelitic and amphibole-bearing rocks. The quartzofeldspathic units are leucocratic, quartz-feldspar-biotite-garnet-bearing rocks which are interpreted to be felsic meta-tuffs and or felsic meta-volcanoclastic greywackes. Pelites vary from leucocratic, quartz-muscovite ± kyanite to melanocratic, biotite-garnet-kyanite rocks which are thought to be felsic tuffs and shales respectively. Amphibolites which contain amphibole ± garnet ± biotite, are ubiquitously intercalated with pelites and quartzofeldspathic rocks throughout the area. The proposed protoliths of the amphibolites are mafic sills/dikes and/or mafic tuffs. The amphibolites are tholeiitic and have a chemical affinity with ocean floor basalts. The geochemistry of all the rocks defines an essentially bimodal sequence of rhyolites/dacites and tholeiites.

Structures recognized in the study area are interpreted to be the results of four episodes of deformation. The earliest, D1, is represented by isoclinal, recumbent folds affecting what is considered to be a primary layering. D2

is defined by a phase of tight, upright to inclined (towards the NE) folds associated with the formation of the regional S2 foliation. D3 is a minor phase manifested by a faint crenulation cleavage, axial planar to asymetric folds. D4 is defined by kinks, chevron folds and faults.

The Isle aux Morts Prospect area lies within a medium-pressure, Barrovian-type, metamorphic facies series terrane. The amphibolite facies paragenesis garnet-kyanite-biotite ± staurolite is commonly observed in pelites and hornblende ± garnet ± biotite ± epidote in amphibolites. A staurolite-muscovite-quartz zone and staurolite-quartz zone are recognized. The area lies within bathozone 5. Estimated pressures and temperatures from the garnet-plagioclase geobarometer and garnet-biotite geothermometer average 6.7 kb and 650^{o}C. U-Pb dates from zircon rims and sphenes from an amphibolite, give a metamorphic age of 410 ± 5 Ma.

Three textural types of mineralization are identified viz., a massive type comprising greater than 50% sulphides; a disseminated type in semipelitic, quartz-muscovite ± kyanite rocks and a banded type occurring in quartzitic rocks. The mineralization occurs at the contact between supposed felsic meta-tuffs to the north and felsic meta-volcanoclastic rocks with intercalated mafic meta-tuffs and pelites to the south. The felsic meta-tuffs contain ubiquitous disseminated pyrite and locally disseminated and banded chalcopyrite, sphalerite and galena. The pelites

contain ubiquitous coticules thought to represent Mn-rich chemical sediments. Average $\delta^{34}S$ values are 10 permil, typical of many volcanic-associated massive sulphide bodies.

The sulphides record the same deformational effects as the enclosing rocks and are pre-deformational. The massive type of mineralization exhibits a deformational fabric of rounded silicate fragments in a sulphide matrix characteristic of deformed/metamorphosed massive sulphide bodies. Mineralized semipelites display a K_2O enrichment and Na_2O depletion characteristic of alteration associated with massive sulphide deposits in volcanic/sedimentary lithologies. The observations above are best interpreted by a model in which the mineralization is of the volcanogenic type.

ACKNOWLEDGEMENTS

I am very grateful to D. Strong who offered this thesis to me and has since provided guidance, supervision, ideas and funding. I would also like to thank P. Legein who initially suggested the topic.

I would like to thank T. Rivers who critically read part of the manuscript and gave some useful comments.

Utah Mines Ltd. generously provided financial support for sulphur and lead isotope, and rare earth element analyses. Temporary employment with them for three summer field seasons allowed my stay in St. Johns to be, definitely, more financially viable. Receipt of a two-year Memorial University fellowship is gratefully acknowledged, as well as funding through D. Strong's NSERC Operating Grant # A7975.

Field assistance during two seasons was given by M. Spurrel, C. Ash, D. Holloway, G. Stapleton, J. Hayes and B. Gray. None of these fine fellows succumbed to the terrors of South Coast Fog or ghosts from Isle aux Morts. The legeindary pie-cooking abilities of P. Legein are also heartily acknowledged.

Useful discussions which contributed to this thesis were held with D. Wilton, G. Dunning who also provided the U-Pb zircon and sphene dates, S. Swinden and P. Barrette.

Much appreciated technical assistance was provided by D. Press, G. Veinott, H. Longerich, W. Marsh, P. Finn, G. Andrews, W. Howell and L. Nolan.

Finally but by no means least, are those fellow graduate students of Decadence Alley and, in the later stages of the thesis, the infamous Aquarena House, who have enjoyed or endured!, with me during my stay at MUN. I must also thank the Coniglio Zoo who stimulated my social agenda.

Table of Contents

List of Figures

List of Tables

Chapter 1
INTRODUCTION

1.1 General Perspective

1.1.1 Exploration History and Significance of the Twin Ponds Showing

In 1980 anomalous Pb-Zn values were found in the catchment area of the Isle aux Morts River, SW Newfoundland (Fig. 1-1), as a result of a regional lake geochemical survey carried out by the Newfoundland Department of Mines and Energy. A property, centred on one of these anomalies in Nutmeg Lake (informal name), was staked by Utah Mines Ltd (Fig. 1-2). Subsequent ground prospecting revealed sphalerite-galena-chalcopyrite-pyrite-barite mineralization which was termed the Twin Ponds Showing.

The occurrence is of special interest as it is the first significant mineralization found within the Port aux Basques Complex. Regionally correlated rocks in the La Poile area to the east contain significant volcanogenic gold and sulphide prospects and the presence of the Twin Ponds Showing may indicate similar potential for the Complex.

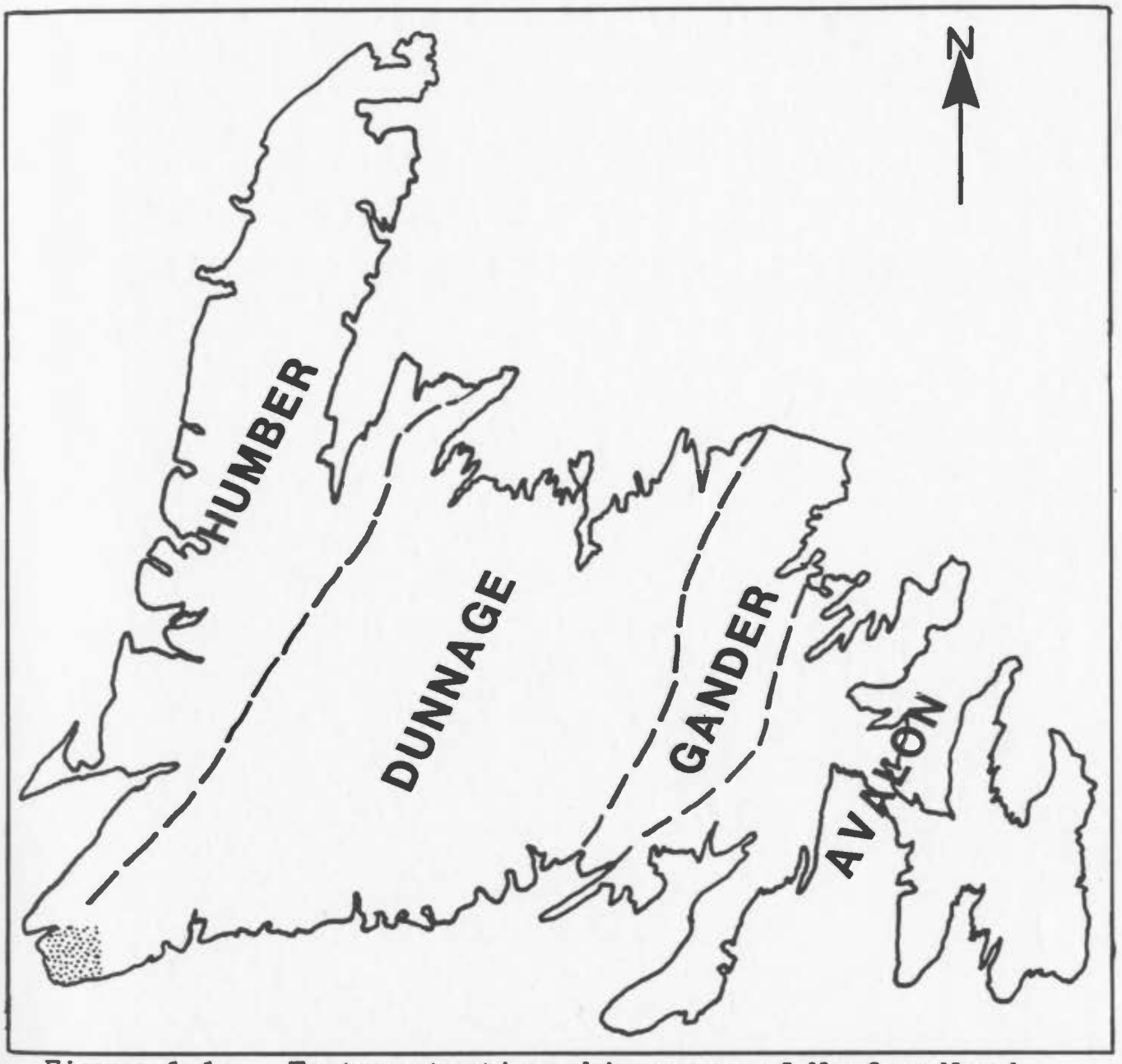

Figure 1-1: Tectonostratigraphic zones of Newfoundland (after Williams, 1979 and Kean, 1983); stippled area contains property and is shown in detail in Figure 1-2.

1.1.2 Purpose and Scope

This thesis is concerned primarily with the origin and geological history of a polymetallic sulphide body which is hosted by medium grade metamorphic rocks. Research on the origin and history of sulphide showings or potentially

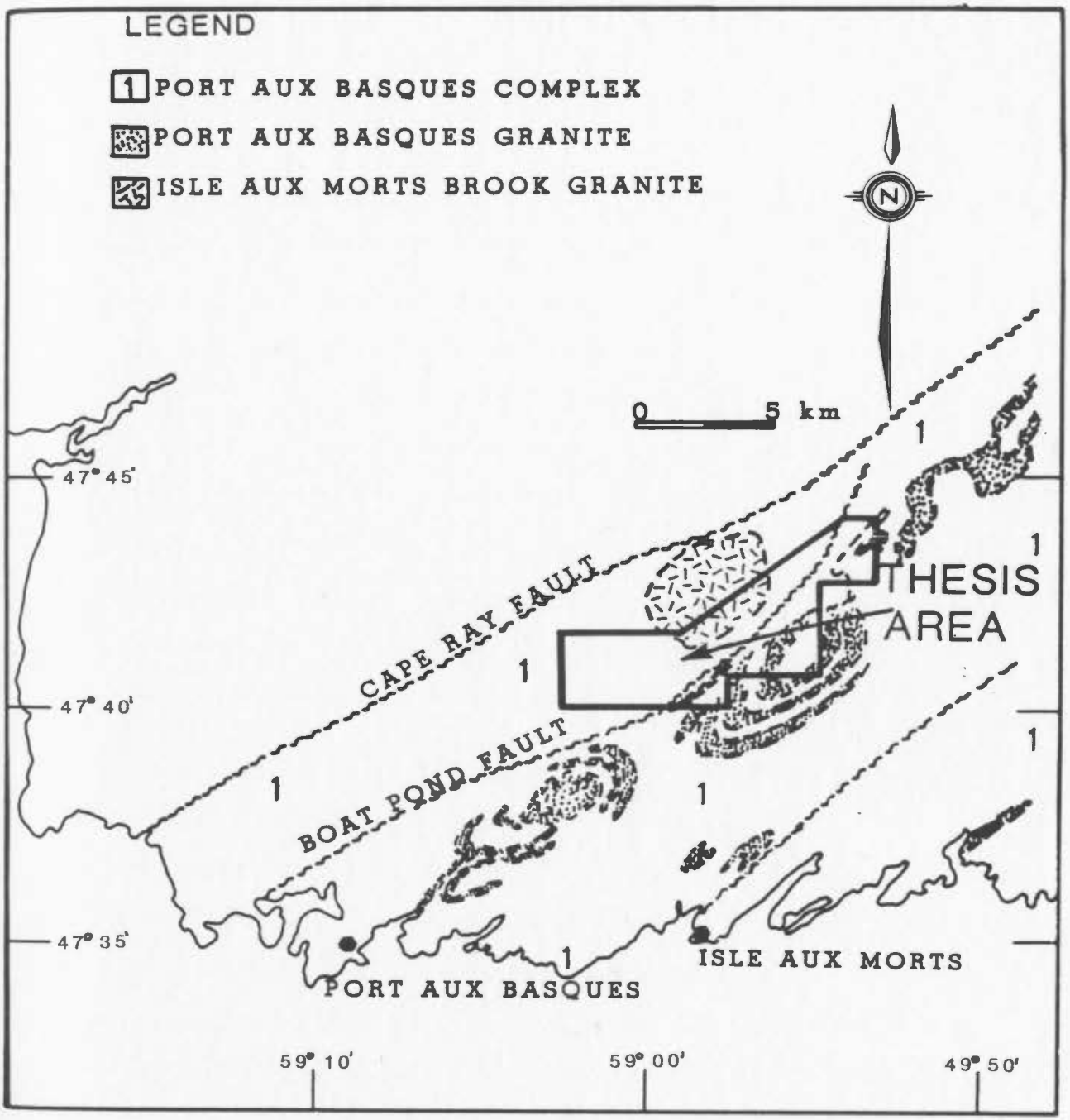

Figure 1-2: Regional geology of southwest Newfoundland (after Chorlton, 1984).

economic mineralization in metamorphic rocks is beset by an array of problems, principally derived from a complete lack or paucity of primary features. An effective ore-genesis model should therefore incorporate a geological-geochemical framework within which protoliths can be identified for the host and surrounding lithologies. This thesis evaluates the basic geological features and history of the host rocks independently of the mineralization, and thus defines a framework within which the mineralization is studied.

After reasonably consistent primary lithological and geochemical constraints have been placed on the host rocks, and their metamorphic/deformational history is outlined, the study focuses on the actual mineralization.

The aims of the thesis are therefore threefold:

(1) To describe and evaluate the lithological, structural, metamorphic and geochemical aspects of the local geology.
(2) To describe all relevant aspects of the mineralization and evaluate its origin and history.
(3) To integrate the new metamorphic, geochemical and geochronologic data from the study area with that of previous workers with the hope of providing new insight into the local tectonostratigraphic setting.

1.2 Location and Access

The thesis area is located in the southwest corner of the island of Newfoundland, between north latitudes 47° 40' to 47° 44' and west longitudes 58° 54' to 59° 02' (Figs. 1-1 and 1-2). The area occupies parts of two contiguous 1:50,000 NTS sheets viz. Rose Blanche (110/10) and Port aux Basques (110/11).

Port aux Basques, the principal community in the region is 12.5 km from the SW corner of the study area and the coastal village of Isle aux Morts (after which the property is named) lies 9 km due south. A rough muskeg track which links the coast road to the Cape Ray gold property provides overland access to the area east of the Isle aux Morts River. Numerous all-terrain-vehicle tracks crisscross the western portion of the property, but these are unsuited to regular use. The most viable means of access is ultimately by helicopter, as all the lakes in the region are too small for float planes.

1.3 Mapping and Sampling Methods

Four partly gridded claim blocks (numbers 1951, 2329, 2327 and 2850, Fig. 1-3) covering approximately 50 sq km, were mapped at a scale of 1" = 200' by the author (Map 1 in the back-pocket is a condensed version of this mapping and Fig. 1-3 is a photoreduction of this map). The area more immediate to the mineralization was mapped at the same scale but in greater detail (Map 2, in back-pocket). The study

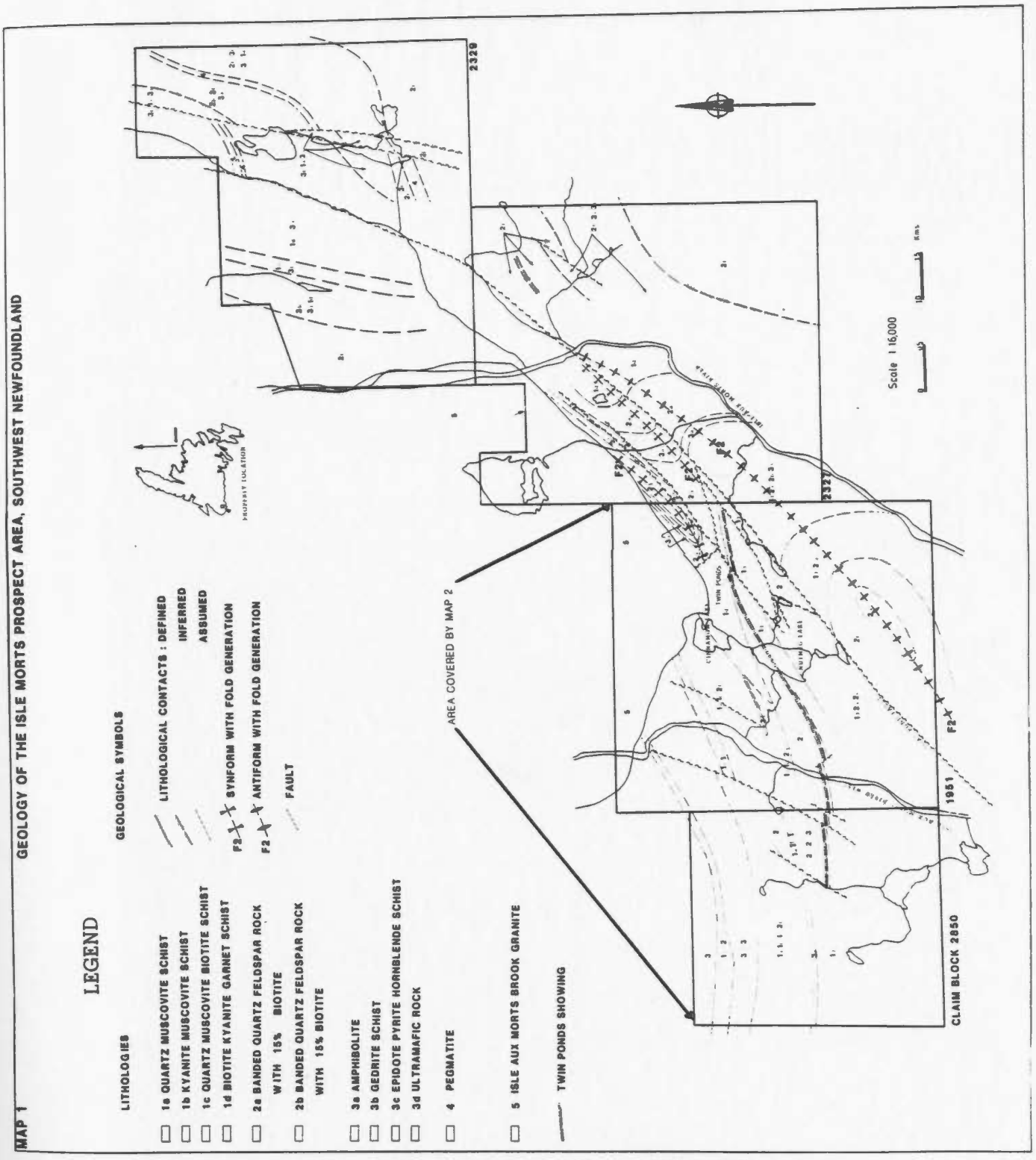

Figure 1-3: Location of the four claim blocks within the study area. This map is a photoreduction of Map 1 in back-pocket.

involved collection of structural and lithologic data and a representative suite of rock specimens. Mineralized samples were collected mostly from trenches which expose the showing, for petrographic, stable isotope, geochemical and mineral chemistry analyses. Diamond drill core was also sampled from nine holes intersecting the Twin Ponds Showing.

1.4 Physiography, Vegetation and Exposure

The Isle aux Morts property is located within the NE-SW trending Long Range mountains. Physiographic features reflect an early to late Wisconsinian, southwesterly directed glaciation (Brookes, 1977). The retreat of the ice left many small and large scale glacial structures. For example, the Isle aux Morts River flows in a U-shaped valley whose sides rise, locally precipitously, from a flat floor at approximately 300 metres above sea-level to plateau level at 500 metres above sea level (see frontispiece). Rôches moutonnées, perched boulders, glacial striae and eskers are other commonly observed glacial effects. Ice movement directions are a major control on the drainage pattern in the area which lies within the catchment basin of the Isle aux Morts River system. The structural grain of the rocks and some regional lineaments also exert a strong influence on flow patterns, for example the Isle aux Morts river flows along the eastern margin of the Isle aux Morts Brook Granite for several km and is diverted sharply southwest by a major NE-SW fault.

A dense undergrowth of stunted timber, colloquially "tuckamore", grows profusely on well drained plateau soil. Large areas between these dwarf-timber stands are covered by peat bogs up to 6 metres in depth. The major river valleys are forested with spruce, fir and minor birch, especially where relief is rugged (see frontispiece).

Rock exposures are poor, less than 5% of the total area, but both Isle aux Morts River and Isle aux Morts River West provide reasonable cross-strike sections. Outcrops on the barrens, i.e. the plateau, are typically small, lichen-covered and mostly follow ridges which reflect the structural grain.

1.5 Regional Geology and Previous Work

1.5.1 Regional Geology

Newfoundland is divided into four major tectonic zones (Williams 1979), the Humber, Dunnage, Gander and Avalon (Fig. 1-1).

The Port aux Basques Gneiss Complex (so defined by Brown, 1973a) has been included (Williams et al. 1974) with the Central Palaeozoic Mobile Belt (Williams, 1964). The Central Mobile Belt comprises an Eastern Crystalline Belt (the Gander Terrane) (Kennedy, 1975), an axial region (the Dunnage Terrane) (Williams et al., 1974) and the Western Crystalline Belt (Kennedy, 1975). The Port aux Basques Complex was considered to be the southwestern extension of the Gander Terrane (Williams et al. (1974). The Dunnage

Terrane representing island-arc volcanic and related sedimentary assemblages, was thought to be pinched out by the Cape Ray Fault (Kennedy, 1976; Brown and Colman-Sadd, 1976).

Rocks of the Port aux Basques Complex were envisaged as comparable to gneisses of the Gander Zone, in the Baie d'Espoir area, which were thought to be correlatives of the basement to the Gander Lake metasediments (Kennedy and McGonigal, 1972). Recent work however, has led to major revisions of the tectonostratigraphic relations of the various terranes in south and southwest Newfoundland. Blackwood (1978) has proposed a conformable relationship (essentially a metamorphic gradient) between the Bonavista Bay Gneisses, originally considered as Precambrian basement to the eastern margin of Iapetus and overlying, pre-Middle Ordovician sediments (Blackwood and Kennedy, 1975). Colman-Sadd (1980) proposed that the Little Passage gneisses of the Baie d'Espoir area are correlatives of the Bonavista Bay Complex. The Little Passage Gneisses were considered to be unconformably overlain by shelf and basinal sequences of the Baie d'Espoir Group in the south and the Gander/Davidsville Groups in the north. The latter groups were thought by Strong et al. (1974) and Colman-Sadd (1980) to have been deposited in a Lower to Middle Ordovician back-arc basin between a central Newfoundland island-arc to the west and the Avalon platform to the east.

Chorlton (1978, 1980a, b, c, 1983) mapping in the La

Poile (sheet 110/9), La Poile River (sheet 110/16) and Grandys Lake (sheet 110/15) areas, has compared rocks on either side of the Cape Ray Fault to those of the Port aux Basques Complex. The La Poile area is considered by Chorlton (1980b) to be underlain by a metavolcanic pile with island arc affinities which grades westwards into a metasedimentary sequence with intercalated amphibolites. These were respectively assigned to the Bay du Nord Group (a polydeformed, staurolite/kyanite grade belt) and the La Poile Group (Cooper, 1954) which is a time-equivalent of the Bay du Nord but at lower metamorphic grade. Both groups were correlated by Chorlton with the Port aux Basques Gneiss.

Chorlton (1984) has proposed that the metamorphic and structural history for the Bay du Nord Group is the same as that of the Port aux Basques Gneiss Complex. She also proposed that the Complex corresponds to the metasedimentary, amphibolitic and migmatitic portions of the Bay du Nord Group. Mafic plutonic rocks in the Grandys Lake area were interpreted by Chorlton (1980a, b) to be ophiolitic segments forming basement to the overlying volcanic sequences south of the Cape Ray Fault zone. Similar relations hold NW of the Fault zone (Chorlton, 1983)

The Hermitage Flexure area, which includes the La Poile and Bay du Nord Groups, contains several important sulphide occurrences, for example the Strickland Prospect (Wynne, 1983) and the Cinq Cerf gold Prospect (Northern Miner,

"Production from Chetwynd possible by year-end, 1988"., April, 1985). If Chorlton's (1984) correlation of these Groups with the Port aux Basques Complex is correct, it has important implications for future mineral exploration in the Complex. Obviously the presence of the Twin Ponds Showing is evidence of such potential.

Swinden and Thorpe (1984), suggested that the La Poile and Bay du Nord Groups are partly derived from melting of continental crust, based on isotopic analyses of lead from such showings as Strickland, Facheux Bay and Barasway de Cerf. These conclusions apparently conflict with those of Chorlton's. Dunning (1984) working in the Annieopsquotch Complex to the north also notes ambiguous geochemistry from the Victoria Lake Group which he considers to reflect a transitional tectonic environment.

Wilton (1982, 1984) has carried out a comprehensive study of the Cape Ray Fault zone which concentrated on granite-related gold mineralization of the Cape Ray Prospect. The present thesis area lies approximately 10 km SE of the Cape Ray Prospect. According to Wilton (1984) the contact between the Port aux Basques Gneiss and the Windsor Point Group, although not well exposed, is sharp, reflecting a 2 kb difference in metamorphic pressure. Geochronologic and structural analyses of the Cape Ray Fault zone (Wilton, 1984) negate the cryptic suture hypothesis of Brown (1973b) and suggest rather that it is a ductile shear zone, developed within the Devonian Windsor Point Group. Similar

conclusions were reached by Chorlton (1984) working further NE. Wilton (1984) also defined the Isle aux Morts Brook Granite (see Map 1) as an A-type, generated by partial melting of depleted granulites. He suggested that the most plausible candidate for the basement is Grenvillian continental crust.

1.5.2 Previous Work in the Port aux Basques Gneiss Complex

Some of the earliest workers of the Newfoundland Geological Survey (Jukes, 1843; Murray and Howley, 1881) described the Port aux Basques Complex as containing "Precambrian crystalline rocks". In 1889 (Murray and Howley, 1918), gold was reported in the Diamond Cove quartz vein, which was further investigated by Howse (1934). The Strickland Prospect was one of the more significant discoveries made in the area (Howse, 1937). Numerous other commodity surveys were carried out, for example Power (1955) mapped a small area on the coast near Isle aux Morts Village and Burnt Island. Tater (1964) and Gale (1967) examined pegmatites on the coastal section for economic potential. The La Poile-Cinq Cerf map area, approximately 80 km to the east, was mapped by Cooper in 1937-1940 (Cooper, 1954) who defined two gneiss complexes, namely the Keepings Gneiss of supposed Precambrian age and a Devonian Dolman Gneiss; However, it was not until 1972 when Gillis published a 1:250,000 map (Sheet 110) and a report for the Port aux Basques area that the geological picture started to take

shape. Gillis (1972) correlated the Keepings Gneiss with the Port aux Basques Gneiss.

Brown (1973a) mapped a coastal strip from Red Rocks to Isle aux Morts Brook as part of an MSc thesis on the structure and metamorphism of the Port aux Basques Gneiss Complex. In 1975 he extended his area further east to Garia Bay, as part of a PhD thesis studying the supposed basement-cover relationships of the Port aux Basques Complex and the Bay du Nord Group respectively. These are the first detailed studies of the Complex and are accompanied by 1:20,000 maps. In 1976 and 1977, Brown, while working for the Newfoundland Department of Mines and Energy, published brief reports and 1:50,000 scale maps of the Port aux Basques (110/11) and Rose Blanche (110/10) sheets.

Brown (1973a, 1975) described the Complex as a polydeformed, banded gneiss raised to sillimanite grade with syn-tectonic granites. This terrane is separated from the Cape Ray Complex to the north by the Cape Ray Fault zone, which he regarded as a major transcurrent fault juxtaposing the Precambrian continental margins of the proto-Atlantic, i.e. a cryptic suture.

The syntectonic Port aux Basques granite was the subject of a BSc thesis (Dingwell, 1980) which focussed on its geochemistry, geophysics and structure. Comparisons were made to two-mica garnetiferous leucogranites of the Gander Zone e.g. Aspen Cove and Round Pond.

Chapter 2

PETROLOGY AND STRUCTURE OF THE ISLE AUX MORTS PROSPECT

2.1 Descriptions of Lithologic Units

2.1.1 Introduction

In this section the geological field relations and macroscopic lithological features of the Isle aux Morts Prospect are described. The geology of the property held by Utah Mines Ltd at the time of writing is illustrated on Map 1 while that of the area more immediate to the mineralization is illustrated on Map 2.

The lithologies are grouped under three major subheadings, viz. quartzofeldspathic rocks, pelites and amphibolites which define an apparently conformable "sequence". This "sequence" is essentially structural and has no stratigraphical implications. Quartzofeldspathic units are leucocratic, banded rocks containing variable amounts of quartz, feldspar, biotite, garnet and muscovite. They dominate the geology in the southern and southeastern portions of Map 1. They are interpreted as being felsic meta-volcanic rocks and/or meta-volcanoclastic sediments.

Pelites comprise leucocratic, muscovite-rich and melanocratic, biotite-, garnet-, kyanite-, staurolite-

bearing units. The two types are distinct and do not occur together. The former are composed of variable proportions of muscovite, kyanite and quartz and occur primarily in the central and northern parts of claim blocks 1951 and 2850. The protolith to these rocks is considered to have been felsic tuffs or reworked tuffs. The dark-coloured pelites are typicallyinterbedded with quartzofeldspathic units south of the mineralized horizon. These pelites are thought to represent metamorphosed shales. Intimately interbedded with the melanocratic pelites are coticules, a distinctive, pink-coloured rock interpreted to be metamorphosed chemical sediments.

Amphibolites, as defined in this thesis, characteristically contain greater than 40% amphibole with variable proportions of garnet and minor biotite and quartz. These are thought to represent mafic meta-tuffs and/or mafic sills or dykes, and locally, proximal mafic meta-fragmental rocks. Amphibole-bearing units i.e. with less than 40% amphibole, occur locally and may represent mafic tuffs. Gedrite-bearing rocks are ubiquitous in the northeast of the area. Two amphibolite bodies (see Map 1) comprising greater than 90% amphibole, are interpreted as metamorphosed ultramafic rocks.

The pegmatitic phase of the Port aux Basques Granite occurs ubiquitously throughout the area in most lithologies, particularly towards the south of Map 2. Only one occurrence of the Granite was noted in the thesis area.

Data from ten diamond drill hole (DDH) logs is incorporated in the descriptions. Mineral assemblages are described in Chapter 3 and the geology of the mineralized horizon is described in detail in Chapter 5.

2.1.2 Pelites and Semipelites: Unit 1

Unit 1 comprises pelitic and semipelitic rock types containing variable amounts of muscovite, biotite, garnet, kyanite, staurolite and quartz. Some quartz-rich varieties (70-80%) are granoblastic in texture but are conveniently included in this group because they are of only local occurrence and are typically associated with certain pelites. Semipelitic types contain quartz and feldspar, perhaps 30 to 60%, but micas are still prominent enough that the rock is obviously schistose.

Unit 1 can be divided into two main groups, a leucocratic group comprising units 1a, 1b and 1c and a melanocratic group, 1d. This first-order subdivision reflects a major mineralogical difference between the two groups and also the fact that they are not seen to occur together. The presence of disseminated and banded sulphides in units 1a, 1b and 1c also distinguishes them from 1d. Units 1a, 1b, 1c and 1d are respectively quartz-muscovite, quartz-kyanite-muscovite, quartz-muscovite-biotite and quartz-biotite-garnet-kyanite-staurolite schists.

Units 1a, 1b and 1c are separated on the basis of mineralogical and lithological criteria. These differences

are locally subtle, probably indicating a common origin. Unit 1a is typically a leucocratic, schistose to granoblastic, quartz-muscovite rock. The quartzitic parts locally contain thin interbands of sulphides. Unit 1a is intimately associated with the mineralized horizon along its entire strike length (however, it is to thin to be shown as a separate band on Maps 1 and 2). Within the quartzofeldspathic rock adjacent to the showing (to the north), unit 1a occurs as 5-30 cm thick bands which increase in abundance towards the mineralization. Quartz veins are a ubiquitous feature of unit 1a. Unit 1b (Fig. 2-1) is distinguished by the presence of positively weathering, pale blue, pale green to grey kyanite comprising up to 60% of the rock.

Figure 2-1: Kyanite schist (unit 1b) openly folded by F2 with axial planar crenulation cleavage, cutting SO//S1.

Disseminated chalcopyrite is also locally present. At Isle aux Morts River West, 1b is locally present, adjacent to the mineralization (however, it is too thin to be shown as a separate band on Maps 1 and 2). The characteristic presence of disseminated pyrite and more rarely chalcopyrite, imparts a distinct yellow, rusty weathering surface to units 1a and 1b. Further northeast in that part of claim block 2329 to the east of Isle aux Morts River, units 1a and 1b crop out together in a 180 m thick band (Map 1).

Unit 1c is typified by a streaky, anastomosing schistosity, defined by minor biotite. This unit also contains a greater proportion of feldspar than either units 1a or 1b. It is also the least prominent member of the leucocratic group of pelites and found only in claim block 2850.

Units 1a, 1b and 1c are intimately associated in the field and their contacts are gradational over several cm. They occur predominantly in the central part of claim block 2850. In the Cinnamon Lake (informal name, Map 2) area, 1a and 1b are subordinate to a grey quartzofeldspathic rock (unit 2b). Westwards, however, they gradually thicken and merge, reaching their greatest combined apparent thickness (550 m) in claim block 2850. Deformation is probably partly responsible for their rapid alternation in claim block 2850. Amphibolites are absent from the pelitic sequence comprising 1a, 1b and 1c in claim block 2850, but they do occur immediately to the south and north; bands of quartzofeldspathic rocks are a minor component.

The aluminous, non-ferromagnesian mineralogy suggests that plausible protoliths are felsic tuffs (or reworked felsic tuffs i.e. siliceous shales).

Unit 1d (Figs. 2-2 and 2-3) typically contains variable proportions of biotite, garnet, kyanite and locally staurolite with minor muscovite and quartz. It locally comprises 10-20% of the sequence, as 30-330 m thick bands, traceable for up to 5 km along strike. This unit only occurs south of Cinnamon Lake in claim block 1951 and south of the mineralized horizon in claim block 2850. In both of these blocks, it is typically interlayered with banded quartzofeldspathic rocks and amphibolites. Further northeast in claim block 2327, it occurs east of the Boat Pond Fault and west of this fault in claim block 2329, where it is a minor component in a mixed sequence of amphibolites and gedrite-bearing rocks, both of unit 3. Contacts between the quartzofeldspathic rocks and the pelites are typically sharp. Deformed quartz veins, boudins and rods are ubiquitous in unit 1d (e.g. Fig. 2-2). Quartz segregations are typically less than 60 cm in longest dimension but some are several m in length. The most spectacular segregation phenomena, only noted in unit 1d, are quartz-kyanite pods in which kyanite forms compact sky-blue, bladed masses up to 10 cm long in the pressure shadows of quartz concentrations.

The most plausible protoliths are shales and/or mudstones. Those clay minerals which have the most suitable composition are illite and montmorillonite, typically

Figure 2-2: Typical tightly folded (F2) biotite schist (unit 1d) with folded quartz veins, exhibiting boudinage structures.

Figure 2-3: Biotite schist (unit 1d) with asymmetrically folded quartz boudins; the darker exposed area was formerly covered by peat bog.

derived from the breakdown of felsic and mafic rocks respectively. Also these two clay minerals are widely associated in shales produced by the weathering of basic rocks if sufficient Mg is present (Deer et al, 1976).

2.1.2.1 Garnetiferous Quartzites: Coticules

Pink garnet-bearing quartzites are a prominent member of unit 1d (Fig. 2-4), and occur rarely in garnet amphibolites.

Figure 2-4: Thin coticule layers in biotite schist (unit 1d) the scale bar is 2 cm.

They vary from mm to several cm thick layers to mm-thin, pancake-like lenses and locally have biotite and/or quartz-rich selvedges. Although they are ubiquitous in unit 1d, it is impossible to trace individual layers for more than several metres because of the combined effects of intense deformation and poor outcrop. They occur south of

the Twin Ponds Showing and are also locally developed in the northeast part of claim block 2327. Contact relations with adjacent rocks are generally sharp.

Field evidence and petrography suggest that these garnet-quartzites are coticules as defined by Renard (1878) *i.e.* rocks rich in spessartine garnet, with up to 35 wt.% MnO in bulk rock composition. This distinctive lithology has now been recognized throughout the Caledonian-Appalachian orogen (Kim, 1975; Kramm, 1976; Kennan and Kennedy, 1983; Docka, 1984). The host rocks are pelitic to clastic sediments of (generally) Ordovician age with associated garnet-amphibolites and carbonates. The tectonic environment is generally in an oceanic or continental margin type setting (Kennan and Kennedy, 1983).

Coticules are found in the Birchy Schist of the Fleur de Lys Supergroup (Kennedy *et al*, 1971) and locally in the La Poile Group of Chorlton (1984) (with which she correlates the Port aux Basques Gneiss). Williams and Kennan (1983) note the spatial relationship of Pb-Zn mineralization to coticules and tourmalinites in metasediments in SE Ireland and similar rocks are also associated with the volcanogenic massive sulphide deposit at Broken Hill, New South Wales (Plimer, 1980).

The salient features of coticules are:

(1) They represent sudden and repeated changes in sedimentation, implying an episodic event which occurs in a relatively short span of time (indicated by the

absence of pelitic material).

(2) They are thin and occur ubiquitously within pelites.

(3) They are spatially associated with volcanogenic mineralization.

(4) They have above-average MnO content.

Suggested protoliths for coticules vary from Mn-enriched ironstones, cherts or mudstones to siliceous sediments rich in montmorillonite clay. The consensus among various authors favours an origin by hydrolysis or hydrothermal processes in deep water, pelagic, sedimentary environments, (Kramm, 1976). The occurrence of coticules interbedded with amphibolites and pelites and their invariably sharp contacts, suggests that they are not produced by hydrolysis of tuffs (Kramm, 1976), in which case gradational contacts would be expected, at least locally. The interpretation favoured here considers coticules as representing episodic pulses of hydrothermal fluids locally, or distally derived, from which precipitate various Mn-rich (clay) minerals.

Coticules are bedding indicators and, as such, imply that transposition during deformation has not totally destroyed all original fabrics. Thus, much of the mineralogic layering which is parallel to coticules may also represent bedding.

2.1.3 Banded Quartzofeldspathic Rocks: Unit 2

Quartzofeldspathic rocks contain variable amounts of quartz, feldspar, biotite, muscovite and garnet. They comprise leucocratic rocks which are banded on a centimetre to metre scale. Individual units vary in thickness from thirty to several hundred metres. The geology south of the showing is dominated by these rocks and they comprise approximately 90% of the sequence south of Boat Pond Fault. In the northeastern part of the property, the presence of approximately 40 to 60% pegmatitic material in these rocks imparts a migmatitic appearance to them. In those quartzofeldspathic units specifically discussed here, pegmatites or leucosomatic material, are not abundant enough to justify calling them gneisses and they are termed banded quartzofeldspathic rocks.

Subdivision of these rocks into two units is based both on mineralogical and macroscopic lithological criteria. Unit 2a is a leucocratic unit with less than 10% biotite (Fig. 2-5). Red garnets occur sporadically and are generally less than 3 mm in diameter. The unit is typically homogenous with fine internal laminations (Fig. 2-5). However, immediately above the mineralization at Twin Ponds (Fig. 1-3), numerous thin amphibolite and biotite-rich bands are locally prominent (Fig. 2-7). One particular band of unit 2a, which thickens considerably westwards, is associated with the mineralization along its entire 4 km strike length. The northern contact which is slightly

Figure 2-5: A leucocratic, quartzofeldspathic rock (unit 2a) with conformable and partly disconformable pegmatite layers.

Figure 2-6: A grey quartzofeldspathic rock of unit 2b with characteristic banding, which may be a primary layering.

Figure 2-7: Quartzofeldspathic unit 2a with amphibolite and biotite/chlorite bands, several feet above (i.e. in the structural footwall) the mineralization.

discordant to the local structural trend, has been intersected in drill hole IAM-82-3 (Map 2) where it is interpreted to be a fault. The surface expression of this fault is a scarp trending westwards from the Twin Ponds to Nutmeg Lake.

Unit 2a is a siliceous unit with possible protoliths being arkosic sandstones, felsic intrusions, flows or felsic volcanoclastic rocks. Its relatively homogenous nature, however, suggests that it may have been of volcanic origin.

Unit 2b is a grey, fine-grained rock containing 10-25% biotite (Fig. 2-6). Garnets, up to 5 mm in diameter, are common. Unit 2b consists of alternating massive and laminated layers, up to approximately 50 cm thick (Figs. 2-6 and 2-8). The essential difference between the layers (in

Figure 2-8: Thinly banded quartzofeldspathic unit 2b; note early fold (F1) closure 10 cm to the right of the lens cap. The principal foliation as seen is S2 which is crosscut by a weak crenulation cleavage (S3), axial planar to the localized F3 in the center of the picture.

Fig. 2-6) is the biotite content (see Appendix Table B-3 for chemical analyses of the laminated and massive layers illustrated in Figure 2-6 and section 4.2.3.1 for discussion). Unit 2b superficially resembles sedimentary rocks such as greywackes, impure sandstones or felsic volcanoclastic rocks.

The conformable sequence of quartzofeldspathic and pelitic rocks (units 1 and 2) dominate the geology of the area south and east of the showing. Exposed contacts between units 1 and 2 are locally sharp, but in general appear gradational due to the effects of deformation and transposition. South of Nutmeg Lake and Boat Pond Fault

both quartzofeldspathic units are interbanded and mutual contacts are sharp.

Thin calc-silicate (± hornblende), amphibolite and biotite (± chlorite) schist layers, typically less than 15 cm thick, occur locally in units 2a and 2b (e.g. Fig. 2-7).

2.1.4 Port aux Basques Granite: Unit 4

The pegmatitic phase of the Port aux Basques Granite is a ubiquitous feature in all lithologies; the granite is only rarely seen. Pegmatites are typically coarse-grained and mineralogically simple comprising quartz, K-feldspar and plagioclase with less than 10% biotite and/or muscovite. South of claim block 1951, large muscovite books, approximately 10 cm in width, occur in a 5 m thick pegmatite vein. Parallel mineralogical layering (alternating quartz and feldspar bands) and a grain size zonation were noted in pegmatite sheets exposed in the major antiformal core on Map 2.

In morphology, pegmatites range from conformable layers exhibiting irregular boudinage structures to crosscutting veins; an example of the latter is seen in the south of claim block 1951 (Map 2). The pegmatites typically occur within quartzofeldspathic and pelitic units as sheets ranging in thickness from a mm to several tens of m. They locally contain screens of quartzofeldspathic rock (Fig. 2-9). Pegmatites cutting tight folds are shown in Figure 2-10 and although clearly intrusive, the contacts are

Figure 2-9: Banded quartzofeldspathic inclusion in pegmatite.

Figure 2-10: Injected pegmatite cutting F2(?).

diffuse. Other pegmatites are folded with the adjacent rocks and were emplaced prior to deformation. Pegmatites occur in pelitic unit 1d in which they are typically less than 5 cm thick and commonly show gradational contacts (in mm) (Fig. 2-11).

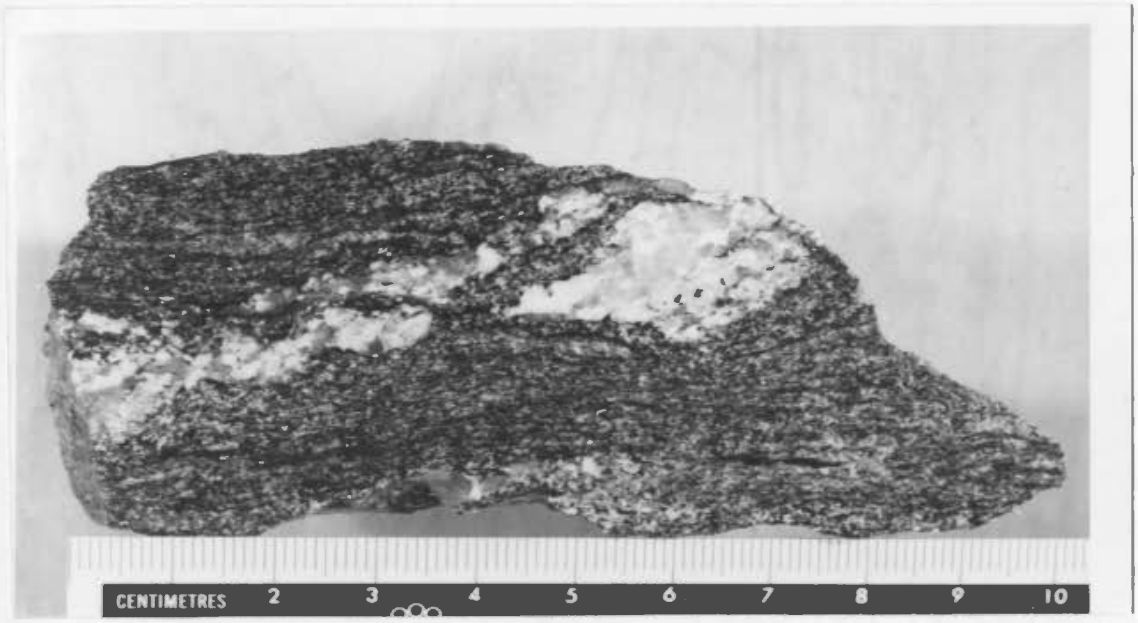

Figure 2-11: Pegmatites in unit 1d; note gradational margins.

Locally they comprise up to 20 % of the rock as conformable lenses or bands. Some have a biotite selvedge indicating either concentration of biotite at the margin of the pegmatite by deformation/segregation or localized partial melting. Although most pegmatite sheets appear intrusive in nature, some, particularly those in pelites to the south of Map 2, which have locally diffuse contacts and constitute a significant proportion of the rock, may be in-situ melts. This is elaborated upon in section 3.5.2.

2.1.5 Amphibolites and Amphibole-bearing rocks: Unit 3

2.1.5.1 Amphibolites: Unit 3a

The term amphibolite as used in this thesis includes those rocks containing 40% (or more) hornblende. There is no distinction made between those amphibolites which exhibit primary structures and those which do not.

Amphibolites generally comprise variable amounts of hornblende (or tremolite locally), plagioclase, quartz, epidote ± garnet ± biotite. Amphibolites are typically melanocratic but become lighter green where the proportion of epidote is significant. Epidote-rich bands, mm to cm thick, are locally common and impart a distinct banding to the rock. Aphanitic, olive-green epidote pods are common in some of the northern amphibolite units. Calcite, quartz and chlorite are present as mm thick veins. Chloritization is locally pervasive, especially in and near fault breccias. Pyrite is common as disseminations and veinlets within the amphibolites, pyrrhotite was noted only in a few places, and chalcopyrite is rare.

In the thesis area, the amphibolites are grouped into garnet-bearing (typically coarse grained) and garnet-absent (usually fine grained) types. The former is more common and is present as interbands in all lithologies S and SW of Cinnamon Lake. Virtually all of the amphibolites associated with unit 1d are of this type and the garnets, up to 2 cm in diameter, may comprise up to 40% of the rock. The

amphibolites in unit 1d, south of the mineralization, are 5 to 10 cm thick and comprise an estimated (from DDH data) 40% of the rock. Exposures (of 1d), however, contain 20-30% amphibolites. Local gradations in both the amount and size of garnets were commonly observed in individual amphibolite bands in drill core.

A streaky foliation, with mm thick, discontinuous, feldspar-rich folia and thicker mafic layers, characterizes the garnet-absent varieties. Their occurrence is apparently restricted to unit 2a, in the footwall to the mineralization and in the NE of claim block 1951. Amphibolites are 50 cm thick on average in unit 2a, adjacent to the Twin Ponds Showing, forming an estimated 10% (based on DDH data) of the unit. In the hanging-wall of the mineralized horizon, a garnet-absent amphibolite unit several m thick in the east and 60 m thick in the west, maintains the same structural level with respect to the mineralization, for a minimum strike length of 5 km. Unit 2b contains similar (to 2a) amphibolite proportions.

In the northern part of CB 2850, the amphibolites reach their maximum (mapped) thickness of 300 m. The amphibolites occur in virtually all lithologies except within units 1a, 1b and 1c in claim block 2850.

The origin of these rocks is uncertain but their mineralogy implies that they are roughly of basaltic composition. They have a similar deformational history to the surrounding rocks and were therefore emplaced/deposited

prior to deformation. At least some of the thin amphibolites which occur interbanded with the pelites and the banded quartzofeldspathic rocks, are thought to be mafic tuffs. Such an origin may apply particularly to those containing garnet, implying a greater Al content. The more localized garnet-absent varieties are possibly sills or transposed dykes.

A noteworthy amphibolite in the NW corner of claim block 2850 contains elongate "clast-like" features which define a lineation in the plane of flattening (Fig. 2-12).

Figure 2-12: An amphibolite in the northeast of claim block 2850, characterized by elongated "porphyroclasts", thought to be relic volcanic clasts.

Their dimensions are >10 cm (along the lineation) : 5-10 cm : 2-4 cm. The "clasts" are richer in modal quartz and poorer in calcite than the matrix, the latter containing accessory epidote and sphene. These rocks are interpreted

to be monolithologic vent-agglomerates or proximal fragmental mafic tuffs. The features defining the lineation are therefore, interpreted to be be porphyroclasts.

Further east within the same amphibolite unit is a poorly exposed green rock containing large olive-green xenoblastic aggregates of epidote (up to 1 cm) crystals set in a matrix of blue-green amphibole. The epidote is extremely turbid with numerous inclusions of amphibole and fine-grained material. The origin of this rock is unknown.

2.1.5.2 Gedrite-bearing rock: Unit 3b

This unit contains variable proportions of gedrite, plagioclase, quartz and magnetite. The orthoamphibole gedrite which characterizes the unit, is a lustrous brown mineral, forming crystals up to 10 cm long and comprising 10-60 % of the rock as compact fibrous masses. The rock is invariably magnetic and weathered to a rusty colour.

Gedrite-bearing rocks crop out mostly in CB 2329 where they are commonly associated with quartz muscovite schists. They also occur locally in claims blocks 1951 and 2327. As no geochemical analysis was done on this rock, major elements were estimated from the modal proportions of the principal minerals. The rock contains approximately 60 wt.% SiO2, 6-10 wt.% (both) MgO and FeO, 3 wt % Na2O and CaO each and 10 wt% Al2O3. This composition is unlike that of any typical igneous or sedimentary rock and is interpreted to be that of an altered rock. As the gedrite-bearing rocks are

distinctive units, the alteration is attributed to some pre-metamorphic process involving hydrothermal fluids leaching e.g. K2O and Al2O3.

2.1.5.3 Epidote-Pyrite-Hornblende-bearing rock: Unit 3c

Unit 3c comprises varying proportions of epidote, pyrite, hornblende, biotite and quartz. It is invariably characterized by 5-10% pyrite ± pyrrhotite. Lithologically, the unit is distinguished by a lumpy-weathered surface which characterizes it in Isle aux Morts River West, where it is best exposed, as bands 30 cm to 4 m thick. The features in raised relief are irregular to ellipsoidal polymineralic aggregates which are coarser than the matrix, ranging up to 10 cm in their long dimension (thus forming a lineation). However, the matrix and the aggregates are compositionally similar. These positively weathering knots are reminiscent of clasts within tuffs and the rock is interpreted to be a mafic tuff.

Many thin (on a decimeter scale), fine-grained hornblende-feldspar (garnet-absent) amphibolite bands are intercalated with this unit in Isle aux Morts River West. Further west, outcrops are small and sparse and the epidote/pyrite lithology apparently thins westwards where a garnet-biotite-hornblende lithology becomes important.

2.1.5.4 Amphibolitized Ultramafic Rock: Unit 3d

A comformable, 30 m thick/600 m long, amphibolite is exposed approximately 300 m NW of Nutmeg Lake and a similar amphibolite block composed of coarsely crystalline amphibole is exposed on the east edge of CB 2327. This rock is composed almost entirely of amphibole with minor plagioclase. These amphibolites are thought to represent ultramafic rocks emplaced early in the geological history, probably pre-D1.

2.2 Structure

The major structural grain of the lithologies within the property describes an arcuate NNE-WNW pattern (Map 1). Many of the macroscopic and mesoscopic structural features are described with reference to Map 2. Four deformation phases D1, D2, D3 and D4 shown schematically in Figure 2-13, have been defined along with their respective fold generations (F1, F2, F3 and F4). Foliations S1, S2 and S3 and lineations L1 and L2, are related to D1, D2 and D3.

2.2.1 Tectonic Fabrics

One principal planar foliation which is developed as a schistosity in the pelites and a banding in the quartzofeldspathic and amphibolitic units is found throughout the area. This foliation trends NNE in claim block 2329 and gradually swings through 90° to NNW in CB 2850 west; dips are generally steep towards the NW or SE. Variations in the modal mineralogy of the common phases define this foliation, which is also locally parallel to thin amphibolite, garnet-quartzite and sulphide-rich layers. Locally this planar fabric is diffuse and is folded around isoclinal folds (Figs. 2-8 and 2-14). This earlier planar fabric which is almost completely transposed, is the earliest recognized in the area and is thought to represent bedding. It is therefore designated S0. Thus S1, which is a regionally recognized planar fabric, is composite in most rocks, being defined by a mineral fabric parallel to S1 and

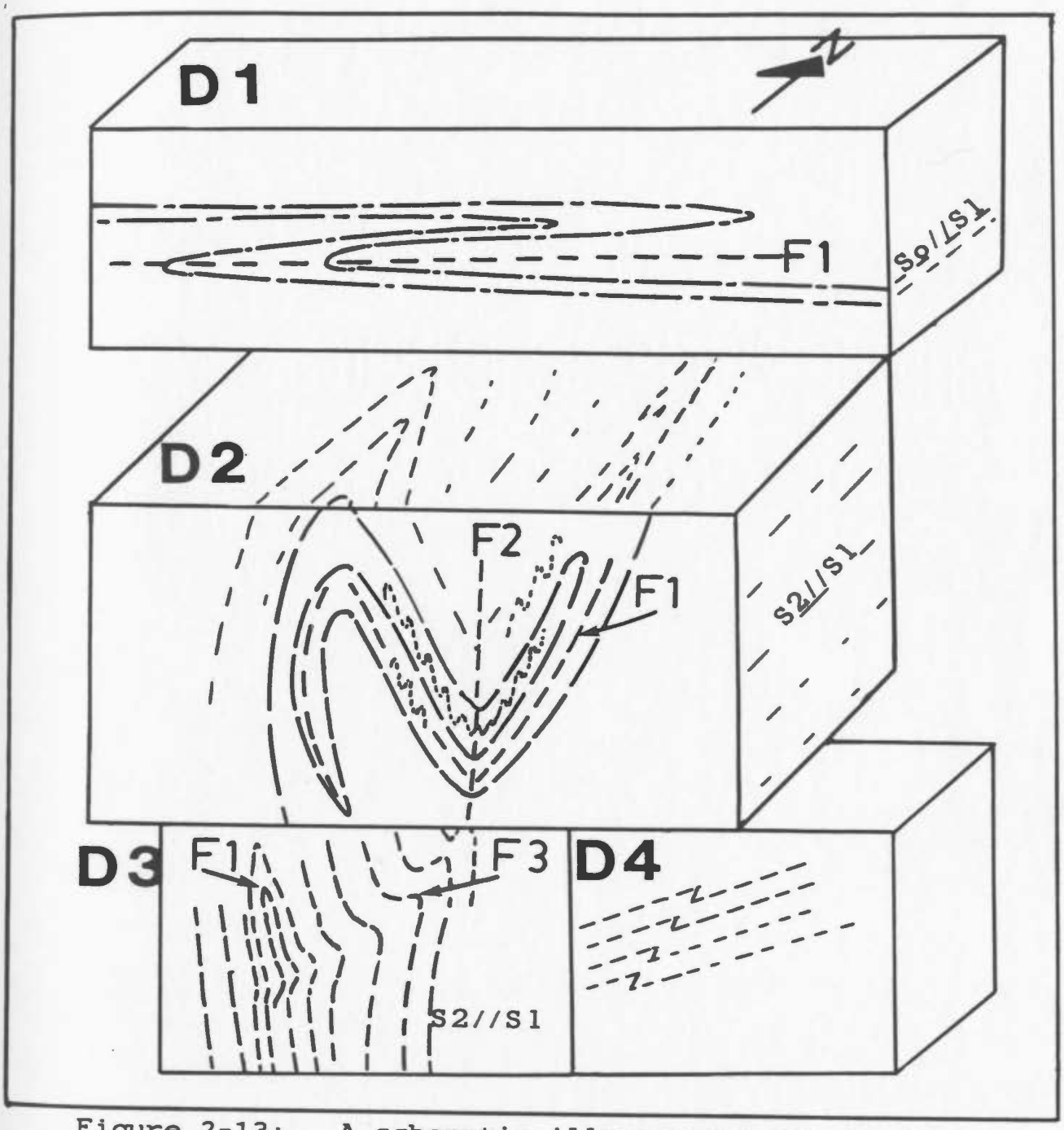

Figure 2-13: A schematic illustration of the four deformation phases recognized in the Isle aux Morts area.

Figure 2-14: The earliest defineable folds (F1) in the Isle aux Morts area; in quartzofeldspathic rocks.

by the parallel to subparallel SO, the original compositional banding/bedding.

Planar fabric elements S1 and S2, are typically parallel or sub-parallel, except in the hinge regions of open F2 folds, (Fig. 2-15A) where a mica foliation (S2) crosscuts the main fabric (SO//S1). The latter fabric strikes NNW and dips shallowly (30^{o}) NE. The vertical (mica) foliation in Figures 2-15A, B is S2 and strikes parallel to S1 (NNE-WNW). Transposition of SO//S1 mineralogic layering into S2 is depicted by Figure 2-15C which is sketched directly from a hand specimen. S2 is locally a domainal crenulation cleavage e.g. in Figure 2-1, in which is illustrated an open fold (F2), with an axial planar fabric S2 defined by 1 cm wide quartz-rich

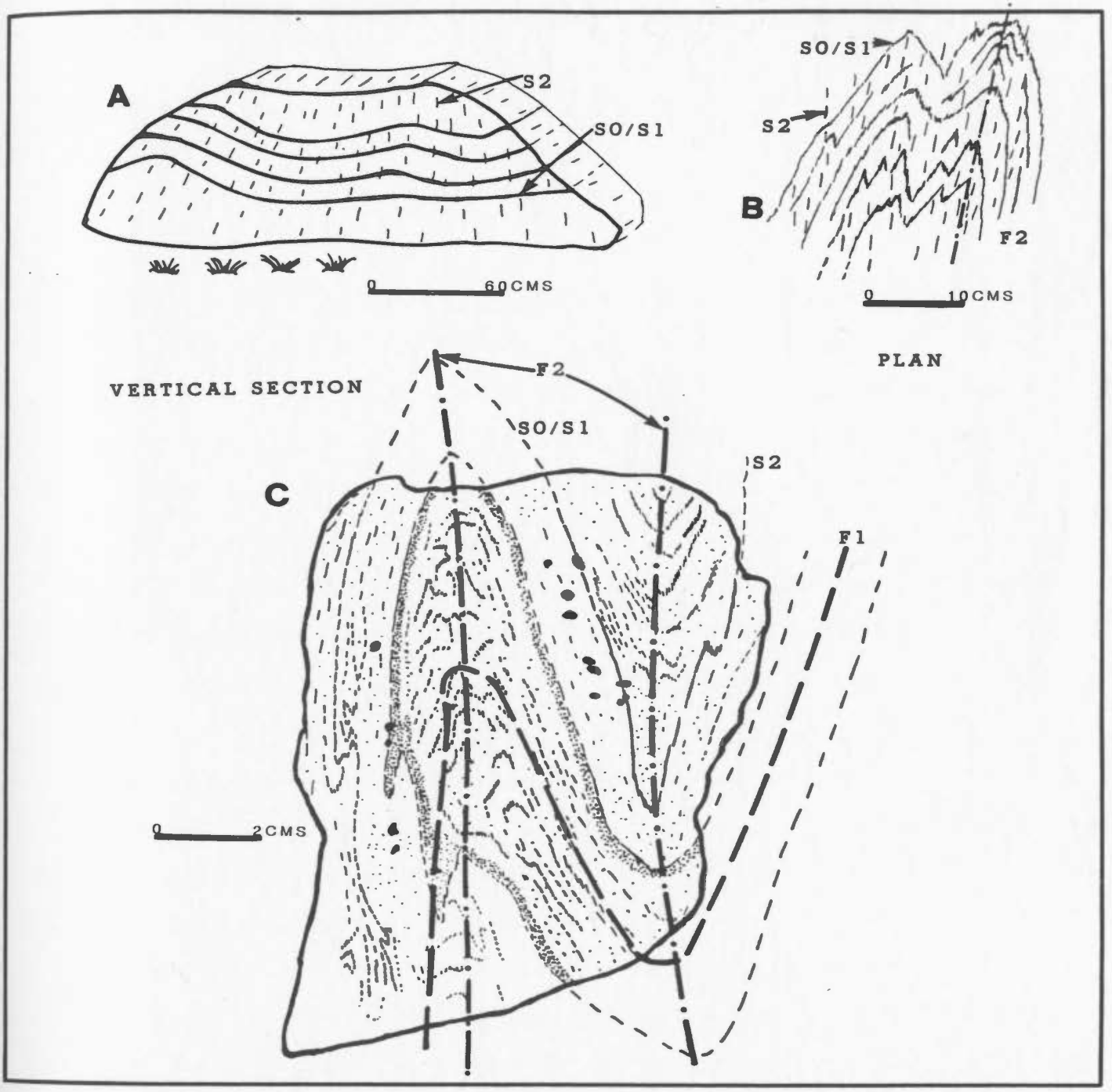

Figure 2-15: A; Open F2 fold in quartzofeldspathic rocks with axial planar S2 schistosity:

B; Tight F2 fold in quartzofeldspathic rocks with axial planar S2 schistosity:

C; Illustration of a refolded fold sketched from a hand specimen; only in the hinge areas can SO//S1 be properly distinguished from S2.

microlithons and thin mica septae cutting the compositionally banded S1. Where F2 folds are tighter, SO//S1 is approximately subparallel to S2.

Micas (and kyanite) locally display a bimodal attitude within the combined S2//S1 foliation (Fig. 2-16) in which the minerals preserve relict F2 fold hinges with dihedral (i.e. inter-limb) angles of 10-30°. These hinge zone micas appear to be strain free and are probably remnant SO//S1; sporadic occurences of short stubby mica (rarely kyanite) oblique to S1//S2 are also thought to be relict SO//S1. Pressure shadow regions of garnet porphyroblasts also locally contain S1//SO which in places is parallel to an internal fabric in the garnet (Fig. 3-7).

An outcrop of the Port aux Basques Granite, occurs NE of Chili Pond (informal name, Map 2). It contains a moderately developed penetrative fabric parallel to S2. The pegmatitic phase of this granite has a locally developed fracture cleavage, approximately axial planar to F2, as noted in the antiform to the south of Map 2, and therefore thought to be S2. The presence of the regional S2 fabric in both phases, implies emplacement prior to D2.

Although most of the lithologies are primarily S>L tectonites, a hornblende lineation locally dominates the fabric in the amphibolites. The linear fabric-forming elements commonly observed are minerals, quartz rodding (Fig. 2-17) quartz boudins, minor fold axes and crenulations (Fig. 2-1). Garnets are locally stretched and broken in

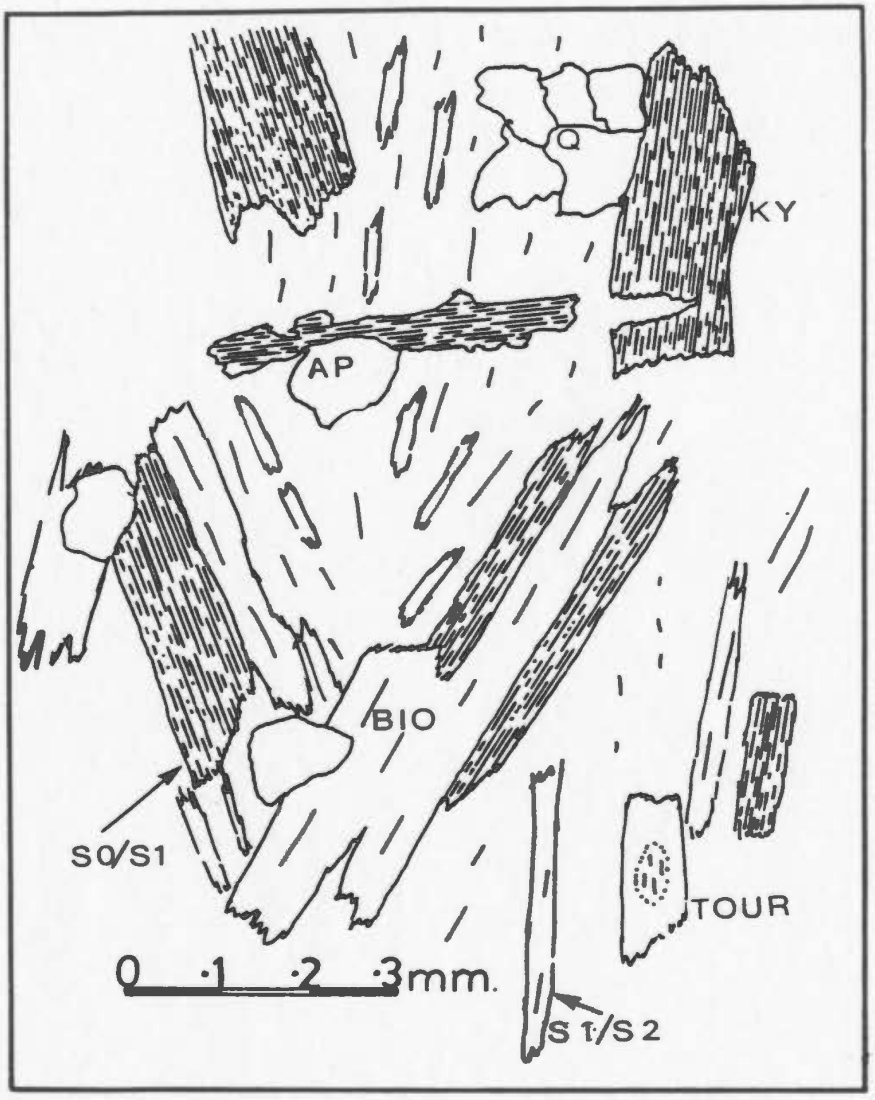

Figure 2-16: F2 fold hinges outlined by recrystallized biotites (BIO) and kyanite (KY); also present are apatite (AP) in S2; note core of tourmaline (TOUR) with oriented inclusions, parallel to S2.

the foliation and they define a minor lineation. Some garnets have an elongate pressure shadow with an aspect ratio of 5 or 6:1. Most of these linear fabrics are symmetrically disposed to the second generation folds (F2). Lineations related to D1 are not commonly observed; Figure 2-18 illustrates a mica lineation lying on the S1(SO) foliation plane, both lineation and foliation have been folded by D2; this lineation is assumed to be related to D1.

Figure 2-17: Quartz rods in a quartz feldspar lithology, unit 2b.

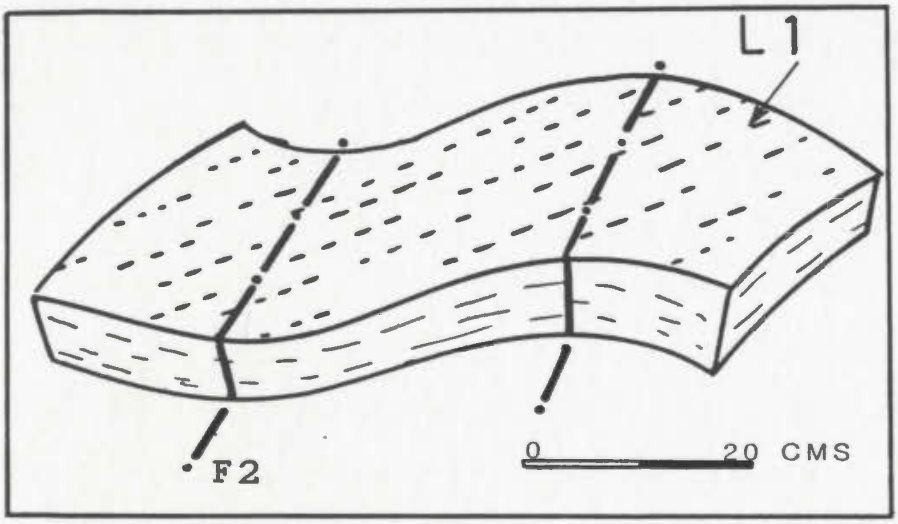

Figure 2-18: Lineation oblique to F2 and considered to be related to D2, in quartz-feldspar lithology

2.2.2 Folds

Two principal fold generations, F1 and F2, and two minor fold generations F3 and F4, related to D1, D2, D3 and D4 respectively, are recognized in the area. F1 folds are recognized on outcrop or hand specimen scale in semipelitic and quartzofeldspathic units. They are isoclinal folds with axial planes that vary from horizontal (Fig. 2-14) in the south of Map 2, to generally steep (Fig. 2-8) north of this area; the F1 fold axis plunges steeply NE in this latter illustration. This deformational phase is correlated with D1 of Chorlton (1984) in which recumbent folds and/or thrust nappes developed, ultimately leading to tectonic thickening of the crust and amphibolite facies metamorphism. Thrusting associated with this phase may explain the discordant southern contact of unit 1d south of Cinnamon Lake.

The F1 axial planes are folded about F2 folds (Figs. 2-15C, 2-19), which are the most commonly observed structures on all scales and in virtually every outcrop. They vary from tight (Figs. 2-20A and D) to open (Fig. 2-15A) and commonly have numerous asymmetric folds developed on their limbs. F2 fold morphology may vary dramatically within one outcrop (Fig. 2-21). These disharmonic folds reflect the competency contrasts between the adjacent layers and typically occur in areas of parallel folding (Hobbs et al., 1976). The F2 folds vary from upright to inclined, plunge predominantly NE at 10-40°, and have axial planes trending NNE-WNW, dipping steeply either SE or NW. The

Figure 2-19: Isoclinal F1 fold tightly folded about an F2; note mineralization approx 10 cm to the left, arrowed.

amphibolite facies rocks of the Bay du Nord Group to the east, contain similar phase 2 structures (Chorlton, 1984). The major antiform in the south of Map 2 is a doubly-plunging F2 with a curved axial trace; this pattern is also commonly observed on outcrop scale (Fig. 2-20C). Overprinting of F2 on F1 has produced the interference patterns illustrated in Figure 2-20B (type 3) and E (type 1-2) (Ramsay, 1967).

The poles to the S2 foliations (collated in CB 1951) define a girdle (Fig. 2-22A), the pole to which coincides with the point maximum for most linear elements (Fig. 2-22B). Hence, the major F2 fold axis (defined by the pole to the S2 girdle) is parallel to the various L2 linear features.

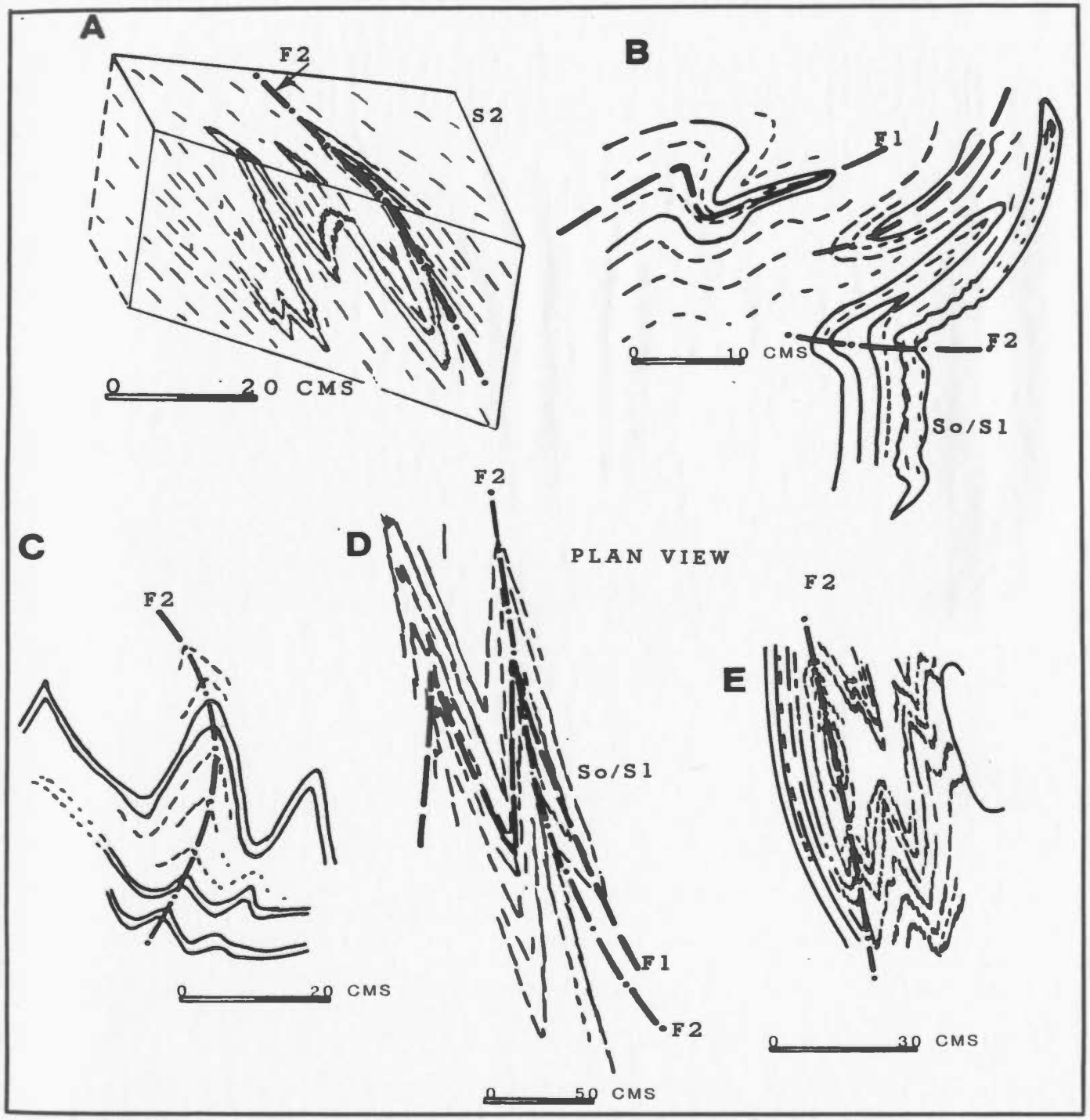

Figure 2-20: A: Tight, mesoscopic F2 folds in semipelites;
B: Variably oriented F2 fold axes with folded F1 in semipelites;
C: F2 fold axes are commonly arcuate, as in this example, in a quartzofeldspathic unit;
D: F1 fold tightly refolded by F2 in semipelite;
E: Shallowly doubly-plunging folds (F2), in semipelite.

Figure 2-21: Varying F2 fold morphology within an outcrop of a quartz-feldspar lithology; unit 2b.

A third phase of deformation (D3) is noted only on a small scale, as in Figure 2-8 where there is a faint crenulation cleavage axial planar to the small asymetric F3 fold in the center of the photograph. F4 folds are sporadically developed as chevron or kink folds, seen in thin section as strained micas bent around tight fold hinges. D4 is therefore a late brittle phase of deformation. No neo-crystallized mineral growth was noted in either D3 or D4 structures. Some F4 crenulations in thin sections seem to nucleate on larger garnet porphyroblasts.

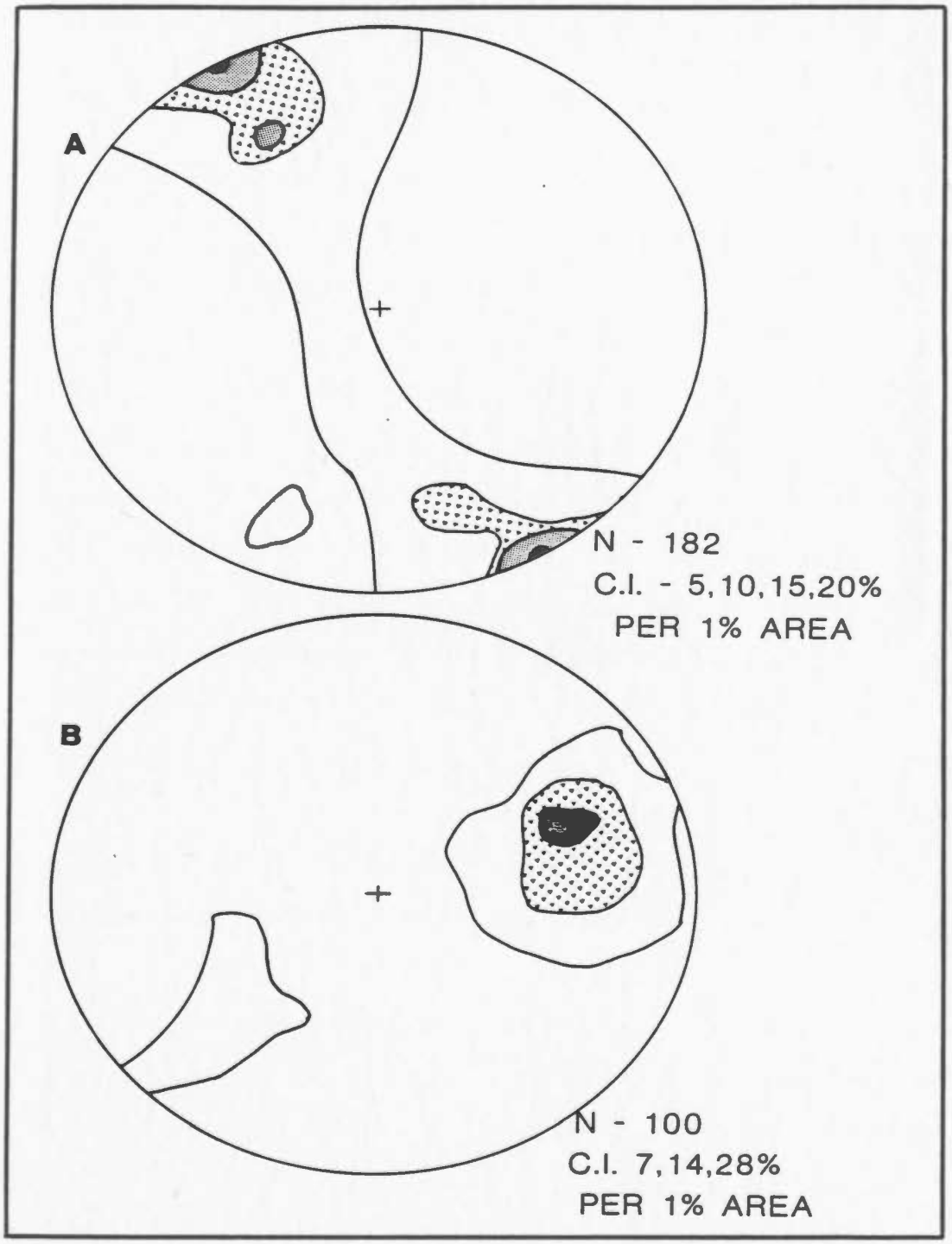

Figure 2-22: A:Stereoplot of poles to the S2 foliations which define a girdle. B:Stereoplot of linear elements i.e. minor fold axes and quartz rods. Note that the pole to the girdle in A coincides with the point maximum for most linear elements in B.

2.2.3 Evidence for Flattening and Shearing

Quartz veins (Figs. 2-2, 2-3 and 2-23), either formed locally as sweats or were injected at some period early in the deformational history syn-D1 or pre-D2. They behaved relatively competently during deformation and display a spectrum of structural features. Locally (Figs. 2-23A and B), the veins are continuous and the parasitic folds are slightly oblique to S2 which apparently refracts through their axial regions. In other cases continuity is lost between the quartz "beads" (Fig. 2-23D) but the small cusps at the tails of the beads suggest that they were originally similar to those in Figure 2-23A. The apparent displacement of the individual beads may indicate either flattening normal to S2 or a shear component along S2. Thus it appears that the hinges are destroyed and the limbs are preserved in, and isolated by S2. In the illustration in Figure 2-23C the competent quartz vein has formed boudinage structures but the matrix has developed tight folds. This apparently indicates extension followed by the development of S2 between the quartz boudins. Features which imply a rotational component in D2 have either sinistral Fig. 2-23E) or dextral (Fig. 2-3) sense of motion. Figure 2-23E shows a quartz pod, the long axis of which is 15^{o} oblique to S2, with S1 remnants in the pressure shadow which has also rotated; however the latter example may also be explained by flattening normal to S2.

Shear phenomena are probably responsible for certain

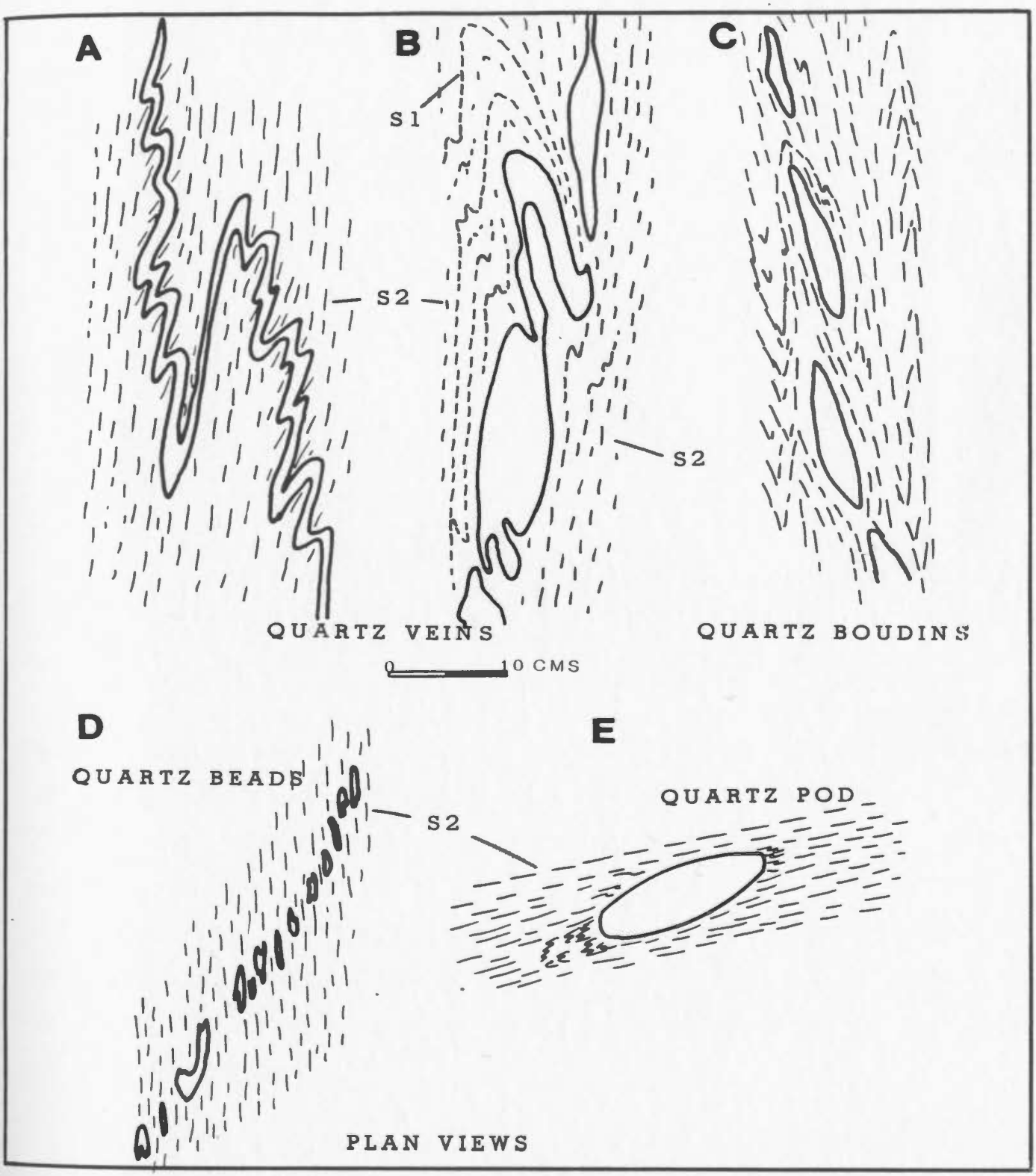

Figure 2-23: Varying modes of behaviour of quartz veins in pelitic rocks; see text for discussion

features that mimic sedimentary structures in quartzofeldspathic rocks; for example in Figure 2-24 there are two sets of foliation surfaces.

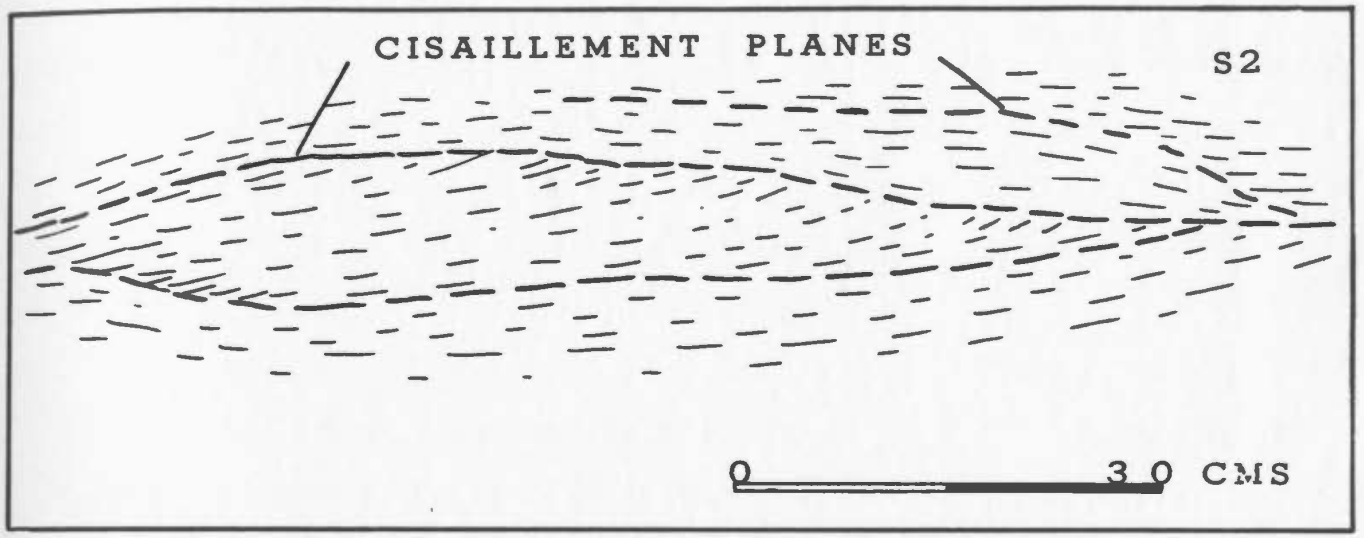

Figure 2-24: C (cisaillement) and S (schistosity) planes in a quartzofeldspathic rock mimicking sedimentary structures.

One fabric is defined by the parallel allignment of minerals and a second fabric consists of sub-parallel surfaces which alternately merge with and crosscut the first set. These appear similar to the S and C surfaces respectively, described by Berthe et. al. (1979), who relate them to the development of mylonite zones. C surfaces are planes of shearing while S is the schistosity plane and typically has a sigmoidal shape.

2.2.4 Faults

Two major fault sets occur in the map area, one trending NE-SW and the other NNE-SSW. Boat Pond Fault (NE-SW set) is the major displacement in the area, traceable for over 13 km and linking with a fault mapped by Brown (1975). This fault continues SW to Grand Bay and northeast towards the Cape Ray Fault, to which it is possibly related as a splay fault. The NNE-SSW fault set is inferred to explain apparent offsets of lithologies. The majority have dextral displacement and lie at a high angle to the regional structural grain. The Isle aux Morts Brook Granite is not offset by any of these faults and must postdate them.

The contact between units 1d and 2a at the northern end of Nutmeg Lake is thought to be a fault for at least part of its length. This may be an oversteepened thrust as it is parallel to lithological boundaries. A fault gouge marks this contact in DDH IAM-82-3 and much of the surface trace is a scarp.

2.3 Summary and Discussion

Complete recrystallization and intense deformation have eliminated most primary features of the protoliths to these metamorphic rocks. Also transposition and microshearing have produced features which may mimic sedimentary structures making an accurate interpretation of the protolith difficult. However, amphibolites and amphibole-bearing rocks locally contain features which are considered

to be primary and suggest a tuffaceous origin for some of them. On this basis, the sequence in CB 2850 can be reduced to mafic volcanoclastic or extrusive rocks (in the north only) with felsic tuffs in the centre, the mineralized horizon then occurs in the eastern half of the claim block and intermixed shales/greywackes to the south. Eastwards the succession is more complex and some quartzofeldspathic units occur interbanded with pelitic units 1a and 1b north of the showing. Mineralization noted in IAM-82-4 may also be the Twin Ponds Showing repeated by faulting or thrusting, as the sequence of rocks is locally the same as that adjacent to the showing. However the sequence is generally similar to that in the west.

The two principal deformational phases to which the rocks were subjected are D1, which resulted in isoclinal folding of a mineralogical layering SO, and D2, defined by tight to open folds (F2) and the regional S2 fabric. The effects of D1 are poorly preserved while F2 folds are present in most outcrops and on all scales. Several interference patterns were produced by D2 overprinting D1, viz., type 3 (Fig.2.19) and type 1-2 (Ramsay, 1967) (elongate antiform) on Map 2. D1 effectively transposed SO to produce S1, the principal foliation in the area. The combined SO//S1 surface was also partly transposed by S2 during D2 deformation. D3 and D4 are minor phases of deformation, locally developed as a faint crenulation cleavage axial planar to asymetric folds (D3), and

chevron/kink folds and faults (D4). F1 fold axes and axial plane attitudes are variable due to the complex history of deformation; F2 fold axes plunge shallowly NE, parallel to most linear elements to which they are probably genetically related. The major fault in the area, Boat Pond Fault, has a gentle arcuate trend following the regional grain developed during D2 and the initiation of this fault is tentatively thought to be pre- or syn-D2.

A single exposure of Port aux Basques Granite contains a fabric parallel to the regional foliation (S2) implying that the granite was emplaced pre-D2. However, the pegmatitic phase of the granite does not contain a fabric in all exposures, suggesting that the emplacement history may extend post D2. Brown (1975), who mapped the granite as conformable sheets between Fox Roost and Port aux Basques, noted two fabrics present which he indicated to be S1 and S2. Thus the granite was emplaced pre-D2 according to Brown.

Deformation histories outlined by Brown (1975) and Chorlton (1984) for their respective areas of SW Newfoundland, are similar to those of the present study and are listed in Table 2-1. The history outlined by Chorlton (1984) is directly comparable: D1 of this thesis correlates with her initial phase of recumbent, isoclinal folds and/or thrust nappes. D2 of this thesis can also be correlated with Chorlton's phase, D2, of upright folds and shear zone development, mostly on the basis of style and orientation of

	Brown (1975)		Chorlton (1984)		This Study
D1	Poorly preserved--inferred from the composite nature of S2.				
D2	Flat lying isoclinal folds overturned to NW; axial planes trend NE and are parallel to "gneissic" banding. D2 preceeded by intrusion of Port aux Basques Granite.	D1	Recumbent isoclinal folds associated with fold/thrust nappes, ultimately led to tectonic burial and amphibolite-grade metamorphism.	D1	Mesoscopic isoclinal folds, variable attitude, which fold pre-existing fabric (S0).
D3	Upright, subisoclinal folds with NE-striking axial planes, overturned to SE.	D2	Responsible for regional foliation of La Poile River Group; moderate to tight folds, numerous NE shear zones.	D2	Upright to inclined, tight to open folds with axial planar regional foliation.
D4	Open monoclinal folds with poor fabric, striking NE.	D3	Inhomogenous crenulation cleavage axial planar to small scale asymmetric folds.	D3	Faint Crenulation Cleavage axial planar to small folds.
		D4	Chevron and kink folds and faults.	D4	Chevron/Kink Folds and Faults.

Table 2-1: Comparison of the deformational histories of Brown (1975) and Chorlton (1984), with that of the present study

folds. Locally, in the study area, there is evidence for shear apparently associated with the regional, S2 fabric.

Wilton (1983, 1984) defined three deformational events affecting the rocks within the Cape Ray Fault zone, to the NW of the study area, but considered that all three post-dated the structural history of the Port aux Basques Complex. The basis of this interpretation is the presence of folded, boudinaged amphibolite bands "close to the fault zone". However in the Isle aux Morts area, folded boudinaged amphibolites occur and are quite compatible with the deformational history above. Thus there may be an overlap of deformational histories between the Windsor Point Group and the Port aux Basques Complex; this is most likely to involve D1 of the fault zone and D2 of the Port aux Basques Complex as they are regionally parallel. An earlier deformation episode (D1) was postulated by Brown (1975) from the composite nature of the D2 foliation in his area but no evidence for this phase was observed in the Isle aux Morts Prospect area.

Chapter 3

PETROGRAPHY AND METAMORPHISM OF THE ISLE AUX MORTS PROSPECT

3.1 Petrography of Pelites, Quartzofeldspathic rocks and Amphibolites of the Isle aux Morts Prospect

3.1.1 Introduction

Results of petrographic and microfabric analyses of 156 thin sections, representative of the pelitic, quartzofeldspathic and amphibole-bearing units (Map 2), are summarized below. The mineral assemblages observed in the area are listed in Table 3-1. The maximum phase assemblage staurolite-kyanite-garnet-biotite in addition to quartz and feldspar, is present in the pelites of unit 1d south of the mineralized horizon on Map 2, whereas the high variance assemblages (i.e. muscovite ± biotite ± garnet, quartz and feldspar) occur in the quartzofeldspathic rocks. Coexisting kyanite-garnet-biotite are used to define an isograd within the area of Map 2; this assemblage is compatible with the breakdown of staurolite in the presence of muscovite and quartz. The assemblage sillimanite-kyanite-biotite in the northeast allows a sillimanite isograd to be defined. The area lies within bathozone 5 of Carmichael (1978) on the basis of the stable mineral assemblages present.

Table 3-1: Mineral assemblages in the Isle Aux Morts Prospect area.

PELITES:

Bio	Musc	Gar	Ky	Sta	K-Fs	Sill	#
X		X	X	X			4
X	X	X	X				7
X		X	X				1
X		X		X			2
X	X		X	X			1
X	X		X				1
X			X				3
X	X	X					10
X		X					2
X	X				X		4
X			X			X	1

All assemblages contain quartz and plagioclase.

AMPHIBOLITES:

Hornblende	Gedrite	Biotite	Garnet	Epidote	
X		X		X	10
	X	X	X		3
	X	X			2
X		X	X	X	1
X			X		1

Some assemblages contain quartz; all contain plagioclase.

Morphologic textural terms e.g. granoblastic and xenoblastic, are used as defined in Spry (1969). The nine-fold classification of porphyroblasts as developed by Zwart (1962) (Fig. 3-1) is used as a convenient reference framework.

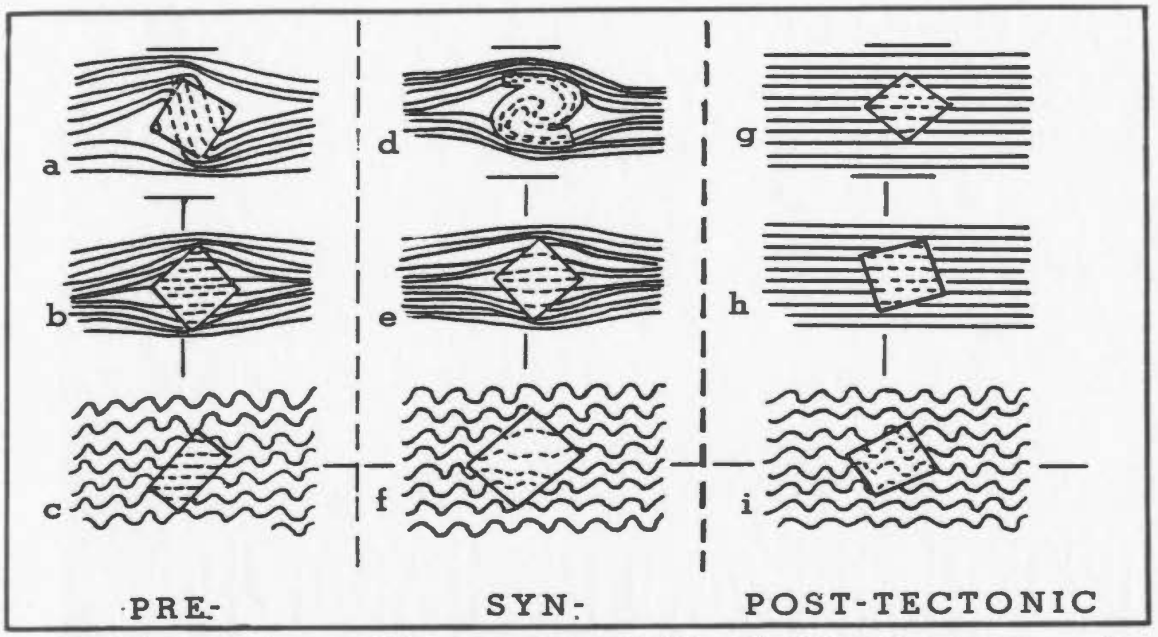

Figure 3-1: Microstructural classification of porphyroblasts (after Zwart, 1962); timing of growth of various minerals in the study area is based partly on these textures.

3.1.2 Pelites, Semipelites and Quartzofeldspathic rocks: units 1 and 2.

Rocks in these units are typically composed of quartz, feldspar and variable proportions of biotite, muscovite, aluminosilicate minerals, garnets, staurolite and accessory phases. Xenoblastic quartz and feldspar range from 0.05-2 mm and have a poor to moderately developed preferred dimensional orientation parallel to the foliation. Locally these inequant grains are also crystallographically oriented parallel to the fabric. Quartz/feldspar grain boundaries range from straight or curved to dentate and (rarely) sutured forms. Although granoblastic polygonal aggregates of quartz and feldspar, indicative of annealing, are locally found in several thin sections, post-tectonic annealing and

recrystallization is generally incomplete and may take the form of a mortar texture i.e. larger grains approximately 1.5 mm long, surrounded by polygonized aggregates of quartz and feldspar. Plagioclase twin lamellae in this situation are commonly diffuse and bent, while larger quartz grains may show subgrain development. A distinctive blue tinge was noted in some quartz, especially near the grain edges. Small rounded quartz inclusions are common in feldspar porphyroblasts; quartz and feldspar in myrmekitic and graphic intergrowths occur in the quartzofeldspathic rocks.

K-feldspar and plagioclase are approximately equally abundant in the quartzofeldspathic rocks while in pelites K-feldspar is rarely present and plagioclase is ubiquitous; however in quartzofeldspathic samples Fs.11, Fs.12a, 82/5/351, 82/3/226 and 83/3/408, modal microcline constitutes 15-30% and plagioclase is less than 5%. Generally, microcline in the quartzofeldspathic rocks is present in small amounts and is always clear, in contrast to the typically (sericite-) clouded orthoclase. String and ribbon perthite are present in some K-feldspar. Plagioclase composition is oligoclase-andesine (range An_{7} to An_{42}).

Retrograde alteration of the common minerals is sporadically developed and is usually indicated by sericite and/or chlorite forming haloes around kyanite and staurolite and filling randomly oriented cracks in garnet. In the pelitic units of the central part of claim block 2850 kyanite and staurolite may locally be almost completely

pseudomorphed by chlorite/sericite. Biotite is occasionally altered wholly, or in part, to chlorite.

Several samples, eg. Fs. 13 and Qtm. 1, all from within several hundred metres of the Isle aux Morts Brook Granite, display a pervasive sericitization which obscures the fabric. The white mica forms spectacular plumose masses (Fig. 3-2) of acicular, radiating aggregates replacing muscovite, minor biotite and the quartz/feldspar matrix.

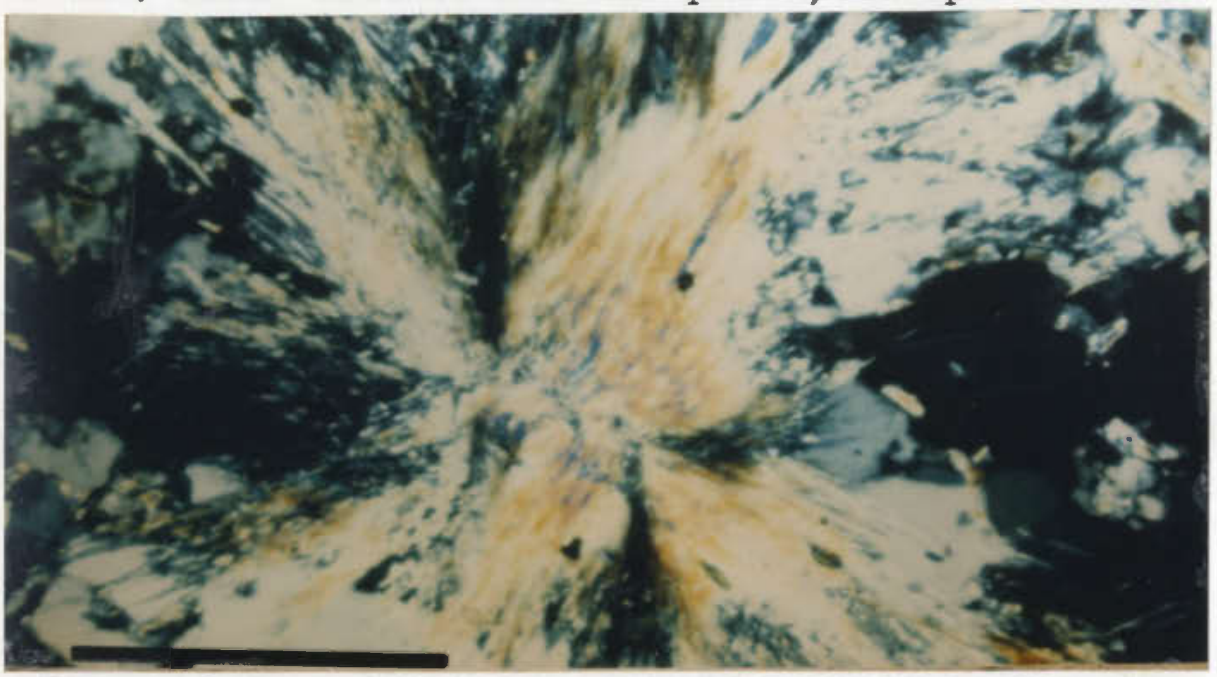

Figure 3-2: Plumose growth of muscovite/sericite noted locally, close to the margin of the Isle aux Morts Brook Granite; scale bar is 1mm.

This post-tectonic growth most likely reflects thermal metamorphism effected by the intrusion of the Isle aux Morts Brook Granite. Further north within the Port aux Basques Gneiss Complex (Wilton, 1984), andalusite has also been found in the contact aureole of this granite. Biotite and muscovite are common to all rock types except unit 1a where

biotite is typically lacking and unit 2a where muscovite is absent. Pleochroism in biotite varies from red to dark brown. Biotite and muscovite laths are up to 3 mm long and typically form equilibrium intergrowths. In places, brown, faintly pleochroic, xenoblastic biotite porphyroblasts with ilmenite lamellae or blebs, are randomly oriented on the fabric.

Garnets are a major phase in unit 1d but are absent from the quartzofeldspathic rocks and occur rarely in units 1a, 1b and 1c. A bimodal distribution of garnet grain size was observed, viz. 0.05-0.2 mm and 0.5-2cm. The smaller garnets are almost always clear and idioblastic, occurring dispersed in both the mica septae and the quartz-feldspar microlithons. Locally, myriads of tiny garnets lie in lensoid clusters and trails parallel to the local foliation, and virtually replace the mica septae. Micas invariably abut these smaller garnets, which commonly form unilateral rational grain boundaries against (001) mica. A thin muscovite corona is sometimes irregularly developed in biotite, in contact with the garnets. This rim may have developed as the garnet grew using FeO and MgO from the adjacent biotite. The larger garnets locally display inclusion zoning i.e. they possess a sieve-textured core with a relatively clear margin. Although matrix-size inclusions of quartz do occur, the tendency is towards smaller grain sizes.

Bladed kyanite is rare in the quartzofeldspathic rocks

and quartz-muscovite schists, but is relatively common in biotite-quartz and biotite-garnet schists. The blades are variably oriented with respect to the main foliation. Micas and kyanite form equilibrium intergrowths (with sharp intergrain boundaries) and smaller garnet inclusions in kyanite also appear stable. Staurolite occurs as poikiloblasts (up to 1 cm) and smaller xenoblastic grains in pelitic unit 1d in the south of Map 2 and comprises less than 5 modal % of this lithology. However, in the southern part of Map 2 it forms a clear equilibrium association with biotite and garnet and is intergrown intimately with kyanite (Fig. 3-3). In the northern part of Map 2 the original staurolite habit is obscured by extensive alteration which precludes definition of the textural relationships with other minerals. Numerous inclusions of quartz in staurolite give it a sieve texture and small idiomorphic garnets are commonly present. Thin section # 83/2/349 contains the stable assemblage kyanite-garnet-biotite, and one garnet crystal encloses a rounded staurolite inclusion.

Fibrolitic sillimanite occurs in quartzofeldspathic rocks in the north east of Map 2 (and also in claim block 2329), coexisting with kyanite, biotite and plagioclase. The sillimanite forms compact, commonly contorted, fibrous masses elongated parallel to the local fabric; this contorted habit is probably growth-related as there is no evidence for deformation in the adjacent biotite, on which it may have nucleated. The sillimanite appears in textural

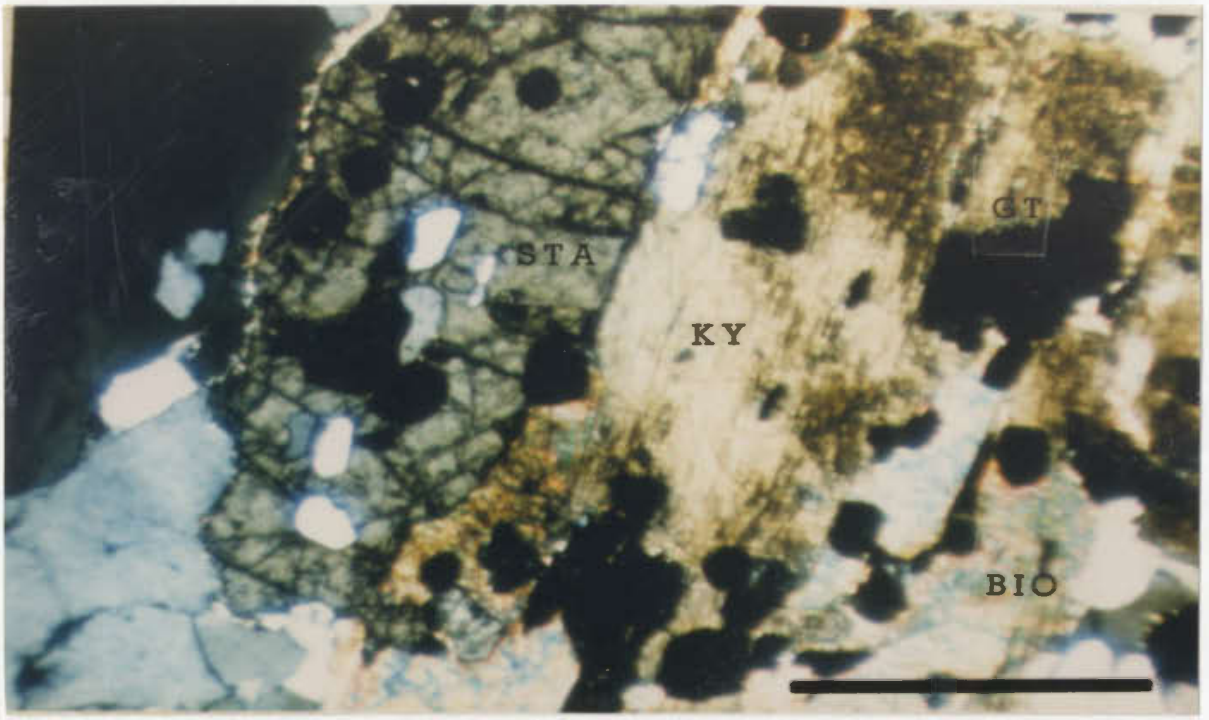

Figure 3-3: Photomicrograph of the low variance assemblage sta-ky-gt-bio which occurs in the south of Map 2; scale bar is 1 mm.

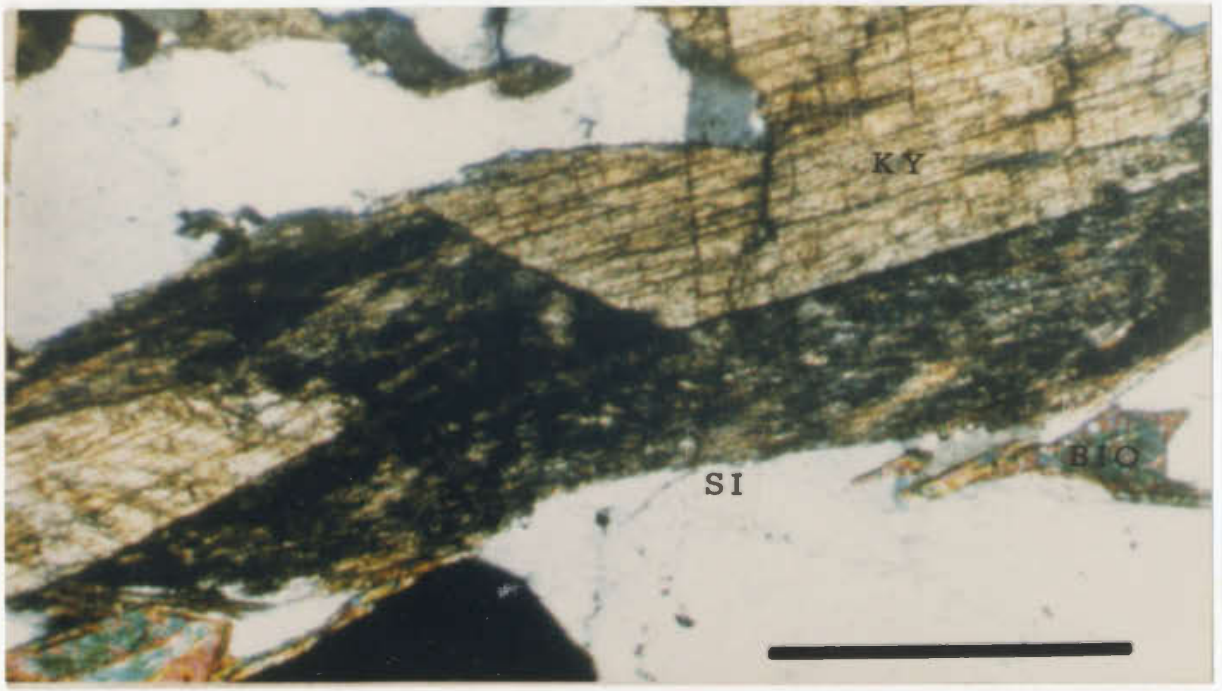

Figure 3-4: Elongate mass of fibrolitic sillimanite in contact with kyanite and biotite; scale bar is 1mm.

equilibrium with both the kyanite and biotite with which it is in contact. No pro-grade muscovite is present, although retrograde muscovite, intimately associated with the sillimanite is abundant. The absence of K-feldspar was confirmed by staining.

Both pelitic and quartzofeldspathic units contain a similar range of accessory minerals viz., epidote, sphene, zircon, apatite, calcite and opaques. These minerals occur as small idiomorphic to rounded grains and as inclusions in the major phases. Tourmaline (var. schorl) however, is only present in unit 1d where it outcrops to the north and the south of the mineralized horizon. It is frequently zoned from a blue-green core with rare oriented inclusions (Fig. 2-16) to an olive-green rim. The zinc spinel gahnite is present in unit 1b in the west end of claim block 2850, associated with staurolite, biotite, chalcopyrite and pyrite. The common opaques in units 1a and 1b, are pyrite, rutile and/or ilmenite and chalcopyrite. Magnetite is an accessory mineral noted in unit 2b in claim block 2850.

Garnet quartzites, contain up to 90% garnet as intergrown, idiomorphic to subidiomorphic crystals (Fig. 3-5) less than 250 microns across, with interstitial quartz, minor sphene and rutile. Up to 25% plagioclase (composition An30, from electron microprobe analyses) may be present in some of the garnet-poor layers. The layers are typically internally homogenous with no obvious planar fabric.

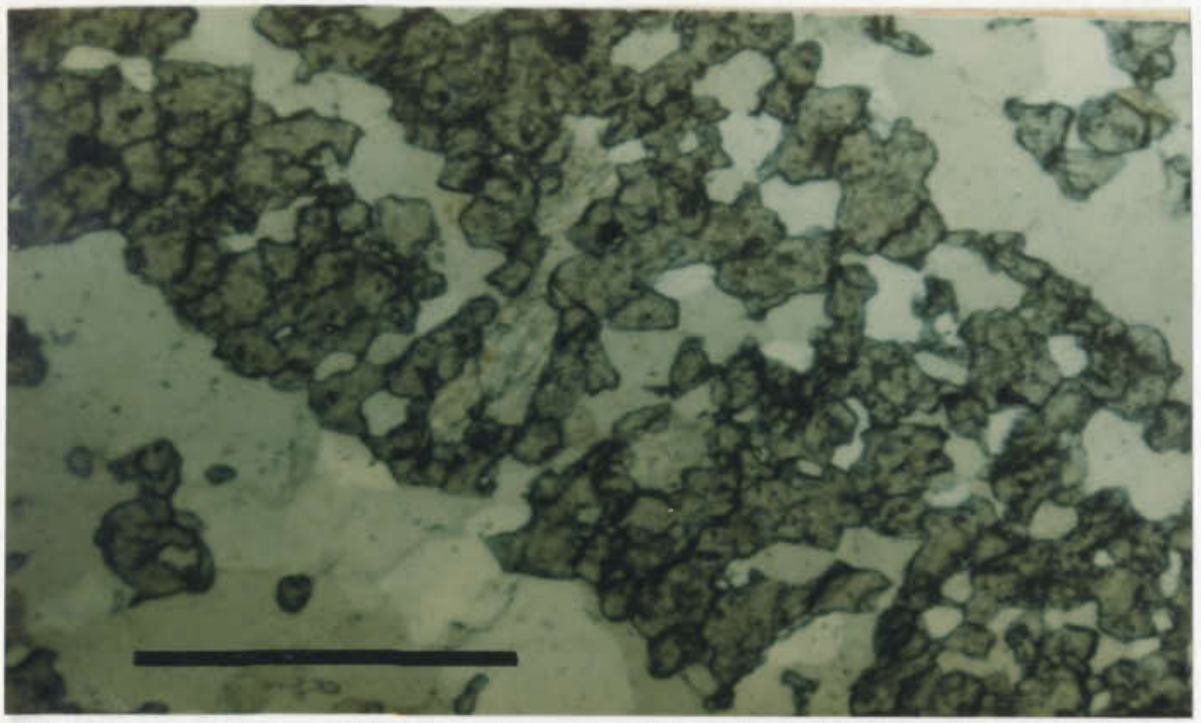

Figure 3-5: Photomicrograph of intergrown garnets in a coticule layer in semipelites; quartz and minor biotite are also present. Scale bar is 1mm.

3.1.3 Microfabrics

Kyanite, staurolite and garnet show a variety of relationships between the fabric within a porphyroblast (Si) and the external matrix fabric (Se). These minerals typically form augen in S2 (Figs. 3-6 and 3-7).

Many kyanite and staurolite porphyroblasts have well preserved internal fabrics (Si) which are continuous with those outside the porphyroblast (Se), although the Si are locally curved at the margin.

Garnets show a great diversity of internal features and of Si/Se relationships. Figures 3-6C to H illustrate garnets with oriented inclusions. A notable difference between the garnets in pelitic rocks and those of

Figure 3-6: Sketches from thin sections.
A: Twinned kyanite in a hard orientation forming an augen in S2; quartz inclusions are probably crystallographically controlled.

B: Two kyanite grains in optical continuity (probably originally one grain) separated by S2 biotites; note small recrystallized kyanite parallel to S2.

D,E: Pre-tectonic (with respect to the enveloping S surface) garnets which form augen in S2; note relict fabric in quartz pressure shadow in E which parallels the Si.

F,G: Syntectonic garnets with Si and Se continuous.

C,H: These two garnets display ambiguous internal fabrics. In C the Si may be syntectonic with either D1 (in which case the Si would be SO/S1) or D2 (and Si would be S1/S2. In H the argument is the same, but note that the core has no oriented inclusions.

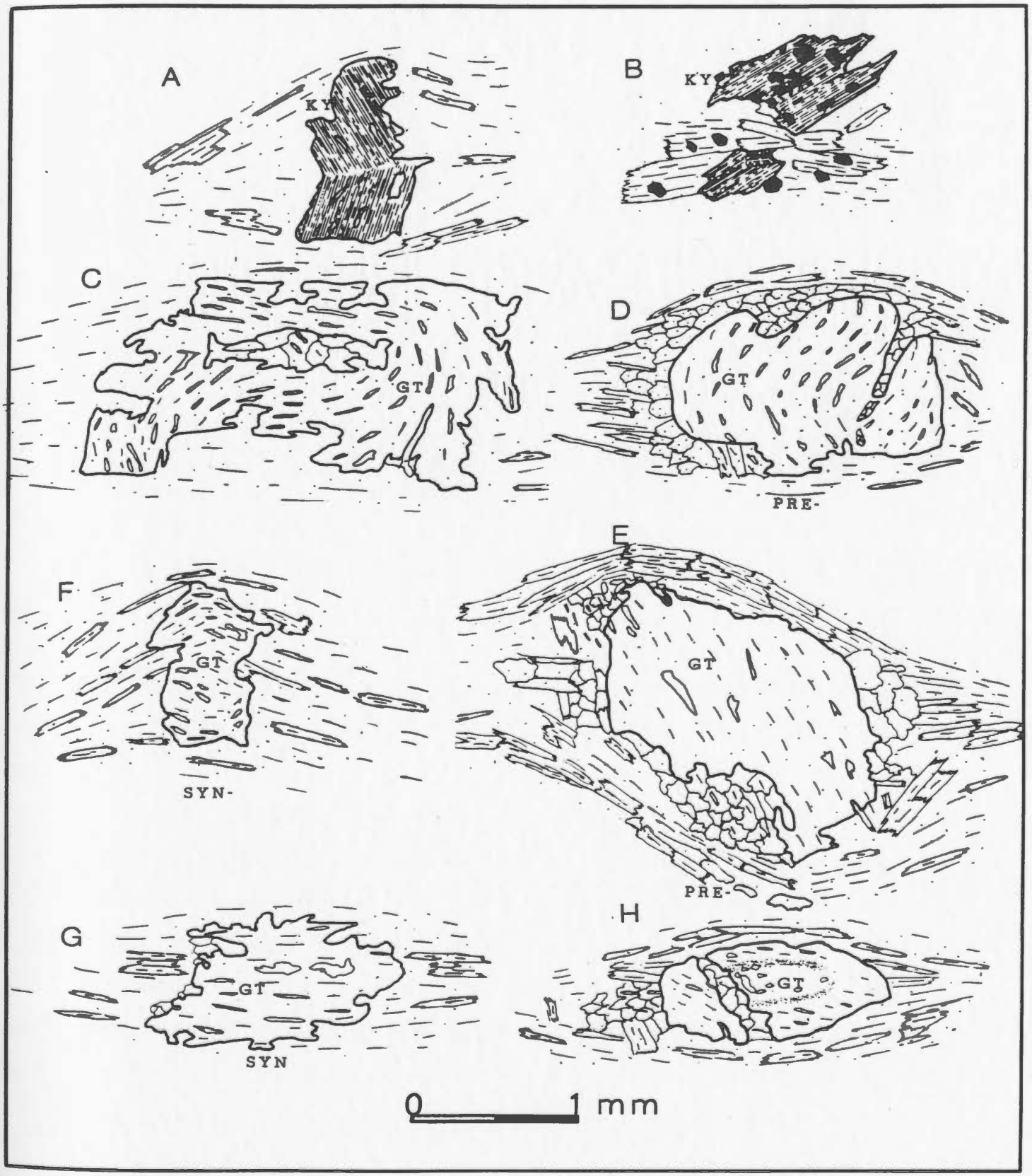
A
KY
B
KY
C
GT
D
GT
PRE-
E
GT
PRE-
F
GT
SYN-
G
GT
SYN
H
GT
0
1 mm

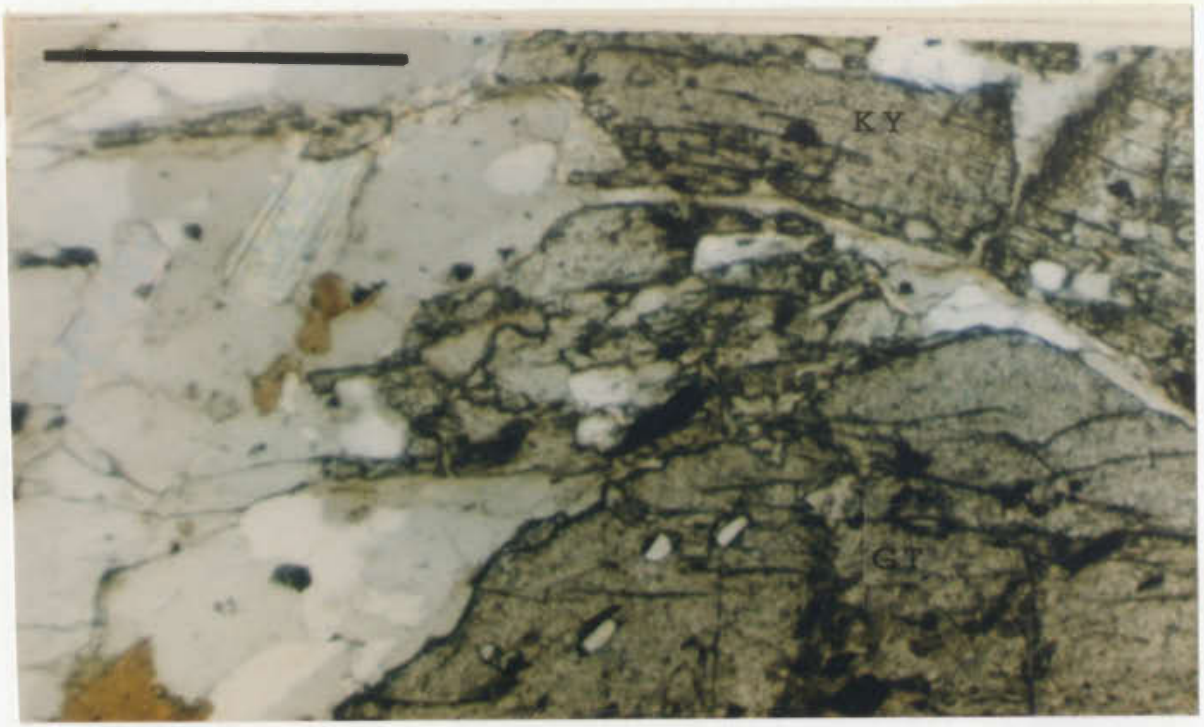

Figure 3-7: Photomicrograph of a garnet, around which a kyanite is bent and which contains an Si parallel to a fabric in the pressure shadow region; this fabric is oblique to the matrix S and is therefore an earlier fabric; scale bar is 1 mm.

amphibolites, is the tendency for Si to be mostly straight in the former while Si in the latter may be spectacularly curved. The trails are best developed in the larger, typically xenoblastic, garnets. Commonly, Si is oblique to Se in pelites and amphibolites, although even within one thin section the angle may vary, resulting in apparently inconsistent timing relations between Si and Se. This may reflect either a real difference in age between the garnets or the operation of a simple shear deformation after porphyroblast growth (Vernon, 1977). However, in Figure 3-7, a garnet contain a fabric which is parallel to Se, the latter (defined by kyanite and biotite) preserved in the

pressure shadow of the garnet and also in the microlithons. This relationship implies that the porphyroblast is pre-tectonic (c.f. Fig. 3-1, a, b and c), (Figs. 3-6D and E). In these the Si is parallel to a relict fabric locally preserved in the matrix, which is considered to be So//S1.

Figures 3-6F and G illustrate syntectonic features in garnets; e.g. the tightly curved fabric in Figure 3-6C has no equivalent in the matrix and the most plausible explanation is that it formed post D1 and rotated synchronously, as it grew, during D2. The clear continuity of Si/Se in Figures 3-6F and G is typical of syn-tectonic growth (c.f. Fig. 3-1 d, e and f). Figures 3-6C and H depict equivocal Si/Se relations where the garnet may have formed synchronously with the early development of S2 or suffered flattening oblique to the foliation, or it may have formed post-tectonically with respect to S1 (which now would be Si). These relationships are discussed later in the "Metamorphic History" section.

3.1.4 Petrography of Amphibolites and Amphibole-bearing rocks: Unit 3

The mineral assemblages common to these lithologies are listed in Table 3-1. Quartz and feldspar display the same petrographic textures noted above in section 3.1.3 for pelites and quartzofeldspathic rocks.

The common amphibole is hornblende. It shows a marked pleochroism from straw/pale green/pale yellow to deep

green/blue-green or olive green. Colour zoning from a blue-green rim to an olive-green core is common. Hornblende crystals vary from idiomorphic to sub-idiomorphic and range up to 3 mm in length. In several samples, larger hornblende crystals lie across the main fabric, suggesting post-D2 growth. Other large hornblende crystals lie on the main fabric and may be mimetic. These larger laths are typically poikiloblastic, with inclusions of quartz ± biotite ± epidote ± opaques, which may be aligned to form an Si.

Biotite and hornblende form equilibrium intergrowths which are locally vermicular. Hornblende within the garnet-(± biotite) bearing amphibolites commonly contains zircon inclusions. Hornblende typically comprises 40-80% of amphibolites and those with higher contents lack garnet and biotite.

In amphibolites retrograde tremolite laths locally overgrow the fabric and a greenschist facies assemblage of chlorite-actinolite-epidote-sphene-calcite is present in an amphibolite adjacent to Boat Pond Fault.

Sample Bi.6b is noteworthy as there are thin coticules present. Accessory sphene is equally abundant in both the amphibole-rich layers and in the coticules; it occurs in the latter as thin seams (100 microns or less) parallel to the foliation. Although there is a mineralogical gradation through increasing quartz and decreasing hornblende towards the coticule, the actual contact is sharp.

Sphene and epidote are the usual accessories with

pyrite ± pyrrhotite ± rutile. Generally calcite is rare, but in 83/97A it forms an estimated 30 (modal) % of the rock. Apatite and zircon are present in minor amounts.

The colourless, poikiloblastic orthoamphibole which is the characteristic constituent of a unit predominant in the NE section of the property, has been identified as gedrite by electron microprobe analysis (Table A-4); it also occurs locally in the area of Map 2. This mineral forms augen within the fabric and is altered to yellowish chlorite and magnetite(?) in places.

Unit 3c, the epidote-hornblende-bearing rock is petrographically similar to the amphibolites. Epidote is a principal phase in the rock, which may comprise up to 65% modal quartz. Calcite is ubiquitous, both as a principal phase and in quartz ± epidote veins. The porphyroclasts (section 2.1.5.2) are composed of aggregates of epidote and calcite. Pyrite ± pyrrhotite, which may form up to 5 modal % of the rock, are typically elongated parallel to the S2 foliation.

The amphibolitized ultramafic rock, unit 3b, is composed (> 90%) of a colourless pale-green fibrous amphibole, probably tremolite, and accessory opaques.

3.2 Metamorphic History

Textural criteria are commonly used in defining the relative timing of metamorphic mineral growth and deformation events. Such criteria may well be equivocal,

particularly with regard to relationships between porphyroblast trails and matrix foliations. Vernon (1977) has reviewed the textural evidence and notes some precautions to be taken in their interpretation.

A relict S1 is defined by micas and kyanite in quartz-feldspar microlithons, garnet pressure shadow regions and in relict F1 hinges. In the latter situation they are invariably recrystallized. The growth of biotite and muscovite occurred during D1 and D2 since they are the principal S1 and S2 fabric-forming minerals. Kyanite blades mostly lie across or on the S2 foliation. The timing of kyanite development is unclear; although it has been shown as defining S1 locally, its tendency towards random orientation is particularly noticeable in hand specimen. However, it is considered to have grown principally either during D1 or mimetically on the S1 fabric and during D2. Much of the kyanite developed during a static phase, accounting for the random orientation of blades.

Staurolite growth may have overlapped D2 in part since Si, considered to be S1, was noted to curve at the margins of several staurolite grains. Staurolite probably formed post-D1 or, late-D1 and pre-D2 and has been noted in rocks of lower grade to the northwest (Wilton, 1984) coexisting with biotite and garnet. The diversity of features shown by garnets is probably indicative of continuous growth throughout the metamorphic history. Development of hornblende porphyroblasts with or without an Si, was probably post D1.

Kyanite blades and mica laths are conspicuously bent around F3 fold hinges but there is no axial-planar foliation associated with D3.

3.3 Mineral Chemistry

3.3.1 Introduction

The common phases in pelites and amphibole-bearing rocks were analysed using a JEOL JXA50 wavelength dispersive electron microprobe. Analytical procedures and analyses are given in Appendix A. Garnets, biotites, feldspars and amphiboles are the principal minerals which were analysed to determine their compositional variation across the area and with lithology. The first three minerals also provide a method of estimating peak metamorphic temperatures and pressures. Several analyses of epidotes and muscovites were also made.

3.3.2 Garnets

Garnet stoichiometry in the analysed samples involves four main components *viz.*, almandine (Alm), grossular (Gr), pyrope (Py) and spessartine (Sp). The relative proportions of these phases (Table 3-2) were calculated assuming the andradite component to be negligible. Average garnet compositions in amphibolites are:

Alm_{59--64}, Gr_{22--18}, Py_{10--14}, Sp_{9--4};

and in pelites

$Alm_{71.5--71.6}$, Gr_{22--18}, Py_{11--15} $Sp_{5.5--6}$
(where arrows indicate core to rim variation).

Distinctive zonation patterns (Table 3-2) in the larger garnets are of increasing MgO and FeO and typically decreasing MnO and CaO from core to rim (although in several garnets a small FeO decrease was noted at the rim). Generally the difference between core and rim composition is less than 5 weight % but sample 83/75 has a 20% increase in FeO content. All the larger analysed garnets from amphibolites are zoned, whereas in pelites, in which both small and large garnets occur, the small type are either unzoned or may display a zoning which is the reverse of the above pattern.

Increasing FeO and MgO and decreasing MnO and CaO in zoned garnets, as seen here, is a feature typical of many metamorphic belts (Miyashiro 1973, Labotka 1980, Ghent et al 1982). Increasing temperature causes the MgO fractionation factor between garnet and coexisting FM phases, to increase (according to Miyashiro and Shido 1973, in Miyashiro, p 221, 1973), and leads to a complementary increase in pyrope content. Higher MgO in pelitic garnets (compared to amphibolites) may reflect available MgO since in amphibolites hornblende is present in abundance and together with garnet comprise much more of the rock than garnet and biotite in pelites. Decreasing MnO from core to rim is attributed by Hollister (1966) and Atherton (1968) to a

Table 3-2: Garnet Stoichiometry from Microprobe Analyses, on the basis of 12 oxygens.

AMPHIBOLITES

Sample#	Alm	Gro	Py	Sp	# of points
Amp3	60→62	25→24	12→12	3→2	2→1
83/75	73→71	12→11	13→17	2→1	2→1
	45→65	29→15	3→13	23→7	2→2
82/1/252	55→60	29→21	10→13	6→6	2→2
	62→53	14→18	12→14	11→6	1→1
		PELITES			
83/12	75→74	8→9	13→13	4→4	2→2
	76	7	13	4	1
83/62	62	13	17	7	3
83/83	67	1	29	3	2
83/86	73→73	6→3	13→17	8→7	2→2
	70→73	5→3	15→18	10→6	2→1
83/87	74	3	15	8	2
83/93	67	6	23	4	4
Bi6A	78→77	3→4	15→7	4→12	1→1
	78	4	10	8	4
82/5/274	73	4	17	6	5
83/2/349	66→65	13→13	17→18	4→4	2→2
	67→68	11→9	19→18	3→3	2→2

Abbrev. Alm = Almandine; Gro = Grossular; Py = Pyrope; Sp = Spessartine;

→ = core to rim molecular proportions variation, average is quoted where more than one point analysed in core or rim.

segregation phenomenon which effectively removes the spessartine-rich garnet core, once crystallized, from the system; MnO is concentrated in the core and becomes quickly depleted in the "matrix". The bulk rock MnO appears to have little influence on spessartine content which is much the same in the pelites and the amphibolites; e.g. sample 83/62

which is a coticule, contains 2 wt. % total MnO (anomalously high) but the spessartine content in the garnet is average compared to pelites. Sample 83/75 has anomalously high MnO (23 % spessartine) in the core of a zoned garnet which has average rim composition. Miyashiro (1973) reports greenschist facies garnets with 19.7 % MnO. However, garnets with rim compositions up to 18% Sp have been reported (Tracey et al., 1976) as having formed at pressures of >5.7 kb and temperatures of 585 to 655 °C. These garnets with high MnO in their cores may have nucleated in either greenschist or amphibolite facies conditions. Note that the Alm-Gro-Py-Sp content of sample 83/62, which is a coticule with relatively anomalous MnO (approximately 2%), is similar to the other samples. The 13 % (average) difference of grossular content between garnets in pelites and amphibolites is a reflection of bulk rock composition (10 % in amphibolites and 1 % in pelites). Gradation in the CaO content may be a result of continuous reactions with plagioclase (Crawford, 1977) although cursory analyses of the feldspars revealed no zoning.

As noted above, the reverse pattern of chemical zoning in which Alm and Py decrease while Gr and Sp increase towards the rim (the latter showing the greatest variation) is displayed by some of the smaller garnets (samples Bi6A and 83/12). This pattern has been ascribed to a retrograde reaction by Tracy et al (1976), Woodsworth (1977) and Ghent et al. (1982), possibly involving exchange of MnO, FeO and

MgO with adjacent reacting species, for example, biotite. Unzoned garnets may have homogenized by a process of volume diffusion which according to Woodsworth (1977) operates at temperatures over 600°C.

3.3.3 Micas

Biotite and muscovite stoichiometries based on microprobe analyses are listed in Table 3-3.

Table 3-3: Mica stochiometry on the basis of 22 oxygens.

	BIOTITES
Sample#	Amphibolites
83/75	$K_{1.6}\{Mg_{3.0}Fe_{2.3}(Al,Ti)_{0.6}\}\{Si_{5.6}Al_{2.4}O_{20}\}(OH,F)_4$
83/97B	$K_{1.6}\{Mg_{3.2}Fe_{2.2}(Al,Ti)_{0.5}\}\{Si_{5.6}Al_{2.4}O_{20}\}(OH,F)_4$
	Pelites
Bi6A	$K_{1.5}\{Mg_{1.6}Fe_{2.8}(Al,Ti)_{1.2}\}\{Si_{5.4}Al_{2.6}O_{20}\}(OH,F)_4$
83/62	$K_{1.4}\{Mg_{2.4}Fe_{2.4}(Al,Ti)_{0.7}\}\{Si_{5.7}Al_{2.3}O_{20}\}(OH,F)_4$
83/93	$K_{1.5}\{Mg_{2.9}Fe_{1.9}(Al,Ti)_{1.0}\}\{Si_{5.6}Al_{2.4}O_{20}\}(OH,F)_4$
	MUSCOVITES
83/86	$(K,Na)_{1.7}(Mg,Fe,Ti,Mn)_{0.4}Al_{3.7}(Si_{6.4}Al_{1.6}O_{20})(OH,F)_4$
83/87	$(K,Na)_{1.6}(Mg,Fe,Ti,Mn)_{0.5}Al_{3.6}(Si_{6.4}Al_{1.6}O_{20})(OH,F)_4$

Biotites in amphibolites are annites, poorer in Al_2O_3 and TiO_2 than pelitic biotites which are siderophyllites. Sample 83/83 is the one exception, lying on the

phlogopite-biotite join and reflecting the high magnesian bulk rock composition. Little compositional heterogeneity exists either within grains, between grains in a single thin section or even between samples of the same rock type. Several muscovites in pelites were analysed and their compositions plot towards the pure muscovite field.

3.3.4 Amphiboles

The typical amphibole is calcic hornblende (Table 3-4) with 1.5-2.0 (atomic proportions) CaO and Na2O+K2O = 0.6 (At. Prop.), using the classification of Miyashiro, 1973.

However, a post-tectonic amphibole in sample 83/97B overprinting the main fabric, was analysed as actinolite-tremolite. The atomic proportions of Na2O+K2O range from 0.15 in the latter example, to 1 in sample 83/80 from the north end of Isle aux Morts River West, in which case the hornblendes are pargasitic. Several rim and core analyses of colour-zoned grains showed only negligible compositional variations.

The orthoamphibole which occurs ubiquitously in the northeast corner of the property, and locally in the south, was probed in two samples, 83/83 and 83/99 (Table 3-4). The composition is that of magnesian gedrite co-existing with magnesian biotite and garnet.

Table 3-4: Amphibole stoichiometry on the basis of 23 oxygens.

Sample#	HORNBLENDE							
83/75	(Na,K) $_{0.6}$	Ca $_{1.7}$	(Mg,Fe,Al)	Si $_{5.0}$	Al $_{6.4}$	O $_{1.6}$ $_{22}$	(OH,F) $_{2}$	
83/80	(Na,K) $_{0.9}$	Ca $_{1.8}$	(Mg,Fe,Al)	Si $_{5.0}$	Al $_{6.3}$	O $_{1.7}$ $_{22}$	(OH,F) $_{2}$	
83/97B	(Na,K) $_{0.1}$	Ca $_{1.8}$	(Mg,Fe,Al)	Si $_{5.1}$	Al $_{7.8}$	O $_{0.2}$ $_{22}$	(OH,F) $_{2}$	
	GEDRITE							
83/83	Na $_{0.6}$	(Mg,Fe)	Al $_{5.6}$	(Si $_{6.3}$	Al $_{1.2}$	O $_{1.7}$ $_{22}$)	(OH,F) $_{2}$	

3.3.5 Feldspars

Plagioclase compositions of pelites and amphibolites are presented in Table 3-5. The average anorthite content in the latter is 32% compared to 21% in the pelites, this difference reflecting the difference in bulk rock chemistry. The orthoclase component is low and no zoning was noted in any feldspars analysed. The feldspar in sample 83/83 is albite (this sample contains magnesian phases and is low in CaO; see section 3.3.4). Both K-feldspar (as orthoclase) and oligoclase were analysed in sample 82/5/274 (however the K-feldspar occurs in thin veinlets and does not form part of the equilibrium assemblage).

Table 3-5: Molecular proportions of albite, anorthite and orthoclase from microprobe analyses (on the basis of 8 oxygens).

Sample#	Ab	An	Or in Mol%
	AMPHIBOLITES		
82/1/252	69.6	30.0	0.4
83/75	70.6	29.3	0.1
83/80	72.0	27.0	1.0
Amp3	57.5	42.0	0.5
	PELITES		
83/62	69.0	30.4	0.6
83/83	92.7	7.2	0.1
83/86	83.9	16.0	0.1
83/87	88.0	11.6	0.4
83/93	75.4	24.4	0.2
82/5/274	81.0	18.5	0.5
83/2/349	62.0	37.5	0.5

3.4 Thermobarometry

3.4.1 Thermometry

The temperature-dependent partitioning of MgO and FeO between coexisting garnets and biotites has resulted in several quantitative methods of estimating temperature. Ferry and Spear (1978) conducted experiments at 2.07 kb and 600 and 700 °C with Alm80 and Py20, to quantify the compositional dependence of the MgO/FeO partitioning coefficient K, in the system Alm-Py-annite-phlogopite. The equilibrium constant K for the expression is MgO/FeO (garnet)/MgO/FeO (biotite). Ferry and Spear derived the expression:

$$12{,}454 - 4.662T(^{o}K) + 0.057P(\text{bars}) + 3RT\text{Ln}K = 0$$

which was used to calculate temperatures of equilibration at an assumed P of 7 kb, consistent with the presence of staurolite and quartz. Garnets and biotites chosen for analysis were separated by minerals inert in any possible exchange reaction e.g. quartz. Garnet-biotite pairs in one to three domains were analysed with the microprobe in each thin section. Domains were approx. 2 mm in diameter and a minimum of 2mm apart. Several biotites were analysed in each domain and an average taken. In most garnets, two points were analysed in both core and rim and averaged separately; only rim analyses were used in temperature estimation since it is most likely that equilibration has been reached between mineral rims and matrix in a domain. This has been postulated by various authors (Ghent, 1976; Pigage, 1976). Values of LnK and estimated temperatures are listed in Table 3-6.

At 7 kb, the calculated average temperature is 655 ^{o}C with a standard deviation of $\pm$39 ^{o}C, determined for 11 samples representing a cross strike distance of 2.7 km. If the apparently anomalous data from samples Bi6A and 83/75 are omitted (and only pelites are considered) the average temperature is 655 ^{o}C with a standard deviation of $\pm$26 ^{o}C. In Bi6A, the lack of equilibration of MgO/FeO partitioning between garnets and biotites is suggested by the large range in LnK values.

Table 3-6: Data from the biotite-garnet geothermometer of Ferry and Spear (1978).

	PELITES					
	Garnets		Biotites			
Sample#	Mg/Fe	Ca+Mn*	Mg/Fe	Al+Ti*	LnK	Temp °C
Bi6A	0.096	0.08	0.324	0.28	-1.21	808
	0.078	0.11	0.321	0.27	-1.41	710
	0.072	0.12	0.325	0.27	-1.50	670
83/12	0.101	0.11	0.480	0.26	-1.55	651
	0.096	0.09	0.519	0.26	-1.68	602
83/39	0.133	0.20	0.591	0.19	-1.49	675
83/62	0.156	0.19	0.717	0.23	-1.50	670
83/83	0.236	0.04	1.200	0.25	-1.62	624
83/86	0.125	0.10	0.565	0.25	-1.50	670
	0.134	0.09	0.576	0.25	-1.45	692
83/87	0.118	0.11	0.579	0.27	-1.59	635
83/93	0.197	0.10	0.858	0.25	-1.47	673
	0.188	0.10	0.794	0.25	-1.44	696
82/5/274	0.131	0.09	0.556	0.27	-1.44	696
	0.129	0.10	0.594	0.28	-1/52	663
83/2/349	0.152	0.17	0.793	0.27	-1.65	613
	0.149	0.12	0.734	0.27	-1.59	635
	AMPHIBOLITES					
83/75	0.109	0.20	0.795	0.34	-1.90	530
	0.140	0.10	0.715	0.34	-1.60	631

Abbreviations: Ca+Mn* = Ca + Mn / Ca + Mn + Fe + Mg
Al+Ti* = Al + Ti / Al + Ti + Fe + Mg

Ferry and Spear (1978) also attempted to quantify the dependence of K on the CaO and MnO contents of garnets, and on the Al(6+) and Ti of biotites. K was calibrated using natural rock samples; comparison with experimental studies indicated that this geothermometer is useful up to approximately 0.2 (CaO + MnO/CaO + MnO + FeO + MgO) in garnet and 0.15 (Al(6+) + TiO2/Al(6+) + TiO2 + FeO + MgO) in biotite. The criteria are met by garnets but not by biotites in the study area; these deviations from ideal mixtures still need to be quantified with respect to temperature dependency. In both anomalous samples, the zoned garnets show the greatest variation from core to rim in MgO and MnO contents. Pigage and Greenwood (1982) assert that such zoning in garnets has a strong influence on the temperatures derived from them. Kyanite-staurolite zone temperatures in Mica Creek, British Columbia, have been estimated at 635 ^{O}C $\pm$ 50 ^{O}C (one standard deviation) using this calibration (Ghent et al. 1979, 1982) which is in reasonable agreement with that of Thompson (1976) and other thermometers. Hodges and Spear (1982) conclude that this method is most accurate in medium-pressure terrains.

Despite these concerns, the present T estimates are reasonably consistent, both internally and when compared with similar metamorphic terrains elsewhere. The analytical uncertainty was determined by Ghent et al (1979), to give a standard deviation of $\pm$ 15 ^{O}C; the "excess" here (15 ^{O}C) over and above the analytical error, is attributed to non-ideality of the (garnet-biotite) mixtures.

3.4.2 Barometry

The partitioning of CaO between coexisting garnet and plagioclase in the reaction:

$$3CaAl_2Si_2O_8 = Ca_3Al_2Si_3O_{12} + 2Al_2Si_2O_5 + SiO_2$$

can be used to derive an expression to estimate pressures from garnet-plagioclase-kyanite-quartz assemblages (Ghent, 1976). The equation so obtained:

$$-3272/T(^{o}K) + 8.3969 - 0.3448(P-1)/T(^{o}K) + \log a(\text{Gr in garnet}) - 3\log a(\text{An in plagioclase})$$

is used here. The activity of grossular in garnet:

$$(a) = X^{3} * \&^{3}$$

where

X= mole fraction CaO (CaO/CaO + MnO + MgO + FeO)

and

&= activity coefficient, given by

$$\text{Ln } \& = (1-x(\text{Gr in garnet}))^{2} (W/RT) \text{ where}$$

$$R = \text{Gas Constant } (1.987 \text{ cal/mol}^{-1} / {}^{o}K^{-1})$$

x= CaO/CaO + FeO

W= interaction parameter for a binary mixture (related to the Gibbs Free energy of mixing), estimated at approx 1000 cal/mol for almandine/grossular (Ganguly and Kennedy, 1974).

The activity of $CaAl_2Si_2O_8$ in plagioclase is:

X (An in plagioclase)*&(An in plagioclase)

where

X= CaO/CaO + Na2O + K2O and &= 1.276 (Orville, 1972)

The pressure estimates and relevant data are presented in Table 3-7.

Table 3-7: Pressure data using the garnet-plagioclase geobarometer of Ghent et al. (1976).

Sample#	X(Plag*)	X(Gt*)	Log (a*)	Pressure (bars)
83/2/349	0.36	0.08	-1.739	8334
	0.52	0.12	-1.724	8374
82/5/274	0.29	0.03	-2.4572	6143
	0.24	0.03	-2.1124	7334
83/86	0.23	0.03	-2.3685	6684
	0.24	0.03	-2.4738	6367
83/87	0.19	0.02	-2.4047	6552
83/93	0.37	0.05	-2.2009	7097
	0.36	0.05	-2.2669	6921

Abbreviations: X(Plag*) = molecular proportions of anorthite in plagioclase.

X(Gt*) = molecular proportions of grossular in garnet.

$$Log(a^*) = Log\, a^{Gt}_{Gross} - 3Log\, a^{Plag}_{An}$$

Assuming a T of 650 °C, the average P is 7085 bars with a standard deviation of 759 bars (for 9 garnet-plagioclase pairs). If sample 83/2/349 is omitted the average P becomes

6723 bars with a standard deviation of 387 bars and a pressure range from 6143 to 7334 bars. These estimates are clearly T dependent; a temperature uncertainty of ± 15 °C with an analytical error of ± 1 mol% Gr and ± 1 mol% An, results in an error of ± 1.6 kb (at two standard deviations) (Ghent et al., 1982). Thus the range of estimated values lies within the error.

P-T conditions of metamorphism estimated from the geothermometer and geobarometer used in this study are illustrated in Figure 3-8. They are consistent with the univariant curves on the grid, in that although the stability of the assemblage staurolite-muscovite-quartz is exceeded, that of staurolite-quartz is not. As noted previously all the maximum phase assemblages lack muscovite, and this has caused the staurolite to remain a stable phase to the right of curve 2. The interpretation of some of the pegmatitic veins as anatectic sweats, is also consistent with the estimated P-T conditions. The presence of sillimanite (with kyanite) in several samples in the northeastern part of Map 1, implies that the stability of kyanite has been exceeded, which is also consistent with the P-T estimates.

3.5 Distribution and Significance of AFM Phases

The mineral assemblages listed in Table 3-1 and estimated pressures and temperatures for the area, are illustrated in the schematic maps of Figure 3-9, along with the estimated temperatures and pressures.

Figure 3-8: Pressure-temperature field and reaction curves relevant to the present study. The stippled area represents the estimated P and T for the Isle aux Morts area:

1: Alumino-silicate triple point from Holdaway (1971)

2: Staurolite breakdown in the presence of muscovite and quartz; unpublished curve from Carmichael (1981), pers. comm. to T. Rivers.

3: Fe-Staurolite breakdown in the presence of quartz (Pigage and Greenwood, 1982).

4: Anatexis (Winkler, 1979)
Ab + Musc + Qz + H2O =
Liq + Al2SiO5

5: Breakdown of muscovite and quartz from Evans (1965)

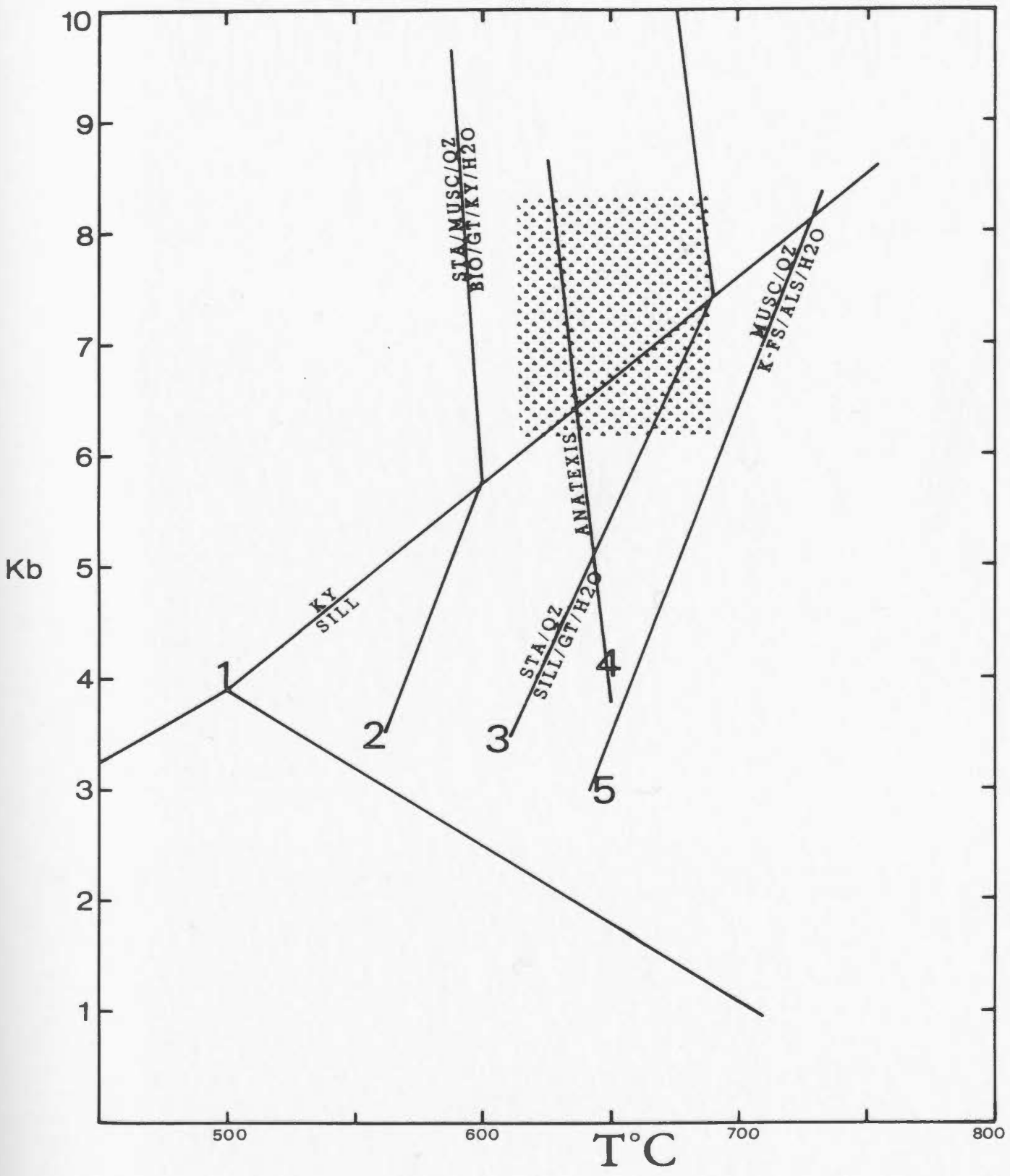
10
9
8
7
6
5
4
3
2
1
Kb
500
600
700
800
T°C
KY
SILL
STA/MUSC/QZ
BIO/GT/KY/H2O
ANATEXIS
STA/QZ
SILL/GT/H2O
MUSC/QZ
K-FS/ALS/H2O
1
2
3
4
5

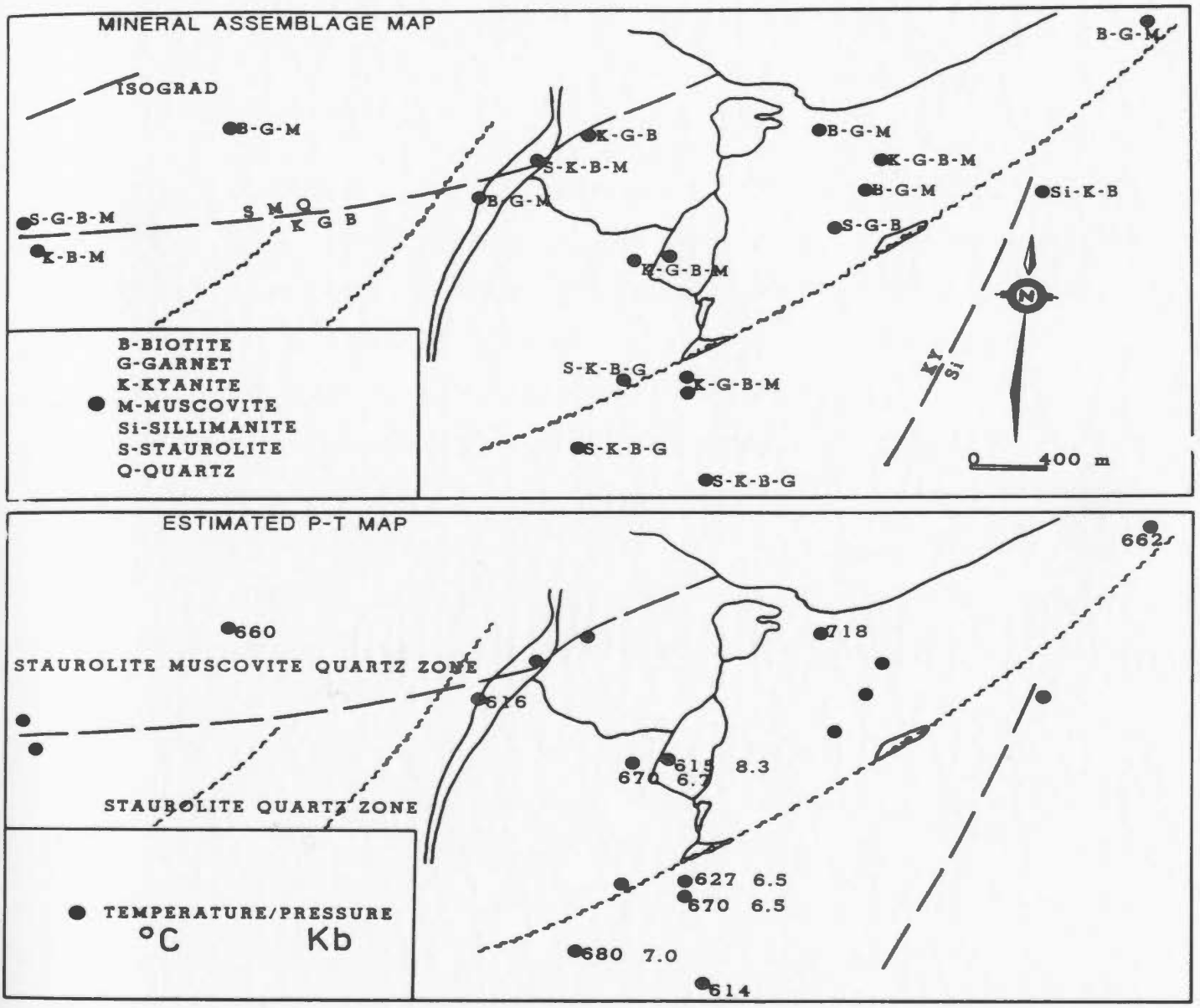

Figure 3-9: A: Distribution of AFM phase assemblages. Two isograds are inferred from these, (1) sta-musc-qz to ky-gt-bio-liq and (2) the transition from kyanite to sillimanite.
B: Distribution of all estimated pressure and temperature data for Map 2. The sta-musc-qz and sta-qz zones are shown, both of which are compatible with bathozone 5 (Carmichael, 1978).

3.5.1 Distribution

The mineral assemblages which are critical for definition of isograds occur in pelites and semipelites throughout the area. The distribution shows that staurolite coexists with muscovite and quartz in the northern part of the mapped area (stippled with triangles). The other members of the three-phase (AFM) assemblages are biotite and either kyanite or garnet. In the central and southern parts of Map 2, the assmblage staurolite + muscovite was not found and the most commonly occurring assemblage is kyanite-garnet-biotite in the south and central parts of Map 2. Muscovite is present in all but one sample, implying that the stability of staurolite has been exceeded. Pelites of unit 1d contain the maximum phase assemblage staurolite-kyanite-garnet-biotite (muscovite absent) found in the south of Map 2. East of Nutmeg Lake, staurolite-biotite-garnet (only occurrence) form an assemblage with muscovite absent. The assemblage sillimanite-kyanite-biotite which is present in one sample in the northeast of Map2, also occurs further northeast in claim block 2329.

The estimated pressures and temperatures are also shown beside each appropriate sample location. Most of these are from the south and there is only one data point from the north. There is no obvious trend in pressure and temperature values, probably reflecting the small area sampled and also local lack of equilibration between the minerals used in geothermobarometry.

3.5.2 Significance

Pelites may be represented in the system FeO-MgO-Al2O3-SiO2-K2O-H2O i.e. KFMASH which assumes that the components CaO, Na2O are incorporated entirely in feldspars, and that MnO and TiO2 contents are small enough to be effectively ignored. Thompson's (1976) AFM projection from muscovite in AKFM space is used, despite the absence of muscovite (or K-feldspar). This is acceptable as the assemblages equilibrated with muscovite prior to the staurolite-muscovite-quartz reaction. The principal assemblages projected are:

kyanite-biotite-garnet
staurolite-kyanite-biotite
staurolite-garnet-biotite
biotite-garnet
biotite-kyanite

On the basis of the foregoing description a zone characterized by kyanite-garnet-biotite can be defined adjacent to a zone containing staurolite and muscovite; these zones are compatible with the terminal discontinuous reaction:

staurolite + muscovite + quartz = kyanite + garnet + biotite + H2O --------- Rxt. 1

which is the breakdown of staurolite in the presence of muscovite. This reaction does however, occur at a lower

temperature than that estimated from the garnet-biotite thermometer. Several explanations arise viz.,

(1) the curve is at too low a temperature
(2) estimates from the thermometer are too high
(3) enhanced stability of staurolite due to excess minor components, eg. MnO or ZnO.

In the staurolite + muscovite zone the stable assemblage staurolite-kyanite-biotite suggests the following continuous reaction:

staurolite + muscovite + quartz = kyanite + biotite + H2O. ---------- Rxt. 2.

This reaction along with other possible reactions depending on the bulk-rock composition, can be schematically outlined using Thompson's (1976) pseudobinary T-X diagram (Fig. 3-10A).

The range of bulk compositions estimated from the modal proportions of the various minerals in the 2- and 3-phase assemblages are also illustrated in Figure 3-10.

In all assemblages analysed biotite has a lower FeO/MgO ratio than garnet. The Mg/Fe ratio of garnets ranges from 0.07 to 0.23 and biotites from 0.32 to 1.2, however no consistent geographic trend is exhibited within this range.

The low variance assemblage staurolite-kyanite-garnet-biotite which cannot be illustrated on the AFM diagrams, may be due to one or more of the following possibilities:

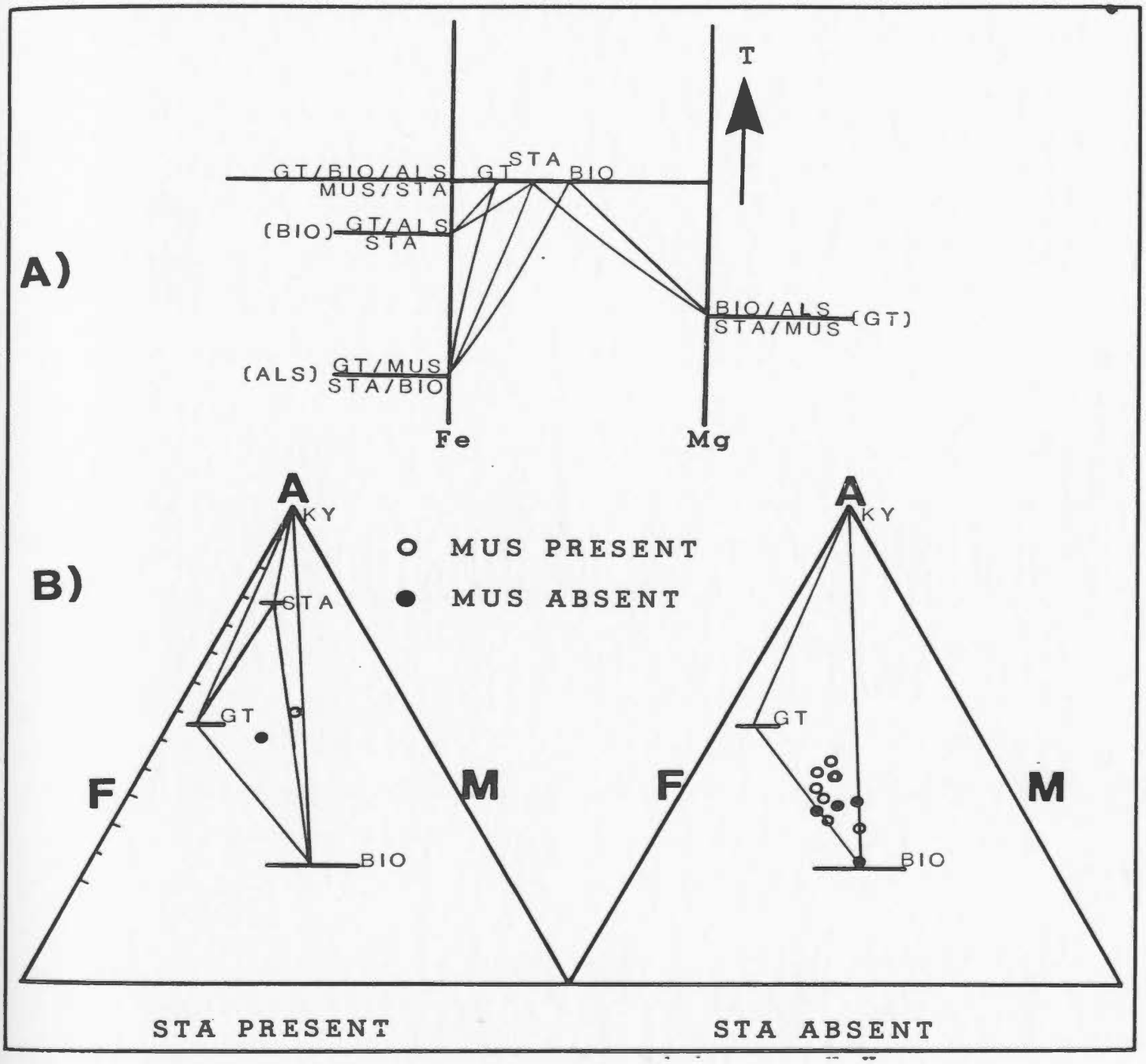

Figure 3-10: A: Schematic pseudobinary T-X diagram illustrating the sequence of continuous reactions postulated to take place from Wilton's (1984) area in the NW, to and including, the study area and the terminal discontinuous reaction involving the breakdown of staurolite with muscovite in the presence of quartz.

B: AFM diagrams (schematic) illustrating the assemblages and their approximate bulk composition.

(1) It may represent the univariant assemblage associated with the discontinuous staurolite breakdown reaction but with muscovite absent, the reaction cannot go to completion. That kyanite-garnet-biotite is the stable assemblage in the south is indicated by staurolite occurring only as an armoured relict in garnet in one sample.

(2) The MnO content of garnet may cause discontinuous Fe-Mg reactions to become continuous Fe-Mg-Mn reactions (Thompson et.al., 1977); TiO2 in biotite and ZnO in staurolite may have the same effect. MnO content is generally low in garnet rims in the south of Map 2. ZnO in staurolite has not been analysed for.

(3) Droop (1981) suggests that the non-reactive nature of some minerals e.g. garnet, may prevent a reaction going to completion, resulting in a metastable low variance assemblage.

These four phase assemblages have been observed in pelites in the Austrian Alps (Droop, 1981) and in Pennsylvania (Crawford, 1977).

Breakdown of staurolite may have occurred approximately synchronously with the production of anatectic pegmatitic melts seen locally as conformable veins in quartzofeldspathic rocks and pelites. Treloar (1985) noted anatectic melts in rocks several metres from those containing staurolite which was breaking down according to the reaction:

staurolite + muscovite + quartz = biotite + kyanite + H2O

Rxt. 3.

Although the pegmatitic bands noted (especially in unit 1d) in the thesis area are locally deformed, they are ubiquitous and are thought to have formed nearby if not in situ. Localized partial melting is quite plausible as the estimated temperature and pressure for the area coincide with the anatexis curve of Winkler (1979) (Fig. 3-8).

Northwest of the study area towards the Cape Ray Fault Wilton (1984) has defined a garnet zone and southeast a staurolite-garnet-biotite zone. The absence of kyanite there can be attributed to bulk-rock composition and is probably developed in more aluminous rocks (further southeast) by the continuous reaction (Rxt. 2) above and/or by:

staurolite + quartz = kyanite + garnet + H2O ------ Rxt. 4

Since these reactions imply no change in the topology of the AFM diagram, no isograds are inferred for the intervening area.

Near Port aux Basques, Brown (1975) has mapped a garnet, staurolite-kyanite-garnet-biotite, kyanite-garnet-biotite and sillimanite zones which appear to correlate with the zones of Wilton (1984) and this study. However extrapolation northeastwards of these zones leads to difficulties as only the isograds representing the

polymorphic transition of kyanite to sillimanite match. Although muscovite is reported for all assemblages containing staurolite in Brown's area, it is unclear whether the disappearance of staurolite is related to the staurolite + muscovite or the staurolite + quartz breakdown reactions. These various isograds are depicted in Figure 3-11.

The limiting stability field of staurolite in the presence of quartz has been the focus of debate in recent literature (Richardson, 1968; Hoschek, 1969; Ganguly, 1972; Rao and Johannes, 1979; Pigage and Greenwood, 1982; Bickle and Archibald, 1984), much of it on the inconsistency between experimental results with a thermodynamic base and P-T estimates from geothermometers and field relationships. In the present study the staurolite + quartz breakdown reaction curve of Pigage and Greenwood (1982) is used (Fig. 3-8) which lies at the estimated upper temperature limit for the area. According to Ganguly (1972) solid solution effects should displace the curve to lower temperatures by no more than 15 ^{o}C and the staurolite + quartz assemblage is stable over a temperature interval of approximately 75 ^{o}C (compatible with the estimated temperature range). The effect of ZnO should increase the thermal stability of the assemblage (Hollister, 1969).

The equilibrium relationship between staurolite and quartz in the south of the area are consistent with the estimated temperatures from garnet-biotite pairs. Since staurolite is usually seen to be in disequilibrium in the

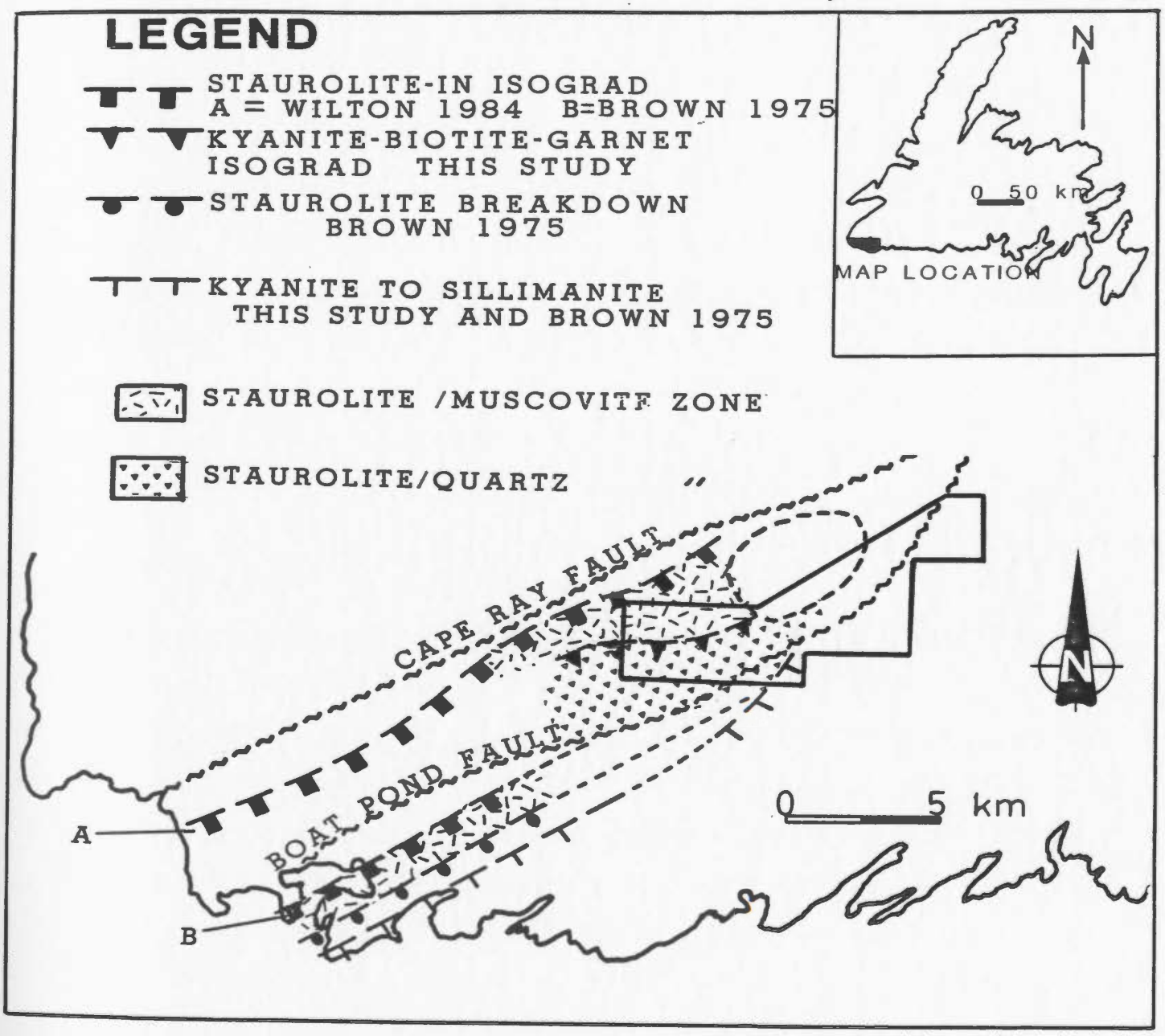

Figure 3-11: Synthesis of isograd data from Brown (1975), Wilton (1984) and this study; teeth are on the high temperature side of the isograds

presence of sillimanite (Pigage and Greenwood, 1982) and as the kyanite + sillimanite transition occurs directly to the southeast, maximum pressure for the area must be approximately 7.5 kb and 690 °C from Figure 3-8.

The bathograd concept of Carmichael (1978) can be

applied to the area as the invariant point defined by the intersection of the kyanite-sillimanite transition and the staurolite + muscovite + quartz = kyanite + biotite + garnet + H2O separates two mineral assemblages, one low pressure (bathozone 4) and the other high pressure (bathozone 5). Thus the area lies within bathozone 5, characterized by the stable assemblage staurolite and muscovite in the north and kyanite, garnet and biotite in the south.

3.6 Summary and Conclusions

Rocks hosting the Isle aux Morts Prospect form part of the Port aux Basques Gneiss Complex (Brown, 1973a), in which a classic medium pressure, Barrovian-type metamorphic facies series is developed. The commonly observed stable pelitic assemblage in the thesis area is the amphibolite facies paragenesis garnet-biotite-kyanite ± muscovite; quartz and plagioclase are ubiquitous and microcline ± orthoclase are present in low variance assemblages. The stable assemblage in the amphibolites is hornblende (or gedrite) + plagioclase ± garnet ± biotite ± epidote ± quartz. Sporadic development of assemblages of muscovite-biotite-chlorite in pelites and blue-green hornblende-chlorite-epidote-calcite ± tremolite in amphibolites suggest greenschist facies retrogression.

An isograd defined by the incoming of the assemblage kyanite-garnet-biotite, products of the breakdown reaction of staurolite in the presence of muscovite, is defined. It is suggested here that staurolite + muscovite + quartz

prograded to a biotite-garnet-kyanite assemblage at peak metamorphic P-T conditions, approximately 650°C and 6.7 kb, but this terminal reaction was incomplete due to a lack of muscovite in some assemblages. During waning P-T conditions, mica replaced the staurolite in a reaction of the type:

staurolite + biotite + quartz + H_2O = chlorite + muscovite

The coincidence of the staurolite + quartz breakdown with the estimated upper temperature limit for the area suggests that this reaction takes place immediately southeast of map 2 and may equate with the northeastwards extrapolation of Brown's staurolite-out isograd.

A synthesis of metamorphic isograds from the Port-aux-Basques Complex is presented in Figure 3-11. Correlation with Wilton's (1984) area to the northwest and Brown's (1975) area to the southeast suggest that the prograding Barovian sequence, i.e. garnet to staurolite-kyanite to sillimanite is repeated on either side of the Boat Pond Fault. However the apparent width of the staurolite zone in the northeast is much greater than in the southwest and may be attributable to bulk rock composition or significant quantities of minor components eg. MnO, TiO_2, ZnO or CaO which would cause enhanced staurolite stability. As the area is structurally complex, the apparent widths may also be a result of unrecognized faulting. Also unlike the lithologies in Wilton's area, the F-M-rich bulk rock

composition in Brown's area delayed the development of kyanite so that it first appears simultaneously with staurolite. It is suggested that the repetition of metamorphic zones is best explained by significant movement on the Boat Pond Fault. The actual disposition of zones also suggests that this motion was scissor-like i.e. the greatest displacement occurred in the southwest and much less in the area immediately southeast of the study area.

The metamorphic history can be correlated on a broad scale with that of the Bay du Nord Group to the east, which according to Chorlton (1984) attained a metamorphic culmination in the upper amphibolite facies during D1 along with the production of synkinematic anatectic melts. A similar pressure-temperature regime existed during D2 which was followed by some differential uplift of the tectonically buried (during D1) terrane and the regional foliation.

Chapter 4
GEOCHEMISTRY

4.1 Introduction

Major and trace elements have been determined from 100 representative samples of all units within the Isle aux Morts prospect area (Map 2). Rare earth element analyses were also carried out on 11 of these samples. The analytical procedures, their precision and accuracy, and the data are given in Appendix B. The samples analysed were unweathered and homogeneous, i.e. with no obvious quartz (with the exception of a coticule sample), calcite and/or epidote veins. Thirty of the samples are from diamond drill core.

This chapter attempts to ascertain the protolith of the lithologies on the basis of their geochemical signatures. Several methods of discriminating igneous and sedimentary rocks are employed. The quartzofeldspathic and pelitic units have been divided into subgroups (Appendix Table B-7) based on lithological features, presence or absence of mineralization and geographic location within Map 2. Table 4-1 gives mean analyses and standard deviations for all subgroups along with published analyses of typical igneous and sedimentary rocks.

4.2 Geochemical Discrimination: Igneous vs. Sedimentary

4.2.1 General Lithogeochemistry

All analyses are plotted on Figures 4-1A and B which show differences in major element chemistry among the lithologies. On both plots, the quartzofeldspathic rocks (QS) and semipelites (QZ: comprising units 1a, 1b and 1c) overlap; the amphibolites (AMP) and epidote-pyrite schist (EPPY) are indistinguishable while the biotite-garnet-kyanite schist (BISC) plots between the two extremes but has closer affinities with the mafic rocks. The majority of the analyses define two clusters on both the alkalies vs. silica plot and AFM diagram. This bimodality also occurs in a histogram of SiO2 distribution for all rocks (Fig. 4-2) which is especially obvious when the pelites are omitted.

Mean analyses of groups and subgroups are plotted in the discriminant diagrams of Figure 4-3. The quartzofeldspathic subgroups plot mostly in the igneous field (Fig. 4-3A), although subgroup 1 lies on the boundary. The semipelite subgroup falls in the sedimentary/igneous boundary while the mineralized group lies well within the sedimentary field. Biotite-garnet-schists plot on the shale trend and the average amphibolite plots precisely as an average tholeiite. The epidote-pyrite schist group falls on a line joining the amphibolites and biotite-garnet schists. In Figure 4-3B, quartzofeldspathic subgroups 1 and 2 plot within the felsic igneous rock spectrum while subgroups 3

Table 4-1: Mean analyses and standard deviations of lithologies from the Isle aux Morts area, with comparative published analyses of common igneous and sedimentary rocks.

	Quartzofeldspathic Rocks							
	QS1	SD	QS2	SD	QS3	SD	QS4	SD
SiO2	68.51	3.2	73.00	2.6	74.14	3.9	72.02	3.0
TiO2	0.47	0.2	0.28	0.1	0.46	0.2	0.41	0.2
Al2O3	13.86	0.8	13.40	1.47	11.71	1.76	13.28	1.13
Fe2O3	4.3	1.2	2.39	0.86	4.25	2.24	3.28	1.58
MnO	0.14	0.1	0.07	0.02	0.12	0.1	0.08	0.05
MgO	1.62	0.9	1.34	0.7	1.34	0.79	1.22	0.66
CaO	2.46	1.86	0.99	0.55	1.21	0.38	1.63	1.07
Na2O	2.74	1.43	3.51	1.06	2.62	1.14	3.86	1.31
K2O	3.64	1.6	2.96	1.14	2.45	1.3	2.90	1.79
P2O5	0.11	0.05	0.05	0.04	0.10	0.07	0.09	0.06
LOI	1.57	0.93	1.20	0.65	0.69	0.33	0.74	0.40
Total	99.42		99.19		99.09		99.51	
#	9		7		8		9	
Pb	100	198	23	26	4	5	18	5
Th	16	5	12	3	10	4	16	5
U	2	3	3	2	3	1	3	2
Rb	100	41	94	40	84	43	73	28
Sr	125	85	103	37	62	30	126	86
Y	31	10	38	18	71	28	41	26
Zr	178	25	161	111	335	125	241	119
Nb	10	1	14	6	22	9	14	8
Zn	200	316	40	13	41	24	40	19
Cu	23	14	14	4	12	8	16	7
Ni	0	0	1	1	5	7	0	1
La	11	7	20	6	19	10	17	10
Ba	1694	1197	1017	449	471	202	1191	507
V	63	35	31	31	33	24	51	41
Ce	31	5	43	14	51	15	41	19
Cr	0	0	0	0	8	15	0	1
Ga	14	2	13	2	16	3	14	3

Abbreviations: QS1-4 are subgroups of quartzofeldspathic rocks (see text for explaination).
SD = Standard deviation.
# = Number of samples meaned.

Mean analyses and standard deviations of semipelites with published data from igneous and sedimentary rocks.

	QZ	SD	MINQZ	SD	WPGIG	ARK	GWCKE
SiO2	72.3	3.2	69.75	5.8	73.70	69.61	66.70
TiO2	0.3	0.1	0.36	0.1	0.34	0.44	0.6
Al2O3	13.0	1.0	13.88	2.0	12.80	12.83	13.5
Fe2O3	2.4	1.3	3.08	1.7	2.7	3.25	5.5
MnO	0.05	0.03	0.03	0.02	0.04	0.06	0.1
MgO	1.9	1.3	1.15	0.98	0.65	1.73	2.1
CaO	0.7	0.6	0.52	0.23	1.5	2.67	2.5
Na2O	2.8	1.2	1.01	0.01	2.1	3.07	2.9
K2O	3.0	1.0	5.8	1.84	6.0	2.75	2.0
P2O5	0.03	0.04	0.02	0.04	0.1	0.14	0.12
LOI	2.2	1.0	3.2	1.2	---	2.91	3.6
Total	98.68		98.8		99.93	99.46	99.62
#	18		6			26	
Pb	41	43	669	866	52	---	---
Th	17	4	17	4	14	---	---
U	3	3	3	3	4	---	---
Rb	79	34	145	45	132	108	---
Sr	83	47	61	15	59	177	---
Y	22	8	27	3	67	30	---
Zr	162	35	154	44	285	191	---
Nb	11	6	12	4	18	10	---
Zn	38	27	1513	1749	69	49	---
Cu	19	20	53	66	19	12	---
Ni	1	0	0	1	11	35	---
La	11	8	11	3	47	26	---
Ba	1758	951	5150	2732	742	753	---
V	52	33	54	27	40	---	---
Ce	28	14	27	10	87	48	---
Cr	0	0	0	0	16	112	---
Ga	13	2	18	6	15	16	---

Abbreviations: QZ= Semipelite; MINQZ= Mineralized semipelite; WPGIG= Ignimbrites, rhyolites and felsic tuffs from the Windsor Point Group (Wilton, 1984); ARK= Average of 26 arkoses (van de Kamp et al, 1976); GWCKE= Average greywacke (Pettijohn, 1963).

Table 4-1, continued

Mean analyses of pelites and a coticule with published values for average granodiorite, shales and a coticule.

	GRAN	BISC	SD	SHALE	COTICULE	GOSCOT
SiO2	66.9	60.0	4.1	58.8	71.0	56.40
TiO2	0.6	1.0	0.2	0.9	0.3	0.24
Al2O3	15.7	18.0	2.0	17.9	10.10	14.60
Fe2O3	3.8	8.9	2.3	7.9	8.5	7.5
MnO	----	0.4	0.2	0.1	2.0	8.9
MgO	1.6	2.7	0.6	2.8	1.6	3.73
CaO	3.5	1.2	1.0	2.0	4.2	3.83
Na2O	3.8	1.7	1.1	1.6	0.6	0.95
K2O	3.1	3.7	0.9	3.6	0.4	1.04
P2O5	---	0.1	1.0	0.1	0.7	0.07
LOI	---	1.7	0.6	5.5	0.2	1.35
Total	99.0	99.4		101.2	99.6	98.4
#	--	16		13	1	1
Pb	---	33	20	---	14	----
Th	---	12	4	---	11	----
U	---	3	3	---	4	----
Rb	120	152	37	251	29	----
Sr	440	83	38	272	26	----
Y	31	41	6	43	52	----
Zr	140	186	28	173	233	----
Nb	---	24	9	12	11	----
Zn	60	97	18	144	47	----
Cu	25	36	15	48	29	----
Ni	15	42	18	92	25	----
La	---	24	6	30	0	----
Ba	500	1043	878	632	0	----
V	--	180	44	---	72	----
Ce	---	55	11	66	29	----
Cr	30	74	27	135	50	----
Ga	18	24	4	24	16	----

Abbreviations: GRAN= Average granodiorite (Taylor, 1968); BISC= Garnet-biotite-kyanite schist; SHALE= Average of 13 shale from Santa Ynez Mts (van de Kamp, 1976); GOSCOT= Coticule from the Gossan Lead District, Gair and Slack (1984).

table4-1, continued

Mean analyses of amphibole-bearing rocks and published values of comparative igneous rocks.

	AMPHIB	SD	OFB	IAT	EPPY	SD
SiO2	50.5	5.0	49.5	52.0	48.5	3.5
TiO2	1.5	0.8	1.4	0.8	0.7	0.2
Al2O3	14.4	1.5	16.1	17.3	16.1	1.9
Fe2O3	11.3	2.3	10.1	7.4	9.0	0.8
MnO	0.3	0.3	----	0.2	0.2	0.0
MgO	7.0	2.9	7.7	7.2	6.5	1.9
CaO	9.5	3.1	11.3	11.5	9.8	2.3
Na2O	2.0	1.1	2.8	2.2	2.2	0.7
K2O	1.0	0.8	0.2	0.4	2.2	1.1
P2O5	0.2	0.1	---	0.1	0.0	0.0
LOI	1.7	2.4	---	0.5	4.4	0.9
Total	99.4		99.1	99.8	99.6	
#	23				5	
Pb	14	21	---	2	37	27
Th	3	4	---	0.5	8	4
U	2	2	---	0.2	3	2
Rb	38	36	1	6	70	40
Sr	225	121	127	340	364	85
Y	39	17	25	---	15	1
Zr	124	83	90	40	65	16
Nb	11	9	13	2	4	2
Zn	127	76	85	---	90	34
Cu	48	35	106	---	109	35
Ni	70	86	135	70	71	81
La	12	12	---	---	6	4
Ba	321	237	12	60	998	493
V	306	101	235	250	263	52
Ce	30	21	---	---	26	7
Cr	156	186	270	180	164	194
Ga	17	4	17	---	15	3

Abbreviations: AMPHIB= Amphibolites; OFB= Ocean Floor Basalts and IAT= Island Arc Tholeiites (BVTP, 1981);
EPPY= Epidote-pyrite-hornblende rock;

Table 4-1, concluded

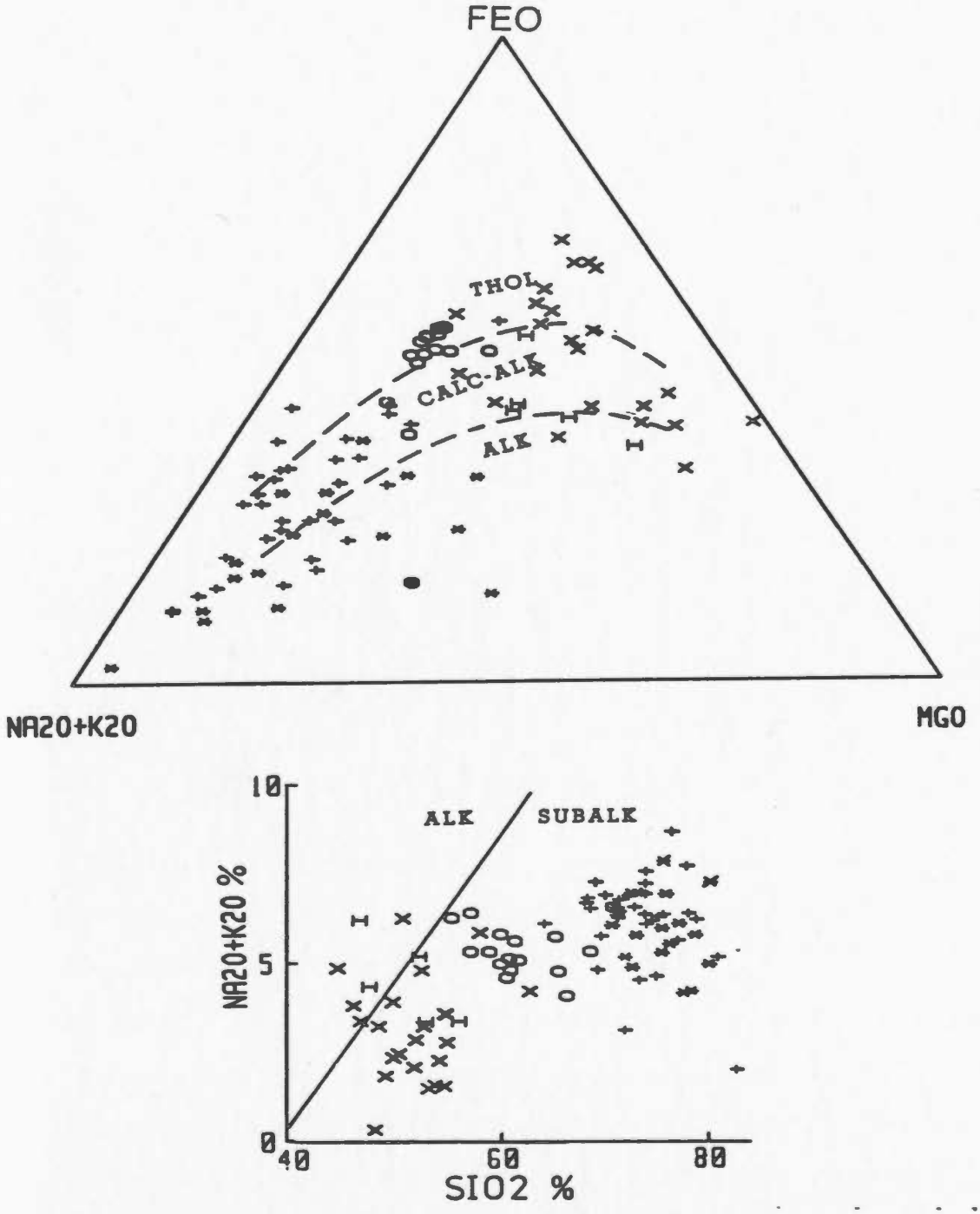

Figure 4-1: These two plots chemically distinguish the three lithologic groupings in the area which are (1) semipelites (*) and quartzofeldspathic rocks (+); (2) pelites (oval); and (3) amphibolites (X) and epidote-pyrite schists (H). These same symbols represent these rocks in following diagrams unless otherwise indicated; fields are from Irvine and Baragar (1971).

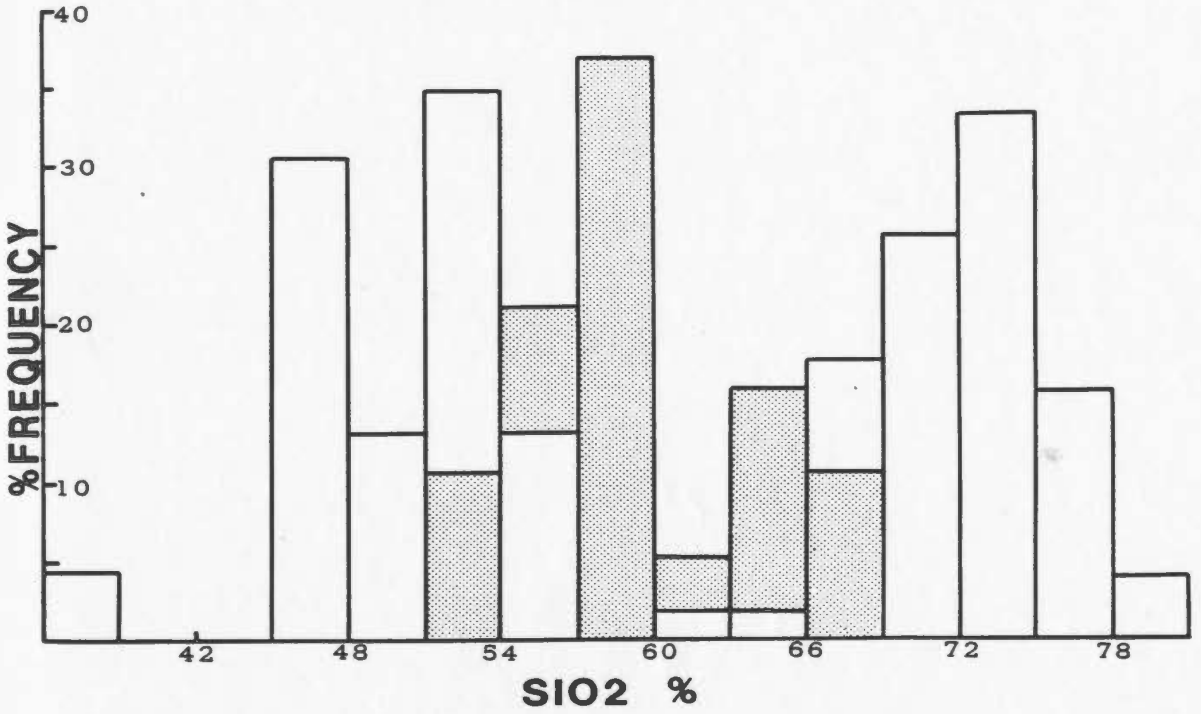

Figure 4-2: SiO2 distribution histogram for all lithologies; note that if the pelites (stippled) are omitted, the sequence is distinctly bimodal.

and 4 lie nearer the greywacke sector of the sandstone field. Semipelitic groups also plot within the felsic field but the mineralized group is closer to the abscissa, indicating K2O enrichment. The biotite-garnet schist mean plots in the shale field (dashed), again forming one end of a line with epidote-pyrite schist and amphibolites, the latter in the mafic igneous area, suggesting a genetic or a metasomatic link between them.

In Figure 4-4A the quartzofeldspathic and semipelitic groups overlap considerably, and along with the amphibolites, show a range in K2O/Na2O contents probably reflecting considerable metasomatism. Mobility and metasomatism involving the major elements mitigates their usefullness, certainly in individual variation diagrams.

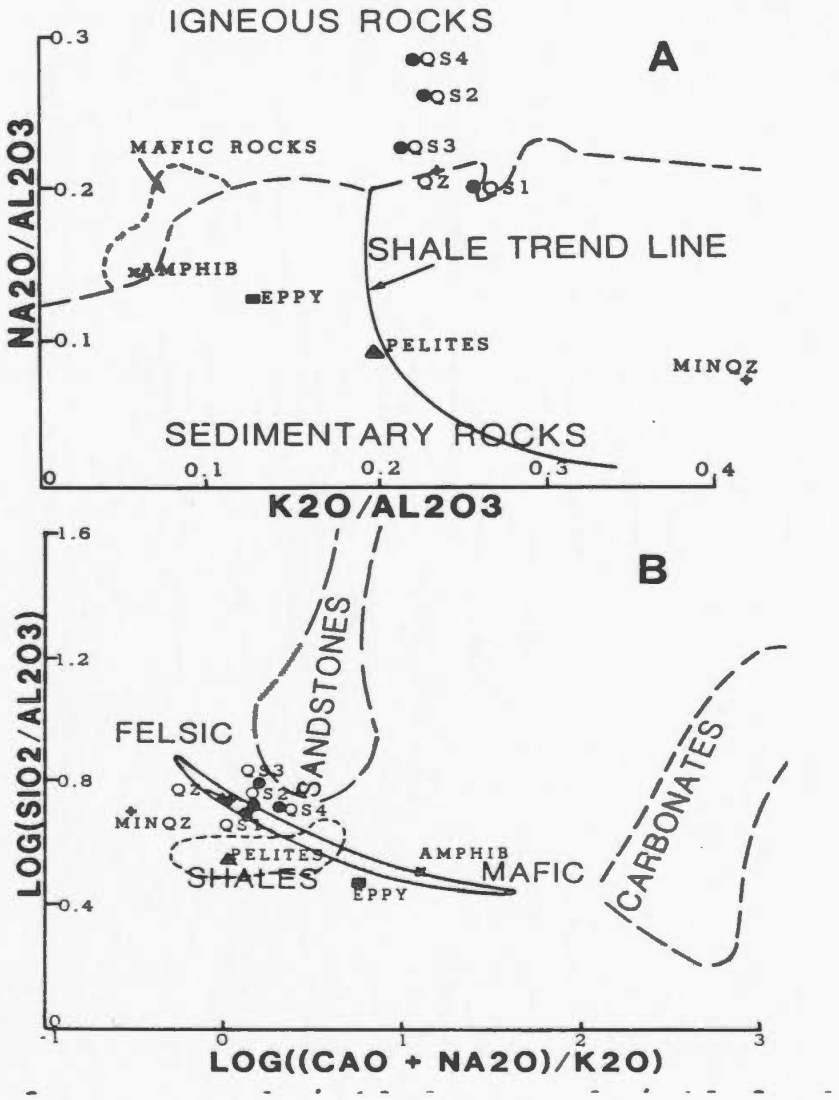

Figure 4-3: A: Na2O/Al2O3 vs. K2O/Al2O3 plot for mean analyses of all lithologies. Symbols are for quartzofeldspathic rocks (QS, closed circles), semipelites (QZ, MINQZ, +), epidote-pyrite schists (EPPY). The shale trend marks an average line drawn through pelitic analyses. B:Log SiO2/Al2O3 vs log CaO+Na2O/Al2O3 for mean analyses of all lithologies. Symbols as above. The stippled field defines the igneous spectrum with felsic rocks at left end and mafic rocks at the right end. Greywackes occupy the bottom part of the sandstone field towards which some quartzofeldspathic rocks migrate. Fields on both diagrams are from Garrels and MacKenzie (1971).

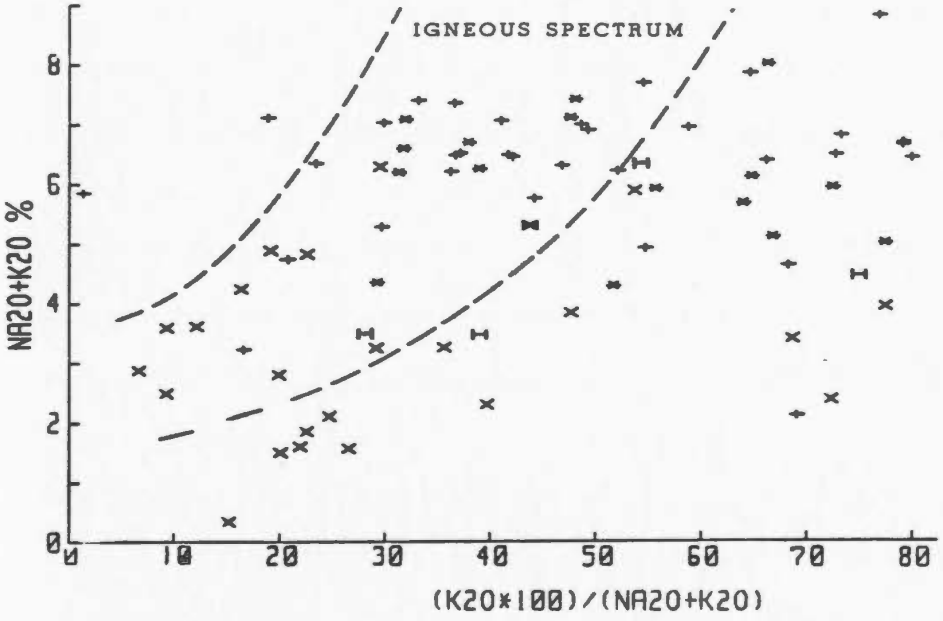

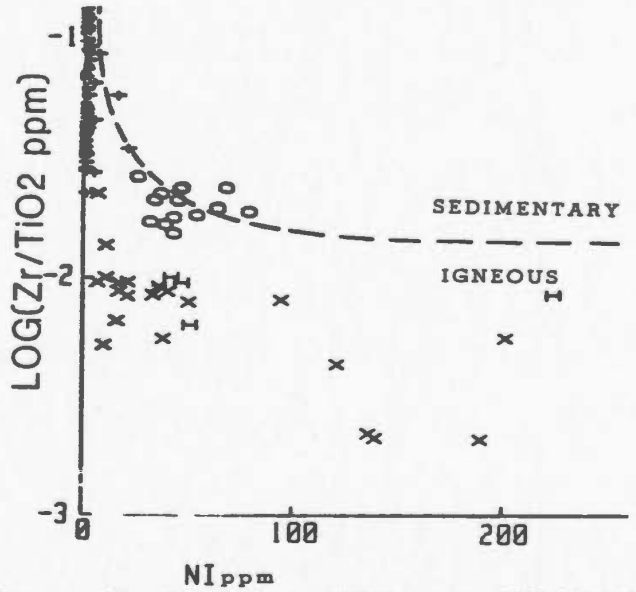

Figure 4-4: A: Na2O + K2O vs. K2O*100/Na2O + K2O plot for all samples except pelites. Igneous spectrum field defined by Hughes (1973).

B: Log Zr/TiO2 vs. Ni plot for all samples most of which fall in the igneous field. Fields are from Winchester et al. (1980)

If, however, a consistent trend is noticeable through a range of plots using various major elements, which can be shown to agree with conclusions from trace element plots, they may prove useful. All of the amphibolite, epidote-pyrite schist, semipelite and most of the quartzofeldspathic groups lie in the igneous field of the Zr-Ti-Ni diagram (Fig. 4-4). Some aberrant quartzofeldspathic samples from subgroup 3 fall near the join while biotite-garnet schist samples straddle it. The elements used in this plot are considered relatively immobile during various alteration processes (Cann, 1970; Winchester and Floyd, 1976; Pearce and Gale, 1976).

A method which is particularly useful in discriminating ortho- and para-amphibolites (Evans and Leake, 1960; Leake, 1964; van de Kamp, 1969; Rehkopff, 1985) employs Niggli mg and c values (Niggli, 1954), as illustrated in Figure 4-5, in which the amphibolites and epidote-pyrite schists coincide with middle stage differentiates on the Karroo trend. However, the important features to note are pelite-carbonate and/or dolomite mixing lines along which the amphibolites and epidote schists would tend to fall if they actually were derived from such mixtures. There is no obvious tendency for the amphibolite and epidote-pyrite schist groups to follow these trends, confirming earlier observations from field evidence that they are not admixtures of pelites and dolomites and/or marls. The biotite-garnet schists samples plot dominantly within the pelite field.

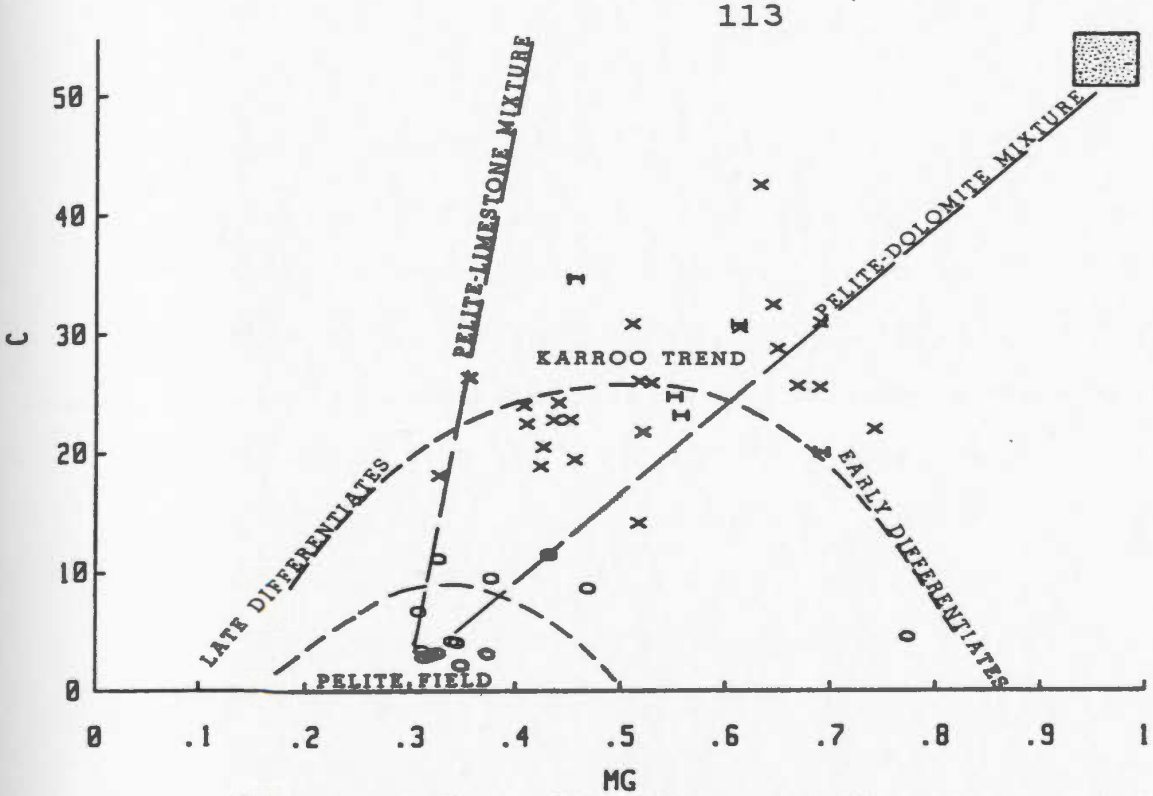

Figure 4-5: Niggli c vs. Niggli mg plot for amphibolites (X), epidote-pyrite schists (H) and pelites (oval). Most of the first two groups cluster on the Karroo trend. Stippled box represents a dolomitic composition.

4.2.2 Quartzofeldspathic Gneisses: Unit 2

The two quartzofeldspathic units (2a and 2b) have been divided into four subgroups (Table B-7. Subgroup 1 (QS1) comprises samples from various 2b units west of Cinnamon Lake; 2 (QS2) samples the leucocratic unit immediately north of the mineralized horizon; 3 (QS3) represents 2a and 2b units immediately north and south of the Boat Pond Fault and subgroup 4 (QS4) samples are from unit 2a in the sector north-east of the east end of the mineralized horizon.

Within these groups silica ranges from 62 to 80% with subgroup 3 having the highest mean value (76%). Total alkalies vary from 2 to 8.6%; subgroup 1 has the highest

mean K2O (3.6%) and subgroup 4, the highest mean Na2O (2.8%). Although the four subgroups have virtually indistinguishable major element abundances (Table 4-1) some trace element contents in subgroup 3 are much lower than in subgroups 1, 2 and 4 viz. Ba (471 ppm) and Sr (62 ppm) compared to 1200 ppm Ba and 115 ppm Sr (average) in the other subgroups; the immobile elements Y, Zr, and Nb are noticeably higher in subgroup 3 also, as are Ni and Cr.

Comparison of the major element chemistry of all four subgroups with that of typical greywackes, arkoses, rhyolites and granodiorites (Table 4-1) allows no genetic discrimination. However, van de Kamp et al. (1976) based on their work on Californian arkoses, advocated using Cr and Ni to discriminate igneous and sedimentary rocks. These elements are totally absent from subgroup 1; four (of 7) subgroup 2 samples have 1 to 4 ppm Ni; one subgroup 4 sample has 4 ppm Ni whereas several subgroup 3 samples have Cr and Ni values up to a maximum of 39 ppm Cr and 20 ppm Ni. In general, these levels are much more compatible with those of felsic igneous rocks (whose average values are 20 ppm Cr and Ni), than of greywackes (average 150 ppm Cr and 50 ppm Ni) or arkoses (112 ppm Cr and 35 ppm Ni).

The application of variation diagrams has the advantage of comparing the lithologies chemically as a group or subgroup to published data; using this approach the idiosyncrasies of individual analyses become less important in terms of an overall trend. Subgroups 1 and 2 cluster

about the igneous spectrum (Fig. 4-6A), but subgroups 3 and 4 do show some scatter towards the greywacke sector of the sedimentary field. All except one analysis of subgroups 1 and 2 define a Na2O/K2O ion exchange trend (discussed later in Ch. 5) and 70% of the samples plot in the igneous field (Fig. 4-6).

4.2.3 Semipelites: Units 1a, 1b and 1c

Although these units are lithologically dissimilar they are chemically indistinguishable and are therefore treated together. Samples comprising the semipelite groups are listed in Table B-7 and mean analyses with standard deviations in Table 4-1. Disseminated mineralization occurs sporadically throughout these units and is treated specifically in Chapter 5. SiO2 content varies from 67 to 77 wt.% in the semipelites (a range typical of rhyolites) and 64 to 80.4 wt.% in the mineralized group. Total alkalies range from 4 to 7.7 wt.% (and up to 8.3 wt.% in mineralized samples). These values are similar to, but more restricted in range than those in the quartzofeldspathic rocks.

In Figure 4-7A, the semipelites range from the felsic end of the igneous spectrum towards the ordinate with increasing K2O and decreasing Na2O. This variation in the K2O/Na2O ratio is also well demonstrated in Figure 4-7B in which the mineralized group plots at the K2O rich end. For comparison, some analyses of felsic igneous rocks are also

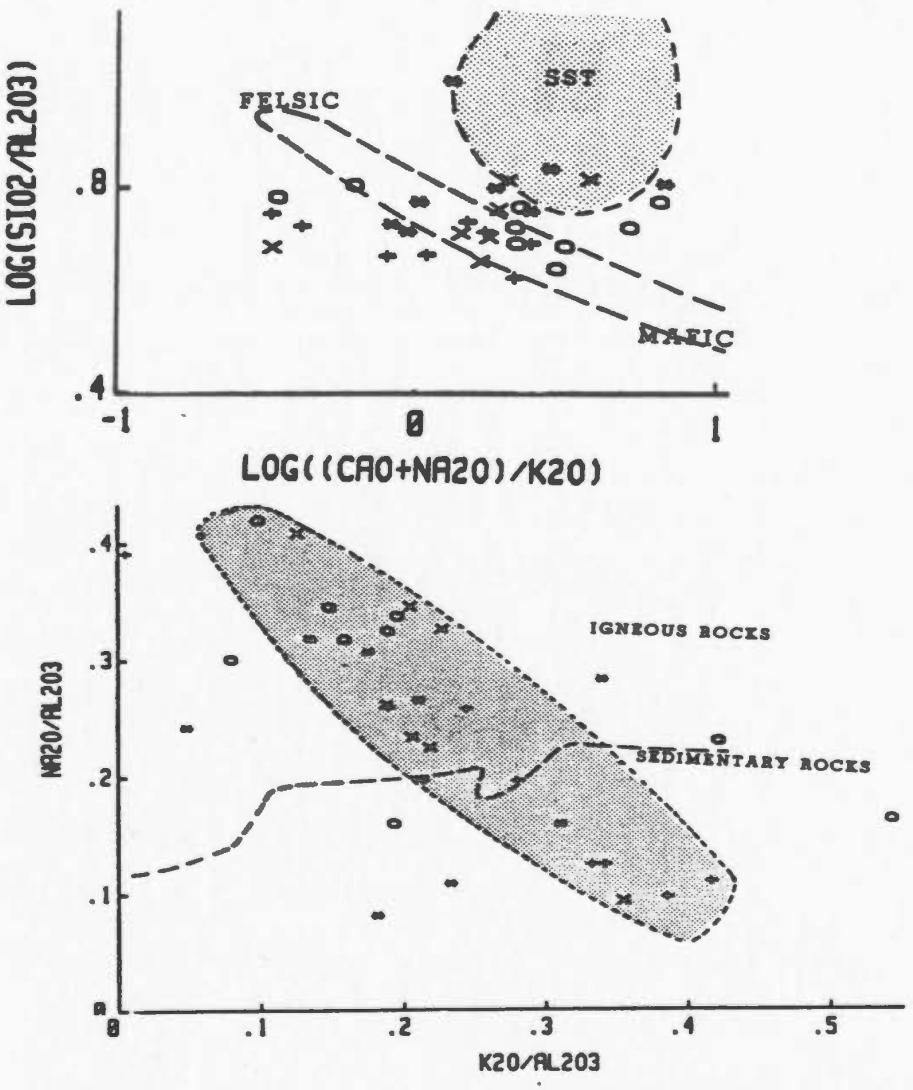

Figure 4-6: Discrimination plots for quartzofeldspathic rocks. Symbols are for subgroups QS1 (+), QS2 (X), QS3 (*) and QS4 (hexagon). Fields are from Garrels and MacKenzie (1971).

A: Log SiO2/Al2O3 vs. log CaO+Na2O/AL2o3. The field of sandstones is stippled; the dashed field defines the igneous spectrum.

B: Na2O/Al2O3 vs. K2O/Al2O3. Field containing QS1, QS2 and some of QS3 and QS4, is stippled. Data overlaps both igneous and sedimentary fields.

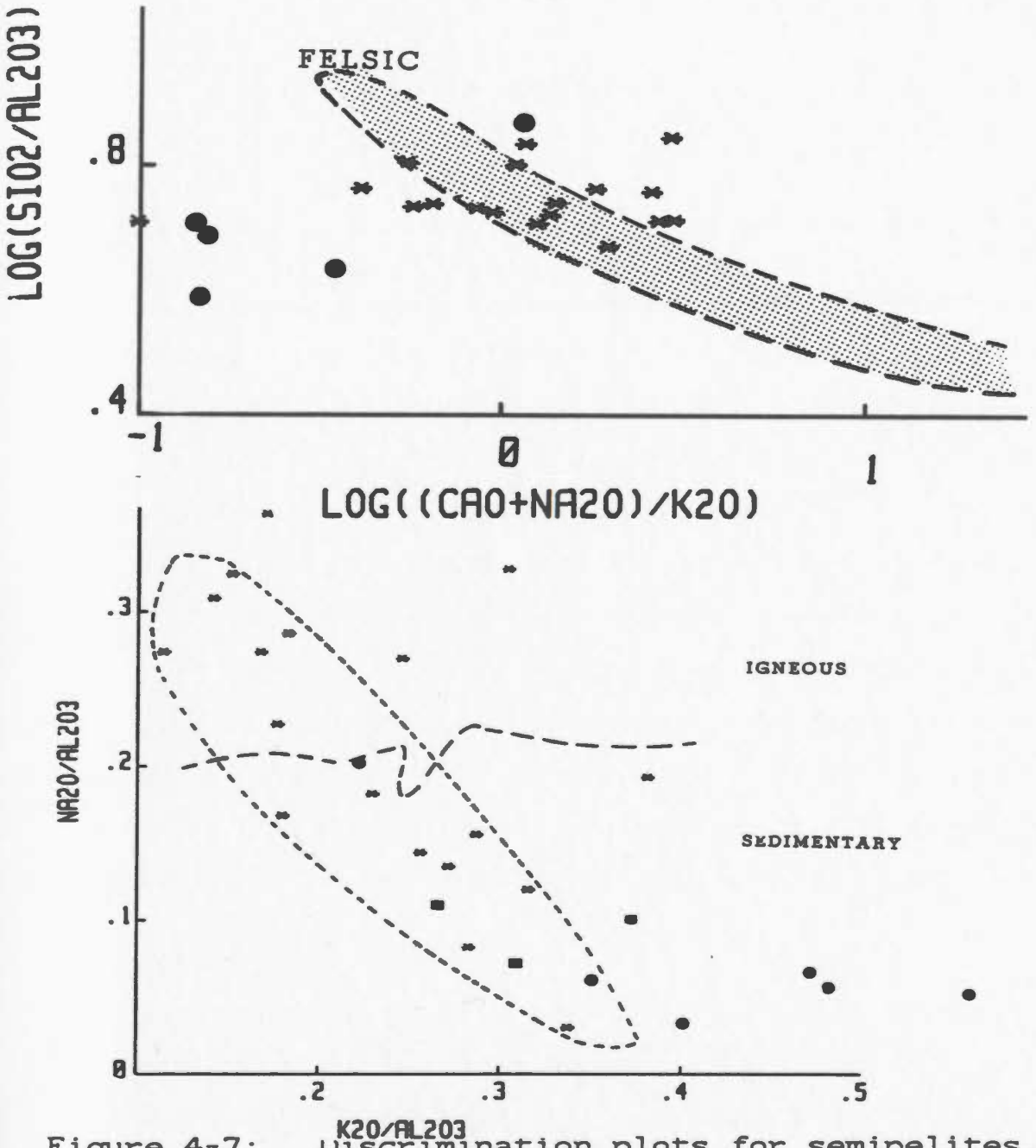

Figure 4-7: Discrimination plots for semipelites. A:Log SiO2/Al2O3 vs log CaO+Na2O/Al2O3 B: Na2O/Al2O3 vs K2O/Al2O3. Fields are as defined in Figure 4-6. Closed circles in both plots are mineralized samples; closed squares in B are felsic flows and tuffs from the Bay du Nord Group (Wynne, 1983)

shown on the plot (note similarity to the trend defined by the quartzofeldspathic groups in Fig. 4-6).

4.2.3.1 Relationship between the Gneisses and Semipelites

The clear chemical similarity between the quartzofeldspathic and semipelitic groups is evident from Table 4-1 and a comparison of the plots discussed. Therefore although there is greater scatter within the quartzofeldspathic group, attributed to its larger population, the two lithologies are treated together.

In a detailed petrographic and provenance/geochemistry study of Californian arkoses, van de Kamp et al. (1976) concluded that a plot of Zr and Niggli al-alk is particularly useful in differentiating igneous and sedimentary trends. Thus the two points to note in the Zr vs. al-alk plot of semipelitic and quartzofeldspathic rocks (Fig. 4-8) are:

(1) the narrow spread of Zr values, although within two groupings (discussed later) and
(2) the marginally positive or flat slope.

Both of these features contrast with:

(1) the spread of values and
(2) the vertical trend (or lack of correlation) exhibited by sedimentary rocks.

This and other Niggli Number plots have been used by several

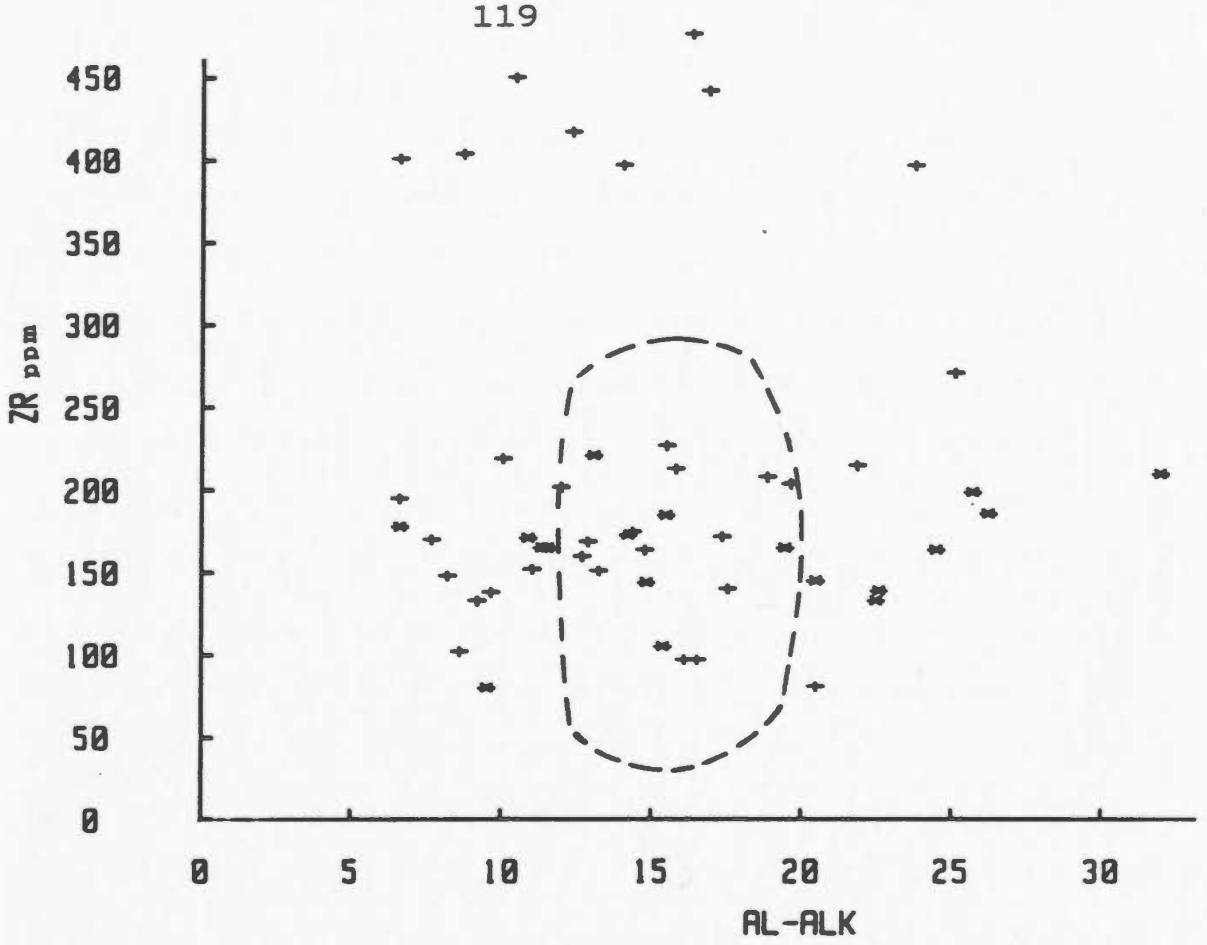

Figure 4-8: Zr vs. Niggli al-alk for semipelites (*) and quartzofeldspathic rocks (+); dashed field is defined for sedimentary rocks (van de Kamp et al., 1976)

authors in discriminating the precursors of highly metamorphosed rocks (Senior and Leake, 1978; Leake, 1980; Rehkoppf, 1985). The quartzofeldspathic subgroup 3 (and 4 to a lesser extent) shows the most scatter (as in Fig. 4-6A). Although subgroup 3 represents both 2a and 2b units, this does not seem to be the underlying reason for its behaviour, as examination of the chemical analyses for samples 7a and 7b shows. These samples represent adjacent bands (actually depicted in Fig. 2-6) however their chemistry is quite different (Appendix Table B-3) suggesting

a sedimentary affinity reinforced by the regular banding. The discriminating methods above, particularly those involving the immobile trace elements, suggest that the semipelites and some of the quartzofeldspathic rocks (subgroups 1 and 2) which occur north of the mineralized horizon, have a stronger igneous affinity than groups 3 and 4. Thus semipelites and groups 1 and 2 are considered more direct products of igneous activity i.e. felsic tuffs. The partial igneous character, as in the Zr-Ti-Ni plot (Fig. 4-4) and lithological characteristics of subgroups 3 and 4 suggest they are volcanoclastic greywackes. The quartzofeldspathic unit 2a (subgroup 2) immediately north of the mineralization, is homogenous, i.e. relatively unbanded (compared to unit 2b), and may represent an extrusive rhyolite.

To substantiate or negate an igneous afinity of the semipelitic and quartzofeldspathic rocks, they are compared (Fig. 4-9) to felsic volcanic and plutonic rocks of Western Chihuahua, Mexico (Bagby et al., 1981). These Mexican rocks were chosen after a literature search for fresh volcanic rocks for which a range of trace and major element plots were available.

Although there is some scatter, both the trends and the abundances of the immobile elements Zr and Nb in the Isle aux Morts rocks are very similar to those of quartz diorites, granodiorites and intermediate rocks from Chihuahua. In the Zr vs. Nb plot (Fig. 4-9A) there is a

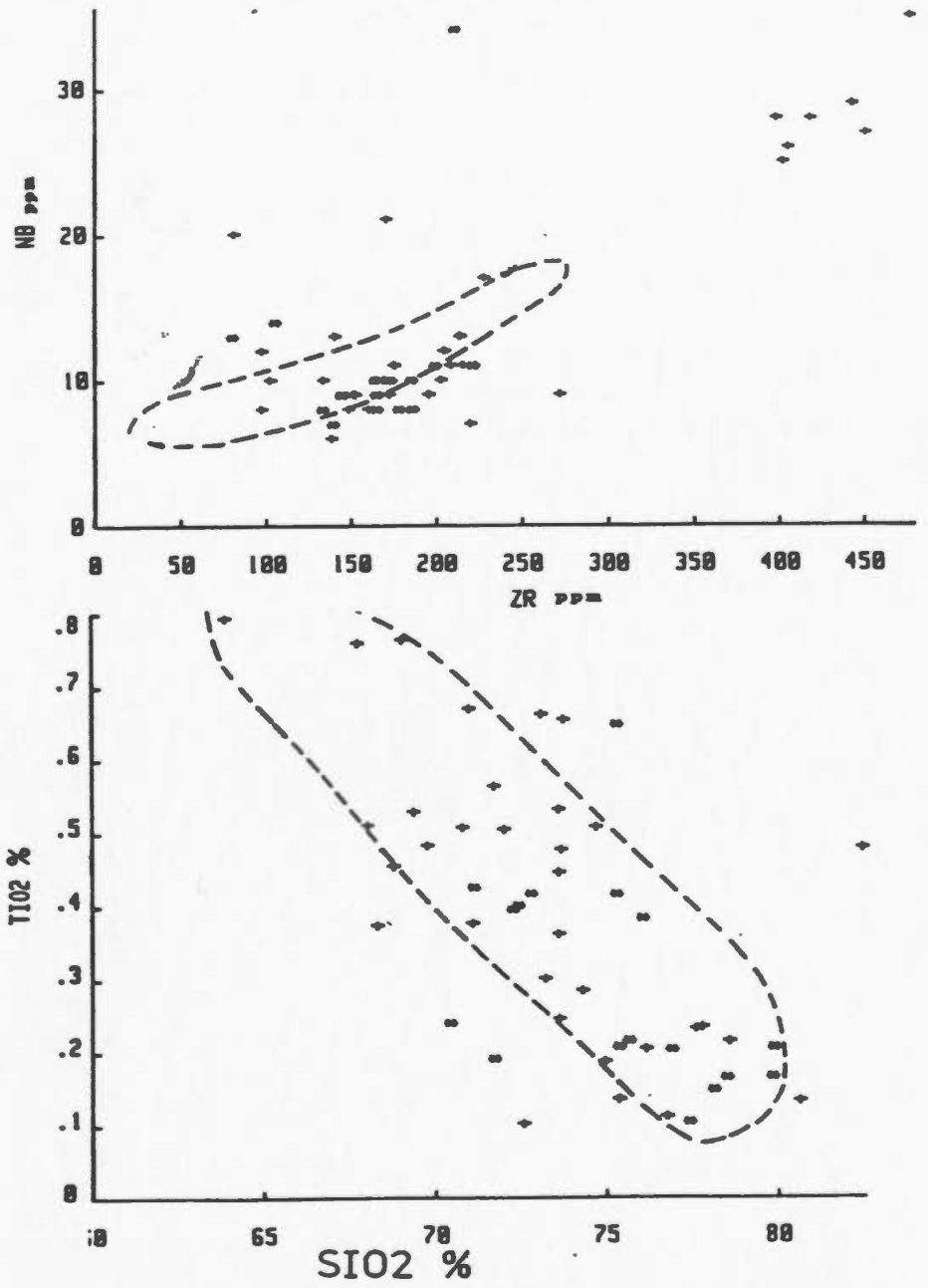

Figure 4-9: A: Nb vs. Zr and
B: SiO2 vs. Sr plots comparing semipelites and quartzofeldspathic rocks from Isle aux Morts to plutonic and volcanic rocks from Chihuahua (fields for the latter rocks are outlined by dashes (Bagby et al., 1981.

minor clustering of quartzofeldspathic samples from subgroups 3 and 4 at approximately 400 ppm Zr and 27 ppm Nb; these samples also have higher Y contents and generally higher Fe2O3 than the main group. Precisely why this minor

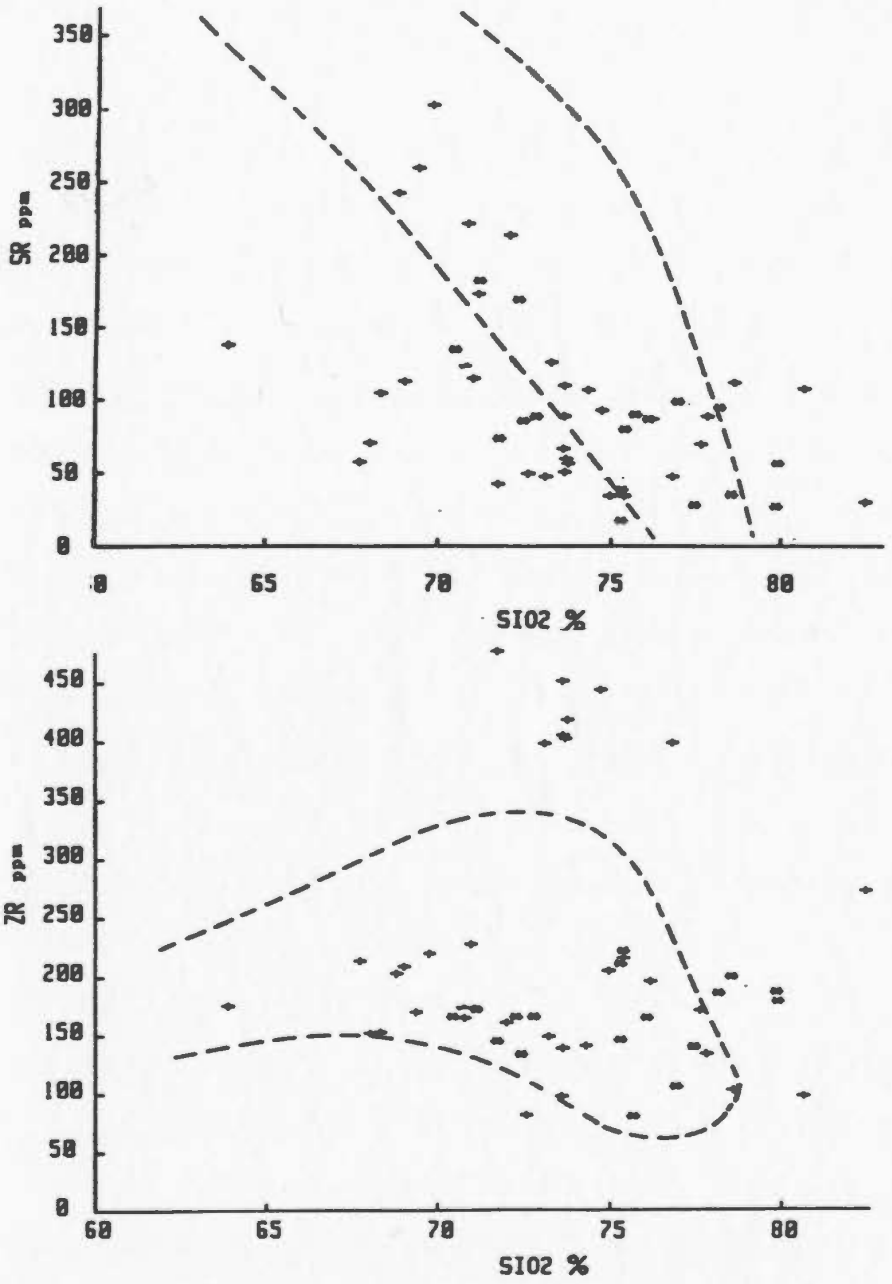

Figure 4-10: A: SiO2 vs. TiO2 and
B: SiO2 vs Zr plots comparing semipelites and quartzofeldspathic rocks from Isle aux Morts to volcanic rocks from Chihuahua (Bagby et al. 1981) Fields represent rhyolitic ignimbrites.

clustering occurs is unclear; as mentioned above, samples Fs7A and Fs7B are interbanded but they actually fall in the different groupings. The combination of a tight clustering

(an igneous feature) with the banding (a sedimentary feature) suggests marginally differing sources providing detritus to felsic tuffs and/or volcanoclastic greywackes.

The absence of the typical spread in values expected from sedimentary rocks may be explained by the relatively small area sampled. Zr also shows two concentrations of values for the same SiO2 value in Figure 4-10B. In SiO2 vs. TiO2 (Fig. 4-9B) there is a minor subgrouping which does not correlate with the minor clustering discussed above. Sr is depleted in all subgroups, particularly in subgroup 1 (and less so in subgroup 3) when compared to the fresh analyses. Most of those samples depleted in Sr are relatively enriched in K2O Op(and therefore Rb). In all these plots there is virtually complete overlap of the semipelite and gneiss groups.

The semipelites are schistose with marginally higher Al2O3 and higher K2O (particularly those that are mineralized). Ubiquitous disseminated pyrite, with galena, sphalerite, chalcopyrite occur less commonly along with occasionally banded sulphides. It is this mineralization that mostly distinguishes the semipelites from the quartzofeldspathic rocks. These sulphides appear to be an integral component of the rock and are therefore thought to be pre-metamorphic. However, whether they were precipitated syngenetically or epigenetically from mineralising fluids or were tuffaceous material is unknown. As the igneous nature of the majority of these quartzofeldspathic and semipelitic

rocks can be reasonably inferred, an igneous classification diagram is applied (4-11).

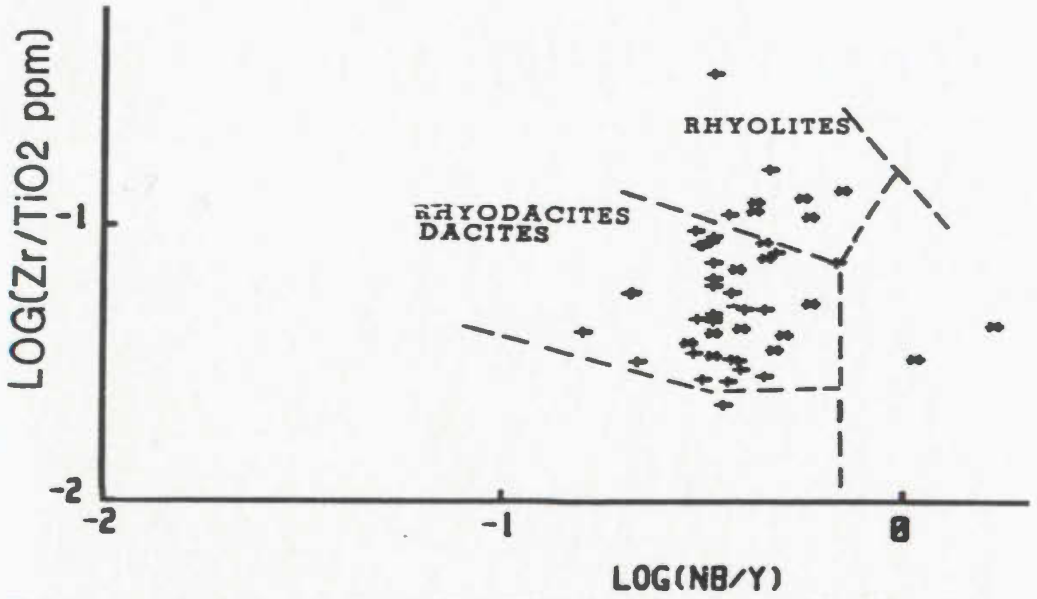

Figure 4-11: Log Zr/TiO2 vs. log Nb/Y plot for quartzofeldspathic and semipelitic rocks; (fields from Floyd and Winchester, 1978)

Virtually all the rocks cluster tightly within the rhyodacite/dacite field on the log Zr/Ti vs. log Nb/Y plot (Fig. 4-11).

The rare earth element pattern for both the quartzofeldspathic and semipelitic groups are very similar and they are described together (Fig. 4-12). Samples done by instrumental neutron activation analysis have broadly similar slopes to those analysed by wet chemical methods. However, Tb data in samples done by XRF at MUN are noticeably higher, especially in semipelites, and at least to some extent, reflect the odd behaviour of Tb in the thin film method (Fryer, pers. comm., 1985). Note however, that

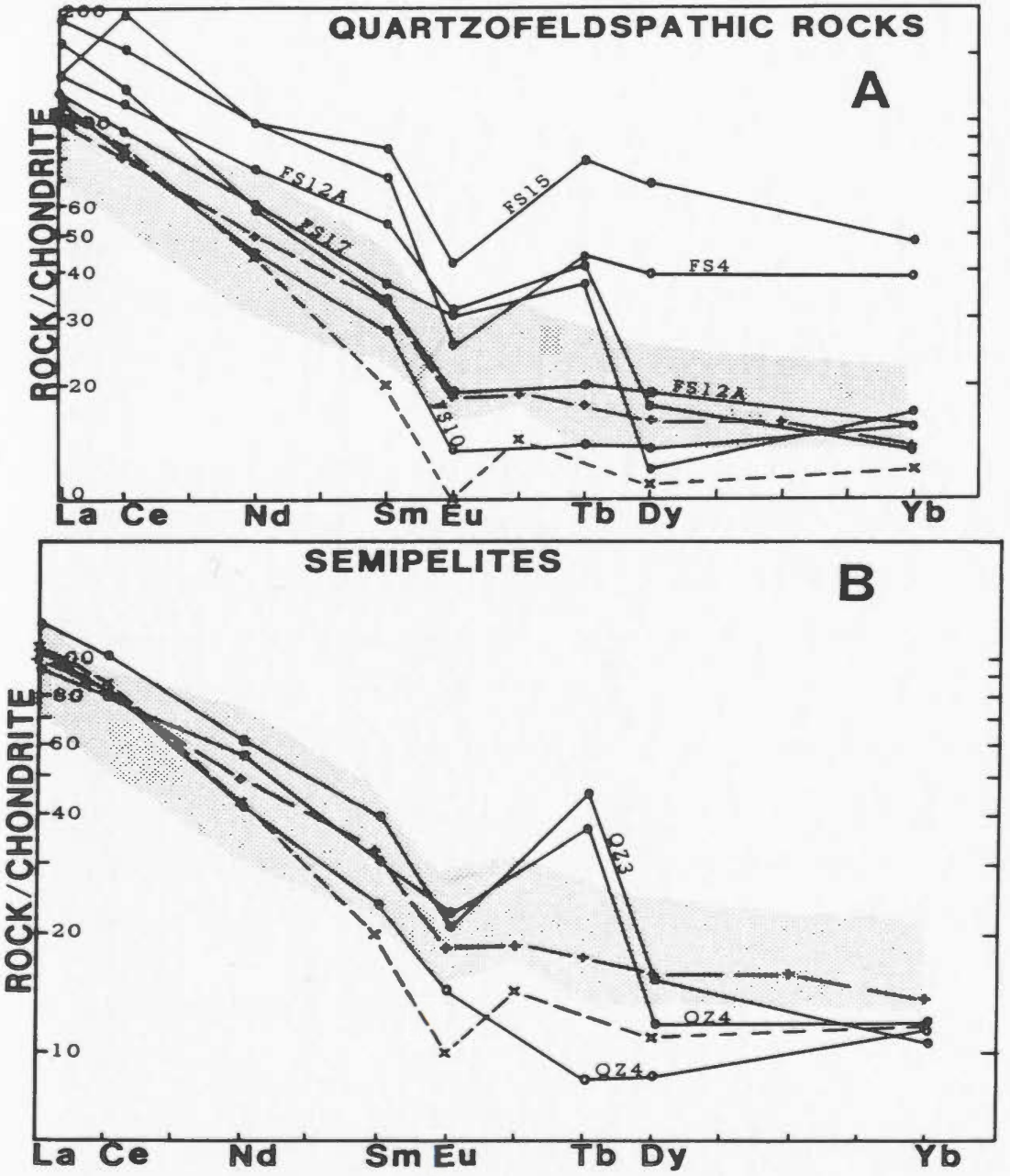

Figure 4-12: Chondrite normalized rare earth element patterns for quartzofeldspathic (A) and semipelitic (B) rocks. Stippled area in both plots defined by rhyolites/dacites from Chihuahua (Bagby et al. 1981). Symbols; Closed circles are those done by the thin film/XRF method (Fryer, 1977) at MUN and open circles are those done by neutron activation analysis. The pattern in crosses (X) defines the average sub-greywacke (Nance and Taylor, 1976) while that in (+) is the North American Shale Composite (Haskin et al., 1968)

Tb in Fs4 in Figure 4-12 (done by NAA) is also relatively elevated. Variable Tb also accounts for the differences between Fs12A and QZ4 by thin film and NAA methods. Both quartzofeldspathic and semipelitic groups show similar patterns with enriched light rare earth elements and Eu anomalies. Patterns for 5 rhyolites and dacites from Western Chihuahua are shown for comparison, as well as some sedimentary trends. Abundances in both semipelitic and quartzofeldspathic rocks are consistently higher than those of the average sub-greywacke. The NASC shale pattern is quite flat from Eu through Yb, as is QZ4 (by NAA but not by thin film; note Tb). The quartzofeldspathic and semipelitic rare earth element patterns are similar to those of the Mexican rhyolites, as in trace and major elements. The semipelite patterns are discussed further in Chapter 5.

4.2.4 Biotite-Garnet Schists: Unit 1d

Samples comprising the biotite-garnet schist are listed in Table B-7 and the mean analyses in Table 4-1. A strong sedimentary affinity has been defined for this unit in section 4.2; this is reiterated in Figure 4-13B in which the biotite-garnet schist group falls in the shale field.

On the Zr/TiO2 vs. Ni plot (Fig. 4-4), the group overlaps both the sedimentary and igneous fields. In Table 4-1, one average shale analysis is given for comparison with the biotite-garnet schist.

The high total Fe, Cr and Ni contents suggest a

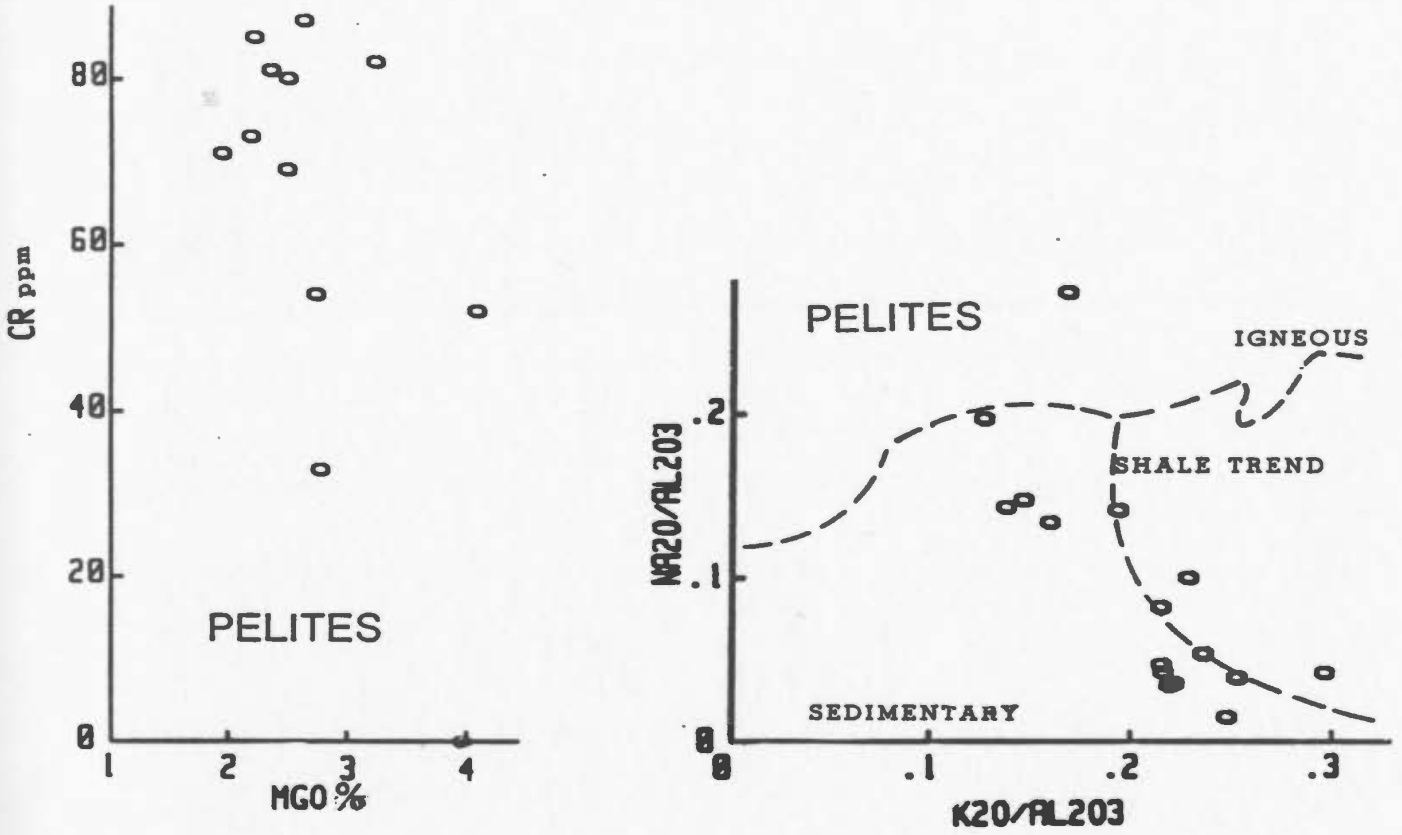

Figure 4-13: A: Cr vs. MgO and
B: Na2O/Al2O3 vs. K2O/Al2O3 plots
for pelites (fields in B from
Garrels and MacKenzie, 1971).

provenance containing mafic igneous rocks. If the Cr and Ni were added as mafic detritus (i.e. a mafic tuff) a positive correlation would be expected with MgO (Figure 4-13A). Although no correlation is evident, the number of samples may not be great enough to produce one. In Figure 4-13B the pelites fall on the shale trend line (Garrels and MacKenzie, 1971) which intersects the sedimentary/igneous join at the composition of the average igneous rock. The pelite trend however, diverges towards the mafic area and suggests a provenance dominated by mafic rocks.

An analysis of a garnet quartzite (coticule) is given

in Table B-5. This unusual rock has 2 wt.% MnO which is very high compared to MnO contents in other rocks. Coticules have been recognized in the Gossan Lead District (Gair and Slack, 1984) and a coticule analysis from there is included in Table 4-1 for comparison. Coticules, by their nature (thinly bedded) are difficult to sample for geochemical purposes, and numerous quartz veins in the sample from Isle aux Morts have probably diluted the MnO content.

4.2.5 Amphibolites and Epidote-Hornblende-bearing rocks: Unit 3

The mean analyses of these rocks are quite similar, except for higher Al2O3, K2O and Ba in the epidote schist and higher maximum values of total Fe, MgO and CaO in the amphibolites. Therefore they are treated together in this section.

A first pass discriminant test on the amphibolite and epidote-pyrite groups has established that the rocks are of mafic igneous origin (e.g. rather than impure dolomites). Field evidence also indicates (section 2.1.5.2) that the epidote-pyrite group probably represents mafic tuffs. A geochemical analysis of one of the amphibolitized ultramafic rocks, is given in Appendix Table B-6); the rock contains approximately 30 wt.% MgO and is similar to a peridotite in composition.

4.2.5.1 Alteration of the Amphibolites

Since the amphibolites may have undergone one or more alteration events, it is important prior to any type of classification, to establish if possible, what elements were mobile and to what extent. For example on Hughes' (1973) diagram the Isle aux Morts amphibolites show much alkali mobility (Fig. 4-4).

In the past decade, many studies (Cann, 1970; Pearce and Cann, 1973; Floyd and Winchester, 1975, 1978; Winchester and Floyd, 1976, 1977; Pearce, 1980) have indicated the relative immobility of the high field strength elements such as Zr, Nb, Y, Ti and the heavy rare earth elements, from low temperature to amphibolite facies conditions, during alteration processes. An excellent review of this topic is given by Goff (1984).

To evaluate the extent of metasomatic alteration of the amphibolites, a procedure suggested by Davies et al. (1979) is adopted (their method is actually a modification of a technique developed by Beswick and Soucie, 1978). As K_2O is incompatible during magmatic fractionation of mafic rocks, it remains constant relative to such elements as Al_2O_3, TiO_2 etc. Plots of these major and trace elements, with K_2O as denominator, will therefore generate straight lines as fractionation proceeds. Since metasomatic processes effectively mobilize K_2O, deviations from straight line graphs can be attributed to such processes (as they will not normally generate straight lines unless different elements are mobilised by precisely equivalent amounts).

Although the 23 amphibolites do generate approximately linear trends, there is obvious scatter in most plots (Figs. 4-14A and B are shown as representative plots).

The results of a number of these plots (which are not all shown) indicate that SiO2, Al2O3 and TiO2 apparently show low mobility, FeO and MgO are moderately mobile and P2O5 is apparently very mobile. The traces Nb and Y are relatively immobile with Zr being moderately immobile and Cr and Ni show the greatest amount of scatter. An analysis of a number of these plots revealed that the same samples were causing the aberations in each plot. These analyses were eliminated from subsequent plots leaving 13 samples which were considered to be reasonably representative of the source rocks, i.e. apparently showing the least effects of any metasomatic alteration. The limited mobility of most elements of interest, for classification purposes, is illustrated in Figures 4-14C and D; these are representative plots. The oxide P_2O_5 and trace element Zr, used in trace element discriminant diagrams later, still display some scatter which needs to be borne in mind during classification.

4.2.5.2 Magmatic Classification

The amphibolites are sub-alkaline basalts in magma-type discrimination diagrams (Fig 4-15).

The diagrams have also been shown to be useful with altered and metamorphosed igneous rocks (Floyd and

Figure 4-14: A: Y/K2O vs. Zr/K2O and B: MgO/K2O vs. Al2O3/K2O are two representative molecular proportion plots illustrating the scatter in values of the amphibolites which reflects varying alteration/mobility of certain elements. Those samples falling off the line are omitted in most future plots. C: Nb/K2O vs Y/K2O and D: Al2O3/K2O vs. SiO2/K2O are two representative plots of screened amphibolites, i.e. those apparently showing the least effects of alteration/mobility. The lines on all plots are visual best fits.

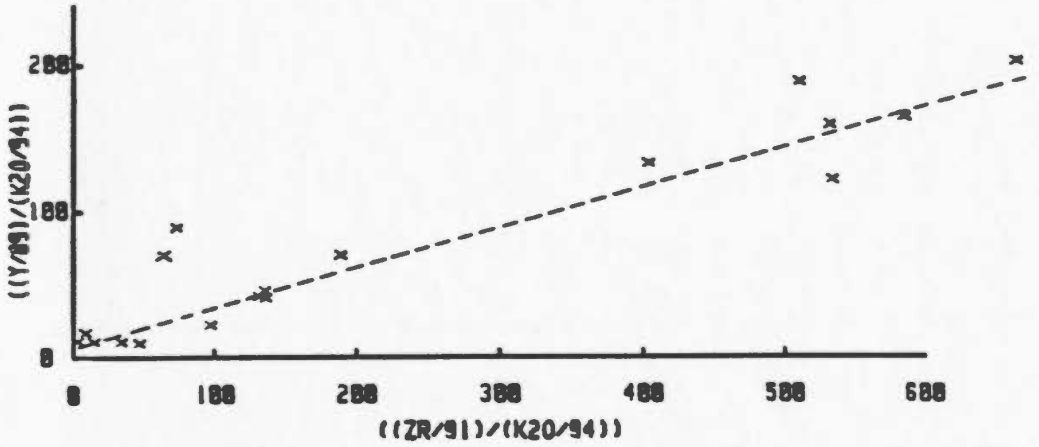

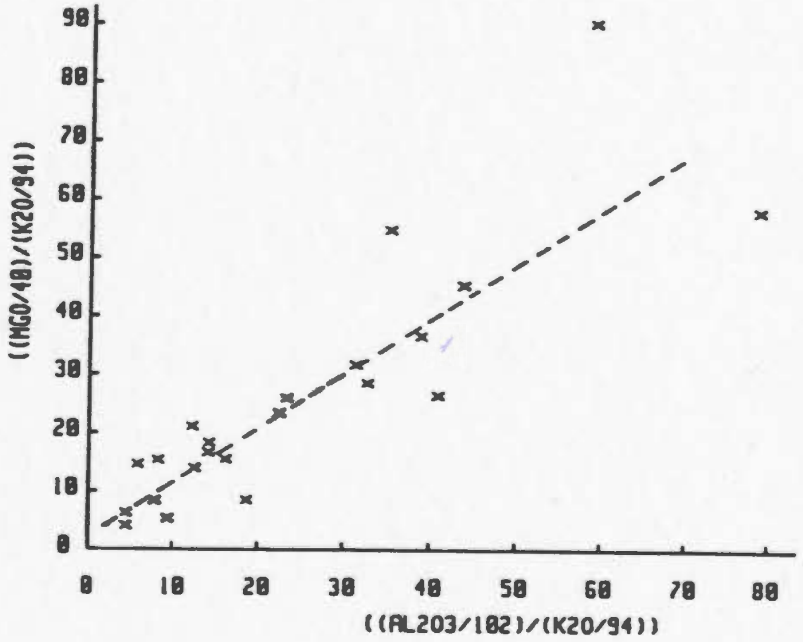

AMPHIBOLITES

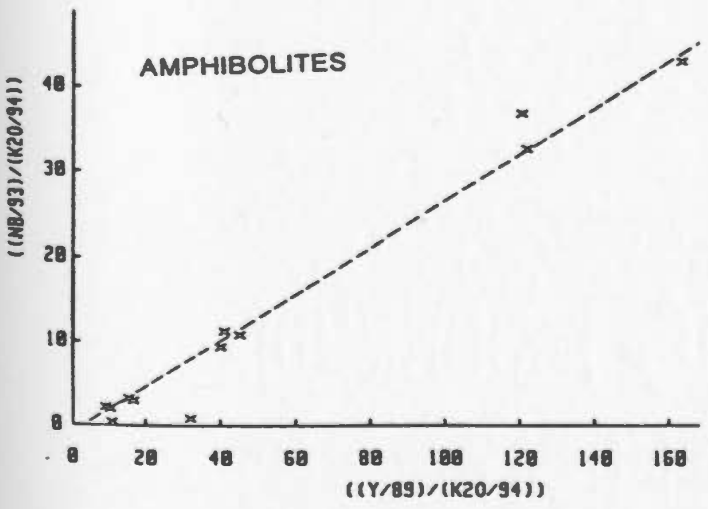

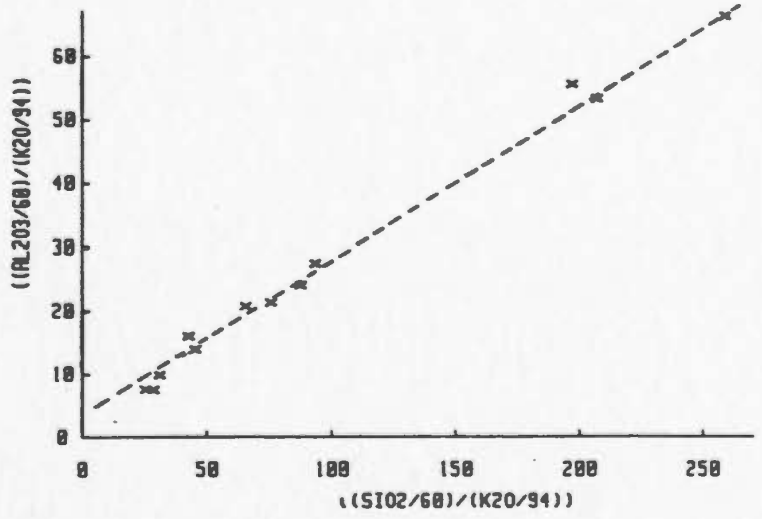

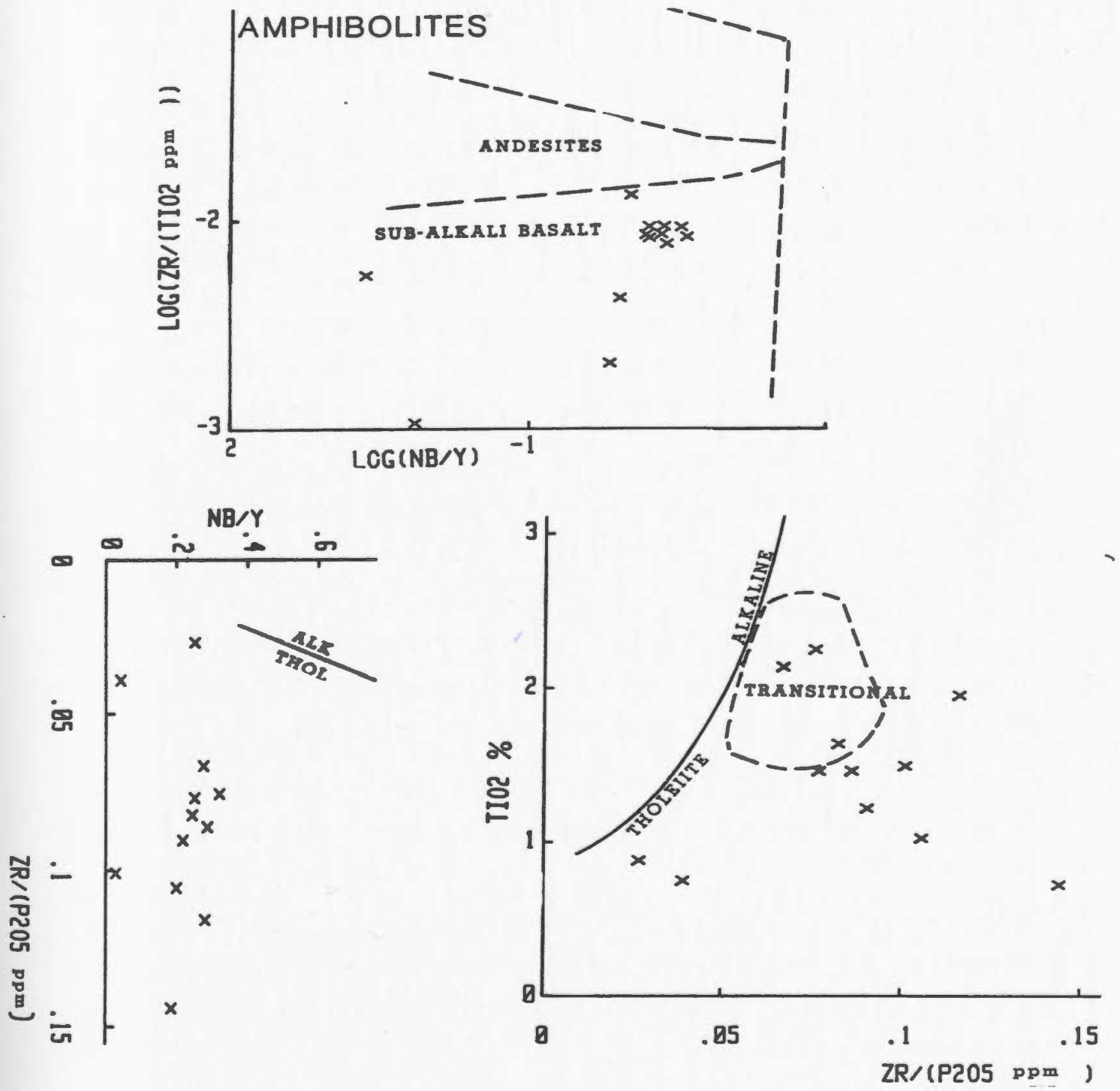

Figure 4-15: Magmatic discrimination diagrams for the Isle aux Morts amphibolites. A: log Zr/TiO2 vs. log Nb/Y (fields from Floyd and Winchester, 1978). B,C: Nb/Y vs. Zr/P_2O_5 and TiO_2 vs. Zr/P_2O_5; fields are from Floyd and Winchester (1975).

Winchester, 1978) as immobile trace elements are used. Their tholeiitic nature is reiterated in Figures 4-15B and C (Floyd and Winchester, 1975) although TiO2 appears to imply a more alkaline condition. However Nb/Y is a more sensitive indicator of alkalinity than TiO2 which, particularly with respect to transitional basalts, is unable to discriminate clearly between tholeiitic and alkaline types (Goff, 1984). The AFM plot similarly, cannot distinguish these amphibolites due to the wide range in alkalies and sharply decreasing FeO/MgO. A more effective method of determining the presence of a trend is illustrated by a Y-T-C diagram (Fig. 4-16) of Davies et al. (1979). TiO2 behaves similarly to FeO (e.g. both are enriched in tholeiitic suites) while Zr and Y typically increase during fractionation (behaving like alkalies) and the variation in MgO content is usually reflected by Cr. Archaean calc-alkaline and tholeiitic trends (Davies et al. 1979) are shown for comparison. However Goff (1984) considered these Archaean rocks to be altered and he redrew the field using Phanerozoic compositions. There is clearly more cohesion between the tholeiitic fields/trends and the amphibolites than with the calc-alkaline suites. Magmatic discriminants therefore indicate a tholeiitic basalt as the original source rock. Note that in Figure 4-16 the amphibolites form two groups, one Cr-rich and one Cr-poor. This grouping will be noted again later.

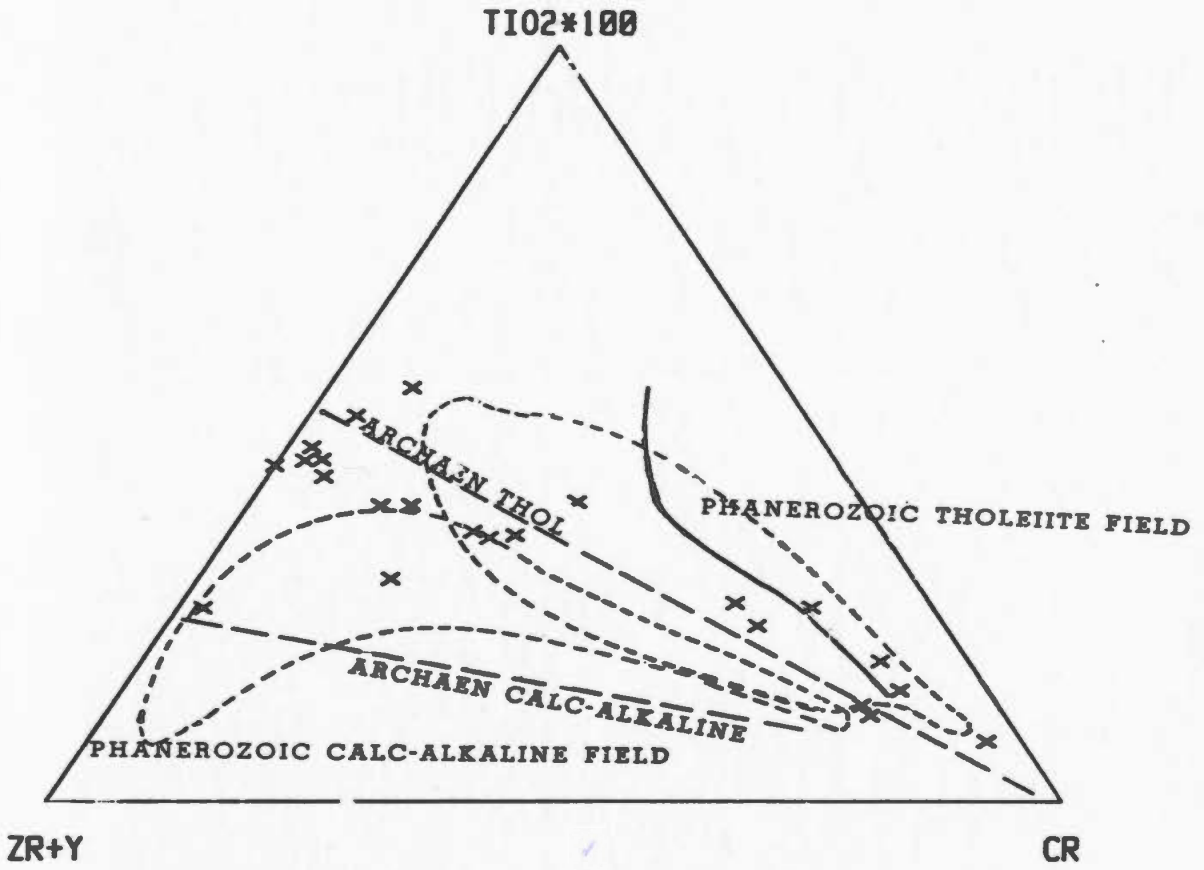

Figure 4-16: Zr+Y-TiO_2-Cr plot for amphibolites with fields from Davies et al. (1979) and Goff (1984).

4.2.5.3 Amphibolites and Tectonic Environment

On a Zr-Ti-Y plot the amphibolites resemble plate margin basalts (Fig. 4-17). Zr contents, which range from 8-300 ppm with a mean of 125 ppm, are equally comparable with island arc and ocean-floor basalt suites (Basaltic Volcanism on the Terrestrial Planets, BVTP, 1981). Whether this variation in Zr which has already been noted during screening of the amphibolites for anomalous samples, is a result of fractionation trends in the source rock, crustal (sialic) contamination or the presence of more than one amphibolite type, is unclear.

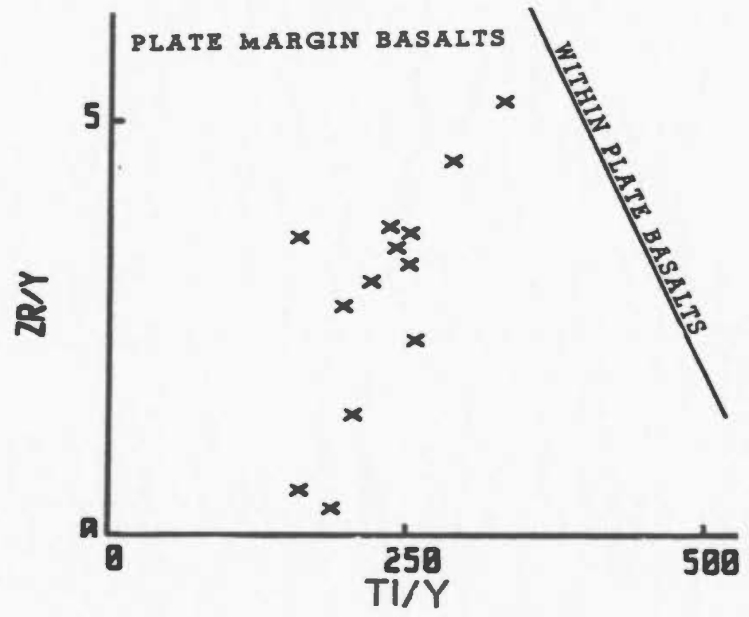

Figure 4-17: Tectonic classification diagram for amphibolites; Zr/Y vs Ti/Y plot (fields from Pearce and Gale, 1977).

Cr was also noted as being variable and this is evident in the Cr vs. TiO2 plot (Fig. 4-18) in which screened amphibolites of a high Cr group fall in the ocean floor basalt field while a low Cr group plot as island arc basalts. In the Cr vs. Y plot the high Cr group of amphibolites have a distinct MORB affinity and virtually all amphibolites are clearly separated from island arc tholeiites (Fig. 4-18B). Mafic rocks of the Victoria Lake Group (Dunning, 1984) are plotted for comparison on this diagram and on a TiO2 vs. Zr plot (Fig. 4-18C). There is virtually complete overlap between these two groups. The Victoria Lake Group is bimodal, comprising rhyolites/dacites and basalts. The Victoria Lake basalts have variable chemistry, alternately suggesting affinities with MORBs and

Figure 4-18: Tectonic setting discriminant diagrams for Isle aux Morts amphibolites; A: Log Ti vs. log Cr plot is unable to distinguish between island arc tholeiites (IAT) and ocean floor basalt (OFB) affinity (fields from Pearce, 1975). B: Cr vs. Y plot shows a distinct correlation with mid ocean ridge basalts (MORBs) (fields from Pearce, 1980). C: TiO_2 vs. Zr plot is similar to B. The fields are from Pearce (1980). In B and C the stippled region defines the field of mafic rocks from the Victoria Lake Group (Dunning, 1984). D: FeO vs. log Zr/TiO_2 (Goff, 1984); note strong positive (tholeiitic) trend of Fe enrichment.

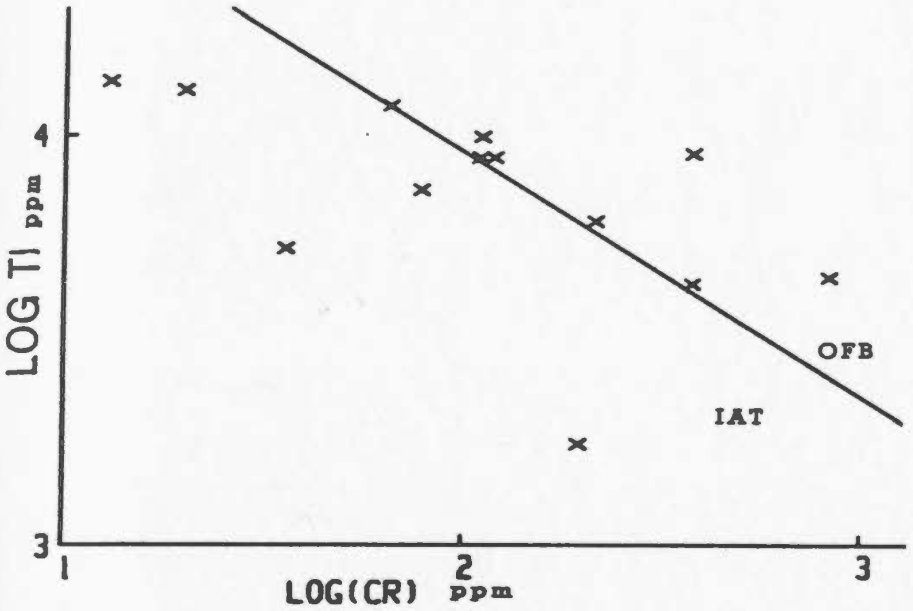
LOG TI ppm
4
3
1
2
3
LOG(CR) ppm
OFB
IAT

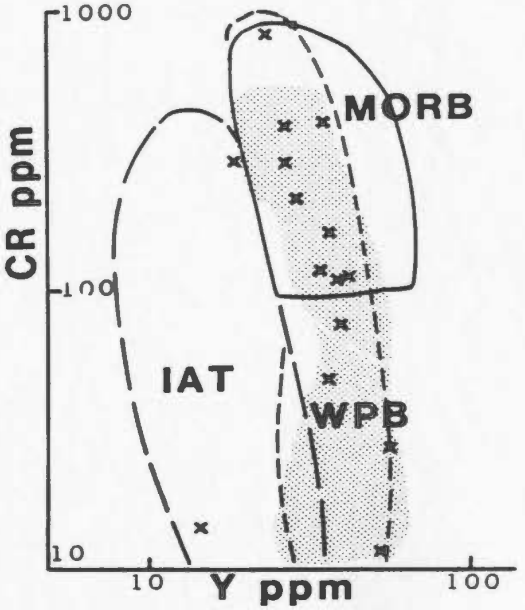
1000
100
10
CR ppm
MORB
IAT
WPB
10
Y ppm
100

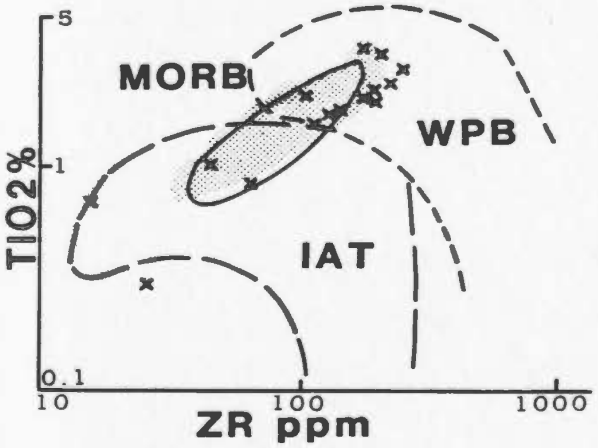
5
1
0.1
TIO2%
MORB
WPB
IAT
10
100
1000
ZR ppm

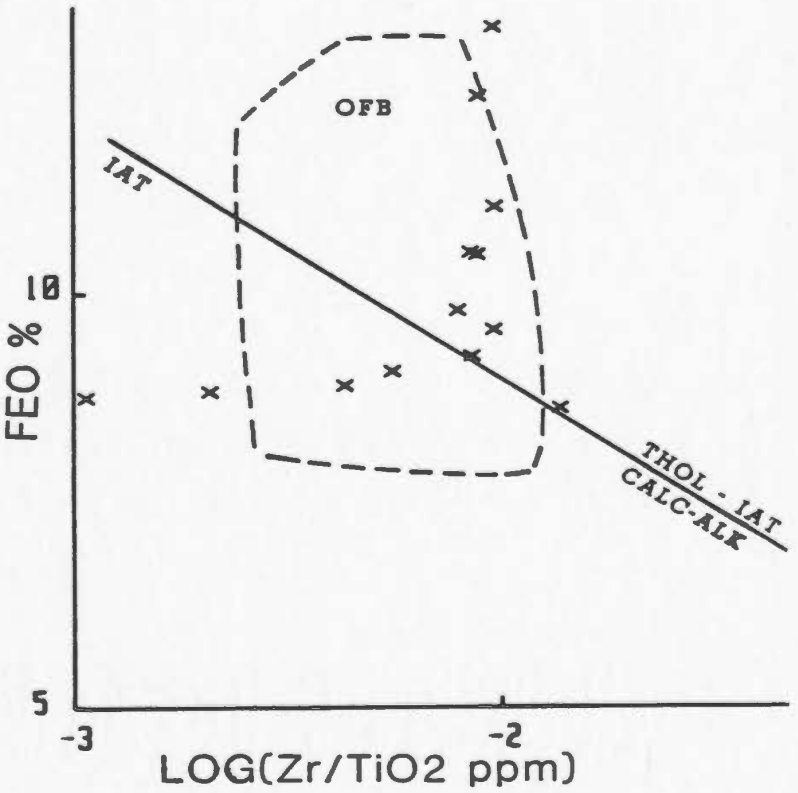
OFB
IAT
10
FEO %
5
-3
-2
LOG(Zr/TiO2 ppm)
THOL - IAT
CALC-ALK

IATs, but trace element data imply MORBs (Dunning, 1984). In the TiO2 vs. Zr plot, although several samples fall in the IAT field, most amphibolites show a distinct MORB affinity also. These were found to be among the samples that define the high Cr group, noted above. Amphibolite data reduction using variation diagrams, revealed two distinct amphibolite groups. Group 1 is characterized by high MgO, CaO, Cr, Ni and consistently low silica, TiO2, P2O5, Nb, Y, Zr and V compared to the second, high silica group (c.f. Fig. 4-2). The epidote, pyrite ± hornblende schists are generally more akin to the low silica group. Two of the amphibolites (i.e. 83/97B which is actually the "porphyroclastic" rock of section 2.1.5.2 and 83/95) from the low silica group are actually associated with these mafic meta-tuffs in the northern part of claim block 2850. The remainder of the low silica group, with one exception, are samples from drill core representing unit 2a, immediately north of the mineralized horizon. The one exception is Tr3-4 which samples the amphibolite on the immediate (structural) hanging-wall (see Map 2). Group two (high silica) amphibolites are not restricted to any particular location or lithology.

Amphibolites of group 1 comprise supposed meta-fragmentals in the north of Map 2 and may represent sills or dykes as seen in unit 2a (adjacent to the Twin Ponds Showing). The suite of tectonic environment classification plots used here, can distinguish ocean floor basalts from

basalts of other regimes with the possible exception of primitive island arc tholeiites (BVTP, 1981).

Although Zr/Nb abundances do not distinguish ocean floor basalts and island arc tholeiites (BVTP, 1981) high Cr and Ni values are more typical of the former suite. However TiO2 levels in the low silica group are similar to those of primitive arc tholeiites (0-1%) whereas TiO2 in the high SiO2 group (1.4-3%) is MORB-like (BVTP, 1981). However the Ti/Zr ratios of both groups of amphibolites of this study are much higher (150:1) than primitive arc basalts (10:1). On MgO vs. Ni plots, MORBs typically show a strong positive trend (as do the Isle aux Morts amphibolites) while arc basalts show a flat trend (BVTP, 1981)

Although the large, low valency cations in the Isle aux Morts amphibolites eg. K, Rb, Sr, and Ba have abundances more typical of arc basalts than ocean floor basalts, these elements are too mobile during alteration and cannot be used for discriminant purposes. Al2O3, TiO2, Cr and Ni abundances are similar to those of ocean floor basalts. Noting the importance of the FeO enrichment trend as being typically tholeiitic, Goff (1984) devised a FeO vs. Zr/TiO2 plot on which calc-alkaline trends are typically negative while tholeiitic are positive. The screened amphibolite which contain samples from both groups show a strong FeO enrichment trend, typical of ocean floor basalts (Fig. 4-18D).

Chondrite-normalized rare earth element (REE) patterns

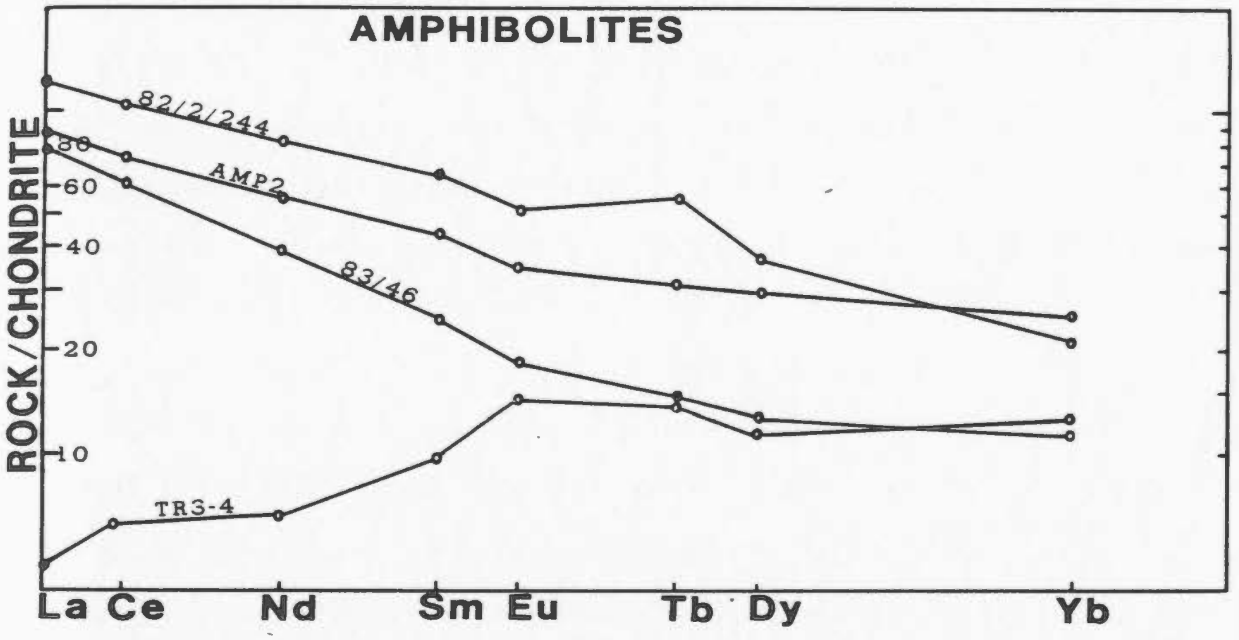

Figure 4-19: Chondrite normalized rare earth element patterns for amphibolites from the Isle aux Morts Prospect. 82/2/244 was analysed by the thin film method and the other three samples were analysed by NAA.

for 4 amphibolites are presented in Figure 4-19. The most divergent patterns and abundances occur in the light REEs, while most heavy REE patterns are flat with abundances from 11 to 25 times chondrite (at Yb). Goff (1984), in a literature review, noted that light REEs are mobile (the extent depending on the alteration process) while heavy REEs are immobile, behaving similarly to Zr, Nb and Y, etc. Menzies et al. (1979) and Hajash (1984) report the results of experimental work on basalts at greenschist and amphibolite facies conditions (150-600 ^{o}C) suggesting that REE abundances and distribution patterns are essentially identical to those of the unaltered rock.

Sample Tr3-4 is from the low silica, high Cr group and

shows light REE depletion at approximately 2 to 10 times chondrite. This particular sample is very fine-grained, homogenous and immediately adjacent to the mineralized horizon. The remaining samples are from the high silica group and have more elevated light REEs. Sample Tr3-4 and heavy REE abundances of the other three samples can be compared to either ocean floor basalts (they are similar to those from the Annieopsquotch Complex, Dunning, 1984) or to island arc tholeiites (as in Jakes and Gill, 1970) e.g. the Sunda Arc basalts (BVTP, 1981). Alternatively, the light REEs may reflect metasomatism. However as basalt fractionation proceeds, negative Eu anomalies develop due to feldspar fractionation. A slight Eu anomaly is evident in 82/2/244 which is apparently the most highly evolved pattern. Such an anomaly suggests that original patterns are retained.

4.3 Summary and Discussion

The geochemical data reviewed above suggest that the majority of the quartzofeldspathic and semipelitic lithologies are felsic tuffs/volcanoclastic rocks of rhyodacitic composition. Elevated K2O, the presence of disseminated and banded sulphides and the schistose nature of the semipelites distinguishes them from the otherwise negligibly different quartzofeldspathic rocks. These features in the semipelites are considered to be genetically related (discussed later in Chapter 5) and to reflect the

effects of syngenetic or epigenetic mineralizing fluids. The fact that those units of 2b interbanded with the semipelites west of Cinnamon Lake are not similarly mineralized suggest that the mineralizing events were syngenetic and sporadic. The semipelites and quartzofeldspathic lithologies are interpreted generally as felsic tuffs and/or volcanoclastic greywackes. The porphyroclastic amphibolite to the north, interpreted as a proximal fragmental or agglomerate, suggests emergent or shallow water conditions which would seem to militate against the presence of greywackes, at least in the northern section; further south the presence of coticules and shales suggests a moderate to deep water basinal environment. Juxtaposition of shallow and deep water facies in such a small area may be an effect of the complex deformational history.

The felsic lithologies are either distal or moderately distal with respect to their source since there is a strong possibility that coarse detritus would be preserved as relicts (as in the presumed mafic tuffs or epidote-pyrite schists, to the north).

The amphibolites are tholeiitic and can be divided into two groups on a geochemical and lithological (section 2.1.5.2) basis. Group 1 amphibolites are characterized by low silica, high MgO, Cr, Ni and depleted light REEs. Group two are typically high in SiO2, low in MgO, Cr, Ni and have highly fractionated REE patterns. The groups do however,

show almost continuous trends in various trace element plots. This observation along with the REE patterns which are considered to be petrogenetically linked rather than to be demonstrating metasomatism, suggests they are related by fractionation. The lack of a complete trend may be due in part, to a sampling bias and the small area sampled.

Although not conclusive, the evidence presented here leads the writer to favour an ocean floor affinity for the amphibolites. The dichotomy produced by this conclusion is emphasized by the local preponderance of felsic rocks which are not typically associated with ocean floor basalts. The amphibolites of the Cr-poor group are garnet-rich and a mafic tuff protolith has been put forward for them in section 2.1.5.2. At least some of the garnet-absent amphibolites are thought to be intrusive and therefore have a local source. This difference in protolith and localized sampling area, are thought to be the main factors giving rise to the two groups. Since trends are apparently continuous, the ultimate magmatic source region may be the same for the different amphibolites.

The felsic rocks are locally predominant and are generally atypical of environments characterized by ocean floor tholeiites. This association may be more easily explained in an island arc regime (with primitive arc tholeiites) but the apparent absence of intermediate rocks, at least in the immediate area, raises problems with this interpretation.

Chapter 5
GEOLOGY, ORE PETROLOGY AND LITHOGEOCHEMISTRY OF THE TWIN PONDS SHOWING

5.1 Introduction

The Twin Ponds Showing is a polymetallic, massive/disseminated, tabular sulphide body, hosted by a quartz-muscovite pelite within a sequence dominated by supposed felsic, meta-volcanoclastic rocks and minor mafic meta-tuffs. The ore mineralogy, morphology and setting, and lithogeochemistry of the host and enclosing rocks suggest an origin similar to that of the Kuroko type, volcanogenic mineralization. Average &34S values are 10 permil and $^{206}Pb/^{204}Pb$ ratios are more primitive than either those of the Hermitage Flexure area or those of pre-Caradocian leads in the Central Volcanic Belt. Comparison of the showing with other Newfoundland ore deposit types on a metal ratio basis, indicates that it is intermediate between Victoria Lake Zn-Pb-Cu dominated and Hermitage Flexure Pb-(Zn)-Ag type.

5.2 Petrology and Structure of the Twin Ponds Showing

The Twin Ponds Showing is hosted by a quartz-muscovite schist bounded on the south side, the structural hangingwall, by a thin amphibolite/biotite-garnet-kyanite schist, and on the footwall by a leucocratic quartzofeldspathic unit. In all drill holes and trenches the mineralization occurred at the quartzofeldspathic rock/amphibolite contact. Map 2 shows that this thin amphibolite unit is immediately adjacent to the showing along its entire srike length, defining a cut-off for assay sections in drill holes and trenches. Pyrite and rarely pyrrhotite were the only sulphides observed in the amphibolite.

The mineralization has a strike length of 4.54 km and is cut off by faults at both ends. It comprises three morphologic types delineated in Figure 5-1. The most distinctive of these types is massive (i.e. with greater than 50%) sulphides which characterize the original showing in trench #4 (Tr 4, Fig. 5-1) in the vicinity of Twin Ponds. This is flanked on one or both sides by disseminated (second type) and banded (third type) sulphides. The minerals comprising all types are pyrite-sphalerite-galena-chalcopyrite in order of decreasing abundance with barite as a constant associate.

In both drill holes and trenches the massive sulphide band generally occurs twice but in some cases only one band is present. In Isle aux Morts River West the massive ore is

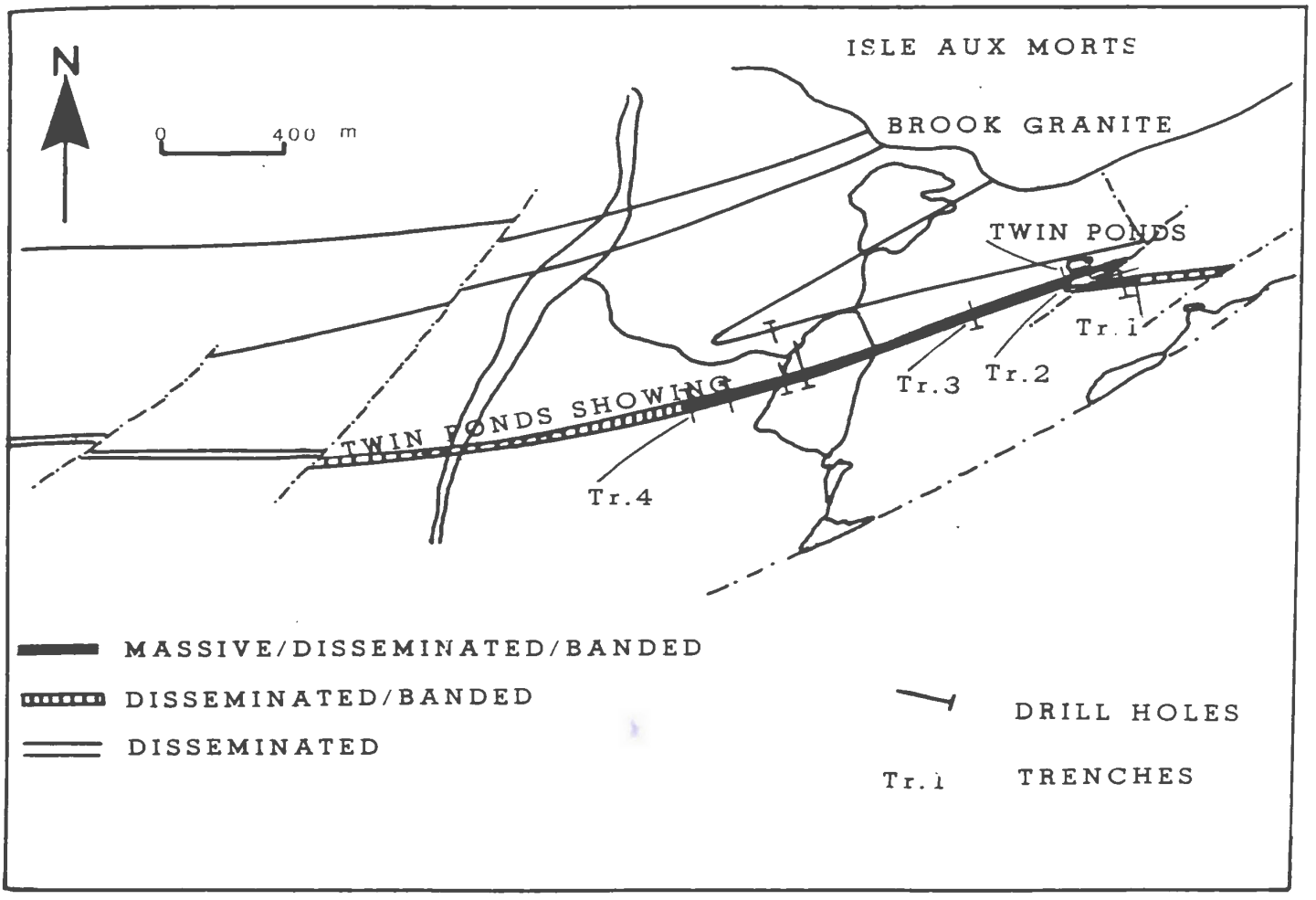

Figure 5-1: Location map for the three morphologic types of mineralization in the Twin Ponds Showing.

absent and the disseminated and banded mineralization is intercalated with amphibolite units (Fig. 5-2). Towards the western and eastern ends of the showing outcrops are sparse and only disseminated mineralization has been noted; where outcrops are absent soil geochemistry has confirmed the presence of mineralization.

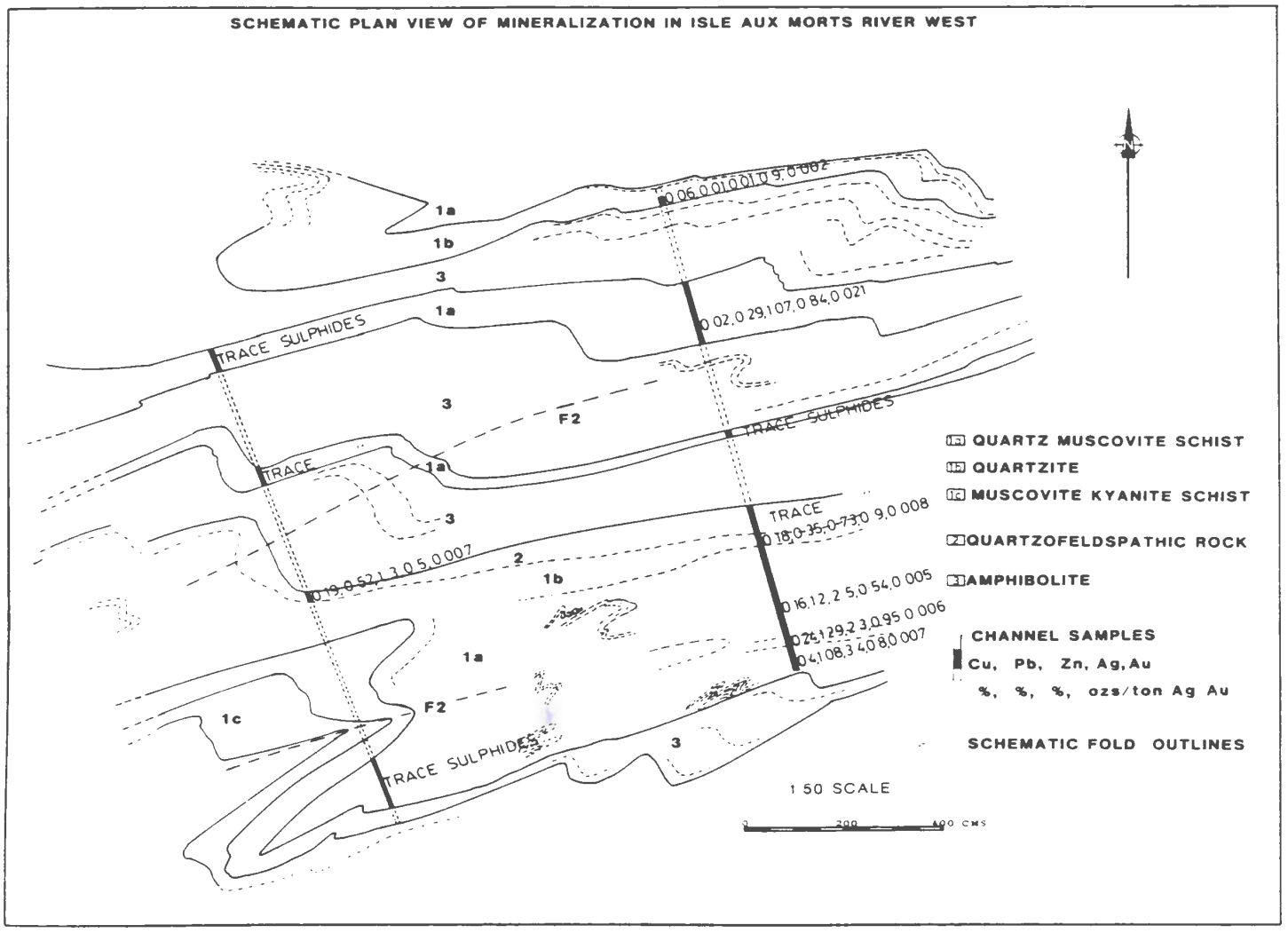

Figure 5-2: Sketch illustrating the structure, lithology and two representative channel sections across the Twin Ponds showing in Isle aux Morts River west.

The massive type of mineralization is a particularly distinctive lithology composed of host rock fragments (quartzofeldspathic, pelitic and vein quartz Figs. 5-3 to 5-7) in a very fine-grained matrix of sphalerite-galena-chalcopyrite and minor pyrite. The fragments are typically

rounded to sub-rounded (Fig. 5-7) and may have white (feldspathic) rims; locally the larger fragments (up to 30 cm across) are angular and exhibit brittle deformation effects (Figs. 5-3 and 5-4). The massive ore which is present in drill holes and trenches is characterized by "Durchbewegung" fabric (Vokes, 1969; Nold, 1983) which is a pseudo-breccia of sulphide ore and adjacent host rock. Although termed brecciation, the process is generally considered to be a ductile phenomenon, occurring at high temperatures and pressures. This is illustrated by Figure 5-6 which clearly shows the disharmonic contorted folding of semipelitic rocks (in the center of the photograph) while further down the folds become dismembered and are incorporated into the sulphides as in Figures 5-4 and 5-5. The enclosed fragments develop the rounded outlines (Fig. 5-7) by the kneading effect of the ductily-flowing sulphides and probably also by aggradation with the other silicate fragments.

The disseminated type of mineralization is typically coarse-grained (up to approximately 0.5 cm) pyrite, sphalerite and galena and generally finer-grained chalcopyrite in a muscovite-rich (Fig. 5-8) to muscovite-poor (Fig. 5-9) quartzose pelite. Minor crosscutting coarse-grained sulphide veinlets occur sporadically in this type of ore and probably represent some minor late stage remobilization. In the subordinate, third type of mineralization, sphalerite-galena-chalcopyrite form

Figure 5-3: Relationship between the massive (under the scale) and disseminated mineralisation below. Scale is 30 cm.

Figure 5-4: The mineralization is commonly stained blue and contains host rock fragments alligned parallel to local foliation.

Figure 5-5: Contorted schist fragment within massive mineralization.

Figure 5-6: Contorted disharmonic folding of semipelitic host rocks adjacent to the massive mineralization within which the folds are disaggregated.

Figure 5-7: Rounded host rock fragments set in a massive sulphide matrix exhibiting "durchbewegung" fabric; scale bar is 1 cm.

bands 1-5 mm thick (Fig. 5-9) which are conformable with the local planar fabric. Sulphides locally concentrate in fold hinges but this feature is not widespread.

The relationship between the massive and disseminated ores is illustrated in Figure 5-3. The contact is clearly discernible on this scale but in Figure 5-4, it is irregular because of deformation. The contact between disseminated and banded mineralization is locally sharp (Fig. 5-9) and parallels the grain size difference in the two, viz. coarse-grain vs fine-grain respectively.

The maximum surface width of the massive ore is 0.6 m and that of combined massive and disseminated (including banded) ore is approximately 2 m. The effects of deformation on the mineralized horizon are varied and

Figure 5-8: Folded muscovite schist with disseminated mineralization; scale bar is 30 cm.

Figure 5-9: Disseminated and banded mineralization sample from Isle aux Morts River west.

complex and include thickening by folding and thinning by boudinage. The widths given here are observed, with no attempt to quantitatively allow for deformation. Diamond drill hole IAM-82-1 had the greatest combined thickness of all types of ore (corrected for drilling angle) of 11.4 m and IAM-83-2 intersected the thickest (1.4 m) massive ore. The minimum proven vertical depth intersection was 106 m in IAM-83-4.

Although a faint foliation is locally developed within the massive type of ore and larger schist and quartzofeldspathic fragments are parallel to the wall rock foliation (Figs. 5-3 and 5-4), a penetrative fabric is not generally present (Fig. 5-7). However in the banded mineralization the sulphides are clearly parallel to a mineralogical layering (Fig. 5-9 and 5-10). Figure 5-10 is a sketch to emphasize the salient points, particularly several F1 fold closures isoclinally folded about F2 folds; a precisely similar structure in semipelites is illustrated in Figure 2.17. Thus the sulphide banding is clearly pre-deformational. A typical F2 style fold within the showing, illustrated in Figure 5-11, is overturned towards the north and plunges north-east at 30^{o}. A plan view of the mineralization as seen in the Isle aux Morts River West is illustrated in Figure 5-2; thickening in the hinge zones is apparent as the folds plunge 20^{o} northeast. At this location and further west the ore breccia is absent.

Contrasting rheologies of amphibolites and massive

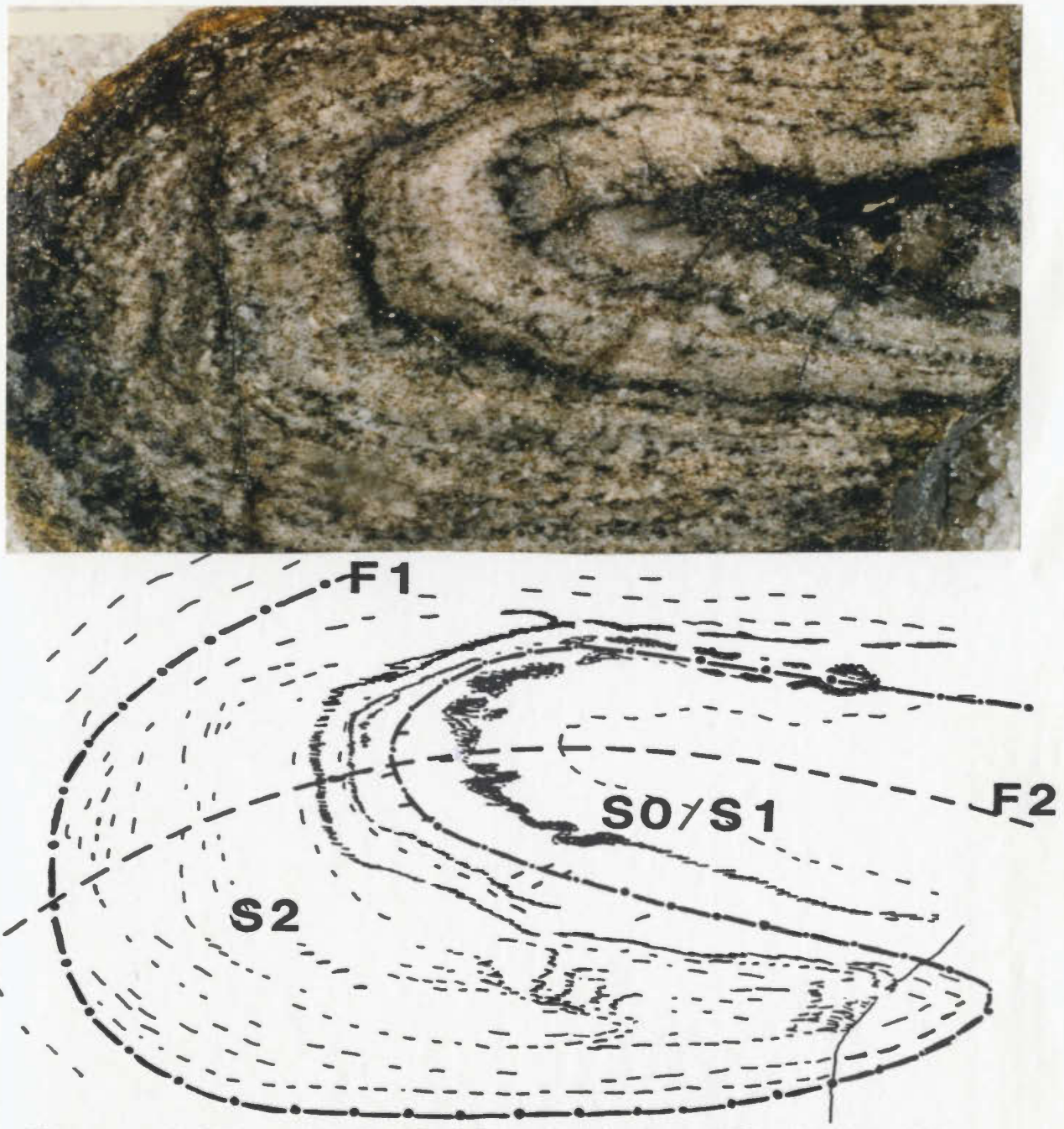

Figure 5-10: Refolded F1 fold (by F2) defined by sulphide bands with a sketch which emphasizes salient points; scale bar is 1 cm.

sulphides are illustrated in Figure 5-12. The competent amphibolite has reacted to deformation by faulting, while the massive sulphide has deformed ductily as is evident to the left of of the center of the scale where the sulphide

Figure 5-11: F2 fold within quartz muscovite schists near Twin Ponds.

Figure 5-12: Apparent behavioural differences between a competent amphibolite and an incompetent sulphide band which has deformed ductily.

fabric is continuous. Because of the ease with which sulphides deform, the ore horizon may have acted as a decollement, initially during D1 when thrusting may have occurred and probably at least sporadically later in D2. Such deformation would eventually lead to extreme attenuation and obliteration of original structures.

5.3 Metal Grade and Distribution in the Twin Ponds Showing

The Twin Ponds Showing was locally exposed by four trenches between Twin Ponds and drill hole IAM-83-1 (Fig. 5-1). All of the trenches were channel-sampled at five feet intervals (along strike). The main trench (Tr 3, Fig. 5-1) at Twin Ponds is shown in Figure 5-13 as an example. Metal distribution (across strike) in the channel and drill hole intersections was examined by plotting metal grades against interval and mineralization type (Fig. 5-14). A plot of metal grades in drill hole IAM-82-3 is shown in this Figure which is representative of all sections examined.

The highest metal concentrations typically occur in the breccia ore mineralization (Table 5-1). Surface grades are similar from the Twin Ponds trench and from the trench at IAM-83-1 location. However, further west grades are lower, as in the sections at Isle aux Morts River West and in claim block 2850. At the eastern extremity of the Twin Ponds Showing the surface mineralization is sparse and apparently of lower grade, although its presence was confirmed by soil geochemistry.

Figure 5-13: Sketch of the original trench adjacent to the Twin Ponds, showing lithology and assay values across the mineralization.

SCHEMATIC PLAN VIEW OF TRENCH #1 MINERALIZATIONALIZATION, ADJACENT TO TWIN PONDS

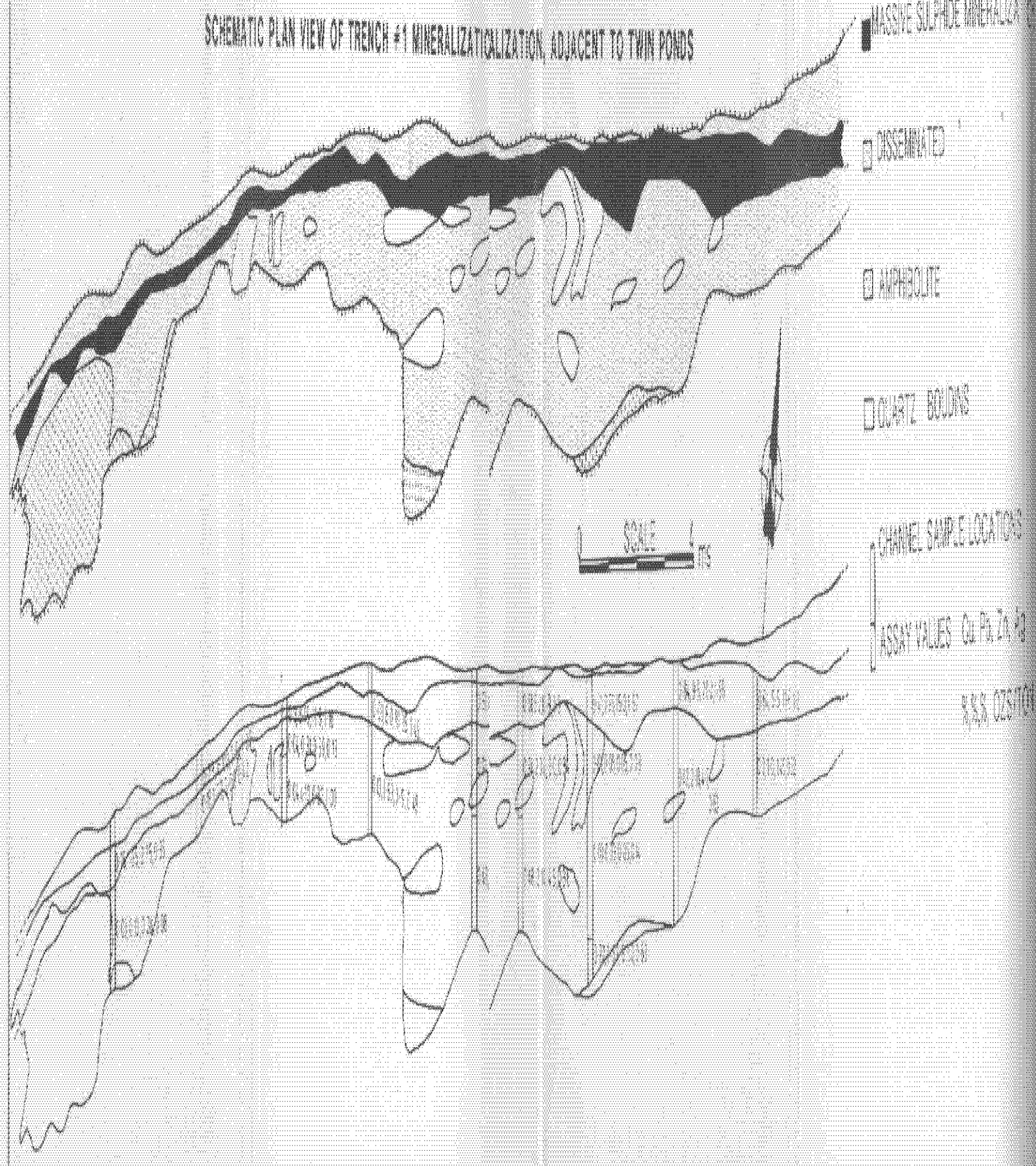

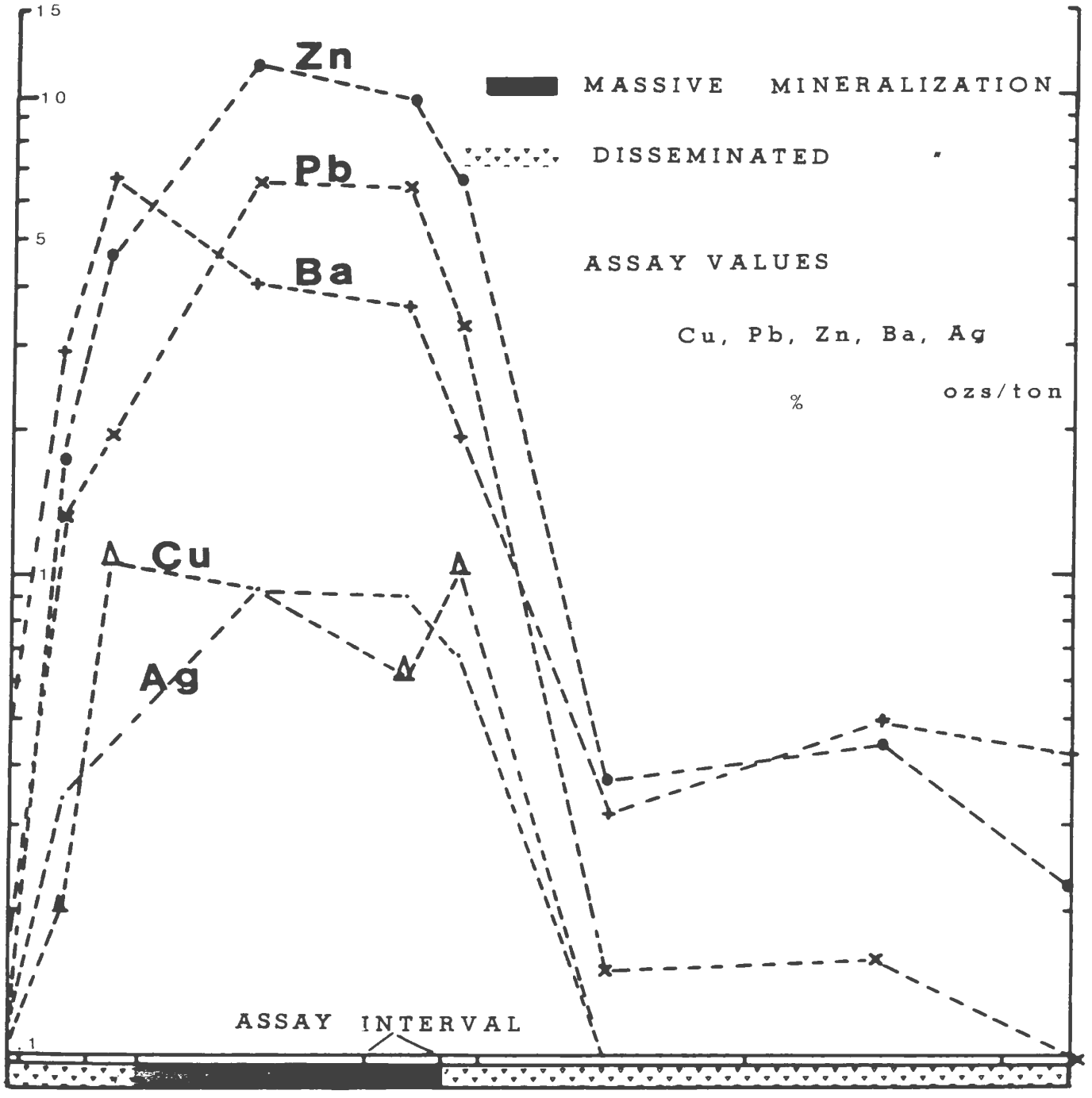

Figure 5-14: Variation in metal grades across the mineralized intersection in DDH-IAM-82-3. Total width of the section is 9 m. Symbols for metal and assay values are placed at the centre of each interval.

Over a srike length of approximately 1.7 km the mineralized horizon shows little variation in metal grades both laterally and vertically. The best grade was

Table 5-1: Best assays along the length of the Twin Ponds Showing.

Massive Ore Grades:

Location	% Zn	% Pb	% Cu	ozs/ton Ag	Interval cm
IAM-82-5	19	9.8	1.1		12
IAM-83-3	18.8	10.4	0.12		10
Trench-2	20.2	9.5	0.84	1.98	17
Trench-4	11	6	1	1.58	60

Disseminated/Banded Ore Grades

IAMRW	3.4	1	0.37	0.8	12
CB2850	1.1	0.52	0.1	0.17	

IAMRW = Isle aux Morts River West
CB2850= Grab sample

approximately 32% combined Zn-Pb-Cu over 17 cm in the Twin Ponds trench.

The metal grades in the disseminated type of mineralization are much lower than in the massive type, varying from 6.6% to < 0.1% Zn, 4 to < 0.1% Pb, 1 to < 0.1% Cu and generally less than 1 oz/ton Ag. A feature present in both drill holes and trenches is the constant sympathetic variation in metals giving the typical parallel slopes in Figure 5-14.

Although the breccia ore does occur twice in most sections, it is impossible to ascertain whether this is an original feature or tectonic repetition of a single band. Due to the spatially restricted nature of the mineralization it seems more likely that there is only one breccia-ore band and one disseminated band. It is also difficult to envisage

a process of formation other than syngenetic deposition that would account for the consistent sympathetic lateral and vertical variation of sulphides and barite.

Sulphides other than pyrite are generally absent from the amphibolite unit in the hangingwall of the showing and from the biotite-garnet-kyanite schist unit. However, in one brecciated pyrite-rich section (unit 1d) in IAM-82-2, up to 0.7% Pb and Zn were assayed. These may have been remobilised from the Twin Ponds Showing along a fault which runs through the ponds. In IAM-83-2 in the quartzofeldspathic unit to the north of the Twin Ponds Showing, sulphides disseminated over 1 cm grade at 1.1% Zn and 0.6% Pb. Many other sulphide occurrences are also known from the sequence in the north of Map 2, whereas sulphides other than pyrite are absent from the sequence south of the mineralization.

Grab samples of mostly massive ore from the trenches were analysed for Cu, Pb, Zn and Ag. The analyses are listed in Appendix Table C-2. The grades are similar to those above for channel and drill hole intersections with the highest grades being 23.5% Zn, 10.9% Pb, 0.07% Cu and 74 ppm Ag in a sample immediately west of Twin Ponds. The highest Cu grade was also in a sample from this locality *viz.* 7.0% Cu, 1.83% Zn, 0.68% Pb and 0.5 ozs/ton Ag, also in massive ore. This anomalously high Cu value may represent concentration by remobilization during deformation or an original Cu-rich area such as a chalcopyrite-ore clast.

The narrow spread of sulphide metal ratios in the Twin Ponds Showing is illustrated in Figure 5-15. The values overlap those of

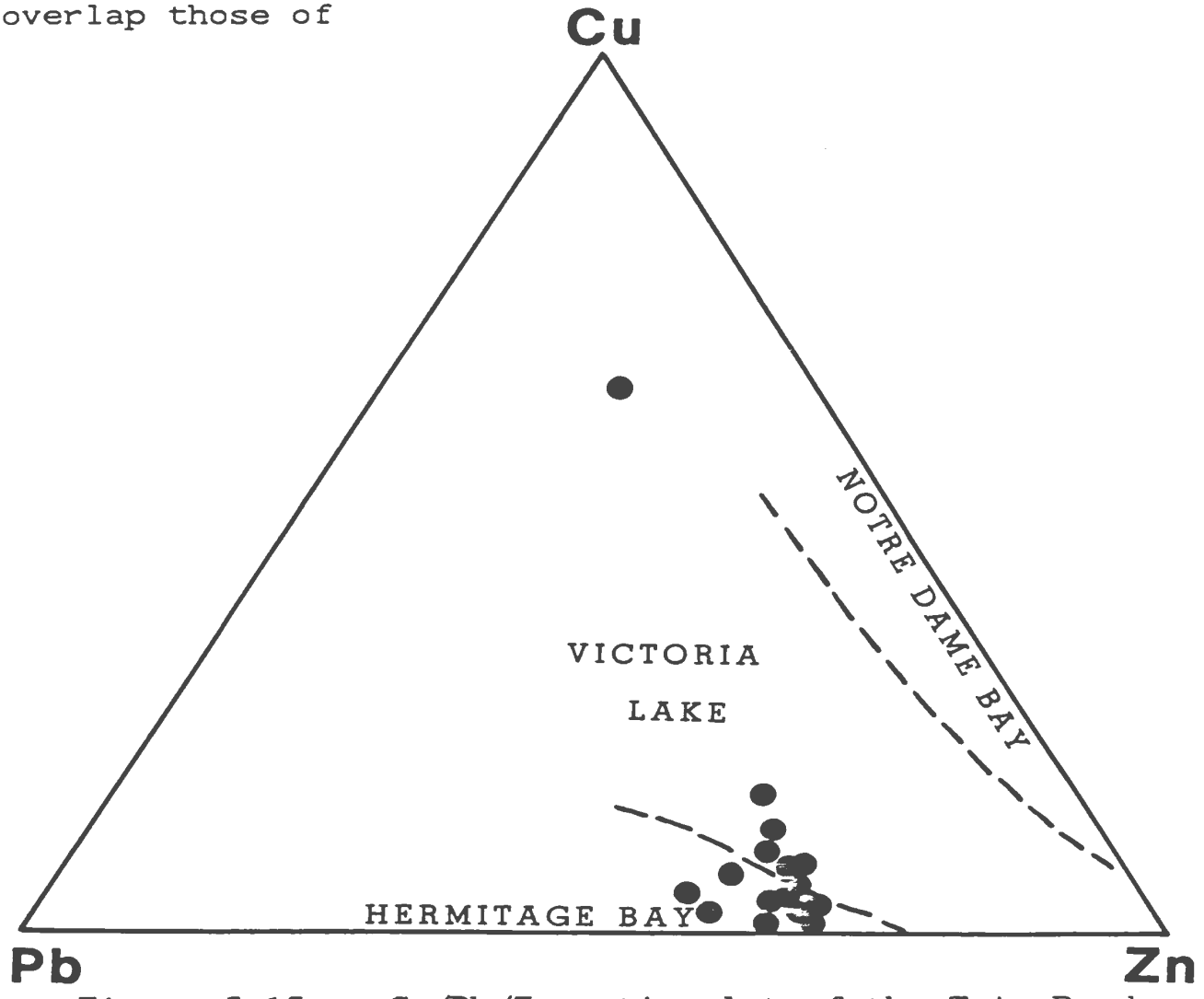

Figure 5-15: Cu/Pb/Zn ratio plot of the Twin Ponds Showing mineralization (circles represent grab and channel samples) compared to other Newfoundland areas; fields from Swinden and Thorpe (1984)

volcanogenic prospects in both the Hermitage Flexure area and those of the Victoria Lake/Tulks Hill areas. In the Hermitage Flexure area, subaerial submarine felsic volcanic rocks are host to polymetallic (Pb-Zn-Ag) sulphide

mineralization e.g. the Strickland Prospect (Wynne, 1984). A strong sialic crustal influence has been postulated by Swinden and Thorpe (1984) for this area.

Submarine mafic volcanic rocks host several polymetallic (Zn-Pb-Cu) deposits in the Victoria Lake/Tulks Hill area. Although the base of this sequence is not exposed, Dunning (1984) states that the ophiolitic Annieopsquotch Complex is in fault contact with the Victoria Lake group.

Metal ratios of the Twin Ponds Showing are equivocal therefore, with respect to derivation from either mafic-dominated or felsic-dominated sequences. This feature may reflect a deeper-seated cause i.e. crustal heterogeneity.

On a metal ratio basis the Twin Ponds Showing equates with the Pb-Zn-Cu type of Lydon (1984) who classified volcanogenic massive sulphide deposits using their ore element chemistry. The presence locally of felsic volcanic/volcanoclastic rocks is also important for the classification of this showing as a Pb-Zn-Cu volcanogenic type in the scheme of Franklin et al. (1981).

5.4 Other Sulphide Occurrences Within the Area

The known sulphide occurrences are typically found within semipelites in the felsic rocks north of the main showing. West of the south end of Cinnamon Lake, drill hole IAM-82-4 (Map 2) intersected approximately 12 m of

disseminated sphalerite-galena-chalcopyrite in quartz-muscovite schist at the contact between an intercalated biotite-garnet-kyanite schist/amphibolite unit and an unmineralized quartz-muscovite schist/muscovite-biotite schist/quartzofeldspathic unit. Grades here range up to 2.9% Zn, 2% Pb, 0.28% Cu, 0.57 oz/ton Ag and 0.048 oz/ton Au over several cm. This sequence is locally similar to that of the Twin Ponds Showing and although grades are much lower it is suggested that the sequence is the same and has been repeated by thrusting.

Of the various occurrences located in Isle aux Morts River West (Map 2) north of the Twin Ponds Showing, the best grab sample graded at 3.2% Zn, 1.6% Pb, 0.04% Cu and 0.45 oz/ton Ag in quartzitic bands within a quartzofeldspathic unit. In a kyanite-muscovite pelite unit 240 m further north, disseminated chalcopyrite occurs in a 1.5 m interval where a grab sample assayed at 0.63% Cu, 0.2% Zn and 0.5% Ba. This type of mineralization is found in a similar unit at the west end of claim block 2850 where a grab sample graded 0.16% Cu, 103 ppm Ag and 0.02 oz/ton Au.

Several other minor occurrences, west of Isle aux Morts River West, are shown on Map 2. Some of these latter showings have similar host rocks to the Twin Ponds Showing as it appears at the river section where the host rocks are more aluminous and contain kyanite.

A significant correlation exists (Lydon, 1984) between the deposit type and the predominant lithologies for 1-5 km

stratigraphically below it. Thus Pb-Zn-Cu types are regionally associated with felsic volcanic rocks in the footwall. These rocks commonly contain disseminated, stockwork mineralization whereas hangingwall rocks are commonly barren. In the Isle aux Morts area, the felsic meta-tuffs to the north of the Twin Ponds Showing, contain ubiquitous disseminated mineralization while sulphides are absent from the felsic volcanoclastic rocks and shales to the south. The group of felsic meta-tuffs to the north are thought to represent the footwall rocks. Large (1977) also notes that volcanogenic-associated sulphide deposits commonly occur at the top of a felsic volcanic pile and depending on their proximal or distal nature, may or may not have interbedded clastic rocks.

5.5 Ore Petrography

The sulphide minerals present in the showing are sphalerite, galena, chalcopyrite, pyrite and minor covellite which probably formed by supergene processes. Barite is a ubiquitous gangue mineral. Sphalerite, galena and chalcopyrite are present as xenoblastic, highly irregular grains in the pseudo-breccia in which they form a typically fine-grained matrix to the silicate fragments. All sulphides occur as inclusions in each other.

Sphalerite inclusions in pyrite and galena are generally rounded but locally they are myrmekite-like in pyrite and more rarely idiomorphic (hexagonal) crystals have

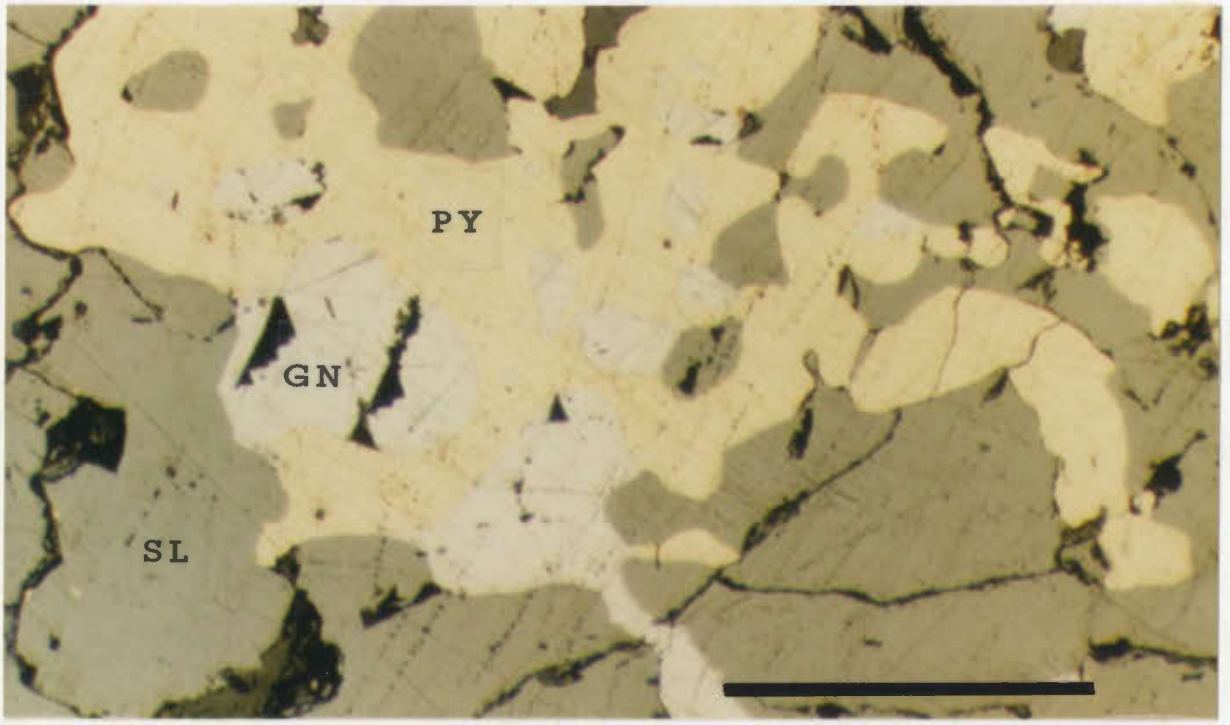

Figure 5-16: Reflected light photomicrograph of intergrown sphalerite (sl), galena (gn) and pyrite (py); scale bar is 1mm.

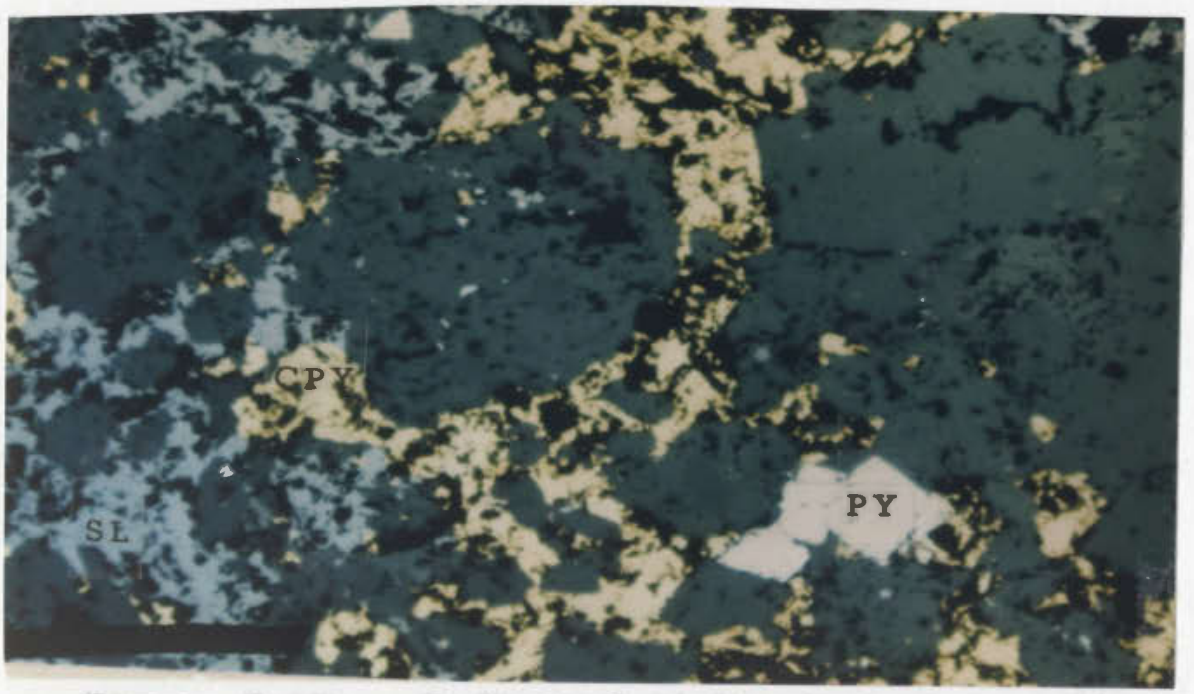

Figure 5-17: Reflected light photomicrograph of silicate fragments in a chalcopyrite (cpy) and sphalerite matrix; massive ore; scale bar is 1 mm.

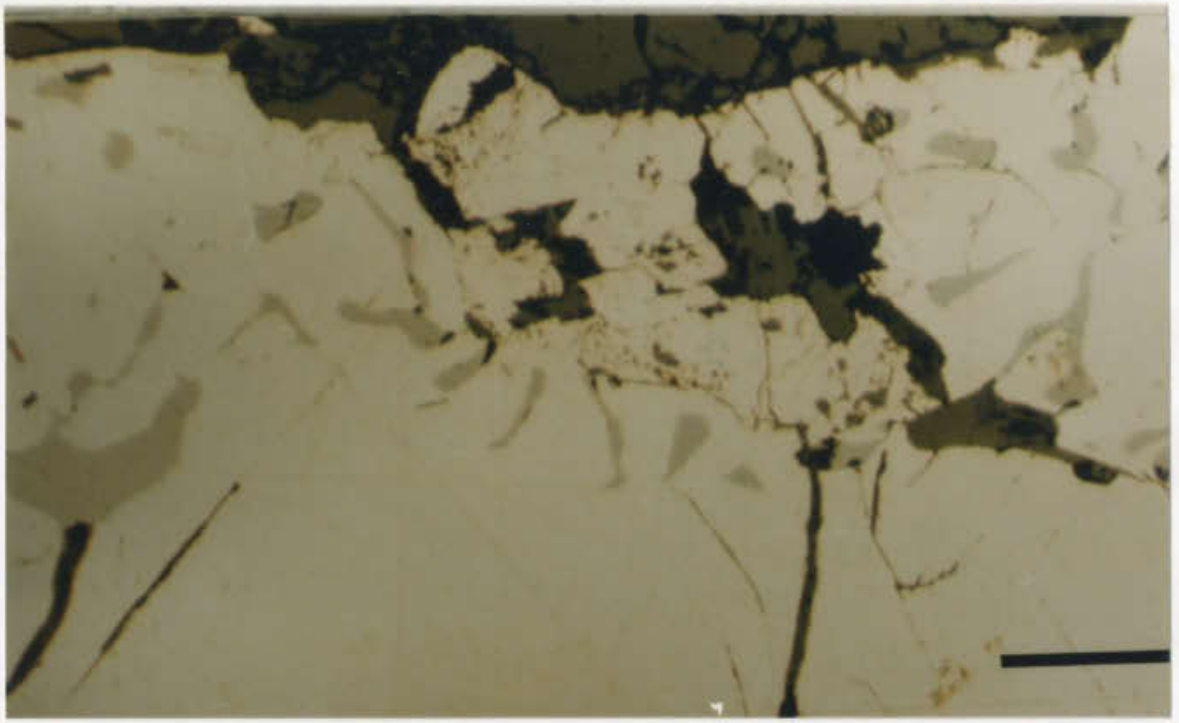

Figure 5-18: Reflected light photomicrograph of pyrite with included myrmekite-like sphalerite; scale bar is 0.2 mm.

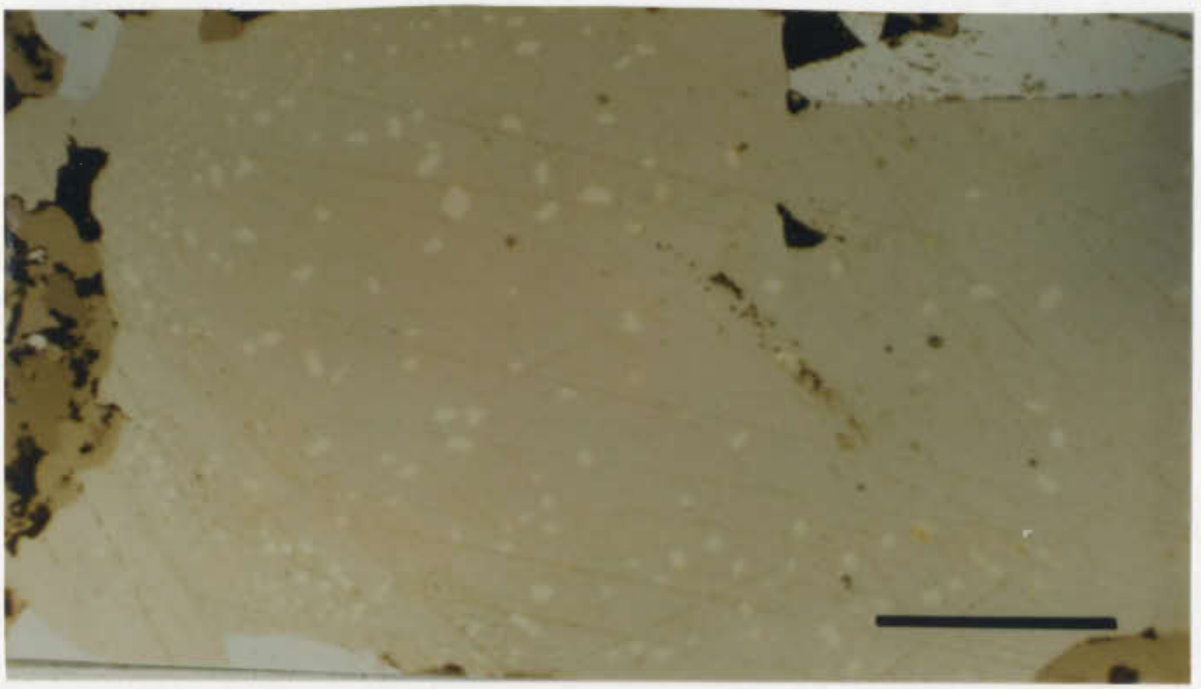

Figure 5-19: Reflected light photomicrograph of chalcopyrite blebs in sphalerite; the blebs decrease in size towards the margin (bottom right) which is actually clear; scale bar is 100 microns.

been observed within pyrite, possibly high temperature relicts. Sphalerite is the dominant matrix ore mineral and has highly variable internal reflections from yellow through shades of orange and red to deep red-brown under crossed nicols.

Chalcopyrite blebs in sphalerite (the feature characterized by Barton 1978, as chalcopyrite "disease") are a distinctive feature. They take the form of small rounded or elongate blebs generally randomly dispersed within the grain but locally apparently parallel to cleavage traces and more rarely parallel to the matrix foliation. The disease is locally abundant in certain sphalerite grains but completely absent in others, even within one polished section. In some grains a gradational decrease in size is present towards the rim but the actual margin is clear (Fig. 5-19). According to Ramdohr (1969) this is an exsolution phenomenon, due to solid solution occurring, at higher temperatures, between sphalerite and chalcopyrite because of their similar structures. Experimental studies on phase relations in the system Cu-Fe-Zn-S (Kojima and Sugaki, 1985) suggest that the amount of CuS dissolved in ZnS is insufficient to produce the observed volume of chalcopyrite blebs in sphalerite. These studies were conducted at temperatures between 300 and 500 ^{o}C. However, the mineralization in the study area is considered to have experienced higher temperatures, approximately 650 ^{o}C (c.f. geothermometric estimates in Chapter 3). At this

temperature, the solubility of CuS in sphalerite may be sufficiently elevated to produce the observed amount of exsolved chalcopyrite blebs at lower temperatures. Kojima and Sugaki (1985) and Barton (1978) cite replacement as being the cause of the disease. Chalcopyrite disease is a common feature of Kuroko deposits (Eldridge et. al., 1983, who also attribute the cause to replacement) where it tends to occur in the more Cu-rich ores. The locally clear margins of sphalerites which have the chalcopyrite blebs in the Twin Ponds Showing, mitigates the replacement argument. Also the absence of free chalcopyrite was noted in one thin section which contained disseminated sphalerite with the disease.

Barite is a common accessory mineral but locally forms up to 50 modal % of the rock. It forms complex intergrowths with hyalophane, a Ba/K feldspar whose presence was confirmed by semi-quantitative analysis using a scanning electron microprobe. Ba feldspars with variable contents of K were found in several sections, from various localities along the showing. However the most spectacular occurrence of hyalophane which has a distinctive green colour, is in a pegmatite intimately associated with the mineralization at Twin Ponds.

The zinc spinel gahnite ($ZnAl_2O_4$), occurring in more aluminous rocks containing disseminated mineralization, was also confirmed by electron microprobe analysis. Gahnite has been observed in many volcanogenic massive sulphide deposits

that have attained amphibolite grade (Franklin et al., 1981).

The coarse grain size of the disseminated sulphides is a feature typical of metamorphosed ore deposits (Vokes, 1969; Rockingham and Hutchinson, 1980). However this contrasts with the very fine-grained nature of the pseudo-breccia ore. Sulphides form up to 70-80 % of this ore which probably remained ductile during waning stages of metamorphism while the enclosing pelites were relatively competent and textures had 'frozen in'. Thus continued late shearing/ductile flow in the massive ore prevented the sulphides from attaining (or preserving) a coarse grain size. Coarsening grain size is a thermally activated process (Stanton, 1972) and the breccia ore, because of its composition, continued to deform ductily at temperatures too low to increase grain size. The relative ease with which these sulphides mobilize under stress is implied by sphalerite, galena and chalcopyrite filling cracks in pyrite. In disseminated mineralization these three sulphides characteristically occur in the pressure shadow regions of pyrite grains (Figure 5-20) which are themselves elongate parallel to the local foliation. In places chalcopyrite and galena appear to have been more mobile than sphalerite defining a sequence of decreasing ductility as Cpy=Gn > Sl > Py. All the sulphides are typically sheared along the foliation in the pelites (Fig. 5-21); locally sphalerite and chalcopyrite occur within mica grains along their 001 cleavage.

Figure 5-20: Reflected light photomicrograph of galena, sphalerite and chalcopyrite in the pressure shadow of a pyrite grain; scale bar is 1 mm.

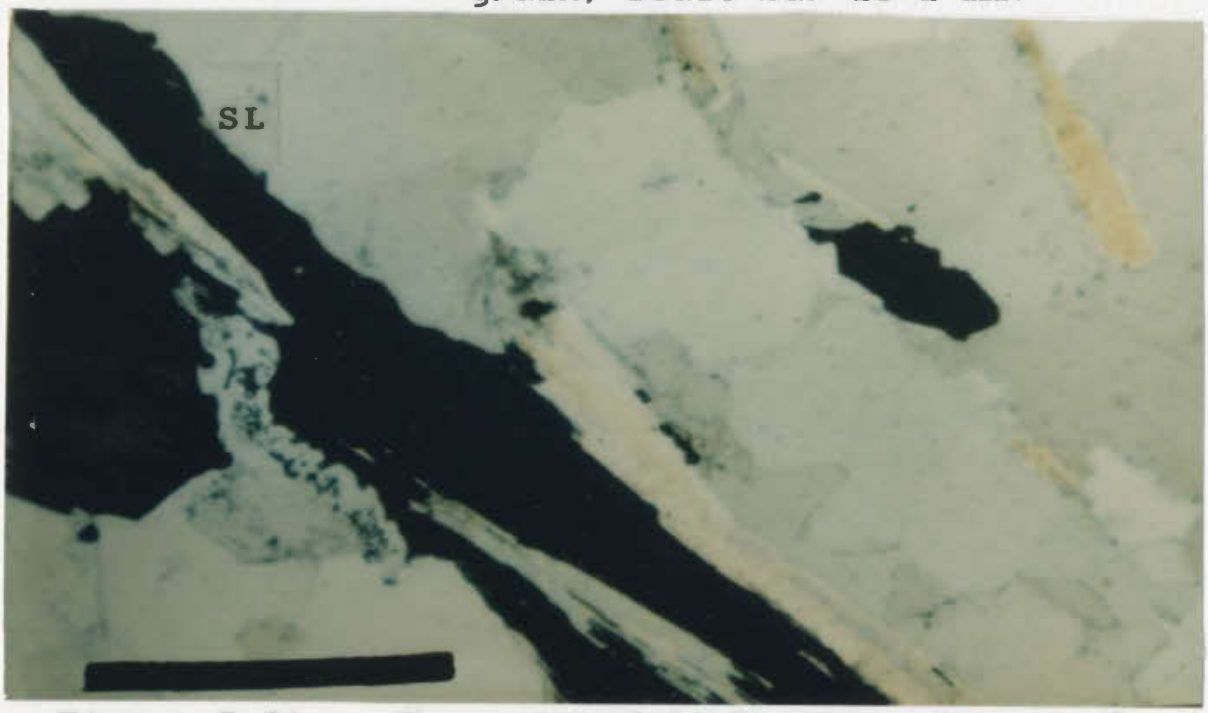

Figure 5-21: Transmitted light photomicrograph of elongate, sheared sphalerite in mica foliation; scale is 1 mm.

All features of deformation may be obliterated by recrystallization and annealing of the 'softer' sulphides during waning temperatures. This may also account for the poor fabric present in the pseudo-breccia which is mostly defined by sparse micas, some elongate silicate fragments and occasional mica beards (Fig. 5-22) joining separate fragments. Chalcopyrite and sphalerite are locally elongate along the 001 cleavage in these micas.

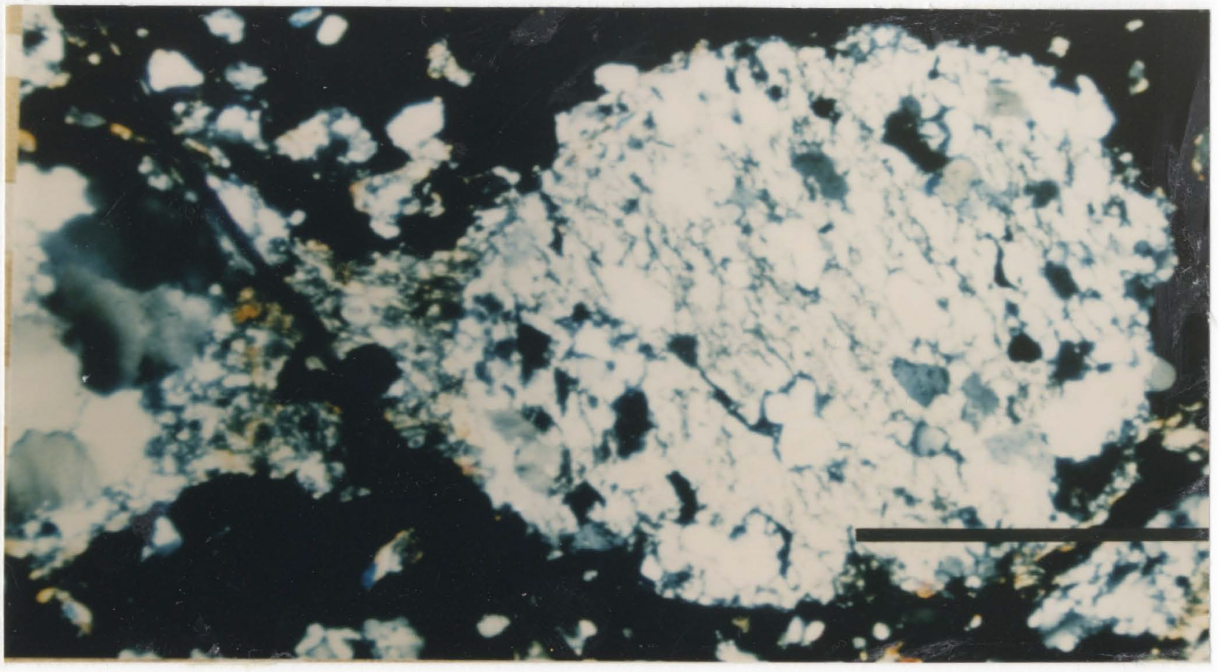

Figure 5-22: Transmitted light photomicrograph of rounded silicate fragments partially joined by mica beards, in massive sulphide matrix; scale bar is 1 mm.

5.6 Ore Mineral Chemistry

The compositions of the principal ore minerals were determined by electron microprobe (see Appendix A for procedures).

Some sphalerite compositions are close to the pure Zn-S

member with less than 2% Fe (Table 5-2) while others range up to 8% Fe. Sphalerites with low Fe content have been noted in metamorphosed sulphide bodies where pyrrhotite is absent (Scott, 1976). The variation in the Fe content probably reflects a lack of equilibration between sphalerites and the matrix and the absence of a S-rich fluid to buffer the sulphide body (Scott, 1976).

Sphalerites with chalcopyrite disease were analysed in sample 6-6-1 (Table 5-2) and the Cu content is the same as that in sphalerites with no evidence of the disease. The Ag content of sphalerites is very low but minor Cd is present, up to 0.22%.

Composition of the several galenas measured is relatively simple, with minor amounts of Bi, Ag and Sb. Ag is generally absent from the other ore minerals and thus galena is the main host of Ag. Chalcopyrites are homogeneous with trace amounts of Zn and Cd.

5.7 Lithogeochemistry of the Twin Ponds Showing and its Host Rocks

Major, trace and rare earth element analyses of 6 mineralized samples are given in Appendix Table B-4. Four of the samples are from drill core, one is from the Twin Ponds Showing and one represents mineralized semipelites in Isle aux Morts River West.

Generally, the mineralized samples have higher K_2O, Fe_2O_3 (total Fe), Rb and lower Na_2O, SiO_2, MgO and Sr than

Table 5-2: Ore mineral compositions as determined by microprobe analyses.

Sample#	S	Fe	Zn	Cu	Cd	Ag	Totals
			Sphalerite				
Tr2B-1	32.02	1.68	67.52	0.04	0.16	0.04	101.46
	0.485	0.013	0.500	0.00	0.00	0.00	0.998
6-6-1	32.64	0.82	65.53	0.14	0.22	0.00	99.36
	0.500	0.008	0.492	0.00	0.00	0.00	1.000
Tr1-3	31.37	7.96	58.03	0.18	0.13	0.00	97.69
	0.484	0.07	0.441	0.00	0.00	0.00	0.996
			Chalcopyrite				
Tr2B-1	34.41	31.39	0.07	33.81	0.17	0.00	99.84
	0.992	0.516	0.00	0.492	0.00	0.00	2.000
			Galena				
	S	Pb	Bi	Ag	Sb		
Tr1-3	13.86	86.3	0.08	0.13	0.15		100.58
	0.508	0.488	0.00	0.002	0.002		1.000
	14.77	83.64	0.46	0.00	0.16		99.17
	0.531	0.460	0.002	0.00	0.002		1.000

First row of each sample is weight %.
Second row of each sample is the structural formula.

the unmineralized group; the remaining major and trace elements are similar in both groups. K2O and Na2O display the greatest differences (Fig. 4.7) and the negative correlation between these elements can be attributed either to an ion exchange or net loss and gain of alkalies. Similar Na2O and K2O depletion and enrichment patterns have been observed by Wynne (1983) in felsic rocks hosting volcanogenic mineralization in the Bay du Nord Group (Fig.

5-23), and in the Japanese Kuroko-type and Canadian Archaen massive sulphides deposits (Urabe et.al., 1983; Ohmoto and Skinner, 1983). SiO2 may be either leached or enriched in these various ores while the lack of any MgO enrichment may be taken as a feature indicative of distal types of exhalative deposits (Large, 1977).

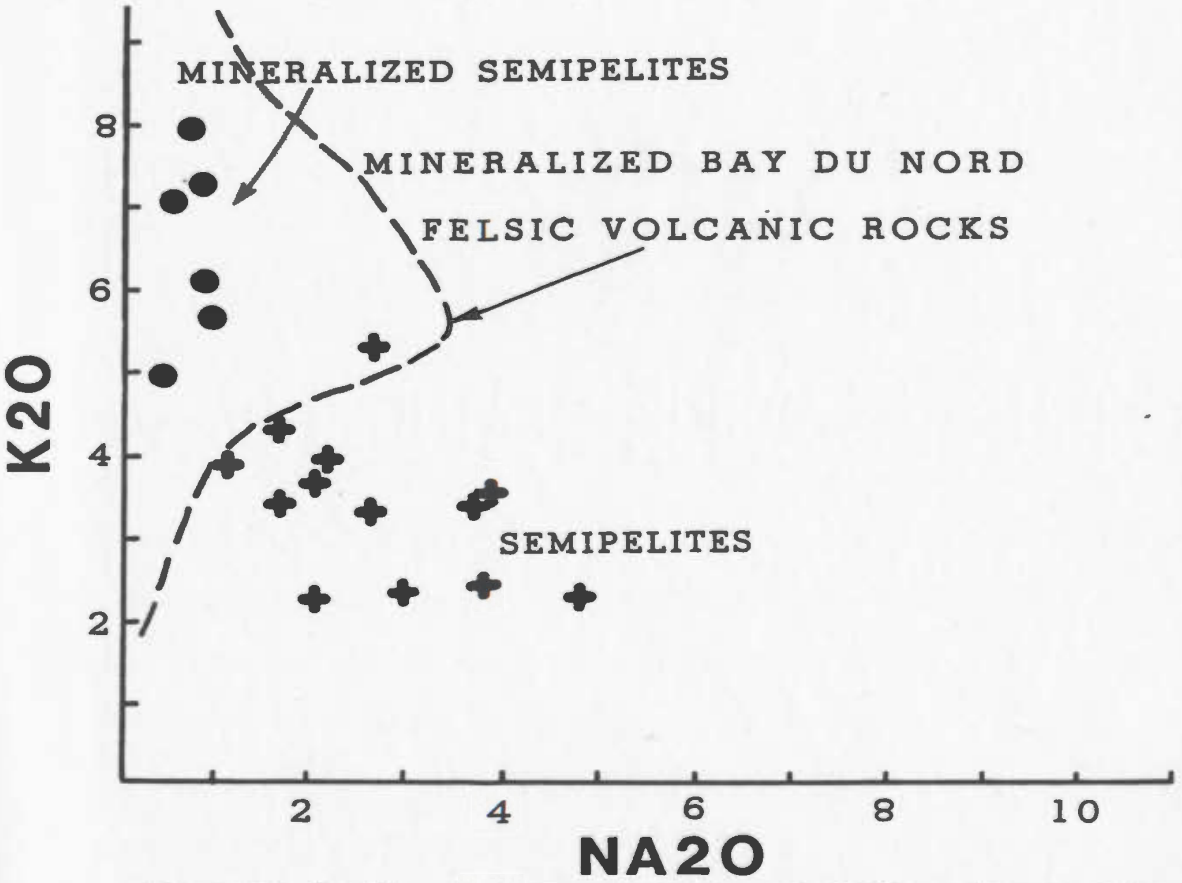

Figure 5-23: Comparaison of K/Na alteration in mineralized felsic volcanic rocks of the Strickland Prospect, Bay du Nord Group (Wynne, 1983) with that of the Twin Ponds Showing.

A similar Na/K trend was also noted in the quartzofeldspathic units intercalated with semipelites west of Cinnamon Lake (Fig. 4.6). Both units are depleted in Sr (Fig. 4.9) and the Rb/Sr behaviour parallels that of K2O and

Na2O. Typically, however, significant enrichment/depletion patterns are restricted to actually mineralized samples in the Twin Ponds Showing or from the sequence to the north. Such trends are absent from the rocks to the south of the Twin Ponds Showing. This general lack of depletion/enrichment patterns is typical of volcanogenic deposits which were deposited distally from their discharge zone (Large, 1977). Ba is typically enriched in all mineralized samples ranging up to approximately 23 wt.% (in trace element analysis) in a sample from Isle aux Morts West. Its presence reinforces analogies with mineralization associated with volcanic terrains.

Chondrite-normalized rare earth element patterns for two mineralized samples and one unmineralized semipelite sample are illustrated in Figure 5-24. Some fresh rhyolites are shown for comparison and a mineralized massive sulphide sample from New Brunswick # 6 deposit (Graf, 1977). Graf attributes the large positive Eu anomaly in the latter to enrichment of Eu in the solutions by interaction of hydrothermal fluids with feldspar. The sulphides were later precipitated from these Eu-enriched fluids. However in the present case the actual abundance of Eu is similar to that in the unmineralized sample; thus rather than absolute Eu enrichment, the light REEs in both samples and heavy REEs in one sample have been depleted, leaving a relative Eu enrichment. This depletion is thought to reflect leaching of host rocks, which occurred synchronously (stockwork?) with the mineralizing event.

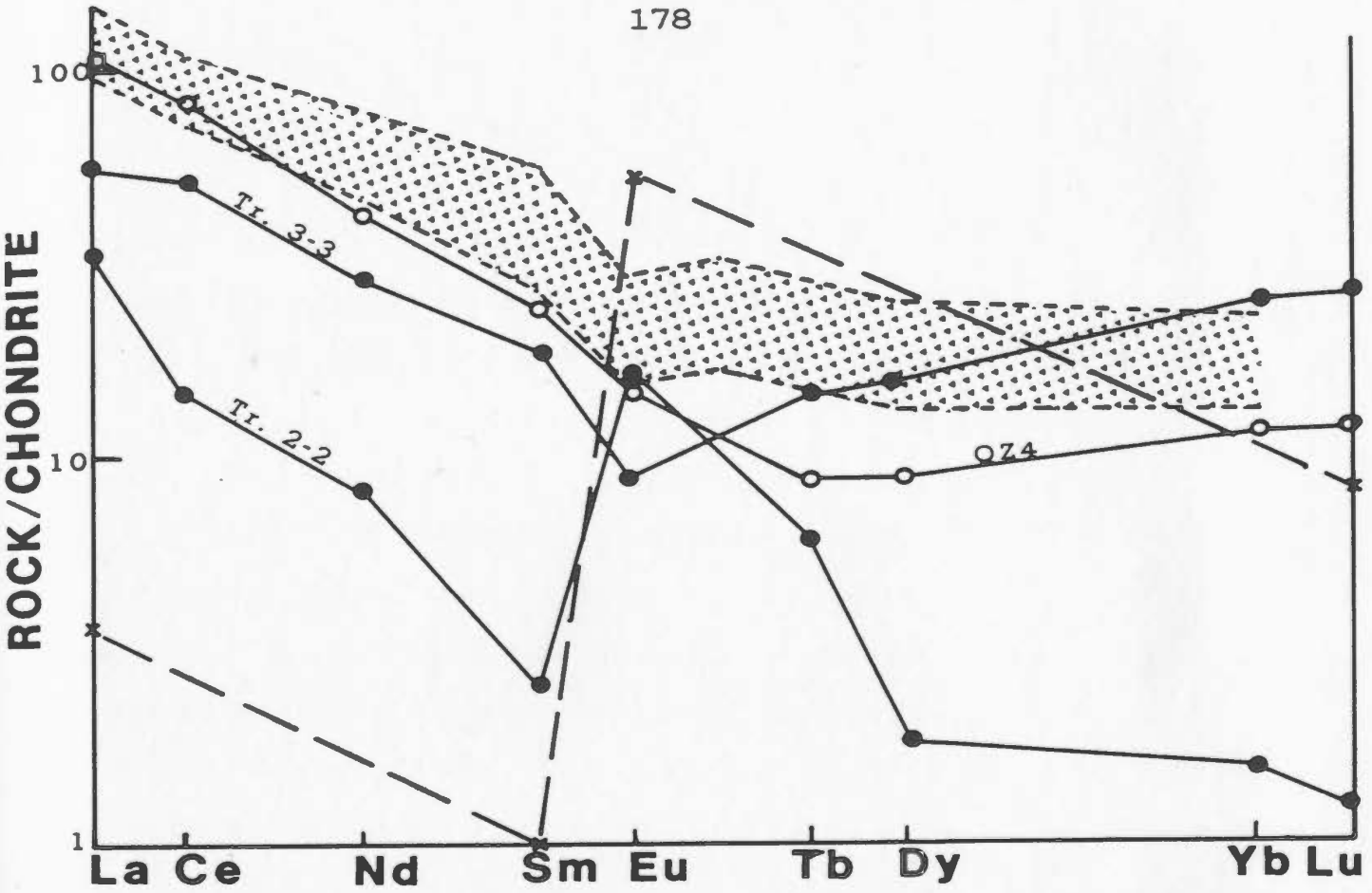

Figure 5-24: Chondrite normalized rare earth element patterns for mineralized (closed circles) and unmineralized (open circles) semipelite samples compared to a mineralized massive sulphide sample (x) from New Brunswick #6 (Graf, 1977).

Stabilization of Eu^{2+} (relative to the other lanthanides) by alumino- and meta-silicate complexes, during anatexis in high grade metamorphic terranes, is postulated by Moeller and Muecke (1984). The case for anatexis in the study area has already been argued in Chapter 3. As the mineralization is intimately associated with feldspathic, muscovite ± kyanite rocks, alumino-silicates are readily available. The sample with highest combined sulphides suffered most leaching; this peculiar behaviour of Eu has also been noted by Fryer (pers. comm., 1985).

Although gedrite-bearing rocks are not directly associated with the mineralization, their presence is thought to be regionally significant with respect to the economic potential of the area. The occurrence and origin of magnesian-aluminous rocks and their possible association with ore mineralization is reviewed by Vrana (1975). The assemblages talc-kyanite-chalcopyrite occurs in the Cu-bearing areas of Katanga; gedrite-kyanite in New Hampshire and gedrite-magnetite-plagioclase in oxidic Fe-formations in Bohemia. The first two are high pressure assemblages and the kyanite-muscovite-chalcopyrite assemblage in claim block 2850 may be a high pressure equivalent (of the first above). Although coexisting kyanite and gedrite were not found, rocks containing quartz-muscovite-kyanite do occur adjacent to gedrite-magnetite-plagioclase units in claim block 2329. This gedrite-bearing rock may represent an oxidic Fe-formation.

5.8 Stable Isotopes

5.8.1 Sulphur

Isotopic ratios of sulphur were determined from a representative suite of sphalerite, galena and chalcopyrite samples collected from the showing between Twin Ponds and IAM-82-5. The analytical procedures and results are tabulated in Appendix 4. The range of values and number of analyses (latter represented by ticks on the mineral bars) are illustrated in Figure 5-25. The ratio of ^{34}S to ^{32}S, the

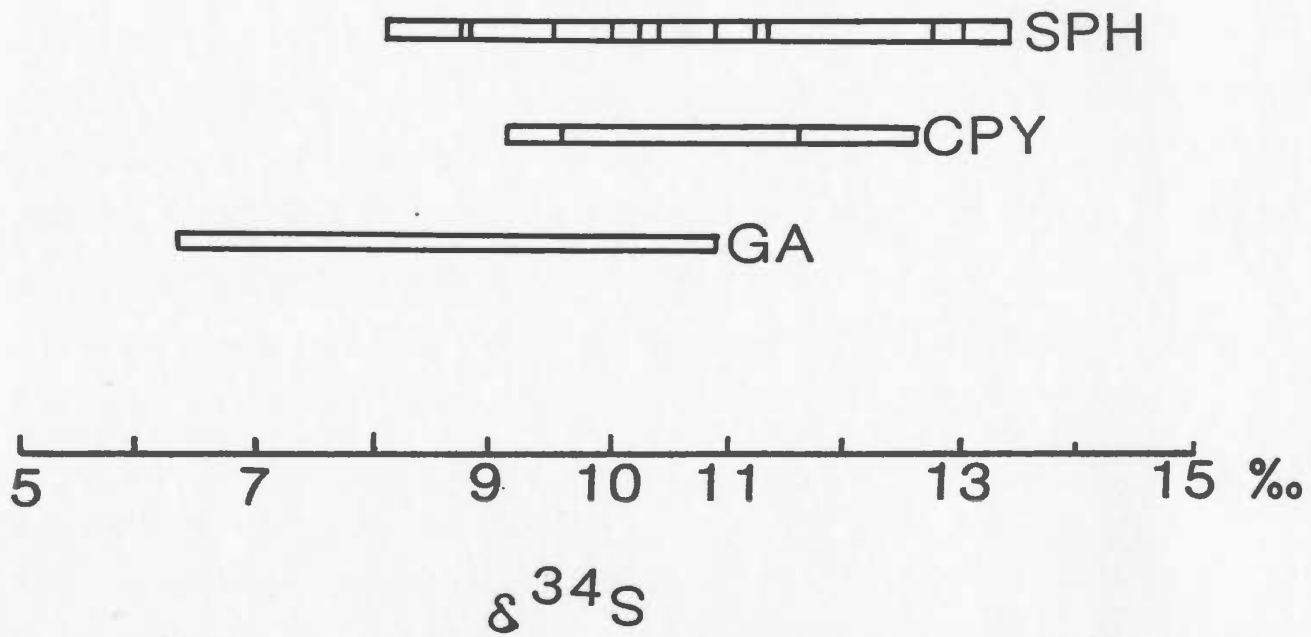

Figure 5-25: Sulphur isotopic ratios in galena (ga), chalcopyrite (cpy) and sphalerite (sph).

two most abundant sulphur isotopes, is generally expressed relative to the standard (Canyon Diablo Meteorite) as:

$$\delta\,{}^{34}S = \frac{({}^{34}S/{}^{32}S\ (\text{sample}) - {}^{34}S/{}^{32}S\ (\text{Std}))*1000}{{}^{34}S/{}^{32}S\ (\text{Std})}$$

The symbol & represents delta, the fractionation factor.

Both organic and inorganic processes lead to sulphur isotope fractionation and it has been established that the $\delta\,{}^{34}S$ values of ore deposits are commonly signatures of the mode of formation of various types of mineralization (Rye and Ohmoto, 1974; Skirrow and Coleman, 1982). In sedimentary deposits for example, where bacterial reduction might produce most of the sulphides, the lighter isotope is concentrated, resulting in typically positive $\delta\,{}^{34}S$ values.

Sulphur isotopic ratios from the Twin Ponds Showing exhibit a narrow range of values from +6.3 to +13.4 permil with a mean of +10 permil. Such values are atypical of those in sulphides from igneous rocks (0 permil *i.e.* unfractionated with respect to the meteoritic standard) and of sedimentary sulphides whose mean values are generally negative. However sulphides in volcanoclastic sequences are typically positive (Stanton, 1972) with a small range of values within deposits.

Figure 5-26 compares $\delta^{34}S$ data from Isle aux Morts with various deposit types (Ohmoto and Rye, 1979) including that of Cape Ray which is situated approximately 5 km to the NW. Volcanogenic sulphides from New Brunswick and the Red Sea give the best comparison with those of the present study. Values are also typical of many volcanogenic massive sulphide deposits as reviewed in Franklin *et al.* (1981). Rye and Ohmoto (1974) conclude from a review of studies on sulphur isotopes that $\delta^{34}S$ variations are generally preserved during metamorphism. One indication that equilibrium has been reached or maintained in the Twin Ponds mineralization is the relative order of $\delta^{34}S$ enrichment *i.e.* sphalerite > chalcopyrite > galena in agreement with theoretical predictions (Kajiwara and Krouse, 1971). However small scale isotopic changes may take place (Ohmoto and Rye, 1974), for example by the conversion of pyrite into pyrrhotite at high temperatures which increases the fS_2 and will preferentially mobilize the lighter isotope (ref).

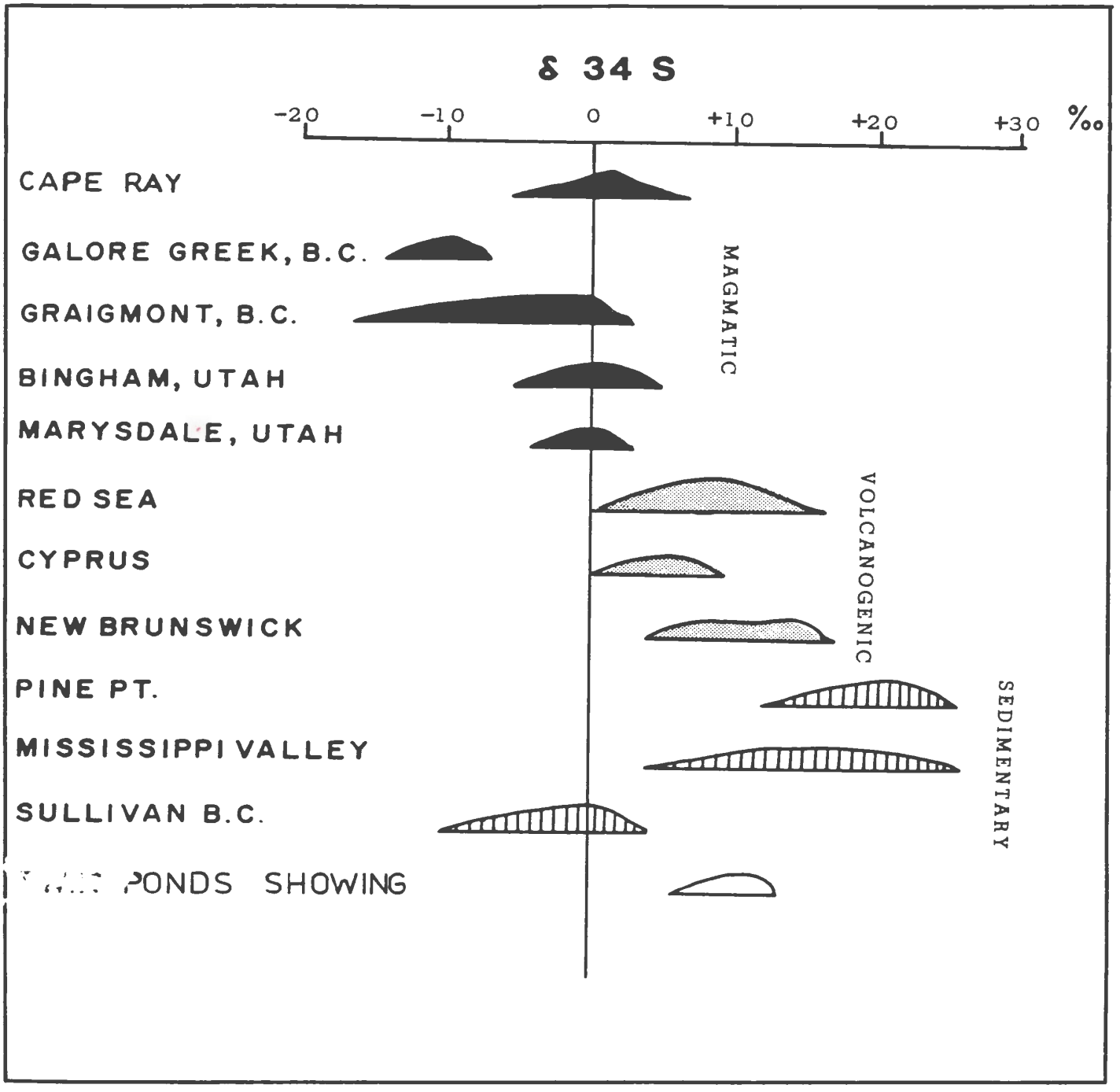

Figure 5-26: Comparison of the sulphur isotopic ratios from Isle aux Morts with those of other environments (from Ohmoto and Rye, 1979; Wilton, 1984).

5.8.2 Lead Isotopes

Six samples of coarse crystalline galena were analysed for 206/204, 207/204 and 208/294 Pb ratios. The results are listed below in Table 5-3; analytical procedures are listed in Appendix 4. Galena samples were taken from mineralized specimens collected near the Twin Ponds Showing.

Table 5-3: Isotopic analyses of leads from the Twin Ponds Showing.

#	206Pb/204Pb	207Pb/204Pb	208Pb/204Pb
Pb1	18.008	15.590	37.828
Pb2	18.013	15.588	37.827
Pb3	18.008	15.589	37.824
Pb4	18.009	15.591	37.828
Pb5	18.011	15.588	37.839
Pb6	17.980	15.588	37.801
Mean	18.010	15.589	37.829
Sigma	0.002	0.001	0.006

First five leads are used in the calculation of the mean.
Sigma = standard deviation of these five leads.

The three radiogenic isotopes of lead are 206, 207 (both produced by the breakdown of U) and 208 (from Th decay). ^{204}Pb, however, is non-radiogenic and is used as a common normalizer for the other leads (Stanton, 1972). Since the mass differences between the various Pb isotopes are negligible, fractionation is unimportant, unlike sulphur isotopes. Thus differences in the isotopic ratios reflect either differing source regions or age of the rocks. This

age will reflect the time at which the lead was separated from the parental U- and Th-bearing sources and concentrated in the mineralization; such leads are known as common leads (Stanton, 1972).

Various lead evolutionary models have been put forward (Cummings and Richards, 1975; Stacey and Kramer, 1975; Doe and Zartman, 1979). A review of these models is given by Koppel and Grunenfelder (1979). The plumbotectonics model of Doe and Zartman (1979) and Zartman and Doe (1981) recognises lead from three distinct environments, viz. mantle, upper continental crust and lower continental crust. However, island and continental arc rocks constitute an important mixing medium, the orogene, which defines an average lead isotopic composition varying with the proportions of respective source rocks.

In Figure 5-27 (Zartman and Doe, 1981) the average lead isotopic value from the study area plots very close to the orogene in both diagrams. Doe and Zartman (1979) have separated two types of Phanerozoic massive sulphide deposits in the island arc regime, viz., primitive (e.g. Buchans) and mature (e.g. Kuroko). The former plot near the mantle curve while the latter are on or close to the orogene. The Isle aux Morts lead data are more compatible with the mature arc interpretation on the basis of lead isotopes. Because of the complex history of the region, these conclusions have to be assessed in relation to the tectonostratigraphic details of SW Newfoundland, which are discussed later.

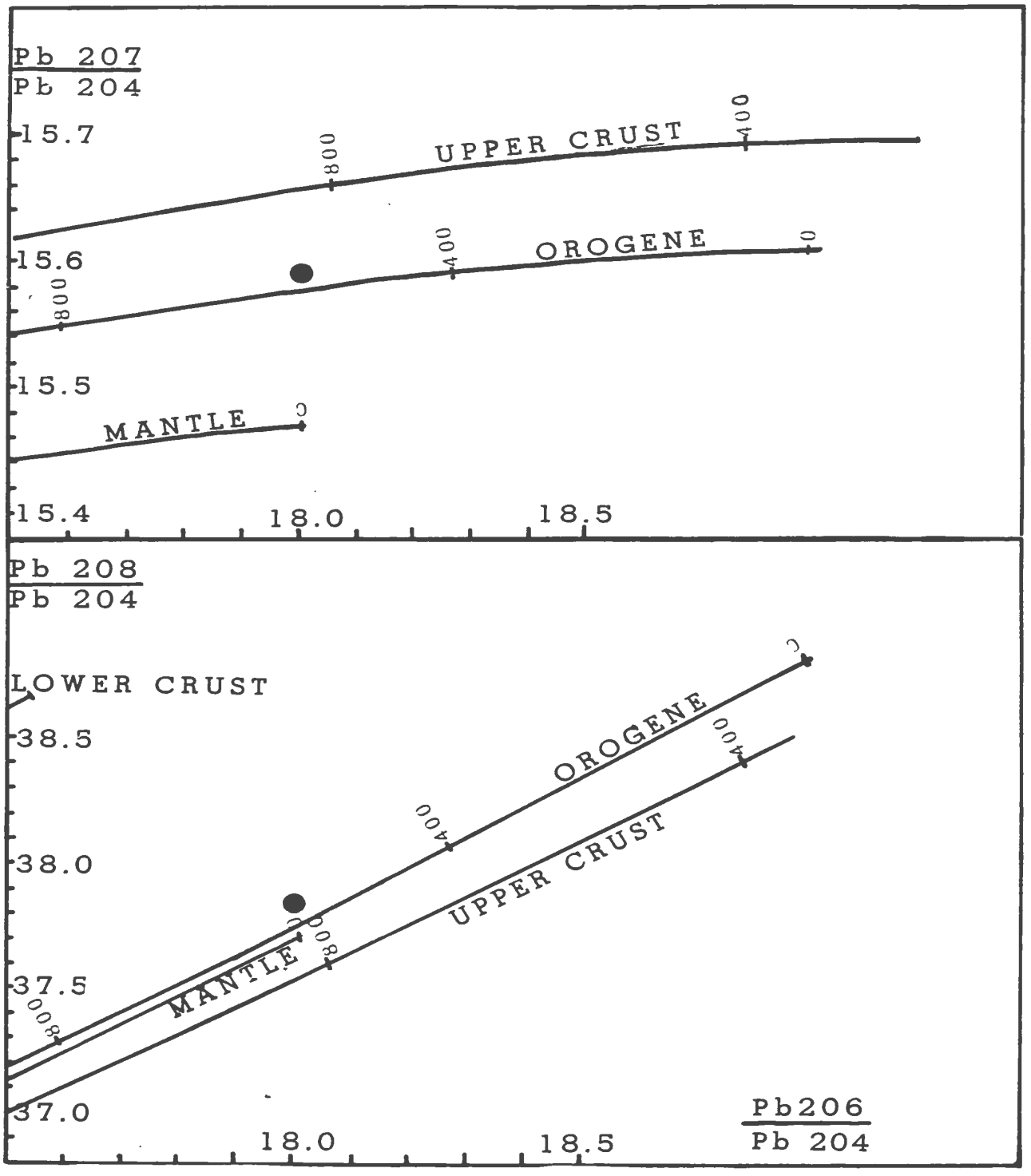

Figure 5-27: Growth curves from Zartman and Doe (1981); in both diagrams the Isle aux Morts leads plot close to the orogene curve.

The diagrams in Figure 5-28 compare the Isle aux Morts lead data to other Newfoundland deposits (Swinden and Thorpe, 1984). In the $^{208}Pb/^{204}Pb$ vs $^{206}Pb/^{204}Pb$ plot the

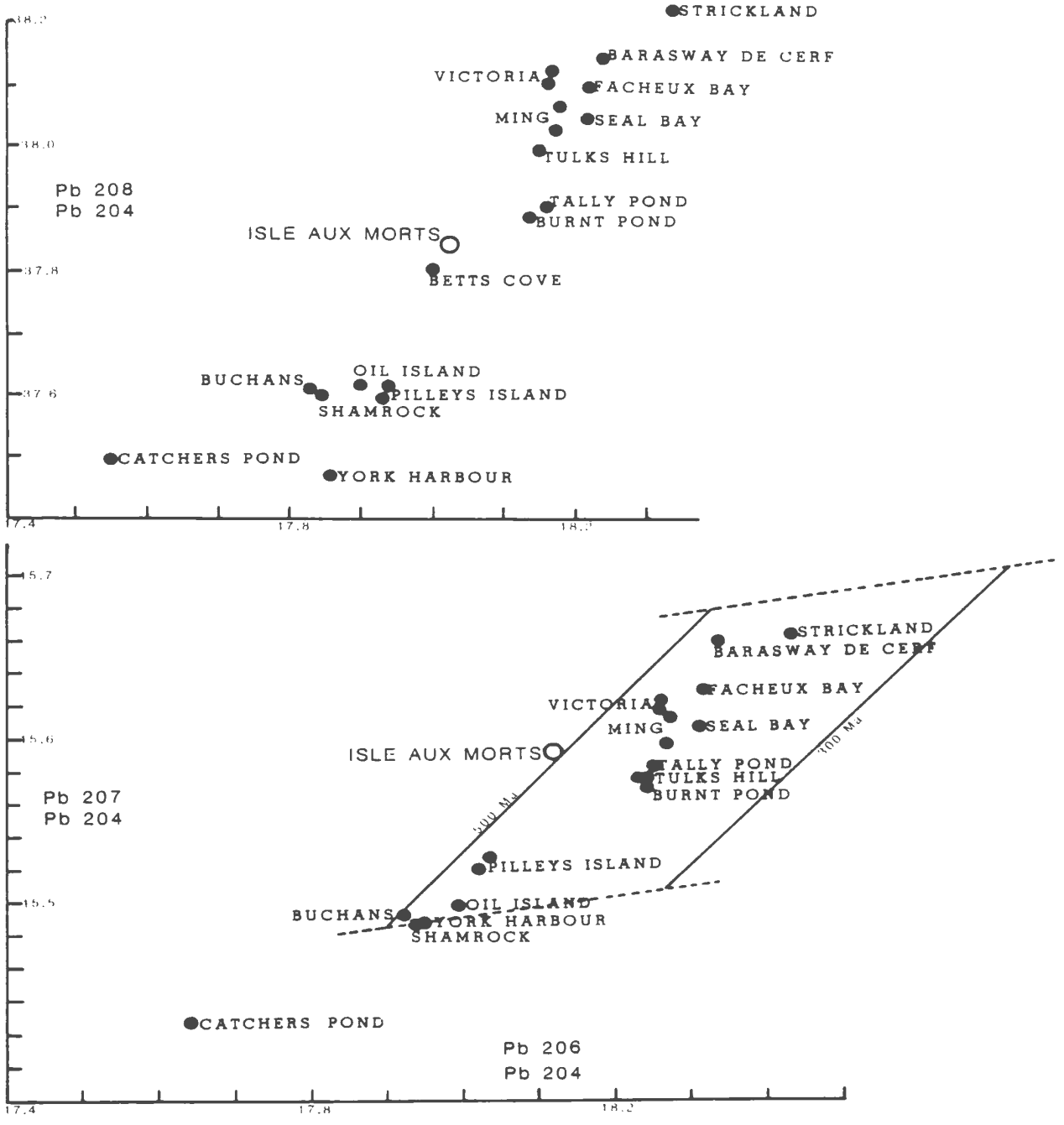

Figure 5-28: The relationship between Isle aux Morts leads and those of deposits through the Central Volcanic Belt (Swinden and Thorpe, 1984); note partly anomalous Pb206 value in lower diagram.

isotopes (this study) fall directly on the linear trend defined by Newfoundland massive sulphides; on the other plot they are marginally off the line. The linear arrays are defined at one end by radiogenic leads from the south coast

e.g. Strickland and the most primitive leads are those of Buchans and Catcher's Pond. Intermediate leads from the pre-Caradocian island arc deposits e.g. Tally Pond, Burnt Pond and Tulks Hill are more radiogenic than the leads of this study, even though the IAM area is dominated by felsic rocks which are subordinate in Tally Pond, etc. (less than 30%, Swinden and Thorpe, 1983). Anomalous leads in the Appalachian system have been discussed by Thorpe et al. (1981), who suggest that lead isotopes from Bathurst indicate crust of Grenvillian age. Variations in lead isotope values from central to southern Newfoundland may be explained (Swinden and Thorpe, 1984) by addition of relatively radiogenic lead, postulated by these authors as Avalonian, to oceanic lead. They suggest that volcanism and generation of sulphide deposits occurred at or near the Avalonian continental margin. A decreasing radiogenic lead component, northwestwards from the Hermitage Flexure area, reflects the waning influence of the Avalon Terrane and an increasing oceanic crustal effect.

That the Isle aux Morts leads are anomalous is also suggested by the tholeiitic nature and ocean floor basalt affinity of the intercalated amphibolites, not generally associated with mature island arcs.

The complex history that common leads may have suffered is not generally recorded clearly in their values and thus model lead ages must be treated with caution. In Figure 5-27 (Zartman and Doe, 1981) model ages are approximately

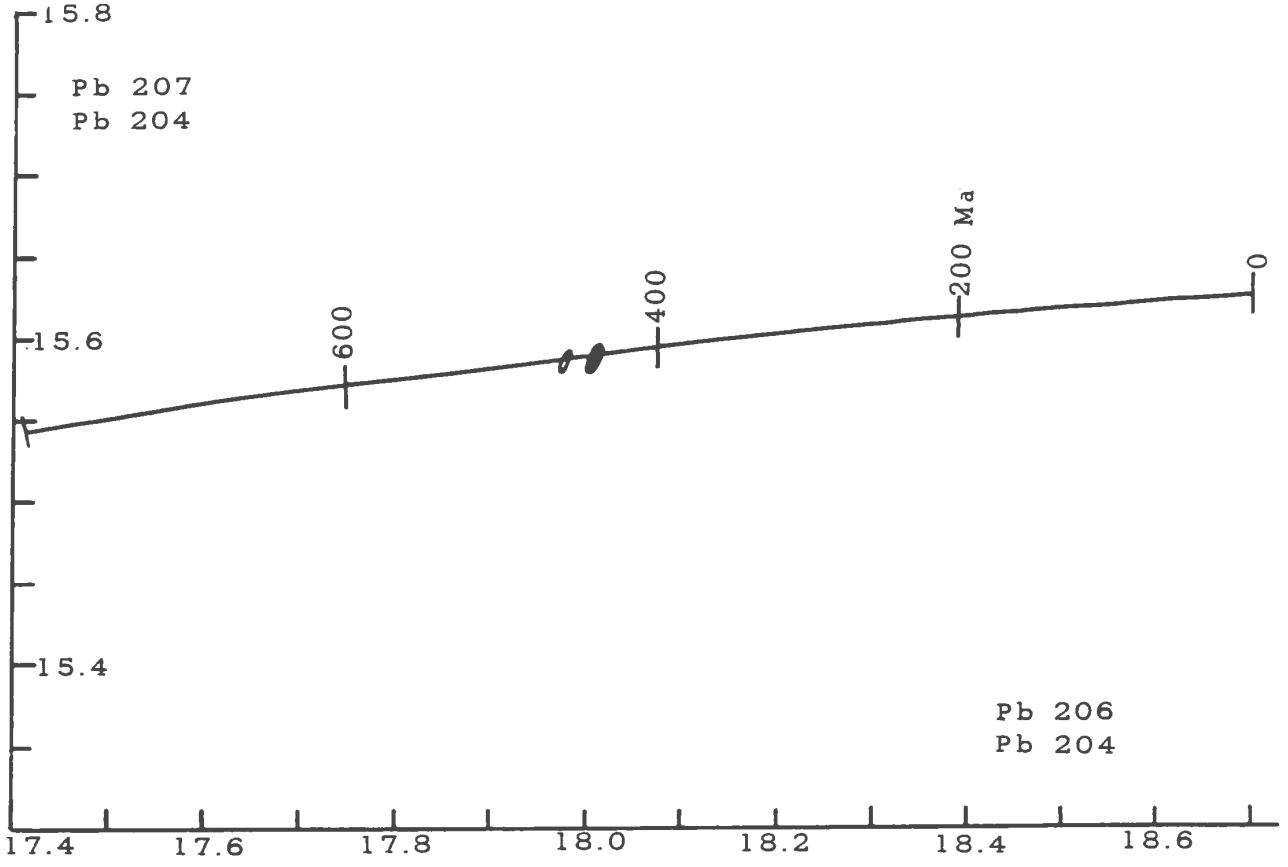

Figure 5-29: Growth curves from Stacey and Kramer (1975) indicating a 440 Ma age for Isle aux Morts leads; the main cluster contains 5 values.

600 Ma; in Figure 5-29 (growth curve from Stacey and Kramer, 1975) the age is 440 Ma; the model age from Cummings and Richards, 1975) is approximately 410 Ma (not shown). The 440 Ma figure accords better with regional dates (Swinden and Thorpe, 1983). However, the 410 Ma date does agree with a U-Pb zircon and sphene date of 410 ± 5 Ma (G.R. Dunning, pers. comm., 1985) from a garnet-bearing amphibolite collected approximately 300 m east of Twin Ponds. Zircons and sphenes both suffer lead loss until their closing temperatures of approximately 650 and 450-500 °C, respectively (Dunning, pers. comm., 1985). Thus 410 Ma

dates the metamorphic event and not the real rock age. The zircons were also found to contain an inherited component, perhaps a core, which gives a date of c.a. 1400 Ma. Wilton (1984) has postulated a Grenvillian source for the A-type Isle aux Morts Brook Granite, inferring a Grenvillian basement to the Port aux Basques Complex. Preliminary U-Pb dates from zircons in amphibolites from the Isle aux Morts area appear to corroborate this.

5.9 Summary and Conclusions

The principal features of the Twin Ponds Showing are listed below:

(1) The showing is polymetallic, i.e. it contains sphalerite, galena, chalcopyrite (up to 32 % combined Cu-Pb-Zn), pyrite, pyrrhotite and barite, minor Ag and trace Au;
(2) It is a tabular, blanket-shaped deposit which is readily interpreted, despite deformation, as stratiform and stratabound;
(3) It comprises massive, disseminated and banded sulphides;
(4) The banded sulphides are conformable with the host rock mineralogical layering and exhibit the same deformational features as them;
(5) Microfabric and petrofabric aspects of the ore minerals e.g. their typically elongated nature, especially in disseminated and banded varieties, and chalcopyrite disease in sphalerite, also imply that they have

suffered the effects of regional metamorphism; gahnite and hyalophane are also produced during amphibolite grade metamorphism;

(6) Massive sulphides form a pseudobreccia or Durchbewegung fabric typically seen in metamorphosed sulphide bodies in high-medium grade rocks;

(7) Average $\delta^{34}S$ value is 10 permil and can be compared to volcanic associated sulphide bodies;

(8) Host rocks to the showing are quartz-muscovite semipelites interpreted as felsic tuffs on a geochemical-lithological basis;

(9) Mineralized samples are enriched in K2O and depleted in Na2O, a typical feature of Kuroko-type deposits.

(10) No lateral or vertical variation in metal content is defineable but there is constant sympathetic variation in Cu-Pb-Zn-Ag-Ba values.

(11) Alteration haloes are undefineable in felsic rocks hosting the main showing or the minor occurrences further north.

(12) Metal ratios are similar to those in the Tulks/ Buchans and Hermitage area deposits which are supposedly floored by mafic and continental crust respectively; however the lead isotope studies indicate a Grenvillian type continental crust which is more compatible in terms of the volume of felsic material present in the Isle aux Morts prospect area.

Chapter 6
SUMMARY AND DISCUSSION

The three principal aims of this study have been to describe and evaluate the history and origin of the Twin Ponds Showing and elucidate the local geological history within a regional context.

The Isle aux Morts Prospect area contains a structurally conformable, and chemically bimodal, group of rocks ranging from felsic to ultramafic types. Mafic meta-fragmental rocks in the north are thought to represent locally shallow, possibly emergent conditions. These are succeeded to the south by supposed felsic meta-tuffs/reworked felsic tuffs containing disseminated and locally thinly banded sulphides. The Twin Ponds Showing, comprised of sphalerite, galena, chalcopyrite, pyrite and barite, forms a marker horizon between these meta-tuffs and banded quartzofeldspathic rocks to the south which are thought to be volcanoclastic tuffs and/or greywackes. Sulphides are absent from these latter rocks, which contain intercalated shales (pelites) and thin mafic meta-tuffs and/or dykes/sills (amphibolites). Numerous coticules occur in the pelites.

The amphibolites are tholeiitic and the chemistry

indicates a strong affinity with ocean floor basalts. Two groups of amphibolites are recognized: 1, a low SiO2, high Cr, Ni and MgO group, and 2, a high SiO2, low Cr, Ni and MgO group. This grouping may reflect at least in part, a sampling bias in a relatively small study area. However, since various chemical trends are continuous, the groups are thought to be cogenetic and may reflect different parts of a fractionated suite.

The similarity with ocean floor basalts does however, conflict with other evidence as to the nature of the local tectonic setting. The preponderance of felsic rocks in the Isle aux Morts area and the presence of much lead in the Twin Ponds Showing, indicates sialic crustal influence. Chorlton (1984) has correlated the Port aux Basques Gneiss Complex with the La Poile and Bay du Nord Groups (of the Hermitage Flexure area) and postulates that these rocks form part of an Ordovician island arc. The bimodal nature of the Isle aux Morts rocks, however, does not equate with this theory. Chorlton (1984) also favours the presence, at least locally in the La Poile/Bay du Nord area, of oceanic crust. Swinden and Thorpe (1984) suggest, on the basis of a lead isotope mixing model, that the Hermitage Flexure area has an Avalonian continental crust but that northwards, towards Central Newfoundland, oceanic crust becomes increasingly dominant. The similarity of Isle aux Morts metal ratios, with those of the Hermitage Flexure and Victoria Lake areas, suggests sialic and simatic influences.

Lead isotopes for the Isle aux Morts area are much less radiogenic than those in the Hermitage Flexure area and less so than those of the Victoria Lake area. Basalts in the Victoria Lake Group have MORB affinity (Dunning, 1984). Thus, the Isle aux Morts leads are too primitive to fit into the mixing model of Swinden and Thorpe (1984).

Continental crust of Grenvillian age (1.2 Ga) and type (i.e. primitive, due to direct derivation from the mantle) has been postulated as the source of the Isle aux Morts Brook Granite (dated by Rb/Sr as 352 $\pm$ 6 Ma, Wilton, 1984). Although lead isotopes ratios from the Cape Ray Fault Zone are quite different (more primitive) from those of Isle aux Morts, the relatively primitive nature of the Isle aux Morts leads is compatible with derivation from Grenvillian crust. Zircon from Isle aux Morts amphibolites have an apparently inherited component, dated at c.a. 1400 Ma which supports the argument for a Grenvillian basement.

Chemistry and lead isotope evidence suggests both continental and oceanic crustal influences exist for the Isle aux Morts area. The bimodal character of the rocks may reflect a local extensional tectonic setting possibly within a Grenvillian-type crust, producing rift-related volcanism tapping a mantle source. Although possibly, locally or initially extensional, the environment ultimately became compressional, at which time the Isle aux Morts rocks were tectonically buried and metamorphosed to amphibolite facies. This metamorphism has been dated by U-Pb methods on zircons

and sphenes at 410 ± 5 Ma. An alternative, possibly related, model involves a transitional tectonic environment, at the interface between continental and oceanic crust. The interbedded shales (pelites) and volcaniclastic greywackes in the study area suggest a deep water basinal setting, possibly a fore-arc or inter-arc basin. The absence of high-pressure, blueschist facies rocks may preclude a trench-type locale. A transitional type setting has also been suggested (Dunning, 1984) for the bimodal Victoria Lake Group, which is chemically similar to the Isle aux Morts amphibolites. These two groups, although spatially separate, may be correlative, at least on the basis of tectonic setting.

Regardless of the type of tectonic setting, volcanism did occur in the Isle aux Morts area and with it, genetically related polymetallic sulphide mineralization of the Twin Ponds Showing. Despite the effects of multiple episodes of metamorphism and deformation, characteristic features of massive sulphide bodies in volcanic suites are retained. However, as sulphide phases are generally unquenchable and do not retain high temperature characteristics, most features observed in the ore minerals are due to re-equilibration at lower temperatures.

Some classification schemes for massive sulphide bodies are based on ore element and host rock composition. These indicate that the Twin Ponds Showing is a Pb-Zn-Cu type.

Massive sulphide bodies typically occur at the top of

felsic sequences or at a felsic-mafic or felsic-sedimentary interface. The latter case seems generally applicable here. The sequence to the north of the Twin Ponds Showing is dominated by felsic rocks with mafic material becoming important near the north end of the mapped area. South of the showing, shales (biotite-garnet schists) and probable volcanoclastic greywackes are present. The mineralizing event which produced the Twin Ponds Showing may have occurred at a hiatus in volcanic activity/sedimentaton which allowed the sulphides to accumulate. Within the felsic tuffs to the north, the ubiquitous disseminated and banded sulphides attest to metal-rich fluids originally present either syngenetically or epigenetically during sedimentation. Local concentrations of disseminated Cu rather than Pb-Zn may reflect varied physicochemical conditions. In the south, the only evidence for chemical precipitation which may indicate continued volcanic activity are coticules, interpreted as manganiferous cherts.

Certain features of the showing which might suggest a distal nature are :

(a) It is Pb-Zn-rich and Cu poor;
(b) It occurs within a mixed sedimentary-volcanic pile;
(c) It has a tabular form;
(d) There is no recognizeable footwall alteration zone;
(e) Metal zoning is absent.

The intense deformation that these rocks have undergone may

have completely transposed and attenuated any alteration zone which might have existed. The only alteration of note i.e. K_2O/Na_2O enrichment/depletion and REE depletion, is localized to actual mineralized samples, suggesting that the sulphides were precipated from fluids whose source was relatively distal from the depositional area. The ubiquitous quartz boudins and pods in the mineralized horizon originally may have been cherts or cherty tuffs which are common associates of syngenetic sulphide bodies.

Although the complex deformation makes exploration difficult, it may concentrate the sulphides, as e.g. at Bathurst where structural interference basins between F1 and F2 have helped to produce the Brunswick #6 and #12 mines. The mineralization type and setting at Bathurst is also similar to the Twin Ponds Showing. Drilling on the Isle aux Morts property has not succeeded in showing any depreciation in metal grades to a minimum depth of 100 metres. Since the massive/pseudobreccia ore is present over a strike length of approx 2 km (locally grading at approximately 30% combined Zn-Pb-Cu) there is much potential for exploration by deep drilling.

Further northeast in claim block 2329, a gedrite-plagioclase-magnetite-bearing rock is characteristally associated with quartz-muscovite schists. A spatial and genetic relationship has been documented between gedrite rocks and alteration haloes associated with volcanogenic mineralization. Some gedrite-magnetite beds in Bohemia have

been interpreted as metamorphosed Fe formations. Gedrite-plagioclase-magnetite rocks may represent oxidic-Fe formations derived from hydrothermal fluids. Gedrite-cordierite assemblages have also been interpreted as alteration pipe material (MacLean and MacGeehan, 1976). The apparent absence of cordierite in the Isle aux Morts area may be compositionally and/or pressure/temperature-controlled. Thus the association of quartz-muscovite schists which is sometimes seen to envelop massive/disseminated sulphide deposits, and gedrite-bearing rocks representing Mg-Fe alteration, could form a useful exploration guide in the Isle aux Morts Prospect area.

BIBLIOGRAPHY

Abbey, S., 1980; Studies in "standard samples" for use in the general analysis of silicate rocks and minerals. Part 6: 1979 edition of "usable values". Geol. Surv. of Canada, Paper 80-14, 30 p.

Atherton, M.P., 1968; The variation in garnet, biotite and chlorite composition in medium grade pelitic rocks from the Dalradian, Scotland, with particular reference to the zonation in garnet. Can. Mineral. and Petrol., Vol 18, pp. 347-371.

Bagby, W.C., Cameron, K.L. and Cameron, M., 1981; Contrasting evolution of calc-alkaline volcanic and plutonic rocks of western Chihuahua, Mexico. in Granites and rhyolites. Special issue of Jour. of Geophysical Research, Vol 86, # B11, pp. 10402-10410.

Basaltic volcanism on the terrestrial planets (BVTP), 1981; Pergamon Press, Inc., New York, 1286 p.

Barth, T.F.W., 1962; Theoretical Petrology. John Wiley and Sons, Inc., New York, 387 p.

Barton, P.B., 1978; Some ore textures involving sphalerite from the Furutobe mine, Akita Prefecture, Japan: Mining Geol., Vol 28, pp. 293-300.

Bence, A.E. and Albee, A.L., 1968; Empirical correction factors for the electron microanalysis of silicates and oxides. Jour. of Geol., Vol 76, pp. 382-403.

Berthe, D., Choukrune, P. and Jegouzo, P., 1979; Orthogneiss, mylonite and non-coaxial deformation of granites: the example of the South Armorican shear zone. Jour. of Struct. Geol., Vol 1, pp. 31-42.

Beswick, A.E. and Soucie, G., 1978; A correction procedure for metasomatism in an Archaen Greenstone belt. Precambrian Research, 6, pp. 235-248.

Bickle, M.S. and Archibald, N.J., 1984; Chloritoid and staurolite stability: implications for metamorphism in the Archaen Yilgarn Block, Western Australia. Jour. of Met. Geol., #2, pp.179-203.

Blackwood, R.F., 1978; Northeastern Gander zone; in Gibbons, R.V., ed., Report of activities for 1977: Newfoundland Dept. of Mines and Energy, Mineral Devel. Div. Report 78-1, pp. 72-79.

Blackwood, R.F. and Kennedy, M.J., 1975; The Dover Fault:

western boundary of the Avalon Zone in northeastern Newfoundland. Can. Jour. of Earth Science, Vol 12, pp. 320-325.

Brookes, I.A., 1977; Geomorphology and quaternary geology of Codroy Lowland and adjacent plateaus, southwest Newfoundland. Can. Jour. of Earth Science, Vol 14, pp. 2101-2120.

Brown, P.A., 1973a; Structural and metamorphic history of the gneisses of the Port aux Basques region, Newfoundland. Unpub. M.Sc. thesis, Memorial University of Newfoundland, St John's, 113 p.

Brown, P.A., 1973b; Possible cryptic suture in southwestern Newfoundland. Nature Phys. Science, Vol 245, pp. 9-10.

Brown, P.A., 1975; Basement-cover relationships in southwest Newfoundland. Unpub. Ph.D. thesis, Memorial University of Newfoundland, St John's, 221 p.

Brown, P.A., 1976; Geology of the Rose Blanche map area (11 O/10), Newfoundland. Mineral Devel. Div., Dept. of Mines and Energy, St. John's, Newfoundland.

Brown, P.A., 1977; Geology of the Port aux Basques map area (11 O/11), Newfoundland. Mineral Devel. Div., Dept. of Mines and Energy, St. John's, Newfoundland.

Brown, P.A. and Colman-Sadd, S.P., 1976; Hermitage flexure; figment or fact?: Geology, Vol 4, pp. 561-564.

Cann, 1970,; Rb, Sr, Y, Zr and Nb in some ocean floor basalts. Earth Planet. Sci. Let., 10, pp. 7-11.

Carmichael, D.M., 1978; Metamorphic bathozones and bathograds: a measure of the depth of post-metamorphic uplift and erosion on the regional scale. Amer. Jour. of Science, Vol 278, pp. 769-797.

Chorlton, L.B., 1978; The geology of the La Poile map area (110/9) Newfoundland. Newfoundland Dept. of Mines and Energy, Report 78-5, 14 p.

Chorlton, L.B., 1980a; Grandy's Lake, west half. in Newfoundland Dept. of Mines and Energy, Report 80-1, Current Research, pp. 74-78.

Chorlton, L.B., 1980b; Geology of the La Poile River area (110/16), Newfoundland. Newfoundland Dept. of Mines and Energy, Report 80-3, 86 p.

Chorlton, L.B., 1980c; Peter Snout, west half. in Newfoundland Dept. of Mines and Energy, Report 80-1, Current Research, pp. 62-73.

Chorlton, L.B., 1983; Early Palaeozoic development of southwest Newfoundland. in Regional trends in the geology of the Appalachian-Caledonian-Hercynian-Mauritanide Orogen, ed. Schenk, P.E., D. Reidel and Co., pp. 381-382.

Chorlton, L.B., 1984; Geological development of the southern Long Range Mountains, southwest Newfoundland: A regional synthesis. Ph.D. Memorial University of Newfoundland, 600 p.

Colman-Sadd, S.P., 1980; Geology of south-central Newfoundland and evolution of the eastern margin of Iapetus. Amer. Jour. of Science, Vol 280, pp. 991-1017.

Cooper, J.R., 1954; La Poile-Cinq Cerf map area, Newfoundland. Geol. Surv. of Can. Mem., 276, 62 p.

Crawford, M.L., 1977; Calcium zoning in almandine garnet, Wissahickon Formation, Philadelphia, Pennsylvania. Can. Min., Vol 15, pp. 243-249.

Cummings, G.L. and Richards, J.R., 1975; Ore lead isotope ratios in a continuously changing earth. Earth and Planet. Science Letters, Vol 28, pp. 155-171.

Davies, J.F., Grant, R.W.E. and Whitehead, R.E.S., 1979; Immobile trace elements and Archaen volcano-stratigraphy in the Timmins mining area, Ontario. Can. Jour. of Earth Science, Vol 16, pp. 305-311.

Deer, W.A., Howie, R.A. and Zussman, J., 1976; An introduction to the rock forming minerals. Longman, London, 528 p.

Dingwell, D.B., 1980; The geology, geophysics and geochemistry of the Port aux Basques Granite. B. Sc. (Hons.) Thesis, Memorial University of Newfoundland.

Docka, J.A., 1984; New England coticules: unusual textures and bulk rock chemistry as evidence of multiple origins. Abstracts with programs: Geol. Soc. of Amer., N.E. section.

Doe, B.R. and Zartman, R.E., 1979; Plumbotectonics; the Phanerozoic. in Barnes, H.L., ed. Geochemistry of hydrothermal ore deposits, New York, John Wiley and Sons, pp. 22-70.

Droop, G.T.R., 1981; Alpine metamorphism of pelitic schists in the southeast Tauern Window, Austria. Schweiz. Mineral. Petrog. Mitt., Vol 61, pp. 237-273.

Dunning, G.R., 1984; The geology, geochemistry, geochronology and regional setting of the Annieopsquotch Complex and related rocks of southwest Newfoundland. Unpub. PhD Thesis, Memorial University of Newfoundland, St. John's, 402 p.

Dunning, G.R. and Herd, R.K., 1980; The Annieopsquotch ophiolite complex southwest Newfoundland, and its regional relationships. in Current Research, Geol. Surv. of Can., Paper 80-1a, pp. 227-234.

Eldridge, C.S., Barton, P.B. and Ohmoto, H., 1983; Mineral textures and their bearing on the formation of the Kuroko and related volcanogenic massive sulphide deposits. Econ. Geol. Monograph 5, pp. 241-281.

Evans, B.W. and Leake, B.E., 1960; The composition and origin of striped amphibolites of Connemara, Ireland. Jour. of Petrol., Vol 1, pp 337-363.

Evans, B.W., 1965; Application of a reaction rate method to the breakdown equilibria of muscovite and muscovite plus quartz. Amer. Jour. of Science, 263, pp. 647-667.

Ferry, J.H. and Spear, F.S., 1978; Experimental calibration of the partitioning of Fe and Mg between garnet and biotite. Contrib. Mineral. Petrol. 66, pp. 113-117.

Floyd, and Winchester, 1975; Magma type and tectonic setting discrimination using immobile elements. Earth Planet. Sci. Let., 27, pp. 211-218.

Floyd, P. and Winchester, J.A., 1978; Identification and discrimination of altered and metamorphosed volcanic rocks using immobile elements. Chem. Geol., 21, pp. 291-306.

Franklin, J.H., Sangster, D.M. and Lydon, J.W.,1981; Volcanic associated massive deposits. in Seventy-fifth Anniversary Volume, 1905-1980: Econ. Geol. pp. 485-627.

Fryer, B.J., 1977; Rare earth evidence in iron formations for changing Precambrian oxidation states. Geochim. et Cosmochim. Acta, Vol 41, pp. 361-367.

Gair, J.E. and Slack, J.F. 1984; Deformation, geochemistry and origin of the massive sulphide deposits, Gossan Lead District, Virginia. Econ.Geol., Vol 79, #7, pp. 1483-1520.

Gale, G.H., 1967; Economic assessment of pegmatites. Unpub. report, Mineral Resources Division, Newfoundland Dept. of Mines, Agriculture and Resources, St. John's.

Ganguly, J., 1972; Staurolite stability and related parageneses; Theory, Experiments and Applications. Jour. of Petrol., Vol 13, part 62, pp. 335-365.

Ganguly, J. and Kennedy, G.C., 1974; The energetics of natural garnet solution. 1. Mixing of the aluminosilicate end members. Contrib. Mineral. Petrol. 48, pp. 137-148.

Garrels, R.M. and Mackenzie, F.T., 1971; Evolution of sedimentary rocks. W. Norton and Co. Inc., New York, 397 p.

Ghent, E.D., 1976; Plagioclase-garnet-aluminosilicate-quartz: a potential geobarometer-geothermometer. Amer. Mineral. 61, pp. 710-714.

Ghent, E.D., Robbins, D.B., and Stout, M.Z., 1979; Geothermometry, geobarometry and fluid compositions of metamorphosed calc-silicates and pelites, Mica Creek, B.C. Amer. Mineral., 64, pp. 874-885.

Ghent, E.D., Knitter, C.C., Raeside, R.P. and Stout, M.Z., 1982; Geothermometry and geobarometry of pelitic rocks, upper kyanite and sillimanite zones, Mica Creek area, B.C. Can. Mineral. Vol 20, pp. 295-305.

Gillis, J.W., 1972; Geology of Port aux Basques Map area, Newfoundland; report and map 1340A, Geol. Surv. Can. paper 71-42, 6 p.

Goff, S.P., 1984; The magmatic and metamorphic history of the East Arm, Great Slave Lake, N.W.T. Ph.D. thesis, University of Alberta, 295 p.

Graf, J.L. 1977; Rare earth elements as hydrothermal traces during the formation of massive sulphide deposits in volcanic rocks. Econ. Geol., Vol 72, pp. 527-548.

Hajash, A. (Jr), 1984; Rare earth element abundances and distribution patterns in hydrothermally altered basalts: experimental results. Contrib. Mineral. and Petrol., vol 85, pp. 409-412.

Haskin, L.A., Frey, F.A. and Wildeman, T.R., 1968; Relative and absolute terrestrial abundances of the rare earths. in Origin and distribution of the elements., ed. Ahrens, L.H., Int. Ser. Monogr. Earth Sci., Vol 30, pp. 689-912.

Hobbs, B.E., Means, W.D. and Williams, P.F., 1976; An outline of structural geology. John Wiley and Sons, Inc., 571 p.

Hodges, K.V. and Spear, F.S., 1982; Geothermometry and geobarometry and the aluminosilicate triple point at Mt. Moosilauke, New Hampshire. Amer. Mineral., 67, pp. 1118-1134.

Holdaway, M.J., 1971; Stability of andalusite and the aluminosilicate phase diagram. Amer. Jour. of Science, 271, pp. 97-131.

Hollister, L.S., 1966; Garnet zoning: an interpretation based on the Rayleigh fractionation model. Science, Vol 154, pp. 1647-1651.

Hollister, L.S., 1969; Metastable paragenetic sequence of andalusite, kyanite and sillimanite, Kwoiek area, B.C. Amer. Jour. of Sci., Vol 267, pp 352-370.

Hoschek, G., 1969; The stability of staurolite and chloritoid and their significance in metamorphism of pelitic rocks. Can. Min. and Pet., Vol 22, pp. 208-232.

Howse, A., 1934; Supplementary report on the Rose Blanche area. Newfoundland Dept. of Natural Resources. Unpub. Rep.

Howse, A., 1937; Preliminary report on the grade and ore occurrences of the Bay du Nord area, La Poile Bay, Newfoundland. Newfoundland Dept. of Mines and Energy unpub. report, 6 p.

Hughes, C.J., 1973; Spilites, keratophyres and the igneous spectrum. Geol. Mag., 109, pp. 513-527.

Irvine, T.N. and Baragar, W.R., 1973; A guide to the chemical classification of the common volcanic rocks. Can. Jour. of Earth Science, Vol 8, pp. 523-548.

Jakes, P. and Gill, J., 1970; Rare earth elements and the island arc tholeiite series. Earth and Planet. Science Letters, 9, pp. 29-33.

Jukes, J.B., 1843; General report of the Geological Survey of Newfoundland, 1839-1840. Pub. by John Murray, London, 160 p.

Kajiwara, Y. and Krouse, H.R., 1971; Sulphur isotope partitioning in metallic sulphide systems. Can. Jour. of Earth Science, Vol 8, p. 1397.

van de Kamp, P.C., 1969; Origin of amphibolites in the Beartooth Mountains, Wyoming and Montana: new data and interpretations. Geol. Soc. of Amer. Bull., 82, 2, pp. 1127-1135.

van de Kamp, P.C., Leake, B.E. and Senior, A., 1976; The petrography and geochemistry of some Californian arkoses with application to identifying gneisses of metasedimentary origin. Jour. of Geol., Vol 84, pp. 195-212.

Kean, B.F., 1983; Geology of the King George IV lake map area (12A/4). Mineral Devel. Div., Nfld. Dept. of Mines and Energy. Report 83-4, 67 p.

Kennan, P.S. and Kennedy, M.J., 1983; Coticules; a key to correlation along the Appalachian-Caledonian orogen? in Regional trends in the geology of the Appalachian-Caledonian-Hercynian-Mauritanide orogen. Paul Schenk, editor, pp. 355-361.

Kennedy, M.J., 1971; Structure and stratigraphy of the Fleur de Lys Supergroup in the Fleur de Lys area, Burlington Peninsula, Nfld. Proc. Geol. Assoc. of Canada, 24, (1), pp. 59-71.

Kennedy, M.J. and McGonigal, M.H., 1972; The Gander Lake and Davidsville Groups of northeastern Newfoundland; new data and geotectonic implications. Can Jour. of Earth Science, Vol 9, pp. 452-459.

Kennedy, M.J., 1975; Repetitive orogeny in the northeastern Appalachians- new plate tectonic models based on Newfoundland examples. Tectonophysics, Vol 9, pp. 452-459.

Kennedy, M.J., 1976; Southeastern margin of the northeastern Appalachians: Late Precambrian orogeny on a continental margin. Geol. Soc. Amer. Bull., Vol 87, pp. 1317-1325.

Kim, S.W., 1975; Geology of the Middle Ordovician coticules of western New England. Jour. of Geol. Soc. Korea, Vol 11, #1, 36-68.

Kojima, S. and Sugaki, A., 1985; Phase relations in the Cu-Fe-Zn-S system between 300 and 500 °C under hydrothermal conditions. Econ. Geol., Vol 80, pp. 151-171.

Koppel, V. and Grunenfelder, M., 1979; Isotope geochemistry of lead. in Lectures in isotope geology. ed. Jager, E. and Hunziltev, J.C., Springer-Verlag, Berlin, 329 p.

Kramm, U., 1976; The coticule rocks (spessartine quartzites) of the Venn-Stavelot Massif, Ardennes; a volcanoclastic metasediment. Contrib. Mineral. and Petrol.., 56, pp. 135-155.

Labotka, T.C., 1980; Petrology of a medium-pressure regional metamorphic terrane, Funeral Mountains, California. Amer. Mineral., Vol 65, pp. 670-689.

Large, R.R., 1977; Chemical evolution and zonation of massive sulphide deposits in volcanic terrains. Econ. Geol., Vol 72, pp. 549-572.

Leake. B.E., 1964; The chemical distinction between ortho- and para-amphibolites. Jour. of Petrol., Vol 5, part 2, pp. 238-254.

Leake, B.E., 1980; Some metasomatic calc-magnesian silicate rocks from Connemara, western Ireland: mineralogical control of rock composition. Amer. Mineral., Vol 65, pp. 26-36.

Lydon, J.W., 1984; Ore deposit models-8. Volcanogenic Massive Sulphide Deposits. Part 1: A descriptive model. Geoscience Canada, Vol 11, #4, pp. 195-202.

MacLean, W.H. and MacGeehan, P.J., 1976; Garon Lake mine; case history 76-1. Montreal, McGill University, Mineral Exploration Research Institute, 67 p.

Menzies, M. and Seyfried, W. (Jr), 1979; Experimental evidence of rare earth element mobility in greenstones. Nature, Vol 282, # 5737, pp. 398-399.

Miyashiro, A., 1973; Metamorphism and metamorphic belts. John Wiley and Sons, New York, 492 p.

Miyashiro, A. and Shido, F. 1973; Progressive compositional change of garnet in metapelite. Lithos 6, pp. in Miyashiro (ibid.).

Moeller, P. and Muecke, G.K., 1984; Significance of Europium anomalies in silicate melts and crystal-melt equilibria: a reevaluation. Contrib. Mineral. Petrol., Vol 87, pp. 242-250.

Mookherjee, A., 1975; Temporal and genetic relationships. in Handbook of strataabound and stratiform ore deposits. Vol 4, Tectonics and Metamorphism, ed Wolf, K.H., pp. 203-260.

Murray, A. and Howley, J.P., 1881; Reports of the Geol. Surv. of Newfoundland for 1866-1880; Stanford.

Murray, A. and Howley, J.P., 1918; Report for 1899. in Report of the Geol. Surv. of Nfld. from 1881-1909. Published by Robinson and Co. Ltd.

Nance, W.B. and Taylor, S.R., 1976; Rare earth element

patterns and crustal evolution: 1. Australian post-Archaen sedimentary rocks. Geochim. et Cosmochim. Acta 40, pp. 1539-1551.

Niggli, P. 1954; Rocks and mineral deposits. W.M. Freeman and Co., 559 p.

Nold, J.L., 1983; The Holden mine, a metamorphosed volcanogenic deposit in the Cascade Range of Washington. Econ. Geol., Vol 78, pp. 944-953.

Ohmoto, H. and Skinner, B.J., 1983; The kuroko and related volcanogenic massive sulphide deposits: Introduction and summary of new findings. in The Kuroko and related volcanogenic massive sulphide deposits. Monograph 5, Econ. Geol., pp. 1-8.

Ohmoto, H. and Rye, R., 1979; Isotopes of sulphur and carbon. in Geochemistry of hydrothermal ore deposits. New York, John Wiley and Sons, pp. 509-567.

Orville, P.H., 1972; Plagioclase cation exchange equilibria with aqueous chloride solution: results at 700°C and 2000 bars in the presence of quartz. Amer. Jour. of Science, 272, pp 234-272.

Pearce, J.A., 1980; Geochemical evidence for the genesis and eruptive settings of lavas. Panayiotou, A., ed. Geol. Surv. Dept. Cyprus, pp. 261-.

Pearce, J.A. and Cann, J.R., 1973; Tectonic setting of basic volcanic rock, determined using trace element analysis. Earth and Planet. Science Letters, 19, pp. 290-300.

Pearce, J.A. and Gale, G.H., 1976; Identification of ore-deposition environment from trace element geochemistry of associated igneous rocks. In, Ore-forming processes in volcanic rocks.

Pettijohn, F.J., 1963; Chemical composition of sandstones, excluding carbonate and volcanic sands. in Data of Geochemistry, U.S.G.S. Paper 440-S, 19 p.

Pigage, L.C., 1976; Metamorphism of the Settler Schist, southwest of Yale, B.C. Can. Jour. of Earth Science, Vol 13, pp. 405-421.

Pigage, L.C. and Greenwood, H.J., 1982; Internally consistent estimates of pressure and temperature; the staurolite problem. Amer. Jour. of Science, Vol 282, pp. 943-969.

Plimer, I.R., 1980; Exhalative Sn and W deposits associated

with mafic volcanics as precursors to Sn and W deposits associated with granites. Mineral. Deposita, Vol 15, pp. 275-289.

Power, W.R., 1955; The south coast of Newfoundland in and around the villages of Isle aux Morts and Burnt Island. Unpub. report on summers field work, part 1, Newfoundland Dept. Mines and Resources, St John's.

Ramdohr, P., 1969; The ore minerals and their intergrowths. Pergamon Press, Oxford, 1174 p.

Ramsay, J.G., 1967; Folding and fracturing of rocks. McGraw-Hill, New York, 568 p.

Rao, B.B. and Johannes, W., 1979; Further data on the stability of staurolite and quartz and related assemblages. Neues. Jahrb. Mineralogie. Monatsh., pp. 407-447.

Rehkopff, A., 1985?; Origin of the quartzofeldspathic supracrustals in the Marranguitkangilerssua area, Nordre Stromfjord region , the central part of the Nagssugtoqidian of West Greenland. Rapp. Gronlands Geol. Unders. in press.

Renard, A., 1878; Sur la structure et la composition mineralogique du coticule. Mem. Cour. et Mem. des Sav. Acad. Royal de Belgique, 16.

Richardson, S.W., 1968; Staurolite stability in a part of the system Fe-Al-Si-O-H. Jour. of Petrol., Vol 9, pp. 467-488.

Rockingham, C.J. and Hutchinson, R.W., 1980; Metamorphic textures in Archaen Cu-Zn massive sulphide deposits. Can. Inst. of Min. Bull. April, pp. 104-112.

Rye, R.O. and Ohmoto, M., 1974; Sulphur and carbon isotopes and ore genesis: a review. Econ. Geol., Vol 69, pp. 826-842.

Scott, S.D., 1976; Application of the sphalerite geobarometer to regionally metamorphosed terrains. Amer. Mineral., Vol 61, pp. 661-670.

Senior, A. and Leake, B.E., 1978; Regional metamorphism and the geochemistry of the Dalradian metasediments of Connemara, western Ireland. Jour. Petrol., Vol 19, pp. 585-625.

Skirrow, R. and Coleman, M.L., 1984; Origin of sulphur and geothermometry of hydrothermal sulphides from the 86^{o} W. Galapogos Rift, Nature, Vol 299, pp. 142-144.

Spry, A., 1969; Metamorphic textures. Pergamon Press, 350 p.

van Staal, C.R. and Williams, P.F., 1984; Structure, origin and concentration of the Brunswick 12 and 6 orebodies. Econ. Geol., Vol 79, # 7, pp. 1669-1692.

Stacey, J.S. and Kramers, J.D., 1975; Approximation of terrestrial lead isotope evolution by a two stage model. Earth and Planet. Science Letters, Vol 26, pp.207-221.

Stanton, R.L., 1972; Ore Petrology. McGraw-Hill, 713 p.

Strong, D.F., Dickson, W.L., O'Driscoll, C.F., Kean, B.F. and Stevens, R.K., 1974; Geochemical evidence for an east-dipping Appalachian subduction zone in Newfoundland. Nature, Vol 248, No 5443, pp. 37-39.

Swinden, H.S. and Thorpe, R.I., 1984; Variation in style of volcanism and massive sulphide deposition in early to Middle Ordovician, island-arc sequences of the Newfoundland Central Mobile Belt. Econ. Geol., Vol 79, pp. 1596-1619.

Tater, J., 1964; A field report on pegmatic occurrences of Newfoundland. Unpub. report, Mineral Resources Division, Newfoundland Dept. mines, Agriculture and Resources, St. John's.

Taylor. S.R., 1968; Geochemistry of andesites: Origin and distribution of the elements. in L.E. Ahrens, ed., Physics and Chemistry of the Earth. New York, Pergamon Press, pp. 559-583.

Thompson, A.B., 1976; Mineral reactions in pelitic rocks: I. Prediction of P-T-X(Fe-Mg) phase relations. II. Calculation of some P-T-X(Fe-Mg) phase relations. Amer. Jour. of Science, 276, pp.401-454.

Thompson, A.B., Lyttle, P.T. and Thompson, J.B., 1977; Mineral reactions and A-Na-K and A-F-M facies types in the Gassetts Schist, Vermont. Amer. Jour. of Science, Vol 277, pp. 1124-1151.

Thorpe, R.I., Sangster, D.F. and Franklin, J.M., 1981; Evolution of lead in massive sulphide ores of Bathurst district, New Brunswick, Canada, (abs.) Institute of Mining and Metall. Trans., Vol 90, section B, pp. B55-B56.

Tracey, R.J., Robinson, P. and Thompson, A.B., 1976; Garnet compositions and zoning in the determinations of temperature and pressure of metamorphism, central Massachusetts. Amer. Mineral., Vol 61, pp. 762-775.

Treloar, P.J., 1985; Metamorphic conditions in central Connemara, Ireland. Jour. Geol. Soc. Lon. Vol 142, pp. 77-86.

Upadhyay, H.D. and Smitheringale, W.G., 1972; Geology of the Gullbridge Copper deposit, Newfoundland: Volcanogenic sulphides in cordierite-anthophylite rocks. Can. Jour. of Earth Science, Vol 9, #9, pp. 1062-1073.

Urabe, T, Scott, S.D. and Hattori, K., 1983; A comparison of footwall-rock alteration and geothermal systems beneath some Japanese and Canadian volcanogenic massive sulphide deposits. in The Kuroko and related volcanogenic massive sulphide deposits. Monograph 5, Econ. Geol., pp. 345-364.

Vernon, R.H., 1977; Relationships between microstructures and metamorphic assemblages. Tectonophysics, Vol 39, pp. 439-452.

Vokes, F.M., 1969; A review of the metamorphism of sulphide bodies. Earth Science Reviews, 5, pp. 99-143.

Vrana, S., 1975; Magnesian-aluminous rocks, the associated ore mineralization and the problem of magesium-iron metasomatism. Krystalinikum, 11, pp. 101-114.

Williams, F.W. and Kennan, P.S., 1983; Stable isotope studies of sulphide mineralization on the Leinster Granite margin and some observations on its relationships to coticule and tourmalinite rocks in the aureole. Mineral. Deposita, Vol 18, pp. 399-410.

Williams, H., 1964; The Appalachians in northeastern Newfoundland - a two-sided system. Amer. Jour. of Science, Vol 262, pp. 1137-1158.

Williams, H., 1979; Appalachian orogen in Canada. Can. Jour. of Earth Science, Vol 16, pp. 792-807.

Williams, H., Kennedy, M.J. and Neale, E.R.W., 1974; The northeastern termination of the Appalachian Orogen. in Ocean basins and margins, ed. Nairn, A.E.H., Vol 2, Plenum, New York, pp. 79-123.

Wilton, D.H.C., 1982; The geology and structural history of the Cape Ray Fault zone in southwestern Newfoundland. Can. Jour. of Earth Science, Vol 20, 1119-1133.

Wilton, D.H.C., 1984; Metallogenic, tectonic and geochemical evolution of the Cape Ray Fault zone with emphasis on Electrum mineralization. Ph.D. thesis, Memorial University of Newfoundland.

Winchester, J.A. and Floyd, P., 1976; Geochemical magma type discrimination: application to altered and metamorphosed basic igneous rocks. Earth and Planet. Sci. Let., 28, pp. 459-469.

Winchester, J.A. and Floyd, P., 1977; Geochemical discrimination of different magma series and their differentiation products using immobile elements. Chem. Geol., Vol 20, pp. 325-343.

Winchester, J.A., Park, R.G. and Holland, J.G., 1980; The geochemistry of Lewisian semipelitic schists from the Gairloch District, Wester Ross. Scott. Jour. of Geol., Vol 16 (2/3), pp. 165-179.

Winkler, H.G.F., 1979; Petrogenesis of metamorphic rocks. Springer-Verlag, New York, 348 p.

Woodsworth, G.J., 1977; Homogenization of zoned garnets from pelitic schists. Can. Mineral., Vol 15, pp. 230-242.

Wynne, P.J., 1983; A lithogeochemical study of the host rocks of the the Strickland showing. Unpub. M.Sc. thesis, Memorial University of Newfoundland, 313 p.

Wynne, P.J. and Strong, D.F., 1984; The Strickland Prospect of Southwestern Newfoundland; a lithogeochemical study of metamorphosed and deformed volcanogenic massive sulphides. Econ. Geol., Vol 79, #7 pp. 1620-1642.

Zartman, R.E. and Doe, B.R., 1981; Plumbotectonics, the model. Tectonophysics, Vol 75, pp. 135-162.

Zwart, M.J., 1962; On the determination of polymetamorphic mineral associations and its application to the Bosost area (central Pyrenees). Geol. Rundsch., 52, pp. 38-65.

Appendix A

Electron Microprobe Techniques

Sulphide and silicate minerals were analysed using a JEOL JXA-5OA electron probe microanalyser at Memorial University. The analyser is a wavelength dispersive type with three spectrometers, controlled automatically by the Krisel system, and run at an operating voltage of 15 kv and a beam current of 0.22 mA.

Silicate data reduction was performed with the Alpha correction program, using the method of Bence and Albee (1968) and the Krisel Magic program was used to correct the sulphide analyses. The majority of garnet and feldspar composition totals fell within the acceptable range of 100 ± 1.5 wt. % while the biotite and muscovite totals consistently totalled 94 ± 2 wt %.

Silicate standards used for calibration were ACPX (Kakanui augite) and KGNT (Kakanui pyrope). Sulphide standards were cubanite (for chalcopyrite), sphalerite, AuAg5 for Ag and PbS.

Appendix Table A-1 shows replicate analyses for ACPX and KGNT.

Table A-1: Replicate analyses for ACPX and KGNT

	Av. of 5 spots		Std. Dev.		H.I.		Pub. value	
	ACPX	KGNT	ACPX	KGNT	ACPX	KGNT	ACPX	KGNT
SiO2	50.00	42.82	0.14	0.07	1.5	0.52	50.73	41.46
TiO2	00.78	00.36	0.02	0.01	2.21	1.18	0.74	0.47
Al2O3	8.02	23.04	0.09	0.17	1.35	1.18	7.86	23.73
Cr2O3	0.13	0.05	0.01	0.01	4.18	7.68	----	-----
FeO	6.16	10.04	0.11	0.19	1.49	2.13	6.77	10.67
MnO	0.11	0.25	0.02	0.02	3.88	1.39	----	0.28
MgO	16.00	19.46	0.18	0.18	1.62	1.25	16.65	18.50
CaO	15.88	4.81	0.29	0.06	3.35	1.5	15.82	5.16
Na2O	1.38	0.01	0.04	0.02	0.61	5.33	1.27	-----
Total	98.5	100.86					99.84	

Pub. = Published value from Abbey (1980).

H.I. = Homogeneity Index is the ratio of the observed standard deviation of the uncorrected metal compositions wt % to calculated values based on counting statistics.

Table A-2: Garnet compositions from microprobe analyses in pelites and amphibolites.

APPENDIX TABLE A-2

Garnet compositions in the pelites On the basis of 12 Oxygens.

Sample #		Mg	Al	Si	Ca	Ti	Mn	Fe	Totals	# of analyses
83/93	wt%	6.14	20.39	39.23	2.22	.00	1.75	31.07	101.39	av. of two
	At. prop.	.708	1.913	3.046	.184	.000	.114	2.016	7.976	
	wt%	5.92	20.66	38.65	2.11	.00	1.84	31.30	100.61	av. of two
	At. prop.	.691	1.913	3.035	.177	.00	.122	2.06	7.998	
83/62	wt%	4.52	20.05	38.78	4.54	.13	3.29	28.85	100.23	av. of three
	At. prop.	.531	1.866	3.063	.382	.007	.218	1.906	7.979	
83/87	wt%	3.95	20.19	38.04	.97	.00	3.70	33.44	100.30	av. of two
	At. prop.	.470	1.904	3.047	.082	.000	.244	2.241	7.994	
83/86	wt%	3.26	20.21	37.6	2.09	.02	3.65	33.15	100.05	av. of two cores
	At. prop.	.39	1.917	3.029	.18	.000	.248	2.232	7.498	
	wt%	4.19	20.39	37.95	1.23	.00	3.06	33.52	100.39	av. of two rims
	At. prop.	.497	1.919	3.03	.105	.000	.206	2.238	7.996	
	wt%	3.88	20.2	38.15	1.73	.02	4.59	32.43	101.04	av. of two cores
	At. prop.	.46	1.894	3.037	.147	.000	.206	2.158	7.996	
	wt%	4.45	19.88	37.88	1.14	.00	2.61	33.15	99.25	one rim
	At. prop.	.535	1.889	3.054	.097	.000	.177	2.233	7.996	
83/83	wt%	7.37	21.34	39.16	.49	.00	1.45	31.12	100.96	av. of two
	At. prop.	.850	1.949	3.03	.039	.000	.093	2.017	7.98	

APPENDIX TABLE A-2 (cont'd)

Garnet Compositions in the pelites.

Sample #		Mg	Al	Si	Ca	Mn	Fe	Totals	# of analyses
83/2/349	Wt% At. prop.	4.25 .497	21.05 1.952	38.65 3.043	4.52 .379	1.94 .129	29.89 1.466	100.32 7.466	av. of two cores
	Wt% At. prop.	4.57 .537	20.7 1.925	38.35 3.027	4.88 .412	1.64 .108	29.97 1.978	100.20 7.99	av. of two rims
	Wt% At. prop.	4.75 .557	20.52 1.904	38.89 3.062	3.47 .335	1.58 .104	30.21 1.990	100.14 7.972	av. of two cores
	Wt% At. prop.	4.68 .546	20.36 1.887	39.13 3.075	3.21 .270	2.05 .136	31.23 2.053	100.69 7.967	av. of two rims
82/5/274	Wt% At. prop.	4.41 .515	20.92 1.933	38.72 3.036	1.45 .122	2.68 .177	33.60 2.202	101.85 7.984	av. of three
	Wt% At. prop.	4.18 .497	20.3 1.911	38.64 3.088	1.50 .126	2.65 .178	32.16 2.147	99.49 7.947	av. of two
B1 6A	Wt% At. prop	3.38 .399	20.18 1.892	38.64 3.077	1.19 .100	2.38 .159	35.05 2.332	100.96 7.965	av. of two
	Wt% At. prop	2.68 .321	20.21 1.916	38.09 3.066	1.25 .106	3.68 .25	34.22 2.303	100.20 7.965	av. of three
83/12	Wt% At. prop.	3.15 .373	20.3 1.900	38.71 3.076	2.98 .251	2.38 .158	33.02 2.194	100.74 7.971	av. of two
	Wt% At. prop.	3.34 .394	20.86 1.953	38.52 3.058	2.95 .249	1.71 .114	32.87 2.181	100.37 7.964	av. of two

APPENDIX TABLE A-2 (cont'd)

Garnet compositions in the amphibolites

Sample #		Mg	Al	Si	Ca	Ti	Mn	Fe	Totals	# of analyses
82/1/252	wt%	2.32	20.06	38.69	10.79	.07	3.27	25.43	100.68	av. of two cores
	At. prop.	.273	1.864	3.053	.812	.002	.217	1.677	8.005	
	wt%	3.18	20.51	38.96	7.77	0.00	2.75	28.1	101.31	av. of two rims
	At. prop.	.370	1.892	3.052	.650	.000	.181	1.841	7.988	
	wt%	3.11	20.47	38.05	4.96	.09	4.69	28.87	100.3	one core
	At. prop.	.367	1.923	3.032	.423	.004	.315	1.923	7.987	
	wt%	3.63	20.61	38.91	6.79	.07	2.77	29.16	101.97	one rim
	At. prop.	.421	1.893	3.035	.565	.002	.183	1.902	8.001	
83/75	wt%	.85	20.00	38.40	10.44	.10	9.08	20.81	99.96	av. of two cores
	At. prop.	.11	1.88	3.08	.894	.009	.613	1.395	7.981	
	wt%	3.26	20.64	38.17	5.40	.03	3.035	29.9	100.435	av. of two rims
	*At. prop.	.385	1.926	3.02	.457	.000	.286	1.981	8.05	
	wt%	3.38	20.58	38.79	4.23	.01	.73	32.7	100.53	av. of two cores
	*At. prop.	.397	1.918	3.072	.357	.000		.097	2.165	
	wt%	4.56	20.53	38.88	4.06	.03	.32	32.54	100.96	av. of two rims
	At. prop.	.532	1.899	3.054	.341	.000	.020	2.186	7.988	
Amp. 3	wt%	2.97	20.74	38.92	8.92	.06	1.43	27.66	100.78	av. of two cores
	At. prop.	.347	1.916	3.05	.747	.004	.094	1.817	15.95	
	wt%	3.29	20.36	38.71	8.9	.02	.75	27.94	100.05	one rim
	At. prop.	.384	1.843	3.056	.753	.000	.048	1.844	15.97	

Table A-3: Biotite, muscovite and epidote compositions from microprobe analyses in pelites and amphibolites.

APPENDIX TABLE A-3

BIOTITE COMPOSITIONS ON THE BASIS OF 22 OXYGEN ATOMS

AMPHIBOLITES

Sample #		Na	Mg	Al	Si	K	Ti	Mn	Fe	Totals	# of analyses
83/80	Wt % At. prop.	.13 .038	10.65 2.46	14.45 2.63	35.64 5.87	8.33 1.72	2.5 0.286	.26 0.037	21.38 2.84	93.34 15.87	av. of two analyses
83/75	Wt % At. prop.	.11 .025	13.54 3.06	15.63 2.79	37.39 5.39	8.71 1.68	1.5 0.164	.09 0.007	17.02 2.259	94.01 15.38	av. of two analyses
	Wt % At. prop.	.11 .026	13.04 2.97	16.20 2.90	36.63 5.58	8.32 1.61	1.34 .15	.09 .008	18.24 2.33	94.14 15.574	av. of two analyses
83/97B	Wt % At. prop.	.21 .057	14.26 3.20	14.93 2.65	37.48 5.65	8.41 1.61	1.84 0.208	.09 .008	17.46 2.198	94.9 15.581	one analysis
PELITES											
83 93	Wt % At. prop.	.30 .080	12.98 2.88	17.96 3.15	37.42 5.57	8.14 1.55	2.25 0.248	.07 .003	15.12 1.88	94.26 15.361	av. of two analyses
	Wt % At. prop.	.29 .083	12.43 2.77	18.03 3.18	37.1 5.5	8.47 1.62	2.23 0.250	.12 .013	15.65 1.96	94.36 15.376	av. of two analyses
83/62	Wt % At. prop.	.17 .049	12.28 2.79	15.42 2.86	37.18 5.67	8.3 1.44	2.26 0.254	.12 .013	17.11 2.18	93.39 15.256	av. of three analyses
83/87	Wt % At. prop.	.34 .099	10.13 2.342	17.66 3.23	35.76 5.55	8.32 1.645	2.36 0.273	.13 .013	17.47 1.999	92.21 15.151	one analysis
83/86	Wt % At. prop.	.24 .071	10.52 2.40	17.75 3.20	35.89 5.50	8.36 1.63	2.28 0.260	.11 .013	18.61 2.38	93.81 15.454	av. of two analyses

APPENDIX TABLE A-3 (cont'd)

Pelites (cont'd) Biotite Compositions on the basis of 22 Oxygen Atoms

Sample #		Na	Mg	Al	Si	K	Ti	Mn	Fe	Totals	
83/83	Wt% At. prop.	.76 .219	15.38 3.42	16.82 2.95	38.27 5.71	6.59 1.25	1.55 .17	.03 .000	13.06 1.62	92.48 15.339	av. of two analyses
83/2/349	Wt% At. prop.	.45 .127	12.05 2.70	17.94 3.18	37.55 5.65	7.51 1.44	2.30 .26	.04 .003	15.19 1.9	93.10 15.267	av. of two analyses
	Wt% At. prop.	.16 .044	11.78 2.68	18.20 3.27	36.51 5.57	7.16 1.39	2.08 .24	.06 .004	16.04 2.05	92.05 15.248	av. of two analyses
82/5/274	Wt% At. prop.	.33 .094	10.12 2.30	18.20 3.27	36.85 5.62	7.05 1.37	2.02 .23	.06 .004	18.19 2.32	92.89 15.208	av. of two analyses
Bi 6A	Wt% At. prop.	.10 .026	7.10 1.63	20.11 3.65	35.03 5.40	7.82 1.54	1.9 .22	.17 .02	21.89 2.82	94.24 15.356	one analysis
	Wt% At. prop.	.10 .027	6.98 1.62	18.61 3.43	35.33 5.53	7.35 1.46	2.16 .25	.18 .022	21.74 2.84	92.58 15.179	av. of two analyses
83/12	Wt% At. prop.	.00 .000	10.16 2.29	18.52 3.29	36.91 5.58	7.62 1.47	1.54 .17	.07 .004	19.84 2.50	94.75 15.306	one analysis
	Wt% At. prop.	.00 .000	9.95 2.24	18.63 3.31	37.14 5.60	8.10 1.56	1.67 .16	.04 .004	19.17 2.17	94.75 15.064	one analysis
83/86	Wt% At. prop.	.24 .071	10.34 2.35	17.51 3.15	36.43 5.56	8.25 1.60	2.72 .31	.09 .009	17.44 2.29	93.61 15.34	

APPENDIX TABLE A-3 (cont'd)

MUSCOVITE COMPOSITIONS ON THE BASIS OF 22 OXYGEN ATOMS

PELITES

Sample #		Na	Mg	Al	Si	K	Ti	Mn	Fe	Totals	# of analyses
83/87	Wt % At. prop	.87 .227	.83 .17	32.49 5.28	46.94 6.38	8.34 1.44	.83 .083	.03 .000	1.18 .13	92.04 13.411	one
83/86	Wt % At. prop.	.80 .213	.97 .14	32.46 5.23	46.54 6.37	8.17 1.42	1.14 .12	.01 .000	1.22 .13	91.42 13.673	one

EPIDOTE COMPOSITION ON THE BASIS OF 13 OXYGEN ATOMS

AMPHIBOLITE

Sample #		Na	Mg	Al	Si	Ca	Ti	Mn	Fe	Totals	# of analyses
83/80	Wt % At. prop.	.01 .000	.02 .000	21.84 2.24	37.91 3.293	22.82 2.123	.11 .005	.12 .007	12.41 .899	95.24 8.568	av. of four analyses

Table A-4: Amphibole compositions from microprobe analyses in the amphibolites.

APPENDIX TABLE A-4

Amphibole Compositions: On the basis of 23 Oxygen Atoms

Hornblendes

Sample #		Na	Mg	Al	Si	K	Ca	Ti	Mn	Fe	Total	# of Analyses
82/1/252	Wt%	1.32	10.11	12.68	44.0	.57	11.13	.93	.14	16.7	97.63	av. of 3
	At. prop.	.375	2.238	2.221	6.542	.104	1.772	.099	.017	2.073	15.441	
83/80	Wt%	2.12	8.33	12.31	40.82	1.49	11.25	1.0	.27	20.39	98.04	
	At. prop.	.630	1.904	2.224	6.264	.288	1.846	.112	.031	2.615	15.914	1
83/75	Wt%	1.79	10.03	14.20	43.00	.37	10.66	.66	.05	15.3	96.07	1
	At. prop.	.514	2.239	2.509	6.447	.069	1.711	.069	.004	1.918	15.480	X Section Centre
	Wt%	1.65	11.01	12.99	44.06	.43	10.52	.63	.08	15.2	96.55	1
	At. prop.	.471	2.441	2.276	6.558	.078	1.677	.064	.008	1.892	15.470	X Section R I M
83/97B	Wt%	.52	18.07	1.75	55.05	.04	11.65	.05	.04	9.96	97.22	Lath Overprint
	At. prop.	.141	3.830	.292	7.82	.004	1.773	.004	.007	1.180	15.723	S2 Fabric
	Wt%	1.61	12.34	10.04	46.74	.28	11.17	.46	.21	14.36	97.29	Lath in
	At. prop.	.477	2.818	1.814	7.173	.054	1.833	.049	.027	1.841	15.051	S2 Fabric
Amp 3	Wt%	1.47	10.32	13.6	44.59	.4	11.16	.85	.04	15.08	97.55	av. of 3
	At. prop.	.418	2.26	2.355	6.555	.072	1.756	.090	.004	1.851	15.361	
		Gedrites										
83/83	Wt%	2.19	14.01	16.85	42.52	.00	.09	.28	.29	20.46	96.69	av. of 3
	At. prop.	.622	3.078	2.926	6.273	.000	.012	.029	.034	2.524	15.498	
Ant.	Wt%	1.57	17.93	12.89	46.26	.01	.44	.18	.97	17.02	97.29	av. of 2
	At. prop.	.435	3.856	2.188	6.671	.000	.067	.017	.118	2.053	15.405	

Table A-5: Feldspar compositions from microprobe analyses in pelites and amphibolites.

APPENDIX TABLE A-5

Table : Feldspar compositions On the Basis of 8 Oxygens

Sample #		Na	Al	Si	K	Ca	Totals	# of analyses
In the amphibolites:								
82/1/252	wt% At. prop.	8.56 .736	24.29 1.27	60.83 2.7	.07 .004	6.7 .317	100.5 5.072	av. of three
83/80	wt% At. prop.	8.83 .76	23.69 1.24	61.46 2.73	.24 .013	6.02 .285	100.38 5.03	av. of six
83/75	wt% At. prop.	8.02 .695	23.52 1.241	61.32 2.748	.04 .001	6.05 .289	99.04 4.974	av. of two
Amp. 3	wt% At. prop.	6.67 .585	25.66 1.37	57.51 2.604	.1 .005	8.8 .427	98.77 4.997	one
	In the pelites:							
83/93	wt% At. prop.	9.39 .803	23.14 1.203	62.59 2.762	.05 .002	5.51 .26	100.76 5.031	av. of two
83/62	wt% At. prop.	8.21 .704	23.95 1.249	61.66 2.728	.16 .007	6.58 .312	100.62 5.000	one
83/87	wt% At. prop.	11.13 .946	20.62 1.065	66.14 2.901	.16 .003	6.58 .124	100.62 5.039	one
83/86	wt% At. prop.	9.99 .863	21.29 1.118	64.16 2.859	.04 .001	3.45 .165	98.98 5.007	av. of two

APPENDIX TABLE A-5 (cont'd)

Table : Feldspar compositions in the pelites

Sample #		Na	Al	Si	K	Ca	Totals	# of analyses
83/83	wt% At. prop.	11.37 .971	20.55 1.067	66.17 2.916	.03 .001	1.61 .075	99.75 5.030	av. of three
83/2/349	wt% At. prop.	7.40 .641	25.55 1.347	58.85 2.632	.08 .004	8.13 .388	100.06 5.012	av. of two
	wt% At. prop.	8.10 .705	23.83 1.261	60.45 2.713	.09 .004	6.62 .317	99.15 5.000	av. of three
82/5/274	wt% At. prop.	9.53 .827	22.01 1.162	63.05 2.824	.10 .005	3.96 .189	98.7 5.006	one
	wt% At. prop.	.24 .022	18.46 1.028	63.64 3.010	13.77 .830	.00 .000	96.21 4.891	av. of two

Appendix B

Procedures for the geochemical analyses of major, trace and rare earth elements

B.1 Major Element Analysis

All samples for analyses were slabbed beforehand to remove oxidized parts, pegmatite, epidote, calcite and/or quartz veins which were considered to be extranneous material. The slabbed samples were crushed into chips and then pulverized for 2-3 minutes using a tungsten carbide puck mill, producing a powder of approximately 100 mesh.

The major elements viz., SiO_2, Al_2O_3, TiO_2, Fe_2O_3 (as total Fe), MnO, MgO, CaO, Na_2O and K_2O were determined by atomic absorbtion spectrophotometry on a Perkin-Elmer Model 370. It was found necessary to digest the garnet-rich samples in aqua regia, for up to seven days, to ensure their complete dissolution.

P_2O_5 was determined colourimetrically using a Bausch and Lomb Spectronic 20 model.

L.O.I. (loss on ignition) was determined by weighing approximately 1 gram of sample into a porcelain crucible and heating it to 1000 ^{O}C for 2-3 hours to volatilize S, CO_2, H_2O etc. The samples were then weighed and % LOI calculated.

The accuracy of determination of the major elements is presented in Table B-1.

Note: (1) Total Fe was analysed as Fe2O3 and (2) all values listed as O in trace element analyses are below the detection limits of the XRF.

B.2 Trace Element Analyses

Pellets for trace element analysis were made by mixing 10 gm of sample powder with approximately 1.5 gm of binding resin which were pressed and then baked for 10 minutes at 200°C. Analyses were made using a Phillips 1450 X-Ray Fluourescence Spectrometer equipped with a Rhodium tube.

Samples were run in batches of 8 with two international standard pellets. A monitor which is saturated with trace elements is used to calibrate the machine against standard values and corrects for instrument drift.

Replicate analyses of standard W1 are given in Table B-2.

B.3 Rare earth element analyses

Rare earth elements were determined at Memorial University using the thin film/XRF method of Fryer (1977). Ten samples were also analysed at McMaster University (commercially) by Instrumental Neutron Activation.

In the thin film method the sample is repeatedly digested by HF, HCl and $HClO_4$. Elution of the REE solution (HCl) in an ion exchange resin separates the REEs, Y and Ba.

Table B-1: Accuracy of major oxide determinations.

GSP-1 (Granodiorite)				
	Pub. %	# of analyses	Mean Wt%	Std. Dev.
SiO2	67.27	7	68.85	0.60
TiO2	0.65	7	0.60	0.08
Al2O3	15.18	7	14.77	0.22
Fe2O3	4.26	8	4.22	0.07
CaO	2.06	8	1.94	0.07
MgO	0.98	7	0.96	0.03
Na2O	2.77	8	2.74	0.06
K2O	5.50	6	5.44	0.12
MnO	0.04	8	0.04	0.01

Published values from Abbey (1980).

Table B-2: Replicate analyses of standard W1 over 10 runs.

	Mean wt%	Std. Dev.	Published Value
Pb	6.6	4.0	8.00
Th	6.4	3.4	2.40
U	4.5	4.0	0.58?
Rb	24.4	1.8	21.00
Sr	185.0	2.1	190.00
Y	25.6	1.3	25.00
Zr	91.2	2.5	105.00
Nb	9.0	1.4	9.50?
Zn	85.2	4.4	86.00
Cu	112.5	4.1	110.00
Ni	78.6	3.0	76.00?
La	2.8	3.9	9.80?
Ba	187.8	5.1	160.00
V	255.3	3.5	260.00
Ce	16.4	2.2	23.00?
Cr	103.3	3.9	115.00?
Ga	14.7	1.8	16.00

Published values from Abbey (1980).

Ba is removed as $BaSO_4$ precipitate by addition of sulphuric acid. After a second elution, the REEs (in HCl) are concentrated by evaporation and taken up on an ion exchange paper. The paper discs were then analysed by XRF. Figure B-1 shows the accuracy of analyses.

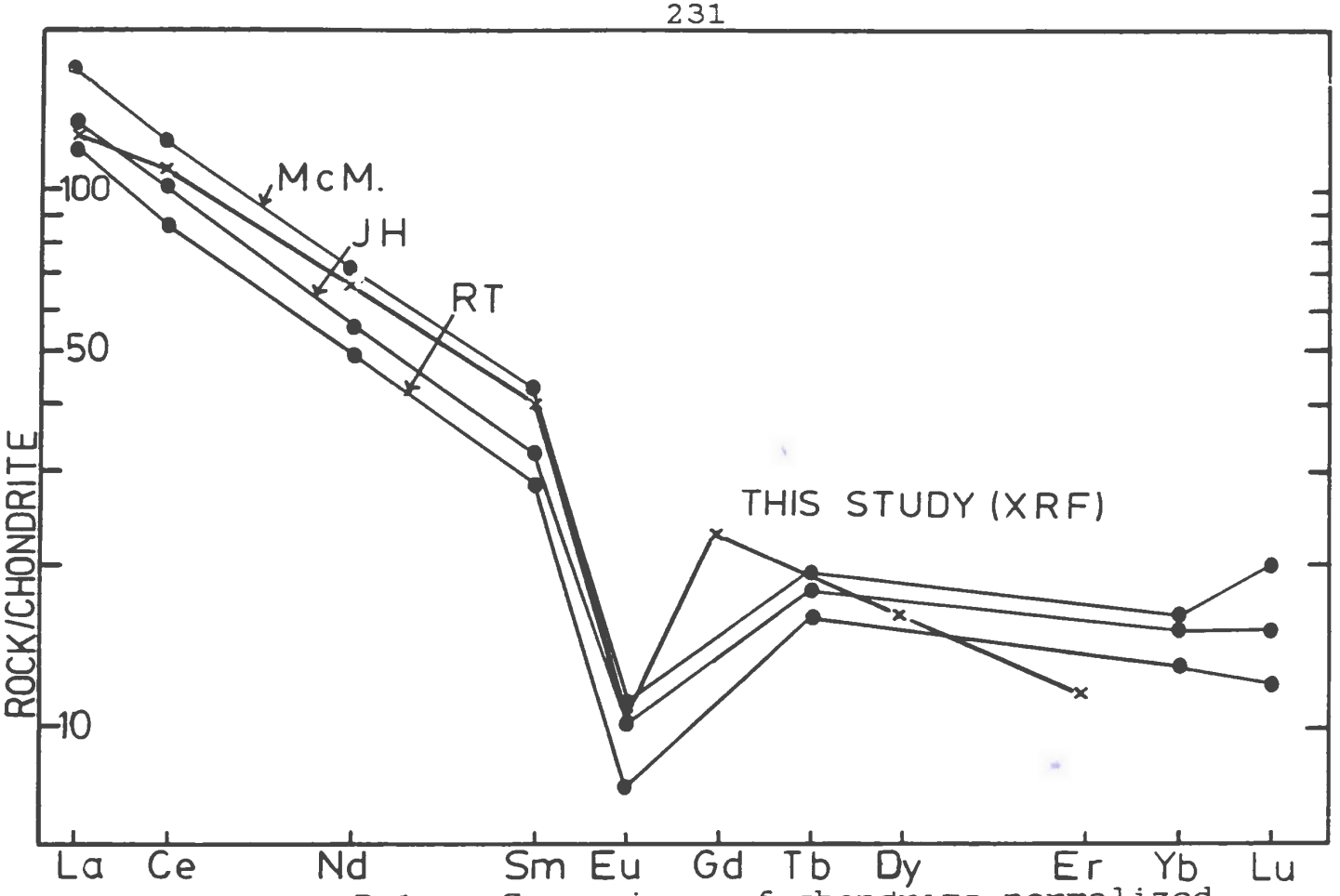

Figure B-1: Comparison of chondrite-normalized rare earth element patterns for MUN 1, an internal granite standard at Memorial University. McM data from McMaster University by NAA, for this study. JH data produced by J. Hoertgen, courtesy of D. Strong. RT data produced by R. P. Taylor, courtesy of D. Strong. Data for this study (x) was produced by the thin film/XRF method of Fryer (1977).

Table B-3: Major and trace element analyses of quartzofeldspathic rocks.

APPENDIX TABLE B-3

QUARTZOFELDSPATHIC ROCKS

	FS7A	FS7B	FS9	FS16	BI1
MAJOR ELEMENTS					
SiO2	80.90	72.10	72.70	78.80	71.90
TiO2	.47	.64	.47	.13	.24
Al2O3	7.90	12.60	12.20	11.40	13.50
Fe2O3	4.28	3.87	3.90	1.00	1.79
FeO	0.00	0.00	0.00	0.00	0.00
MnO	.12	.09	.08	.03	.08
MgO	1.06	.89	.83	.52	1.79
CaO	1.25	1.48	.85	.69	1.14
Na2O	.64	3.86	3.44	3.62	4.54
K2O	1.43	2.20	4.14	1.53	2.63
P2O5	.07	.08	.09	.01	.06
LOI	.59	.30	.43	.69	1.47
TOTAL	98.71	98.11	99.13	98.42	99.14
TRACE ELEMENTS					
Pb	0	1	0	4	12
Th	6	13	13	6	13
U	3	4	4	4	6
Rb	78	78	114	46	52
Sr	30	56	59	107	80
Y	43	84	80	24	29
Zr	271	417	401	97	133
Nb	9	28	25	8	6
Zn	22	23	25	6	34
Cu	9	9	17	11	25
Ni	15	4	0	0	0
La	38	25	20	13	23
Ba	314	719	693	210	1443
V	51	18	20	7	74
Ce	59	77	33	36	38
Cr	25	0	0	0	0
Ga	10	20	18	11	11

APPENDIX TABLE B-3 (cont'd)

QUARTZOFELDSPATHIC ROCKS

	83/38	83/32	83/66	FS13	FS17
MAJOR ELEMENTS					
SiO2	71.40	69.80	66.90	72.00	72.40
TiO2	.50	.50	.75	.18	.13
Al2O3	13.80	14.20	14.40	12.80	13.60
Fe2O3	3.36	3.96	5.73	3.59	2.92
FeO	0.00	0.00	0.00	0.00	0.00
MnO	.06	.07	.18	.04	.02
MgO	.89	.83	1.76	.79	.57
CaO	2.18	2.82	2.17	.38	.18
Na2O	3.55	3.67	1.79	1.23	1.69
K2O	3.37	2.68	4.92	4.93	4.52
P2O5	.07	.09	.19	.13	.04
LOI	.63	1.07	1.14	2.93	2.82
TOTAL	99.81	99.69	99.93	99.00	98.89
TRACE ELEMENTS					
Pb	28	17	18	114	24
Th	14	19	19	5	20
U	0	0	0	3	8
Rb	102	86	138	141	108
Sr	212	220	57	34	34
Y	37	27	29	33	24
Zr	160	164	213	204	215
Nb	8	10	13	12	11
Zn	35	73	141	284	0
Cu	51	10	12	21	31
Ni	0	0	0	0	0
La	15	12	7	22	17
Ba	976	1055	1131	2604	4159
V	65	67	52	35	19
Ce	37	31	31	43	33
Cr	0	0	0	0	0
Ga	11	13	16	16	15

APPENDIX TABLE B-3 (cont'd)

QUARTZOFELDSPATHIC ROCKS

	83/22	82/5/3	82/3/3	FS10	FS15
MAJOR ELEMENTS					
SiO2	76.70	69.90	71.30	76.20	72.70
TiO2	.21	.37	.35	.23	.44
Al2O3	11.60	15.30	14.00	11.60	12.60
Fe2O3	1.35	2.57	2.14	1.93	4.01
FeO	0.00	0.00	0.00	0.00	0.00
MnO	.06	.08	.05	.07	.11
MgO	.77	1.17	1.82	.72	.60
CaO	.73	2.06	.94	.79	1.29
Na2O	4.73	3.43	3.65	4.00	4.10
K2O	1.45	3.34	2.62	2.37	2.86
P2O5	.02	.11	.02	.06	.08
LOI	.66	1.57	1.42	.63	.46
TOTAL	98.28	99.90	98.31	98.60	99.25
TRACE ELEMENTS					
Pb	82	23	27	10	3
Th	20	8	12	9	13
U	5	2	4	5	6
Rb	58	87	88	48	95
Sr	111	172	109	88	88
Y	30	27	33	27	78
Zr	102	172	97	133	404
Nb	10	9	12	10	26
Zn	32	34	33	48	22
Cu	17	22	12	15	11
Ni	0	0	4	1	2
La	19	25	25	21	19
Ba	613	1744	852	918	648
V	8	98	40	29	21
Ce	38	39	40	34	65
Cr	0	0	0	0	0
Ga	13	14	12	10	19

APPENDIX TABLE B-3 (cont'd)

QUARTZOFELDSPATHIC ROCKS

	83/56	83/57	83/81	83/59	FS1
MAJOR ELEMENTS					
SiO2	73.40	73.60	73.00	69.40	76.60
TiO2	.53	.50	.30	.48	.23
Al2O3	12.60	12.30	13.70	14.20	11.90
Fe2O3	4.70	4.18	2.93	4.51	1.16
FeO	0.00	0.00	0.00	0.00	0.00
MnO	.08	.14	.05	.07	.03
MgO	.59	.38	1.38	2.02	.58
CaO	1.25	2.64	1.20	1.73	.44
Na2O	4.08	3.69	5.74	4.89	2.73
K2O	2.37	.97	1.34	2.09	5.01
P2O5	.16	.15	.08	.11	.04
LOI	.34	.46	.50	.64	.44
TOTAL	100.10	99.01	100.22	100.14	99.16
TRACE ELEMENTS					
Pb	12	15	21	23	14
Th	19	26	17	12	16
U	5	4	4	0	4
Rb	75	55	34	57	117
Sr	66	92	125	301	69
Y	86	89	20	23	31
Zr	450	442	148	219	170
Nb	27	29	8	7	21
Zn	67	40	29	55	13
Cu	16	11	16	28	9
Ni	0	0	0	0	0
La	9	25	3	3	22
Ba	820	248	1203	1339	1532
V	12	9	77	93	9
Ce	42	84	20	17	56
Cr	0	0	0	0	0
Ga	18	20	13	14	12

APPENDIX TABLE B-3 (cont'd)

QUARTZOFELDSPATHIC ROCKS

	82/5/3	83/78	83/94	FS4	FS6
MAJOR ELEMENTS					
SiO2	71.10	70.00	71.30	71.80	75.50
TiO2	.10	.66	.56	.65	.11
Al2O3	14.60	13.40	11.00	13.30	11.90
Fe2O3	2.82	4.66	8.80	4.94	2.52
FeO	0.00	0.00	0.00	0.00	0.00
MnO	.06	.08	.40	.08	.10
MgO	2.39	1.60	3.03	1.70	1.06
CaO	.34	1.82	.93	1.16	1.50
Na2O	1.36	2.12	2.66	1.44	3.15
K2O	5.18	4.16	.53	3.10	2.50
P2O5	.03	.15	.24	.10	.02
LOI	2.26	1.30	.64	.55	1.04
TOTAL	100.24	99.95	100.09	98.82	99.40
TRACE ELEMENTS					
Pb	10	15	8	4	4
Th	15	17	15	6	6
U	4	0	4	6	6
Rb	170	163	15	92	92
Sr	49	114	42	47	47
Y	42	57	114	84	84
Zr	81	227	476	397	397
Nb	20	17	35	28	28
Zn	53	51	65	68	68
Cu	8	31	9	6	6
Ni	1	20	6	0	0
La	25	19	0	22	22
Ba	1559	676	268	444	444
V	6	75	55	19	19
Ce	62	50	39	60	60
Cr	0	39	2	0	0
Ga	15	15	18	18	18

APPENDIX TABLE B-3 (cont'd)

QUARTZOFELDSPATHIC ROCKS

	82/4/2	83/67	83/77	83/1	83/2/6
MAJOR ELEMENTS					
SiO2	65.40	67.70	68.20	62.80	73.10
TiO2	.49	.37	.52	.78	.28
Al2O3	14.00	12.50	14.50	14.90	14.10
Fe2O3	4.72	3.23	4.54	6.65	1.92
FeO	0.00	0.00	0.00	0.00	0.00
MnO	.32	.26	.11	.20	.06
MgO	2.92	2.07	1.85	2.87	1.92
CaO	1.53	6.33	2.73	3.66	.81
Na2O	2.74	1.37	5.67	2.92	3.29
K2O	3.92	5.20	.08	3.18	2.90
P2O5	.11	.08	.13	.15	.02
LOI	2.48	1.34	.44	1.26	1.40
TOTAL	98.63	100.45	98.77	99.57	99.80
TRACE ELEMENTS					
Pb	623	33	6	39	12
Th	12	22	14	17	13
U	1	8	0	0	0
Rb	87	131	3	100	117
Sr	70	104	258	137	106
Y	23	57	26	31	29
Zr	151	152	169	175	140
Nb	9	9	10	11	13
Zn	1015	68	63	121	58
Cu	39	11	13	19	13
Ni	0	0	0	0	0
La	23	5	0	6	7
Ba	2247	1641	15	1245	785
V	101	47	49	137	17
Ce	31	25	23	32	25
Cr	0	0	0	0	0
Ga	18	9	16	15	11

APPENDIX TABLE B-3 (cont'd)

QUARTZOFELDSPATHIC ROCKS

	FS8	FS12A	83/58
MAJOR ELEMENTS			
SiO2	67.80	74.40	68.10
TiO2	.75	.20	.45
Al2O3	13.70	12.20	15.40
Fe2O3	5.50	1.34	3.45
FeO	0.00	0.00	0.00
MnO	.19	.03	.06
MgO	1.76	.63	1.83
CaO	3.59	.31	2.35
Na2O	2.18	1.98	4.88
K2O	2.64	6.62	2.43
P2O5	.15	0.00	.07
LOI	1.33	.68	.82
TOTAL	99.59	98.39	99.84
TRACE ELEMENTS			
Pb	23	28	21
Th	12	9	25
U	0	2	6
Rb	89	113	66
Sr	112	86	241
Y	35	30	30
Zr	208	195	202
Nb	11	9	10
Zn	69	20	36
Cu	11	9	25
Ni	0	0	4
La	30	25	19
Ba	697	1833	1609
V	76	7	106
Ce	45	34	39
Cr	0	0	4
Ga	19	14	13

Table B-4: Major and trace element analyses of mineralized and unmineralized semipelites.

APPENDIX TABLE B-4

SEMIPELITES

	83/48	83/52	83/53	QTM1	QTM4
MAJOR ELEMENTS					
SiO2	68.80	73.60	70.00	77.00	72.60
TiO2	.38	.37	.40	.16	.40
Al2O3	13.00	13.70	13.80	12.10	13.30
Fe2O3	4.17	1.50	3.36	1.44	2.41
FeO	0.00	0.00	0.00	0.00	0.00
MnO	.04	.02	.04	.02	.04
MgO	1.49	1.02	1.49	.66	1.32
CaO	2.39	1.01	1.42	.17	.39
Na2O	1.07	1.97	2.51	1.63	2.07
K2O	3.67	3.50	3.16	3.28	3.81
P2O5	0.00	.10	0.00	0.00	.10
LOI	4.26	2.62	2.95	2.21	2.56
TOTAL	99.27	99.41	99.13	98.67	99.00
TRACE ELEMENTS					
Pb	31	14	40	6	10
Th	21	21	20	13	13
U	3	0	5	7	5
Rb	84	79	72	118	76
Sr	85	86	88	27	38
Y	24	6	18	19	19
Zr	133	164	165	186	145
Nb	8	10	9	8	9
Zn	18	13	38	5	28
Cu	10	14	15	95	14
Ni	0	0	0	0	0
La	8	1	0	20	14
Ba	907	1859	1152	2653	1986
V	115	72	83	17	84
Ce	30	6	9	43	25
Cr	0	0	0	0	0
Ga	13	15	14	13	14

APPENDIX TABLE B-4 (cont'd)
SEMIFELITES

	83/10	83/30	83/44	QTM3A	QTM3B
MAJOR ELEMENTS					
SiO2	68.60	77.60	72.90	67.90	76.20
TiO2	.33	.20	.20	.18	.16
Al2O3	14.70	11.40	13.50	12.40	13.20
Fe2O3	2.11	.23	1.06	4.74	.92
FeO	0.00	0.00	0.00	0.00	0.00
MnO	.11	.01	.01	.06	.02
MgO	3.84	.25	1.02	4.12	.69
CaO	.74	.26	.32	.23	.12
Na2O	4.02	3.73	2.60	2.81	1.58
K2O	2.46	3.46	5.13	2.19	4.16
P2O5	.10	.03	0.00	.05	.02
LOI	2.18	1.08	1.64	4.04	1.69
TOTAL	99.19	98.25	98.38	98.72	98.96
TRACE ELEMENTS					
Pb	99	16	27	8	14
Th	15	18	18	15	11
U	1	0	2	5	1
Rb	44	62	95	64	170
Sr	123	56	79	73	35
Y	27	18	19	20	26
Zr	173	178	221	144	199
Nb	10	8	11	9	11
Zn	104	1	16	51	7
Cu	18	14	14	23	20
Ni	0	0	0	0	1
La	13	5	13	16	25
Ba	3083	1961	2084	727	3301
V	78	11	19	87	20
Ce	29	24	34	31	36
Cr	0	0	0	0	0
Ga	15	11	13	11	12

APPENDIX TABLE B-4 (cont'd)
SEMIFELITES

	83/47	83/19	83/70	83/71	83/50
MAJOR ELEMENTS					
SiO2	74.30	70.40	73.90	67.60	69.70
TiO2	.10	.42	.14	.23	.38
Al2O3	11.80	13.70	10.60	13.20	13.30
Fe2O3	3.25	3.13	1.40	3.59	3.48
FeO	0.00	0.00	0.00	0.00	0.00
MnO	.05	.10	.07	.12	.07
MgO	2.06	3.03	3.79	4.43	1.69
CaO	.32	1.64	.55	.88	.80
Na2O	1.98	4.44	2.90	4.07	3.58
K2O	2.12	2.07	1.20	1.86	3.26
P2O5	0.00	.06	.04	0.00	0.00
LOI	3.03	1.04	1.63	2.06	1.96
TOTAL	99.01	100.03	96.22	98.04	98.42
TRACE ELEMENTS					
Pb	78	22	66	9	28
Th	9	17	22	17	18
U	0	1	6	0	0
Rb	50	68	35	44	71
Sr	28	181	94	134	168
Y	10	30	18	21	23
Zr	139	171	185	165	165
Nb	7	10	10	8	9
Zn	53	44	46	57	30
Cu	13	12	13	13	13
Ni	0	0	0	0	1
La	3	5	6	7	4
Ba	3947	1183	1230	1130	1607
V	60	54	17	85	59
Ce	1	29	28	23	24
Cr	0	0	0	0	0
Ga	13	13	12	13	13

APPENDIX TABLE B-4 (cont'd)

SEMIPELITES

	QTM5	82/1/1	83/4/2
MAJOR ELEMENTS			
SiO2	72.10	75.60	73.70
TiO2	.62	.20	.21
Al2O3	14.10	13.10	12.90
Fe2O3	2.81	1.14	1.73
FeO	0.00	0.00	0.00
MnO	.02	.04	.04
MgO	.82	1.57	1.01
CaO	.04	.53	.93
Na2O	.43	3.74	4.68
K2O	4.75	2.39	2.20
P2O5	.10	0.00	.02
LOI	3.06	1.01	.89
TOTAL	98.85	99.32	98.31
TRACE ELEMENTS			
Pb	179	49	40
Th	14	21	26
U	6	6	2
Rb	140	90	67
Sr	17	98	89
Y	32	24	45
Zr	210	105	80
Nb	34	14	13
Zn	86	42	50
Cu	2	19	14
Ni	0	0	0
La	20	27	12
Ba	969	553	1316
V	42	3	33
Ce	63	38	33
Cr	0	0	0
Ga	18	13	12

APPENDIX TABLE B-4 (cont'd)

MINERALIZED SEMIPELITES

	83/3	IAM11	82/5/3	83/2/2	83/2/2
MAJOR ELEMENTS					
SiO2	69.40	80.40	70.60	64.00	65.30
TiO2	.42	.11	.42	.53	.29
Al2O3	12.40	11.00	14.60	16.60	15.20
Fe2O3	5.33	.42	2.24	4.49	2.60
FeO	0.00	0.00	0.00	0.00	0.00
MnO	.03	.02	.02	.03	.06
MgO	.51	.80	.69	1.25	3.08
CaO	.61	.53	.26	.43	.90
Na2O	.83	2.22	.82	.54	.93
K2O	5.83	2.43	7.02	6.64	5.30
P2O5	0.00	0.00	.09	0.00	.04
LOI	3.80	1.26	2.74	4.36	4.36
TOTAL	99.16	99.19	99.50	98.87	98.06
TRACE ELEMENTS					
Pb	2317	160	274	938	23
Th	11	19	17	25	17
U	0	0	9	7	5
Rb	145	67	142	160	164
Sr	65	45	46	65	86
Y	31	22	26	31	31
Zr	187	75	165	202	144
Nb	10	12	20	9	15
Zn	4571	139	427	2364	41
Cu	62	15	45	182	12
Ni	0	0	0	0	3
La	9	7	18	11	10
Ba	2926	6709	5835	8872	1201
V	34	12	76	87	51
Ce	16	18	21	43	30
Cr	0	0	0	0	2
Ga	27	10	17	24	13
DF	0	0	0	0	0

APPENDIX TABLE B-4 (cont'd)

MINERALIZED SEMIPELITES

	83/3/4
MAJOR ELEMENTS	
SiO2	68.80
TiO2	.40
Al2O3	13.50
Fe2O3	3.37
FeO	0.00
MnO	.02
MgO	.55
CaO	.36
Na2O	.71
K2O	7.55
P2O5	0.00
LOI	3.02
TOTAL	98.28
TRACE ELEMENTS	
Pb	307
Th	17
U	2
Rb	172
Sr	62
Y	26
Zr	156
Nb	9
Zn	1537
Cu	7
Ni	0
La	12
Ba	5358
V	67
Ce	34
Cr	0
Ga	17
DF	0

Table B-5: Major and trace element analyses of pelites i.e. biotite-garnet-kyanite-staurolite schists and coticule.

APPENDIX TABLE B-5 PELITES

	BI3	BI6A	BI8	82/2/2	FS2
MAJOR ELEMENTS					
SiO2	55.90	59.00	59.20	58.70	65.10
TiO2	1.06	1.05	.85	.87	.98
Al2O3	19.50	18.90	19.50	19.40	15.90
Fe2O3	10.72	8.82	9.47	10.11	8.52
FeO	0.00	0.00	0.00	0.00	0.00
MnO	.47	.28	.47	.67	.78
MgO	2.90	2.10	2.28	2.47	2.13
CaO	1.03	.55	.60	.74	.63
Na2O	1.95	.29	.92	.70	.68
K2O	4.45	4.68	4.19	4.29	3.43
P2O5	.17	.13	.15	.15	.15
LOI	1.49	2.46	1.83	2.24	2.18
TOTAL	99.64	98.26	99.46	100.34	100.48
TRACE ELEMENTS					
Pb	21	19	17	28	26
Th	6	16	6	11	11
U	1	5	5	5	5
Rb	181	188	168	191	165
Sr	50	65	91	69	47
Y	44	43	42	51	42
Zr	196	195	183	209	208
Nb	31	24	48	30	21
Zn	105	80	63	119	90
Cu	13	35	30	49	37
Ni	53	42	33	67	44
La	28	31	25	30	21
Ba	1007	774	583	744	693
V	201	170	160	198	150
Ce	61	54	70	61	58
Cr	102	85	81	102	73
Ga	25	27	25	29	21
DF	0	0	0	0	0

APPENDIX TABLE B-5 (cont'd)
PELITES

	82/2/1	83/12	83/10	82/4/5	BI2
MAJOR ELEMENTS					
SiO2	52.90	66.50	68.60	57.80	58.40
TiO2	.01	.95	.33	.85	.98
Al2O3	9.80	15.60	14.70	18.20	19.80
Fe2O3	19.92	6.10	2.11	9.97	9.23
FeO	0.00	0.00	0.00	0.00	0.00
MnO	.06	.14	.11	.40	.39
MgO	.69	1.87	3.84	3.16	2.28
CaO	.34	.49	.74	2.54	.64
Na2O	.84	.66	4.02	2.68	.78
K2O	5.38	4.62	2.46	2.66	5.00
P2O5	.08	.15	.10	.14	.15
LOI	9.49	2.22	2.18	1.07	1.96
TOTAL	99.51	99.30	99.19	99.47	99.61
TRACE ELEMENTS					
Pb	2228	45	99	34	15
Th	23	16	15	9	11
U	5	0	1	3	3
Rb	99	169	44	136	200
Sr	142	51	123	142	45
Y	18	37	27	42	37
Zr	128	236	173	201	171
Nb	12	21	10	17	34
Zn	26606	92	104	105	75
Cu	360	46	18	41	18
Ni	13	25	0	45	31
La	24	15	13	27	31
Ba	16686	1243	3083	650	800
V	59	135	78	205	174
Ce	11	34	29	54	57
Cr	0	71	0	82	81
Ga	30	22	15	26	24
DF	0	0	0	0	0

APPENDIX TABLE B-5 (cont'd)

PELITES COTICULE

	FS12B		83/85
MAJOR ELEMENTS			
SiO2	64.20		71.00
TiO2	.68		.26
Al2O3	16.50		10.10
Fe2O3	8.54		8.53
FeO	0.00		0.00
MnO	.48		1.98
MgO	2.43		1.61
CaO	.38		4.17
Na2O	.89		.58
K2O	3.89		.40
P2O5	.14		.75
LOI	1.80		.24
TOTAL	99.93	TOTAL	99.62
TRACE ELEMENTS			
Pb	42		14
Th	11		11
U	5		4
Rb	147		29
Sr	46		26
Y	34		52
Zr	115		233
Nb	19		11
Zn	74		47
Cu	35		29
Ni	38		25
La	20		0
Ba	573		0
V	165		72
Ce	51		29
Cr	69		50
Ga	25		16
DF	0		0

Table B-6: Major and trace element analyses of amphibolites, epidote-pyrite schists and calc-silicate rocks.

APPENDIX TABLE B-6

AMPHIBOLITES

	BI68	AMP2	AMP3	AMP4	AMP5
MAJOR ELEMENTS					
SiO2	53.70	54.00	53.00	54.40	52.00
TiO2	2.15	2.23	2.09	2.13	2.49
Al2O3	15.50	13.90	14.20	13.90	16.20
Fe2O3	13.40	14.57	14.40	13.72	13.06
FeO	0.00	0.00	0.00	0.00	0.00
MnO	.80	.28	.25	.23	.48
MgO	3.95	5.53	5.79	5.14	4.69
CaO	9.00	6.92	8.72	6.39	8.64
Na2O	1.25	1.14	1.20	3.24	2.69
K2O	.35	.41	.30	.33	.19
P2O5	.28	.28	.24	.28	.13
LOI	.85	.40	.12	.65	.22
TOTAL	101.23	99.66	100.31	100.41	100.86
TRACE ELEMENTS					
Pb	6	0	7	12	1
Th	6	0	3	4	0
U	0	0	8	5	2
Rb	21	13	10	13	2
Sr	163	90	229	254	180
Y	52	47	57	51	62
Zr	179	213	192	187	247
Nb	20	15	15	14	17
Zn	102	112	126	101	72
Cu	12	5	72	66	23
Ni	21	17	36	17	11
La	27	33	26	25	19
Ba	197	138	86	167	111
V	384	402	370	453	410
Ce	50	58	58	51	50
Cr	11	13	27	20	0
Ga	20	16	20	22	20

APPENDIX TABLE B-6 (cont'd)
AMPHIBOLITES

	AMP6	83/20	83/80	83/84	83/95
MAJOR ELEMENTS					
SiO2	53.30	45.40	49.90	52.40	47.10
TiO2	1.90	3.07	.87	1.46	.29
Al2O3	13.10	15.40	18.60	14.40	10.90
Fe2O3	10.06	15.38	10.52	11.65	10.12
FeO	0.00	0.00	0.00	0.00	0.00
MnO	.21	.22	.14	.19	1.66
MgO	5.38	6.45	4.13	6.67	13.33
CaO	10.71	9.16	8.33	9.76	14.83
Na2O	2.18	1.99	4.38	2.29	.28
K2O	.54	1.81	1.83	.94	.05
P2O5	.15	.43	.31	.15	0.00
LOI	1.82	1.02	.80	.76	1.80
TOTAL	99.35	100.33	99.81	100.68	100.36
TRACE ELEMENTS					
Pb	2	8	20	8	24
Th	0	0	4	6	7
U	0	3	0	1	4
Rb	18	66	60	43	6
Sr	206	596	483	169	438
Y	36	37	16	40	9
Zr	101	171	84	123	25
Nb	6	38	4	10	3
Zn	77	120	119	84	118
Cu	27	32	44	25	1
Ni	10	38	7	33	33
La	19	7	5	0	0
Ba	167	527	487	350	0
V	277	454	360	311	167
Ce	26	53	22	26	0
Cr	159	47	36	109	194
Ga	15	19	20	16	7

APPENDIX TABLE B-6 (cont'd)

AMPHIBOLITES

	83/97B	82/1/2	82/2/2	82/4/1	82/1/1
MAJOR ELEMENTS					
SiO2	38.90	50.00	52.40	48.30	47.50
TiO2	.34	2.97	1.42	.73	.69
Al2O3	12.60	12.60	15.40	14.00	14.50
Fe2O3	7.20	15.56	10.58	8.89	9.39
FeO	0.00	0.00	0.00	0.00	0.00
MnO	.19	.28	.21	.36	.22
MgO	6.39	5.53	5.80	8.44	10.70
CaO	18.08	7.88	9.02	13.40	10.60
Na2O	3.47	1.53	1.34	2.17	.63
K2O	.82	.50	.88	.22	1.64
P2O5	0.00	.19	.13	.02	.01
LOI	12.13	.28	1.16	1.87	2.66
TOTAL	100.12	97.32	98.34	98.40	98.54
TRACE ELEMENTS					
Pb	2	12	9	13	8
Th	2	4	0	0	0
U	0	0	0	0	3
Rb	13	16	41	7	53
Sr	260	162	235	157	160
Y	9	64	35	19	27
Zr	31	201	115	16	15
Nb	2	18	10	3	5
Zn	42	148	185	292	81
Cu	84	25	66	135	24
Ni	94	16	50	139	189
La	0	36	16	1	16
Ba	383	243	326	111	429
V	190	525	276	227	230
Ce	7	59	29	0	10
Cr	222	28	118	295	373
Ga	8	22	22	14	14

APPENDIX TABLE B-6 (cont'd)

AMPHIBOLITES

	82/3/2	83/4/4	83/4/2	TR3-4	82/1/4
MAJOR ELEMENTS					
SiO2	45.30	51.00	47.40	47.10	46.70
TiO2	.73	1.60	.98	1.09	1.45
Al2O3	14.20	14.40	14.00	15.20	14.80
Fe2O3	9.49	11.36	9.46	9.88	9.77
FeO	0.00	0.00	0.00	0.00	0.00
MnO	.28	.20	.28	.17	.20
MgO	14.10	6.30	7.76	9.32	10.06
CaO	10.23	7.94	12.12	11.97	10.84
Na2O	1.04	3.64	.85	1.38	2.03
K2O	2.27	1.06	2.91	.40	1.12
P2O5	.02	.17	.04	.03	.08
LOI	2.11	1.88	3.21	2.10	1.67
TOTAL	99.77	99.55	99.01	98.64	98.72
TRACE ELEMENTS					
Pb	6	5	36	7	12
Th	0	7	3	0	0
U	4	3	2	0	0
Rb	91	63	130	17	27
Sr	112	222	209	149	226
Y	24	41	30	27	35
Zr	8	143	44	25	83
Nb	1	10	6	1	1
Zn	114	87	121	174	69
Cu	45	54	65	119	84
Ni	355	40	121	136	201
La	6	0	0	6	11
Ba	686	156	870	436	227
V	189	305	240	282	263
Ce	4	25	2	9	19
Cr	823	110	212	273	373
Ga	11	19	13	17	16

APPENDIX TABLE R-6 (cont'd)

AMPHIBOLITES

	82/5/2	83/79	83/3/2		
	MAJOR ELEMENTS			AMP7	ULTRAMAFIC
SiO2	53.90	62.50	56.50	55.30	40.00
TiO2	1.93	1.33	1.19	1.25	0.33
Al2O3	15.20	13.90	14.70	14.00	6.73
Fe2O3	12.14	9.95	9.36	10.30	10.54
FeO	0.00	0.00	0.00	0.00	0.00
MnO	.26	.28	.50	0.18	0.16
MgO	5.22	2.50	5.31	5.84	29.20
CaO	6.56	4.79	4.32	7.98	4.34
Na2O	3.13	3.53	2.66	2.55	0.06
K2O	.43	.69	3.08	0.39	0.02
P2O5	.16	.37	.18	0.10	0.01
LOI	.76	.26	.99	0.44	7.88
TOTAL	99.69	100.10	98.79	98.34	99.27
	TRACE ELEMENTS				
Pb	9	15	102	21	10.00
Th	0	14	11	19	20.00
U	6	0	7	0	0.00
Rb	21	28	123	8	8.00
Sr	169	170	146	290	13.00
Y	50	75	46	45	0.00
Zr	187	298	166	140	0.00
Nb	14	23	10	9	3.00
Zn	101	98	390	70	49.00
Cu	40	21	39	0	26.00
Ni	21	7	11	8	1280.00
La	18	2	2	20	26.00
Ba	113	335	846	38	0.00
V	353	142	233	269	139.00
Ce	51	46	30	25	0.00
Cr	65	13	78	107	4169.00
Ga	18	22	15	11	4.00

APPENDIX TABLE B-6 (cont'd)

EPIDOTE PYRITE PEL

	83/9	83/13	83/34	83/5	83/7
MAJOR ELEMENTS					
SiO2	49.90	45.60	53.00	44.30	49.90
TiO2	.69	.95	.45	.83	.73
Al2O3	15.00	16.90	13.70	18.60	16.50
Fe2O3	9.39	8.73	7.91	10.03	8.97
FeO	0.00	0.00	0.00	0.00	0.00
MnO	.18	.23	.19	.14	.14
MgO	4.06	7.13	9.15	6.45	5.64
CaO	11.99	12.32	6.98	8.98	8.69
Na2O	1.99	1.07	2.36	2.75	2.84
K2O	1.27	3.20	.92	3.27	2.21
P2O5	0.00	0.00	0.00	0.00	0.00
LOI	5.23	3.14	5.26	4.44	4.01
TOTAL	99.70	99.27	99.92	99.79	99.63
TRACE ELEMENTS					
Pb	22	23	82	17	23
Th	13	6	4	7	11
U	6	3	0	3	1
Rb	43	98	27	123	61
Sr	329	340	259	408	483
Y	14	15	16	14	14
Zr	67	62	40	82	76
Nb	5	4	2	6	5
Zn	69	110	139	79	53
Cu	133	72	157	86	99
Ni	35	50	223	46	41
La	8	2	3	10	9
Ba	910	1006	300	1681	1092
V	217	259	220	344	273
Ce	28	17	21	36	30
Cr	56	110	510	82	63
Ga	14	17	11	17	17

APPENDIX TABLE B-6 (cont'd)

CALC SILICATES

	83/45	83/46
MAJOR ELEMENTS		
SiO2	67.70	65.10
TiO2	.30	.68
Al2O3	13.30	12.80
Fe2O3	2.06	7.58
FeO	0.00	0.00
MnO	.22	.17
MgO	4.19	2.85
CaO	7.95	7.12
Na2O	2.62	1.12
K2O	.13	1.26
P2O5	.05	.08
LOI	1.37	1.16
TOTAL	99.89	99.92
TRACE ELEMENTS		
Pb	12	15
Th	22	6
U	7	4
Rb	5	46
Sr	261	267
Y	48	23
Zr	157	138
Nb	9	7
Zn	57	64
Cu	10	11
Ni	0	0
La	13	0
Ba	94	930
V	46	198
Ce	31	13
Cr	0	0
Ga	13	12

Table B-7: List of samples in groups and subgroups of lithologies in the Isle aux Morts area.

QUARTZOFELDSPATHIC GNEISSES				SEMIPELITES		
QS1	QS2	QS3	QS4	QZ		MINQZ
83/1	83/22	83/78	83/56	83/10	82/1/161	83/3
83/32	Fs10	83/94	83/57	83/19	83/4/245	IAM/11
83/38	Fs15	Fs4	83/58	83/30	QTM1	82/5/351
83/66	82/3/337	Fs6	83/59	83/44	QTM3A	83/2/260
83/67	82/5/364	Fs7A	83/81	83/47	QTM3B	83/2/298
83/77	82/5/397	Fs7B	Fs1	83/48	QTM4	82/5/351
Fs13	83/2/60	Fs9	Fs8	83/50	QTM5	
Fs17		Fs16	Fs12A	83/52	83/70	
82/4/221			Bi1	83/53	83/71	

PELITES		AMPHIB		EPPY	CALCS
83/10	82/1/250	Amp2*	82/1/134*	83/5	83/45
83/12	82/3/367	Amp3	82/1/252	83/7	83/46
Bi2	82/4/58	Amp4*	82/2/244*	83/9	
Bi3	82/5/274	Amp5	82/3/298*	83/13	
Bi6A	82/5/334	Amp6	82/4/101	83/34	
Bi8	83/2/349	83/20	82/5/289*		
Bi10	83/85	83/79	83/3/220*		
Fs2		83/80*	83/4/241*		
Fs12B		83/84*	83/4/410*		
		83/95*	Tr3-4		
		83/97B	Bi6B		
		82/1/43*			

Abbreviations: AMPHIB=Amphibolite; EPPY=Epidote-pyrite schist; CALCS=Calc-silicate samples;
Amp3* (eg) denotes a screened amphibolite.

Appendix C

Analytical procedures for metal assaying and results

The metal grades quoted in text for mineralization in drill hole intersection and in trenches were determined at the laboratories of Atlantic Analytical Services Ltd., Springdale, Newfoundland.

Twenty mineralized samples from trenches and drill holes were also analysed by the Dept. of Mines and Energy, St John's, Newfoundland, using the atomic absorption spectrophotometric method. In each of three runs of the 20 samples, two standards, MP-1 and UM-1, were alos analysed. The mean, standard deviation and published values for MP-1 are presented in Table C-1. Values for UM-1 wre also within acceptable limits of precision and accuracy. The metal assays are presented in Table C-2

Table C-1: Replicate analyses of MP-1: 3 runs

Metal	Mean wt%	Std. Dev.	Published Value
Cu	2.00	0.016	2.09
Pb	1.92	0.042	1.88
Zn	15.54	0.112	15.90
Ag ppm	55.90	0.754	57.90

Table C-2: Metal assays from trench and drill hole intersections

Sample	Cu	Pb	Zn	Ag
Tr.3-1	0.88	7.53	15.14	35.7
Tr.1-3	0.77	6.24	14.70	36.5
82/2/141	0.99	2.82	5.54	22.9
Tr.5-1	2.90	7.21	14.44	57.2
Tr.2A	0.07	10.9	23.55	74.4
Tr.4-1	1.18	8.93	18.30	53.6
Tr.5-3	0.11	7.90	14.43	39.3
Tr.2Lc	2.34	8.64	19.83	117.5
Tr.3-3	0.65	1.09	2.17	22.5
Tr.51G	0.36	2.00	4.16	37.6
Tr1-5	0.38	2.37	4.50	15.3
Tr.3-2	1.38	5.05	10.88	32.2
Tr.2-7	0.06	6.94	12.87	41.7
Tr.1-7	0.14	0.21	4.10	1.3
Tr.1-1	0.59	0.16	0.19	2.2
Tr.1-6	1.14	6.48	13.48	36.1
Tr.2-1	1.21	5.87	9.76	48.2
Tr.2-3	0.03	0.49	0.73	3.8
Tr.2-2	0.28	2.36	5.38	18.8
Tr.2B	0.03	8.41	18.92	54.3

Cu, Pb and Zn in wt%; Ag in ppm.

Appendix D

Analytical techniques for the determination of the Stable Isotopes of Sulphur and Lead

D.1 Lead Isotopes

The stable isotope analyses of lead were perfomed commercially by GEOSPEC CONSULTANTS LTD (Edmonton). Six samples of galena were analysed on a Micromass MM-30 mass spectrometer using the silica-gel-phosphoric acid technique. The Pb sulphide was first purified by fractional crystallization and a one microgram sample was then loaded on a Re filament and placed in the mass spectrometer.

Replicate measurements on NBSRM 981 standard indicate a precision at one sigma of 0.17, 0.22 and 0.28 permil respectively for the isotopic ratios.

D.2 Sulphur Isotopes

Twenty-one hand-picked sulphide samples were analysed for isotopes of S in the Nuclear Research Building, Dept. of Geology, McMaster University by Professor C. E. Rees.

Sulphide samples were converted to sulphur dioxide by reaction, under vacuum with copper oxide at 1200 ^{o}C. Carbon dioxide was removed from the sulphur dioxide by fractional

distillation at the temperature of freezing liquid pentane. The sulphur dioxide was separated from water by fractional distillation at dry ice temperatures.

Sulphur dioxide samples were stored in pyrex tubes prior to mass spectrometry. Delta ^{34}S values were determined by analysis in a double inlet mass spectrometer with a 6" radius, 90^{o} magnetic sector analyser.

Precision of measurement was $\pm$ 0.2 permil.